Magma Chamber Dynamics in the Peralkaline Magmas of the Kakortokite Series, South Greenland

Emma Joanne Hunt

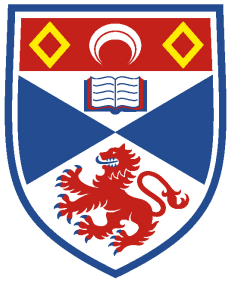

University of
St Andrews

This thesis is submitted in partial fulfilment for the degree of PhD
at the
University of St Andrews

February 2015

1. Candidate's declarations:

I Emma Joanne Hunt hereby certify that this thesis, which is approximately 31,000 words in length, has been written by me, that it is the record of work carried out by me, and that it has not been submitted in any previous application for a higher degree.

I was admitted as a research student in August, 2011 as a candidate for the degree of Doctor in Philosophy in August, 2011; the higher study for which this is a record was carried out in the University of St Andrews between 2011 and 2015.

Date: 23rd February 2015 Signature of candidate:

2. Supervisor's declaration:

I hereby certify that the candidate has fulfilled the conditions of the Resolution and Regulations appropriate for the degree of Doctor of Philosophy in the University of St Andrews and that the candidate is qualified to submit this thesis in application for that degree.

Date: 23rd February 2015 Signature of supervisor:

3. Permission for publication: (*to be signed by both candidate and supervisor*)

In submitting this thesis to the University of St Andrews I understand that I am giving permission for it to be made available for use in accordance with the regulations of the University Library for the time being in force, subject to any copyright vested in the work not being affected thereby. I also understand that the title and the abstract will be published, and that a copy of the work may be made and supplied to any bona fide library or research worker, that my thesis will be electronically accessible for personal or research use unless exempt by award of an embargo as requested below, and that the library has the right to migrate my thesis into new electronic forms as required to ensure continued access to the thesis. I have obtained any third-party copyright permissions that may be required in order to allow such access and migration, or have requested the appropriate embargo below.

The following is an agreed request by candidate and supervisor regarding the publication of this thesis:

PRINTED COPY
Embargo on all or part of print copy for a period of 2 years (maximum five) on the following ground(s):

- Publication would be commercially damaging to the researcher, or to the supervisor, or the University
- Publication would preclude future publication
- Publication would be in breach of laws or ethics

Supporting statement for printed embargo request:

An embargo on all of the printed copy is requested for 2 years, as publication of the thesis would preclude future publication of the data and models presented within the thesis.

Although this PhD was not commercially funded, it worked closely with a company who allowed us access to cores and gave support in the field. Since this thesis is about an area of wider commercial interest, we also request the embargo to ensure that this work can have no knock-on effect on the value of the tenement

ELECTRONIC COPY
Embargo on all or part of electronic copy for a period of 2 years (maximum five) on the following ground(s):

- Publication would be commercially damaging to the researcher, or to the supervisor, or the University
- Publication would preclude future publication
- Publication would be in breach of law or ethics

Supporting statement for electronic embargo request:

An embargo on all of the electronic copy is requested for 2 years, as publication of the thesis would preclude future publication of the data and models presented within the thesis.

Although this PhD was not commercially funded, it worked closely with a company who allowed us access to cores and gave support in the field. Since this thesis is about an area of wider commercial interest, we also request the embargo to ensure that this work can have no knock-on effect on the value of the tenement

Date: 23rd February 2015 Signature of candidate:

Date: 23rd February 2015 Signature of supervisor:

Please note initial embargos can be requested for a maximum of five years. An embargo on a thesis submitted to the Faculty of Science or Medicine is rarely granted for more than two years in the first instance, without good justification. The Library will not lift an embargo before confirming with the student and supervisor that they do not intend to request a continuation. In the absence of an agreed response from both student and supervisor, the Head of School will be consulted. Please note that the total period of an embargo, including any continuation, is not expected to exceed ten years.
Where part of a thesis is to be embargoed, please specify the part and the reason.

Acknowledgements

I would like to thank the following people for their support, advice and general assistance during the production of this thesis. First and foremost I thank my supervisors Adrian Finch and Colin Donaldson for their encouragement, constructive discussions and general patience throughout the project and production of the thesis.

The project could not have been completed with the fieldwork in Greenland and special thanks have to go to my field assistant Rachel Gwynn who went above and beyond the call of duty. I would also like to thank Greg Barnes and Hans Kristian (Hank) Schønwandt at TANBREEZ Mining Greenland A/S for their support in accessing drill core and arranging helicopter support. I would also like to thank Henning Bohse for his assistance in the field, with discussions and keeping us fed with fresh fruit, mushrooms and fish during the fieldwork.

I would like to thank a number of people for sharing their technical expertise throughout the project. In St Andrews Donald Herd provided invaluable assistance during the very long hours of carrying out EPMA analyses. I also would like to thank Andy Mackie for preparing all the sections used in the project and Mark Stacey for his assistance in preparing samples for sectioning. I am very grateful to Angus Calder for help with producing the XRD and XRF analyses on tight deadlines.

I am very grateful to the postgraduate community at St Andrews, especially including Christopher Sargeant, Victoria Oliver, Catherine Cole, Cynthia Brezina and Hannah Fitzpatrick for their support and numerous offers of cups of coffee during the writing of this thesis. I would also like to thank Richard Taylor for helping me to put the data collection phase of the project in perspective and William McCarthy and Hannah Hughes for their support and encouragement during the final stages of writing.

I would finally like to thank my Mother, Carolyn, for her support throughout my education and especially the numerous long distance conversations during the completion of the project.

Abstract

Understanding crystallisation in magma chambers is a key challenge for igneous petrology. It is particularly important to understand the origins of layering in peralkaline rocks, e.g. the kakortokite (nepheline syenite), Ilímaussaq Complex, S. Greenland, as these are commonly associated with high value multi-element economic deposits. The kakortokite is a spectacular example of macrorhythmic (>5 m) layering. Each unit consists of three layers comprising arfvedsonite-rich (sodic-amphibole) black kakortokite at the base, grading into eudialyte-rich (sodic-zirconosilicate) red kakortokite, then alkali feldspar- and nepheline-rich white kakortokite. Each unit is numbered -19 to +17 relative to a characteristic well-developed horizon (Unit 0), however there is little consensus on their development.

This project applies a multidisciplinary approach through field observations combined with petrography, crystal size distributions (CSDs), mineral and whole rock chemistries on Units 0, -8 to -11 and a phonolite/micro-nephelinolite ("hybrid") sequence that crosscuts the layered kakortokite.

Textures and compositions are laterally consistent across outcrop and indicators of current activity are rare. CSDs indicate *in situ* crystallisation with gravitational settling as a minor process. Chemical discontinuities occur across unit boundaries.

The layering developed through large-scale processes under exceptionally quiescent conditions. The discontinuities reflect open-system behaviour; units were formed by an influx of volatile-rich magma that initiated crystallisation in a bottom layer. Nucleation was initially suppressed by high volatile element concentrations, which decreased to allow for crystallisation of arfvedsonite, followed by eudialyte, then alkali feldspar and nepheline to form each tripartite unit. The chemistry of the hybrid indicates mixing between a primitive (sub-alkaline) magma and kakortokite. Thus injections of magmas of varying compositions occurred, indicating a complex plumbing system below current exposure. The lessons learned at Ilímaussaq, which is extremely well exposed and preserved, are relevant to understanding magma chamber dynamics in the more common instances of pervasively altered peralkaline rocks.

Contents

Chapter 1
Introduction

1.1 Project Rationale

Layered intrusions occur over a range of compositions from ultramafic to peralkaline (Naslund & McBirney, 1996) and represent fossilised magma chambers (O'Driscoll *et al.*, 2014). These rocks are key to understanding magma chamber dynamics as they provide excellent records of magmatic processes. Peralkaline layering is however less well understood, partly due to pervasive late-magmatic or sub-solidus alteration, and so is of special interest to petrologists.

Peralkaline complexes are further of economic interest as they are commonly associated with highly valuable, multi-element deposits, e.g. rare-earth elements (REE), Zr, Nb, Ta, P, F, Be, Li and Sr (Kogarko, 1990, Petersen, 2001, Sheard *et al.*, 2012). Many of these, particularly the REE, are in high demand and considered to be of strategic economic importance (BGS©NERC, 2012). This has brought peralkaline complexes to the forefront of current debate into viable deposits as their multi-element nature means that they are not as dependant on the vagaries of single commodity markets. The critical metal potential of Southern Greenland is of interest to the European Union as REE and other critical metals could be supplied to Europe through Greenland's Partnership Agreement. The TANBREEZ Project (TANBREEZ Mining Greenland A/S) focused on the layered nepheline syenite of the Ilímaussaq Complex, is considered to be one of the world's largest potential REE deposits (Schonwandt *et al.*, 2014) and at the time of writing is close to development of the pilot mine. Thus this thesis represents a timely study into the development of these layered rocks and the processes through which the critical metals are concentrated.

The Ilímaussaq Complex was identified as one of the best examples to study peralkaline layering as it has excellent exposure and alteration is often absent. It hosts spectacular macrorhythmic (>5 m) layering in the nepheline syenite (kakortokite, see p.26 for definition) at the base of the complex. This type of layering is considered to be one of the most poorly understood (Irvine, 1987) and there is no consensus on how it developed. One of the current hot topics in igneous petrology is the relative significance of gravitational settling vs. *in situ* crystallisation during layer development. This thesis applies quantitative textural analysis to determine the relative importance of each process through crystal size distribution plots, a technique not previously applied to the complex. The results have been combined with mineral chemistries to develop a conceptual model for the formation of macrorhythmic layering in peralkaline magmas and to gain an insight into the complexity of the plumbing system beneath the Ilímaussaq chamber.

1.2 References

BGS©NERC. (2012). Risk List 2012.

Irvine, T. N. (1987). Processes involved in the formation and development of layered igneous rocks. In: Parsons, I. (ed.) *Origins of Igneous Layering*. Dordrecht: D. Reidel Publishing, 649-656.

Kogarko, L. N. (1990). Ore-forming potential of alkaline magmas. *Lithos* **26**, 167-175.

Naslund, H. R. & McBirney, A. R. (1996). Mechanisms of Formation of Igneous Layering. In: Cawthorn, R. G. (ed.) *Layered Intrusions: Developments in Petrology*. Amsterdam: Elsevier Science B. V.

O'Driscoll, B., Butcher, A. R. & Latypov, R. (2014). New insights into precious metal enrichment on the Isle of Rum, Scotland. *Geology Today* **30**.

Petersen, O. V. (2001). List of all minerals identified in the Ilímaussaq alkaline complex, South Greenland. *The Ilímaussaq alkaline complex, South Greenland: status of mineralogical research with new results* **190**, 25-33.

Schonwandt, H. K., Barnes, G. B. & Ulrich, T. (2014). The world-class REE deposit Tanbreez, South Greenland: its size and structure. *ERES2014: 1st European Rare Earth Resources Conference*. Milos.

Sheard, E. R., Williams-Jones, A. E., Heiligmann, M., Pederson, C. & Trueman, D. L. (2012). Controls on the Concentration of Zirconium, Niobium, and the Rare Earth Elements in the Thor Lake Rare Metal Deposit, Northwest Territories, Canada. *Economic Geology* **107**, 81-104.

Chapter 2
Geological Background

2.1 Introduction

The Ilímaussaq Complex is one of the world's most spectacular examples of igneous layering due to the macrorhythmic scale and excellent exposure. The pervasive alteration commonly associated with peralkaline complexes is typically absent from Ilímaussaq and so it is one of the best examples for distinguishing the primary processes that developed layering. This chapter provides the theoretical background to this thesis through a review of the commonly inferred processes that generate igneous layering. Geological context is provided through a review of selected peralkaline complexes of varying ages and sizes that share characteristics with Ilímaussaq. A brief description of the geology of southern Greenland and a more detailed description of the rocks that comprise the Ilímaussaq Complex completes this chapter.

2.2 Development of Igneous Layering

Layered intrusions are common throughout the geological record and range in composition from ultramafic to peralkaline (Naslund & McBirney, 1996). They represent fossilised magma chambers (O'Driscoll *et al.*, 2014) and as such have proved to be extremely important in understanding magma chamber dynamics, as the rocks within them provide excellent records of the primary processes of igneous layering. Layering develops at the cumulus stage during differentiation of crystals through processes such as gravitational settling or *in situ* nucleation (Irvine, 1987). A cumulate is defined in the present study following Irvine (1982) as an igneous rock characterised by a touching crystal framework, where the crystals were concentrated through fractional crystallisation, therefore crystal settling is a possible but not essential process. The repetitive nature of the layering is controlled by processes including crystal fractionation, mechanical sorting of crystals, liquid replenishment, gain or loss of volatiles, pressure changes or through external factors such as earthquakes (Irvine, 1987).

The types and expressions of igneous layering are highly variable (Naslund & McBirney, 1996) due to variations in thickness, modal composition, grain size, textures (including internal structures such as lamination and deformation) and chemistries (Irvine, 1982, Naslund & McBirney, 1996). Thus a range of processes are required to account for this variety in the styles of layering.

One of the driving mechanisms for crystal nucleation and growth is magma mixing (Huppert & Sparks, 1980, Irvine, 1975). Mixing of magmas of differing compositions, either through the resident magma mixing with a more primitive melt

during a replenishment event (Huppert & Sparks, 1980, Irvine, 1977) or assimilating country rocks (Irvine, 1975, Spandler *et al.*, 2005) will affect the melt composition and and which phase is crystallising. For example mixing with a primitive melt can move a mafic melt composition away from the olivine-chromite cotectic (Fig. 2.1) and force it into the chromite field, resulting in nucleation of chromite either in suspension or *in situ* on the magma chamber walls and/or floor (Huppert & Sparks, 1980). Crystallisation then moves the melt composition back towards the cotectic it was originally crystallising along (Fig. 2.1). Repeated replenishment or assimilation events can produce rhythmic modal layering (Irvine, 1975) through repeated cycles of nucleation.

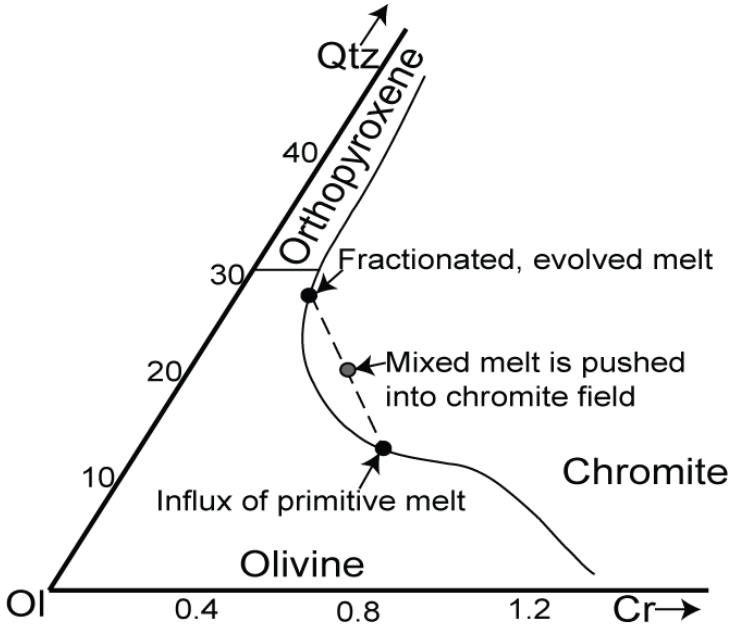

Figure 2.1: Phase diagram indicating how an influx of primitive melt can force the hybrid melt into the chromite crystallisation field. After Irvine (1977).

Replenishment events can further contribute to the formation of primary igneous layering through entrained crystal cargoes (Maier *et al.*, 2013, Mondal & Mathez, 2007). These nucleated in the plumbing system below the chamber or in a lower magma chamber, and the microphenocrysts were entrained as a suspended load (Eales, 2000) and injected into the upper magma chamber. Settling of these crystals from suspension (Mondal & Mathez, 2007) or injection as a crystal-rich slurry (Maier *et al.*, 2013) would lead to the development of stratiform layers on the magma chamber floor and repeated replenishment events would develop the cyclicity of layering. Marsh (2013) advocates layer formation through the emplacement of crystal slurries over rhythmic crystallisation.

Intensive parameters can also affect the development of layering as pressure fluctuations in the magma chamber can control the liquidus phase assemblage. This

affects which phase is nucleating and can develop modal layering (Naslund & McBirney, 1996). Within the Bushveld Complex this mechanism is suggested to have contributed to the formation of the Merensky Reef due to an increase in the pressure of the magma chamber associated with replenishment events. This resulted in sulphur saturation and separation of an immiscible sulphide liquid that contributed to the formation of the Merensky Reef (Cawthorn, 2005).

Fluctuations in oxygen fugacity due to assimilation of country rocks, volatile release, temperature fluctuations or convection currents (Naslund & McBirney, 1996) can vary which phase is nucleating. Thus an oscillating oxygen fugacity can lead to the development of modal igneous layering.

Convection currents and thermal gradients are also proposed to have a role in the formation of primary igneous layering. Thermal gradients through the magma body can result in nucleation at thermal boundaries, i.e. crystallisation fronts. Nucleation occurs at these in response to cooling and subsequent lowering of the magma temperature below the liquidus at the thermal boundary (Tait & Jaupart, 1996). This can result in *in situ* crystallisation at the thermal boundary (Tait & Jaupart, 1996) or convection processes can transport the nuclei away from the thermal boundary where they either dissolve or continue to grow (Martin & Nokes, 1988, Sparks *et al.*, 1993).

Double diffusive convection cells have been invoked by many authors (Huppert & Sparks, 1984, Huppert & Turner, 1981, Larsen & Sørensen, 1987, Naslund & McBirney, 1996) to account for the development of primary igneous layering. These convection cells can occur in magma bodies that have multiple values of molecular diffusivity, i.e. compositional variations (Huppert & Sparks, 1984). These variations lead to the development of convective cells with individual molecular diffusivity and thermal gradients. Crystallisation in these cells progresses along thermal boundaries and the repetitive nature of the layering is developed through multiple convection cells, which can each form one or more layers (Huppert & Sparks, 1984, Huppert & Turner, 1981, Larsen & Sørensen, 1987).

The similarity between each process is that they all act to develop layering through affecting the nucleating phase. The site of nucleation is however controversial, the most often cited is in suspension in the magma body. Crystal settling and sedimentation, driven by gravitational sorting of crystals following Stokes' law develops the layered rocks (McBirney, 2006, McBirney & Hunter, 1995, Naslund & McBirney, 1996, Sparks *et al.*, 1993). The process is commonly cited to contribute to the development of graded layering due to concentration of the densest and coarsest crystals at the base of the layer through density sorting (Naslund &

McBirney, 1996). The modal layering in the Skaergaard Intrusion, E. Greenland, is suggested to have formed through this process (Conrad & Naslund, 1989, Naslund & McBirney, 1996). Alternatively *in situ* crystallisation is receiving attention as an alternative process to gravitational settling (O'Driscoll *et al.*, 2010). Nucleation in these models is controlled by thermal or compositional boundary layers and crystallisation occurs on either on the floor or the walls of the magma chamber (Latypov *et al.*, 2013, O'Driscoll *et al.*, 2010, Tait & Jaupart, 1996). Igneous layering develops as a result of movement of these boundary layers in combination with variations in the intensive parameters.

These potential controls on nucleation will be investigated with reference to their effectiveness in developing layered peralkaline rocks and the relative importance of gravitational settling vs. *in situ* nucleation on the development of the Ilímaussaq rocks.

2.3 Layered Peralkaline Complexes

Peralkaline rocks have developed through extreme fractional crystallisation and as such are characterised by an extraordinary wealth of mineral species (Sørensen, 1997). Many of these are economically valuable, which has acted to further interest and research into the peralkaline rocks that host them. At excessive concentrations of alkalis, peralkaline rocks are termed agpaitic. These rocks have molar ratios of [(Na+K)/Al] > 1.2 (Ussing, 1912), are associated with high volatile contents (F and Cl) and contain complex Zr- and Ti-silicates such as: eudialyte, a Na-zirconosilicate, rinkite a titanosilicate; loparite, a rare-earth titanosilicate; astrophyllite, a Na-rich titanosiliate; and villiaumite, a NaF mineral (Edgar, 1974, Sørensen, 1997). The magmas are inferred to have low solidus temperatures, *c.* 400-500ºC, due to their extremely high volatile contents and often segregate fluid phases, which are typically of Na- or methane-rich compositions (Sørensen, 1997).

These rocks are represented in the geological record by layered intrusions composed almost entirely of agpaitic rocks, e.g. the Ilímaussaq, Khibina and Lovozero Complexes; or through agpaitic rocks incalcated with miaskitic rocks (characterised by zircon, titantite and Fe-Ti oxide minerals (Marks *et al.*, 2011)) within a single intrusion, e.g. the Nechalacho Alkaline Layered Suite, Canada. The layering in these complexes is hypothesised to form through processes of: gravity and/or current driven accumulation of crystals; crystallisation at nucleation fronts due to chemical and/or thermal gradients through the magma; or *in situ* crystallisation when the crystallising phase is of a similar density to the magma (Larsen & Sørensen, 1987, Sørensen, 1969).

These layered peralkaline/agpaitic complexes occur throughout the geological record in association with extensional tectonic settings and range in size from several to hundreds of kilometres in diameter. The following section briefly reviews the characteristics of peralkaline/agpaitic intrusions that represent a range of ages and sizes, discussed from the oldest to youngest.

2.3.1 Nechalacho Layered Alkaline Suite, N.W.T., Canada, 2.1 Ga

The Nechalacho Layered Alkaline Suite (Sheard *et al.*, 2012), also referred to as the Nechalacho deposit, was discovered through drilling in the core of the Thor Lake Syenite (Fig. 2.2) (Sheard *et al.*, 2012). It is situated on the southern margin of the Slave province of the Canadian Shield within the Palaeoproterozoic Blatchford Lake Intrusive Complex (~2.15 Ga) and underlies the Thor Lake Syenite (Fig. 2.2).

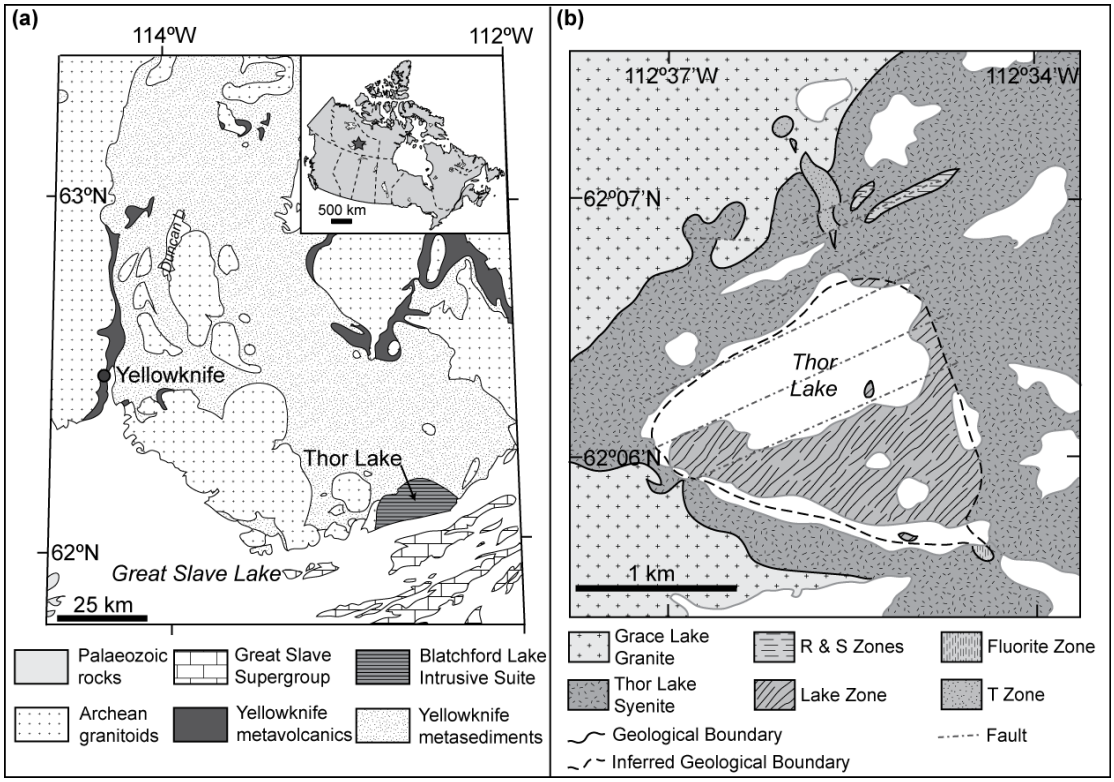

Figure 2.2: (a) Geological sketch map of the Southern Slave Province, Thor Lake Syenite is arrowed. (b) Geological sketch map of the zones of mineralisation within the Thor Lake Syenite. After Pinckston & Smith (1995).

The Thor Lake Syenite contains 5 zones of mineralisation: the R, S, T, Lake and Fluorite Zones (Fig. 2.1b) (Pedersen & LeCouteur, 1991). The main economic elements are Be, Li, Nb, REE, Y and Zr, with the richest deposits occurring in the T (Be, Nb, Ce) and Lake Zones (Nb, Ce, Y, Zr). The Lake Zone overlies the Nechalacho deposit (Sheard *et al.*, 2012) and is the largest of the mineralised zones at ~1.8 km^2. It is composed of altered and brecciated syenite, with the alteration attributed to late-stage magmatic and hydrothermal events (Pinckston & Smith, 1995). The mineralisation is concentrated in the central portions of the Lake Zone, which displays the greatest post-magmatic, hydrothermal alteration (Pinckston & Smith, 1995).

The Nechalacho Layered Alkaline Suite is the youngest intrusive event in the Blatchford Lake Intrusive Complex (Pinckston & Smith, 1995, Sheard *et al.*, 2012)

and although a precise age of the layered suite itself has not yet been determined, a date of 2094 ± 10 Ma (Bowring *et al.*, 1984) is considered to represent either the emplacement age of the suite or the age of the rare metal mineralisation (Sheard *et al.*, 2012). The Nechalacho Layered Alkaline Suite only outcrops in a restricted area, thus has mostly been studied through drill core, through this it is inferred to have a dome shape with a diameter of ~1.5 km (Sheard *et al.*, 2012). The vertical extent of the layered series is unknown but it extends through the 300 m of drill core (Sheard *et al.*, 2012). The alkalinity increases with depth through a sodalite cumulate roof zone; under which is coarse-grained to pegmatitic aegirine ± arfvedsonite syenite; zircon-rich cumulates; and the lowest discovered rock is layered aegirine nepheline syenite, which contains pseudomorphs after inferred cumulus eudialyte (Sheard *et al.*, 2012). This nepheline syenite is sub-horizontally layered at centimetre to metre scales, associated with cyclical variations in the modal mineralogy (Sheard, 2010).

The zircon cumulates and nepheline syenite host the rare metal deposit owned by Avalon Rare Metals Inc., which is comprised of two mineralised zones. The upper zone (15-30 m thick), is hosted by the zircon cumulates, and the lower zone (15-60 m thick), is hosted by the altered eudialyte cumulates (Sheard *et al.*, 2012). These rocks are proposed to have formed through emplacement of a volatile-rich aegirine nepheline syenite into the core of the Thor Lake Syenite. The layering developed in an open system, where convection combined with multiple injections of magma, followed by fractional crystallisation, resulted in repeated saturation and undersaturation in the observed zirconosilicate phases. After the crystallisation of the cumulates a fluid phase, exsolved from nepheline syenite at depth, acted to alter the primary eudialyte to zircon, fergusonite-(Y), bastnäsite-(Ce), allanite-(Ce), parisite-(Ce)/synchysite-(Ce), albite, quartz, biotite, fluorite, kutnahorite and haematite (Sheard *et al.*, 2012).

2.3.2 Pilanesberg Complex, South Africa, 1.2 Ga

The Pilanesberg complex is situated along an extensional structure (Mitchell & Liferovich, 2004) between the Lebowa Granite Suite and the Rustenberg Layered Suite of the Bushveld Complex (Fig. 2.3) (Olivio & Williams-Jones, 1999). It has an area of 625 km^2 (Cawthorn, 2015) and was emplaced at 1250±60 Ma (SACS, 1980) as part of the widespread Pilanesberg Alkaline Province, which is comprised of dykes, central volcanoes and circular intrusions (Cawthorn, 2015).

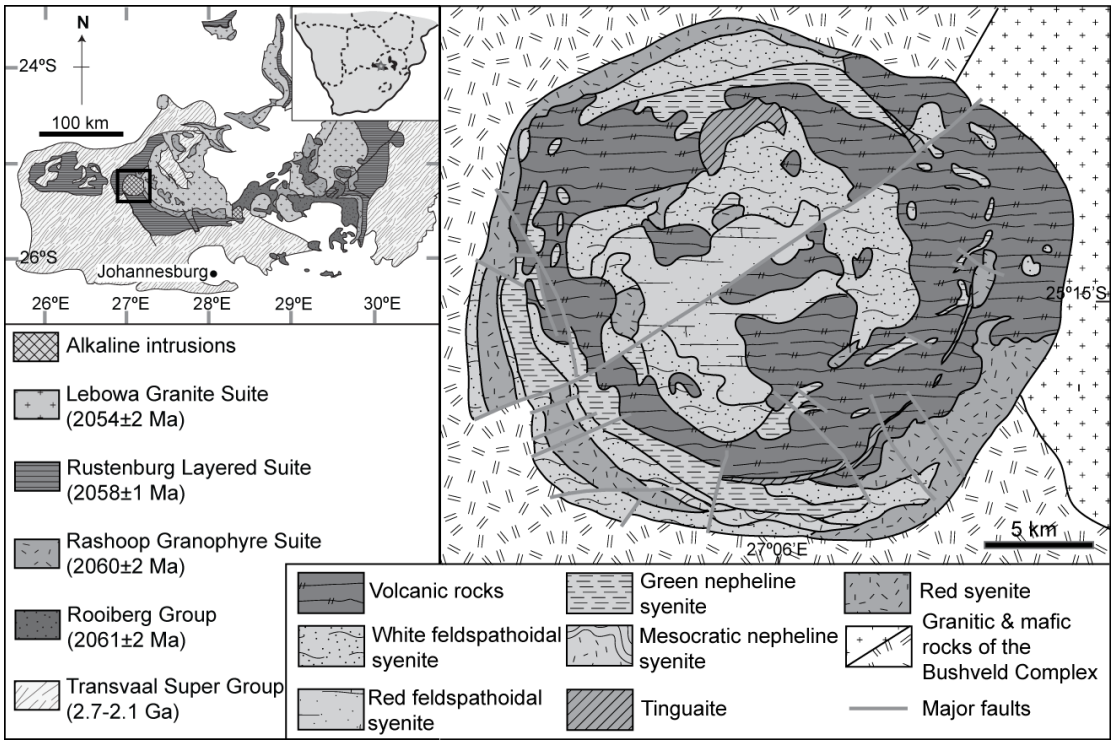

Figure 2.3: Geological sketch map of the Pilanesberg Complex, after Liferovitch & Mitchell (2006). Inset geological map of the Bushveld Complex, top left, after Nex (2004).

Relatively little has been published on the complex due to a lack of exposure and pervasive autometasomatic alteration (Cawthorn, 2015). The most recent study by Cawthorn (2015) suggests that the complex is a gently inward-dipping sheet, composed of units that developed through injections of magma into an unconsolidated, evolving magma chamber.

The complex is composed of phonolitic to trachyitic volcanics (pyroclastics and lava flow sequences) and arcuate intrusive units of agpaitic feldspathoidal syenite that young towards the core of the complex (Mitchell & Liferovich, 2004). From the core outwards the arcuate units are composed of red and white feldspathoidal syenites, green nepheline syenite (aegirine lujavrite), white feldspathoidal syenite, meso-melanocratic nepheline syenite, tinguaite and red

syenite (Fig. 2.3; Liferovich & Mitchell, 2006, Olivio & Williams-Jones, 1999). The red syenites are inferred to have been emplaced first; followed by white foyaites, likely into the centre of the red syenites. Lastly the Green (and Ledig) Foyaites were emplaced within the white syenite (Cawthorn, 2015).

The complex hosts Zr and REE resources within eudialyte-group minerals, with the highest grades hosted in the green nepheline syenite. However exploration for these has ceased due to the complex being located within a designated National Park (Cawthorn, 2015). The green nepheline syenite is layered, coarse-grained and composed of aegirine with microcline, albite, nepheline, sodalite, pectolite, zircon, eudialyte, britholite and fergusonite-(Y) (Olivio & Williams-Jones, 1999).

The layering of the green nepheline syenite is proposed to have formed through processes of crystal sorting and accumulation within a low viscosity peralkaline magma (Mitchell & Liferovich, 2006). Postmagmatic alteration by deuteric alkaline fluids altered primary aluminosilicates, rinkite, eudialyte and fluorapatite to assemblages of secondary minerals (Liferovich & Mitchell, 2006, Mitchell & Liferovich, 2006).

Mineralisation models indicate three stages of alteration contributed to the mineralisation. The first stage of alteration involved replacement of orthomagmatic eudialyte and sodalite by a miaskitic (lower alkalinity) paragenesis. The second stage of alteration occurred in an environment of increasing alkalinity and the final stage of alteration took the form of a miaskitic phase (Mitchell & Liferovich, 2006). This marked evolution from miaskitic to agpaitic and hyperagpaitic back to miaskitic is interpreted as the result of prolonged interaction of the deuteric fluids with the evolving mineral assemblages and the subsequent effect on the Na/Cl ratio and pH of the deuteric fluids (Liferovich & Mitchell, 2006). This requires retainment of the Pilanesberg deuteric fluids in a closed system (Mitchell & Liferovich, 2006).

2.3.3 Khibina & Lovozero Complexes, Russia, 371-362 Ma

The Khibina and Lovozero Complexes are agpaitic intrusions in the Kola Alkaline Province, Kola Peninsula, Russia (Fig. 2.4). The province consists of 24 ultramafic to alkaline intrusions with associated mafic dykes (Kramm *et al.*, 1993), all of which are suggested to be co-magmatic and sourced from the same mantle region (Kogarko, 1987, Kogarko *et al.*, 2010). The Khibina and Lovozero intrusions were emplaced after the formation of the Fennoscandian Shield (Kogarko & Khapaev, 1987) between 377 to 362 Ma (Kramm *et al.*, 1993), despite their close proximity, the intrusions are separate and not linked at depth (Arzamastsev *et al.*, 2000).

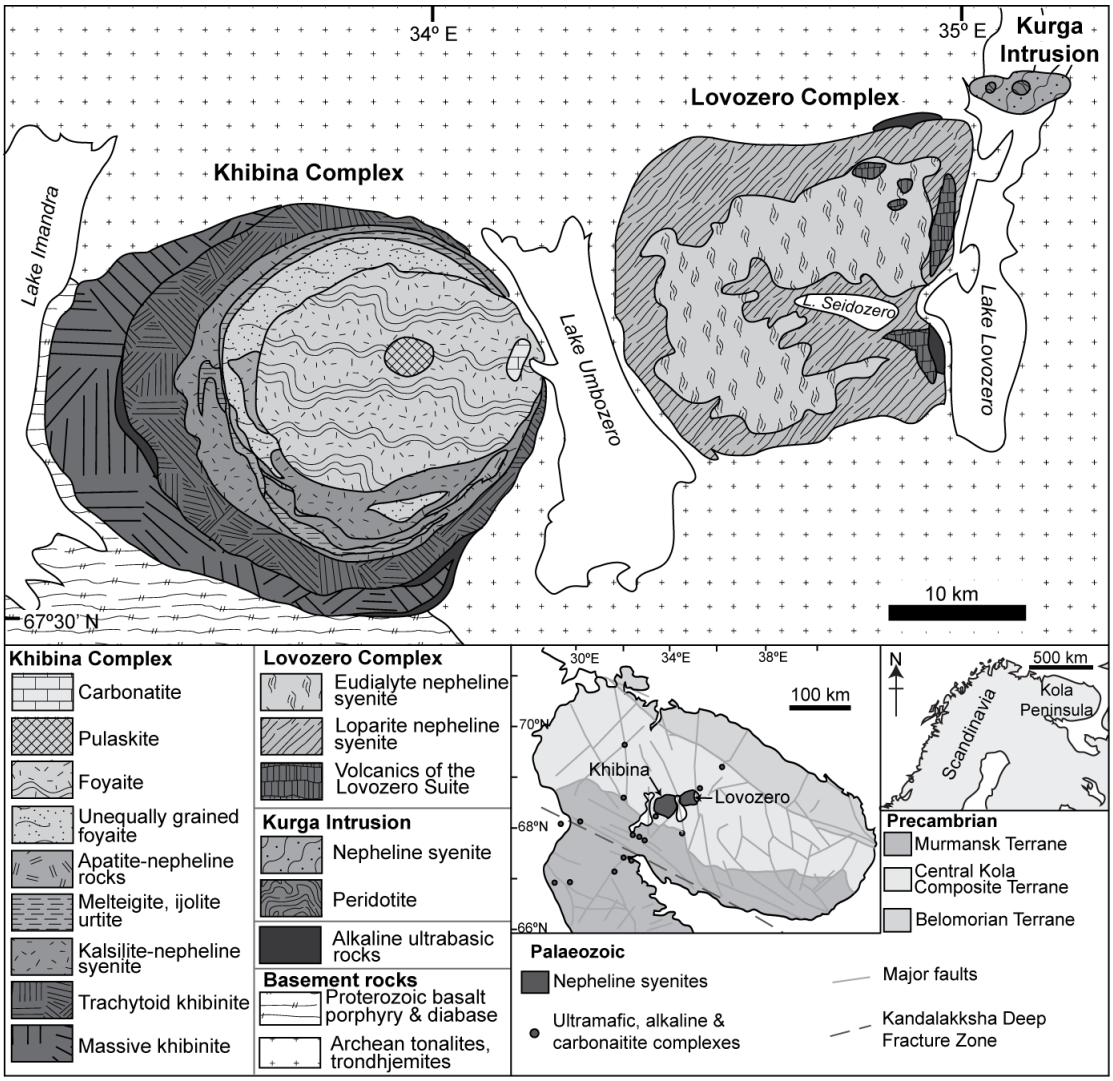

Figure 2.4: Geological sketch map of the Khibina and Lovozero Complexes, after Arzamastsev *et al.* (2000)). Inset map, lower right, of Kola Peninsula after Féménias *et al.* (2005).

The Khibina Complex is one of the largest agpaitic intrusions with an area of 1350 km^2 (Kogarko, 1987). It is polyphase and comprised of 6-7 concentric ring intrusions, which young inwards and dip to a common centre at the eastern margin of

the complex (Kramm *et al.*, 1993). It is divided into eight zones: (1) alkaline and nepheline syenites (oldest); (2) massive khibinite; (3) trachytoid khibinite; (4) kalsilite-nepheline syenite; (5) melteigite, ijolite and urtite; (6) unequally grained foyaite; (7) foyaite; and (8) carbonatite (Arzamastsev *et al.*, 2000, Kogarko *et al.*, 2010).

Although the Khibina complex is classified as a ring intrusion, Zone 5 displays primary magmatic layering. This zone has a thickness of 1-2 km and hosts apatite-nepheline syenite within a layered melteigite-ijolite-urtite series (Kogarko *et al.*, 2010). These rocks are of economic interest as the apatite-nepheline syenite is potentially the world's largest apatite deposit, with additional resources of phosphorous, strontium and REE (Kogarko *et al.*, 2010).

The layering of the tripartite melteigite-ijolite-urtite series is hypothesised to have formed from five zones of crystallisation (Kogarko & Khapaev, 1987). These are: (1) a lower near-contact zone (LCZ); cumulate layers enriched in (2) aegirine, (3) aegirine & nepheline, (4) nepheline; and (5) the upper near-contact zone (UCZ). The formation model is based on data from a single outcrop, but reflects formation of the LCZ through *in situ* crystallisation; the middle three layers through gravitational settling and density sorting; and the UCZ through the freezing of crystals at the roof of the intrusion.

The neighbouring Lovozero Complex (Fig. 2.4) is comprised of three units: (1) an upper volcanic to subvolcanic unit in the east of the complex; (2) a laccolithic, layered nepheline syenite body, which extends to a depth of 2 km; and (3) a lower ring structure with a thickness of at least 7 km (Kramm *et al.*, 1993). The laccolithic unit is comprised of a lower miaskitic nepheline syenite, which passes upwards into a rhythmically layered agpaitic unit (Kramm *et al.*, 1993).

This agpaitic unit has been divided into 5 series: I (uppermost) containing 5 layers; II containing 8 layers; III containing 16 layers; IV containing 11 layers; and V (lowest) containing 3 layers. These series are distinguished by the presence of apatite and/or loparite rich marker horizons (Féménias *et al.*, 2005).

The layers have a generalised tripartite structure of: urtite, enriched in nepheline with apatite; foyaite enriched in nepheline & alkali feldspar; and lujavrite, enriched in aegirine & arfvedsonite (Féménias *et al.*, 2005). Various processes have been proposed for the development of the layering: formation from a stratified magma body (Bussen & Sakharov, 1967); *in situ* crystallisation from the roof downwards through a stagnant magma (Vlasov *et al.*, 1959); gravitational settling (Kogarko & Volkov, 1963) or flotation (Ivanov, 1960); or emplacement of cargoes of entrained crystals, sourced from a lower magma chamber (Féménias *et al.*, 2005).

2.3.4 Tamazeght Complex, Morocco, 44-35 Ma

The Tamazeght Alkaline Complex (also referred to as the Tamazert Complex) is comprised of a range of silica-saturated to silica-undersaturated and carbonatitic plutons and volcanic rocks, located in the northern range of the High Atlas Mountains, Morocco (Fig. 2.5) (Bouabdellah *et al.*, 2010).It is inferred to have a plutonic, layered peralkaline complex at depth below the volcanic series (Berger *et al.*, 2009). Although this is not exposed, the style of mineralisation and post-magmatic hydrothermal alteration has similarities with Ilímaussaq and the Nechalacho Layered Alkaline Suite, thus a review of the complex is included.

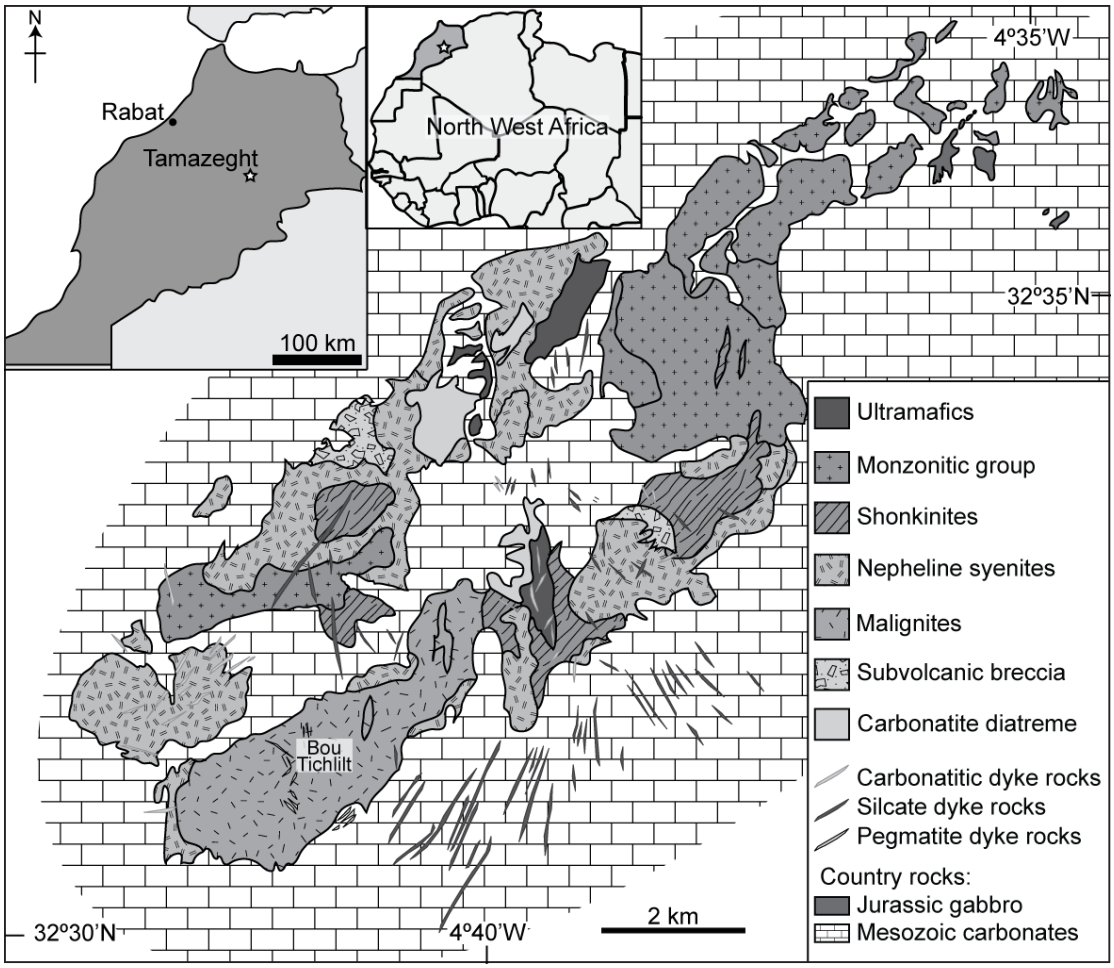

Figure 2.5: Geological sketch map of the Tamazeght Complex. After Marks *et al.* (2009).

The complex is located in an intracratonic rift basin and was emplaced at shallow depths (<3 km) (Salvi *et al.*, 2000) during the middle Eocene (44±2 Ma) (Marks *et al.*, 2008a) into Jurassic carbonates (Marks *et al.*, 2008b). It is a polyphase complex and is suggested to have formed through either fractional crystallisation of a single magma batch (Salvi *et al.*, 2000) or through progressive partial melting of a single mantle source region (Marks *et al.*, 2009). Recent geochemical evidence

supports the latter hypothesis as two evolutionary trends are displayed, indicating the complex did not evolve from a single parental melt composition (Marks *et al.*, 2011).

The emplacement sequence of the Tamagzeght Complex has been identified as an initial alkaline ultrabasite, followed by shonkinite, foïd monzogabbro, plagisyenite, malignite, foïd syenite and finally monzonite (Kchit, 1990). The malignites and nepheline syenites that outcrop in the Bou Tichlit area (Fig. 2.5) are subdivided into zircon-rich miaskitic amphibole; biotite malignite and eudialyte-rich agpaitic nepheline syenite, with intermediate compositions (Salvi *et al.*, 2000). The agpaitic assemblages are represented by pegmatitic dykes, which outcrop in spatially restricted areas. They are interpreted as forming from highly evolved restitic melts (Schilling *et al.*, 2009) and represent the most evolved units of the complex. Their mineralogy has been compared to the nepheline syenite of the Ilímaussaq Complex, S. Greenland, although the extent of hydrothermal alteration has been compared to the Strange Lake and Thor Lake Complexes, Canada (Salvi *et al.*, 2000). The HFSE enrichment in these dykes is associated with eudialyte-group minerals, and detailed textural and compositional analysis of these by Schilling *et al.* (2009) suggests that they underwent a discontinuous two-stage evolution from late-magmatic compositions through to sub-solidus hydrothermal alteration. The eudialyte-group minerals that underwent hydrothermal alteration exhibit much greater contents (one order of magnitude) of light and middle REE than the magmatic eudialyte-group minerals, although the HREE contents do not significantly differ (Schilling *et al.*, 2009). The composition of the fluids responsible for this enrichment is debated. Some authors suggest that the REE, Zr, Ti and Nb were transported as mixed F-OH complexes in a high temperature (500-300ºC) Ca-poor, F-rich fluid (Salvi *et al.*, 2000). Other authors argue that the fluids were sourced from the neighbouring carbonatites and therefore enriched in Ca, Sr, Mn, LREE, MREE, Y, Nb and CO_2 (Schilling *et al.*, 2009). The extent of the hydrothermal alteration is not considered to have been great enough to concentrate the HFSE to ore grades in the currently published literature (Salvi *et al.*, 2000).

2.4 Proterozoic Tectonic Setting of Southern Greenland

The southern Greenland region formed during accretion of the supercontinent Nuna (Hoffman, 1997, Zhang *et al.*, 2012), also referred to as Columbia (Zhao *et al.*, 2002), during the Palaeoproterozoic at approximately 45ºN. The Ketilidian Orogenic belt across the southern tip of Greenland (Fig. 2.6) is suggested to have formed between 1900-1800 Ma (Hoffman, 1997) and fully accreted by 1780 Ma (Zhang *et al.*, 2012). Break-up of Nuna is inferred to have started around 1400 Ma (Zhang *et al.*, 2012), which led to extensional rifting along the margins of the Ketilidian orogen and development of the Gardar Province between 1350-1140 Ma (Upton *et al.*, 2003).

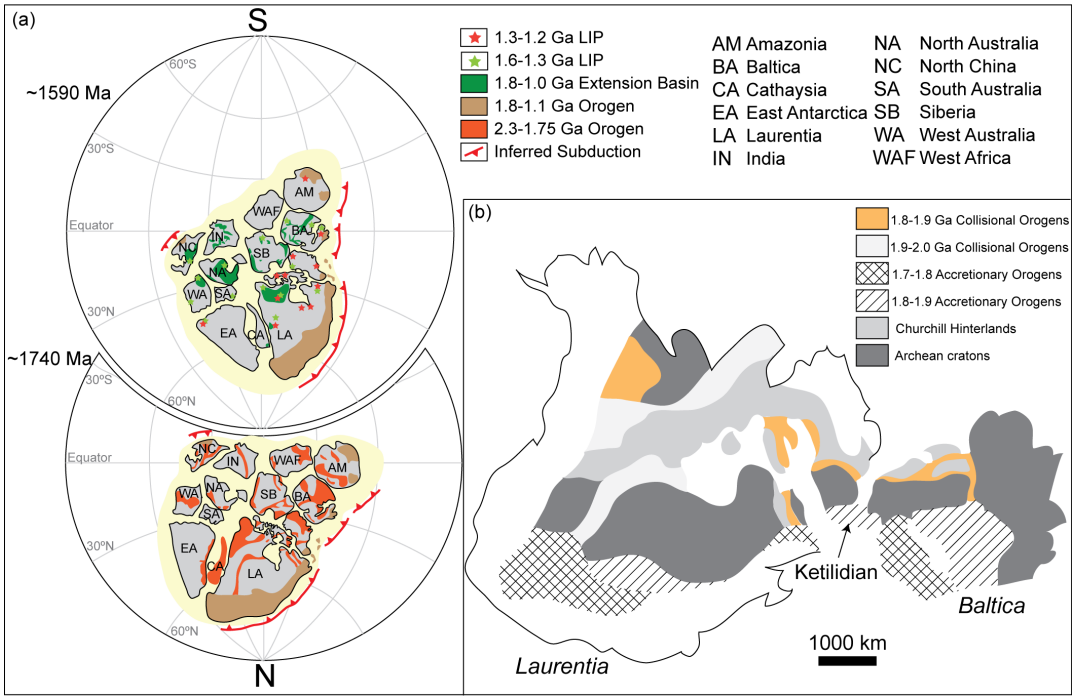

Figure 2.6: (a) Palaeogeographic reconstruction of Nuna at ~1740 Ma and ~1590 Ma suggesting southern Greenland was moving southwards during the Palaeozoic, after Zhang *et al.* (2012). (b) Enlarged view of Laurentia and Baltic showing the position of the Ketilidian Accretionary Orogen across southern Greenland, after Hoffman (1997).

2.5 Geological Overview of Southern Greenland

Southern Greenland is comprised of rocks from the Ketilidian orogeny, bordered to the north by a portion of the Archean North Atlantic craton (Fig. 2.7).

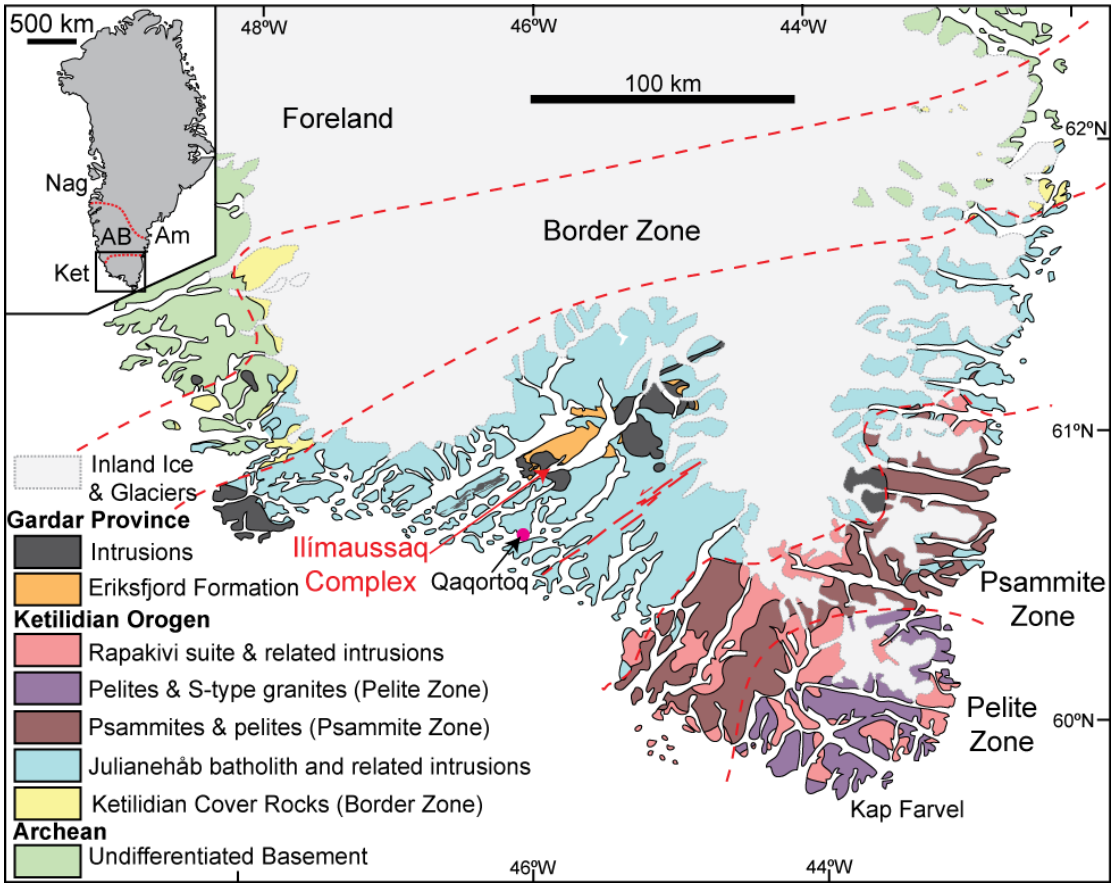

Figure 2.7: Geological sketch map of southern Greenland. After (Garde *et al.*, 2002)

The Julianehåb Batholith was emplaced between 1855-1795 Ma during the Ketilidian orogen (Garde *et al.*, 2002) and is interpreted as the root of a volcanic arc, which formed through oblique convergence between the North Atlantic craton and a subducting oceanic plate to the south (Chadwick & Garde, 1996). The batholith is predominantly composed of granodiorite and granite, with minor bodies of tonalite and diorite with subordinate metagabbro and amphibiolite dykes (Chadwick & Garde, 1996, Garde *et al.*, 2002). The fore-arc basin was filled during the emplacement of the batholith. The coarser sediments formed the proximal Psammite Zone and finer sediments formed the Pelite Zone (Garde *et al.*, 2002). These were metamorphosed between 1795-1785 Ma during a high temperature, low pressure metamorphic event. The final rocks of the Ketilidian orogen, the granites of the Rapakivi suite, were emplaced between 1755-1732 Ma (Garde *et al.*, 2002).

2.6 Gardar Province

The Gardar Province (1.3-1.1 Ga, Upton, 2013) of South Greenland is formed of central complexes predominantly composed of syenite; mafic to intermediate dyke swarms; 'giant dykes', up to 500 m in width, composed of syenogabbro with granitic or syenitic centres; and basin fill sequences of clastic sediments with sub-aerial lavas (Fig. 2.8, Upton *et al.*, 2003). Emplacement of the central complexes was controlled by the dominant ESE Ketilidian or Early Kuanitic faulting, associated with rifting between the Archean craton and the Ketilidian orogen (Piper *et al.*, 1999). The emplacement of the Ilímaussaq Complex was however controlled by local ENE faulting (Ferguson, 1964).

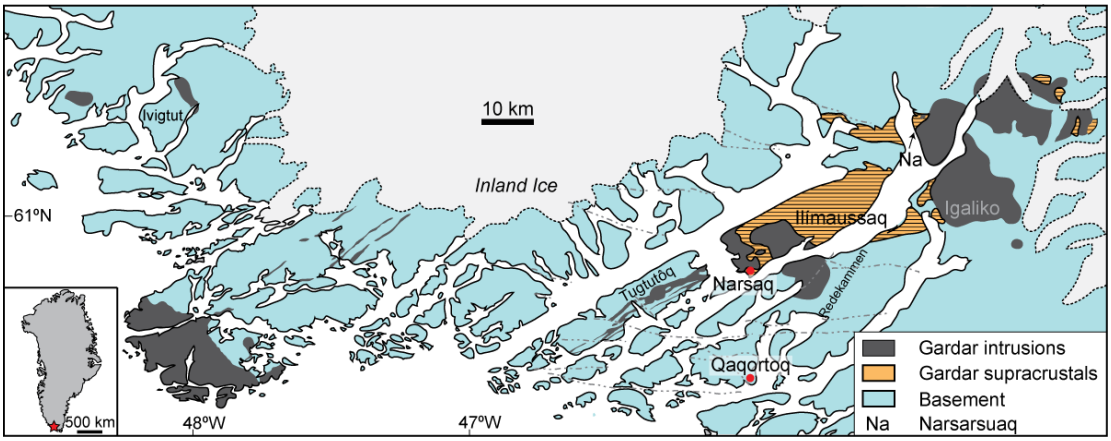

Figure 2.8: Geological sketch map of the Gardar Province, after Sørensen (2001).

The supercrustal Eriksfjord Fm. is comprised of a sequence of clastic sediments and volcanic rocks, ~3.4 km thick. The age is still debated as palaeomagnetic data suggest formation between 1350-1310 Ma (Piper *et al.*, 1999), while Sm-Nd isochrons infer a younger age between 1200-1170 Ma (Paslick *et al.*, 1993). Despite this controversy, the formation must be older than 1273±6 Ma, the age of magmatism at the Motzfeld Centre (McCreath *et al.*, 2012) as the Eriksfjord overlies this intrusion. The formation is composed of ~1.8 km of clastic sediments, subdivided into 3 members; and ~1.6 km of volcanic rocks, also subdivided into 3 members, with the volcanics more prominent upwards through the formation (Piper *et al.*, 1999, Upton *et al.*, 2003).

The clastic sediments are continental in origin and comprise aeolian sandstones, fluvial conglomerates and arenitic sandstones with minor unconformities (Clemmensen, 1988, Piper *et al.*, 1999). The volcanic rocks predominantly consist of basalts and hawaiites, although trachyte lavas become more prevalent upwards through the formation (Piper *et al.*, 1999). These volcanics display a general increase in differentiation upwards between the three Eriksfjord Fm. basalt groups, the

Mussartût, Ulukasik and Ilímaussaq. Piper *et al*. (1999) suggest that this could be related to derivation of the volcanics from either a single magma chamber or a related nest of chambers. These compositional variations were further investigated by Halama *et al.* (2003) through isotopic, rare earth and trace element data. They suggest that the compositional variations could be associated with derivation of the basalts from a mantle plume source with some assimilation of lower crustal material.

In the vicinity of the Ilímaussaq complex, the Eriksfjord Fm. is represented by the 5th member, the Nunasarnaq Mbr of the Ulukasik group (Halama *et al.*, 2003, Piper *et al.*, 1999, Upton *et al.*, 2003). The Nunasarnaq Mbr is ~350 m thick and is composed of aeolian quartz arenites, interlayered with lava flows (Piper *et al.*, 1999). These are overlain by the volcanic Ilímaussaq Mbr., which is mainly comprised of basalts that pass up into hawaiites, trachybasalts, trachyandesites, trachytes and phonolites.

2.7 Ilímaussaq Complex

The Ilímaussaq Complex is a 1160±2 Ma (Waight *et al.*, 2002) peralkaline intrusion, intruded as an elongated laccolith (Fig. 2.9), 17x8 km in plan section, into basement granitoids and the overlying Eriksfjord Formation (Ferguson, 1964).

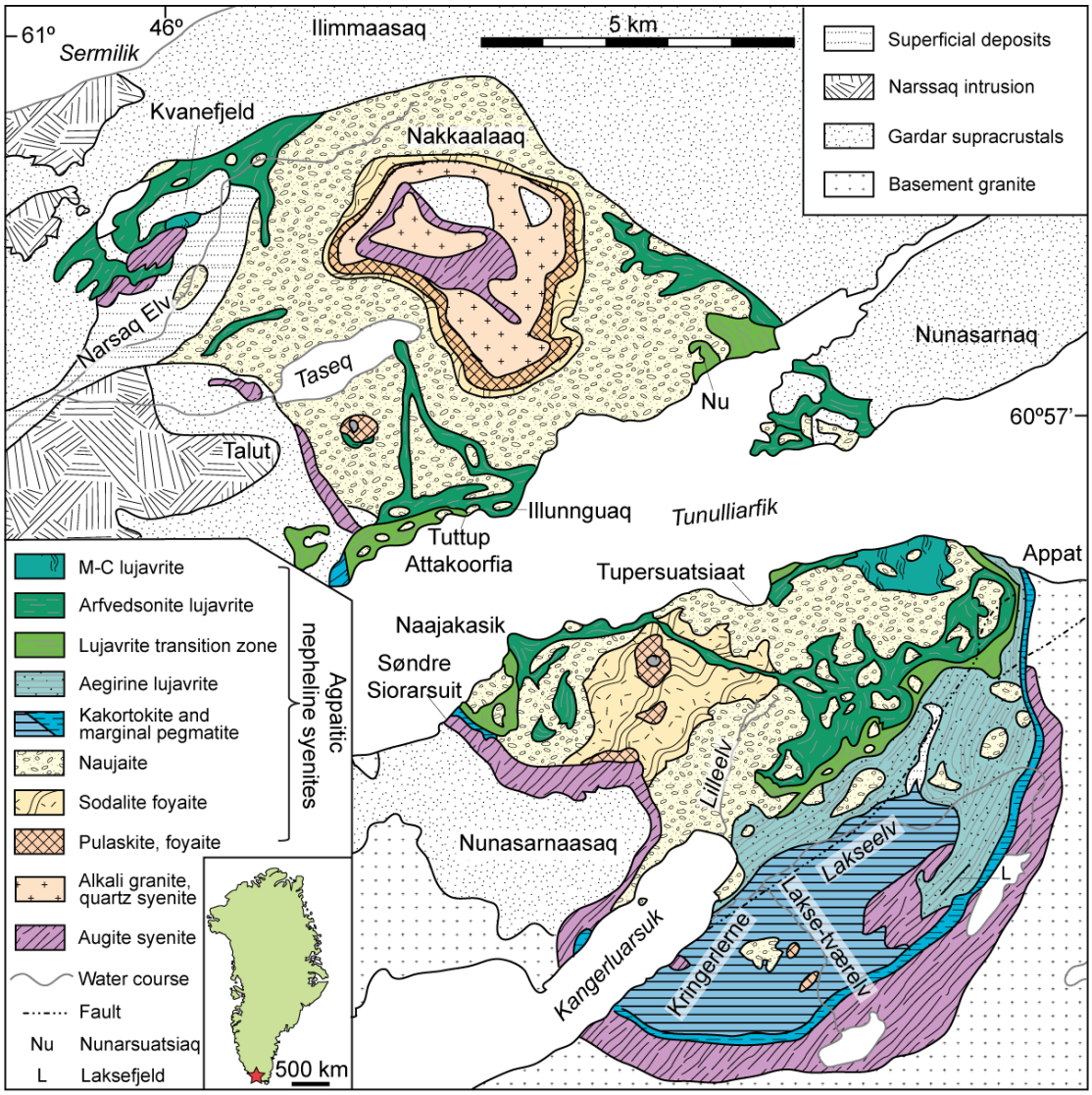

Figure 2.9: Geological sketch map of the Ilímaussaq Complex, after Sørensen (2001).

Much of the language used to describe the complex is derived from early studies (e.g. K.L. Giesecke in 1806 & 1809 and N.V. Ussing in 1900 & 1908 (Sørensen, 2001)), thus many of the names used in this thesis are unique to the complex but are used to retain consistency with the scientific literature. Geographical features are however referred to with the recommended Greenlandic orthography (Geodatastyrelsen, 2013). Where places and features are too small to have been nationally recognised by the naming committees, this work adopts the names used in Sørensen (2001), illustrated in Figure 2.8.

The parental melt is inferred to be sourced from a deep-seated fractionating alkali basalt magma chamber (Larsen & Sørensen, 1987, Markl *et al.*, 2001). Three phases of magmatism (Fig. 2.10) formed the complex (Ferguson, 1964). The first emplaced a slightly silica undersaturated augite syenite into the country rocks, this is preserved at the margins of the complex (Figs. 2.9 & 2.10). The second phase was a relatively small intrusion of peralkaline granite, which may have some genetic relationship with the first phase (Ferguson, 1964) and crops out in the northern part of the complex around Nakkaataaq (Fig. 2.9). The third phase is associated with the agpaitic nepheline syenites that form the main body of the complex (Figs. 2.9 & 2.10). These are subdivided into the roof zone, which consists of sodalite foyaite and pulaskite; naujaite, which developed at the roof of the intrusion; kakortokite, which formed at the base of the intrusion; and lujavrite, which developed in the 'sandwich zone' in the middle of the intrusion (Ferguson, 1964).

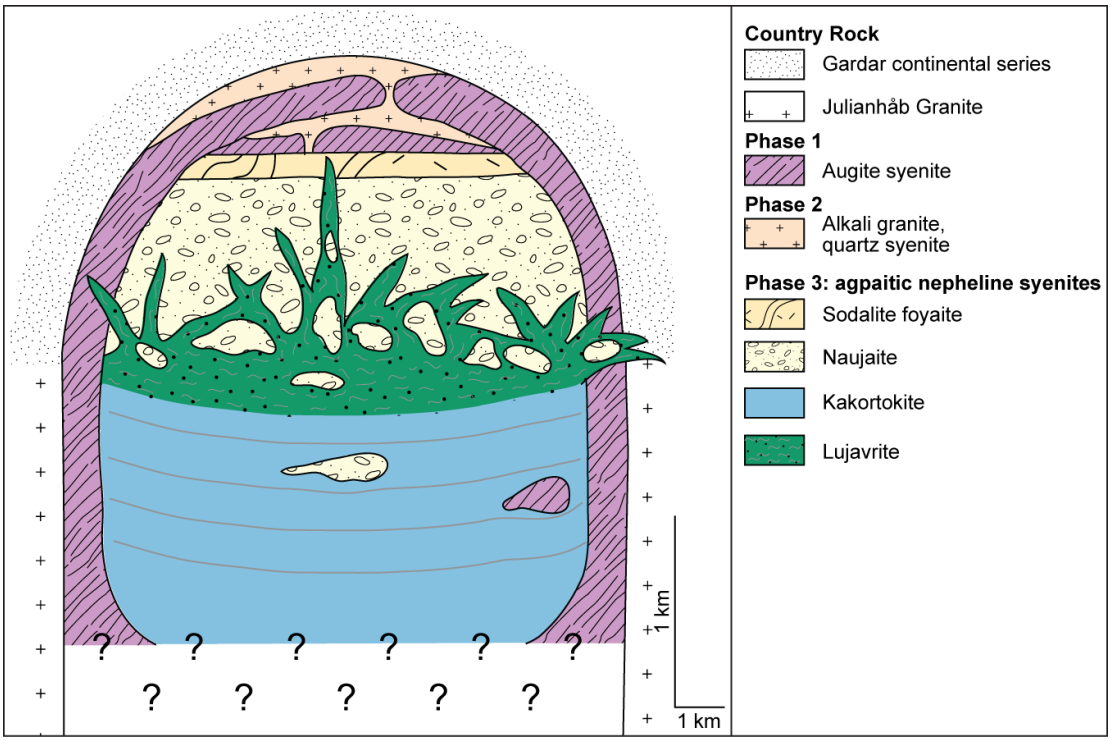

Figure 2.10: Cartoon style cross-section through the Ilímaussaq Complex illustrating the 3 phases of magmatism. Note extreme vertical exaggeration. After Ferguson (1964).

2.7.1 Augite Syenite

The augite syenite was the first intrusive phase (Ferguson, 1964, Marks & Markl, 2001, Ussing, 1912) and is inferred to have formed from an initially homogeneous magma (Marks & Markl, 2001). Heterogeneities developed through closed system fractionation in combination with localised country rock assimilation (Marks & Markl, 2001). Ferguson (1964) observed banding in the augite syenite on the north and south shores of Kangerluarsuk fjord, and adjacent to the kakortokite. This banding is defined by 1-3 cm thick layers of magnetite, augite and olivine that strike parallel to the margin of the intrusion, but are discontinuous (Ferguson, 1964).

2.7.2 Roof Zone

The roof zone rocks are comprised of pulaskite, foyaite and sodalite foyaite. Pulaskite is a nepheline-bearing alkali feldspar syenite with variable amounts of sodic pyroxenes, sodic amphiboles, fayalite and biotite (Le Maitre, 2002). Foyaites were originally defined by Streickeisen (1967) as a feldspathoidal syenite with a feldspar ratio [plagioclase / (alkali feldspar + plagioclase)] of <10% therefore it overlaps with the compositional range of nepheline syenites. The current definition by Le Maitre (2002) includes nepheline syenite with a foliation fabric (foyaitic texture) carried by platy alkali feldspar crystals. Although the foyaites at Ilímaussaq would have been originally classified under Streckeisen (1967), both definitions apply to the rocks. A sodalite foyaite is classified as above, with the addition of sodalite as a modal mineral (Le Maitre, 2002).

The roof rocks crop out to the west of Tupersuatsiaat in the southern part of the Ilímaussaq complex and around Nakkaataaq in the northern part of the complex (Fig. 2.9). The generally accepted formation method is through *in situ* crystallisation onto the roof of the chamber associated with heat loss through the roof (Sørensen, 1969). The rocks are massive with localised ‘inch-scale’ layering (Sørensen, 1969) and are suggested by Larsen & Sørensen (1987) to have formed from a well-mixed magma chamber that was slowly evolving and cooling. There is a continuous evolution from pulaskite to foyaite and sodalite foyaite (Sørensen *et al.*, 2006) with a progressive enrichment in alkalis downwards (Sørensen, 1969).

The pulaskite is a sheet that varies in thickness between 20 to 50 m (Ussing, 1912) with an average thickness of 20 m in the southern part of the complex (Andersen *et al.*, 1981). It crystallised from a slightly silica undersaturated, weakly peralkaline magma, with a water-free, high temperature liquidus mineral assemblage of alkali feldspar, fayalite, hedenbergite, titanomagnetite and apatite (Larsen &

Sørensen, 1987). The foyaite has the same mineral assemblage as the pulaskite, but differs in texture, as it is laminated and heterogeneous with irregular patches of coarse-grained foyaite and pegmatites (Larsen, 1976). The thickness of the foyaite unit was estimated at 60 m by Andersen *et al.* (1981). The foyaite has a gradational contact to the underlying sodalite foyaite (Ussing, 1912), which is the coarsest-grained roof zone rock (Sørensen, 1969). The liquidus mineral assemblage is similar to that of the pulaskite and foyaite, with additional nepheline and sodalite (Larsen & Sørensen, 1987). The unit is suggested to mark the first occurrence of sodalite as a flotation cumulate (Sørensen, 1970) and is the first agpaitic rock to crystallise (Sørensen *et al.*, 2006). The sodalite foyaite has an average thickness of 80 m (Andersen *et al.*, 1981), with a gradational contact to the underlying naujaite over some metres (Ussing, 1912).

2.7.3 Naujaite

The naujaite is the lowermost part of the roof series and is a coarse-grained, weakly layered, agpaitic sodalite syenite (Ussing, 1912). The sodalite is interpreted to have accumulated through flotation, and thus the naujaite is inferred to have crystallised as a flotation cumulate (Ferguson, 1970, Sørensen, 1969, Ussing, 1912). The average thickness of the naujaite is estimated at 600 m (Andersen *et al.*, 1981) and it has sharp contacts to the underlying lujavrite of the 'sandwich zone' within a veined and brecciated zone (Ussing, 1912).

2.7.4 Kakortokite

The kakortokite is the lowest exposed rock and comprises the floor series. Ussing (1912) named the kakortokite after the 10th Century Norse settlement at Qaqortukulooq (presently referred to as Hvalsey) to the south of the complex. It is an IUGS-recognised local term (Le Maitre, 2002) for an agpaitic nepheline syenite with a pronounced cumulus texture and modal igneous layering distinguished by enrichment in arfvedsonite (sodic amphibole – black kakortokite), eudialyte (sodic zirconosilicate – red kakortokite) or alkali feldspar (white kakortokite). Ferguson (1970) applied the term to include the rocks with poorly developed layering that overlie and are in continuation with the main layered series. The exposed kakortokite is ~285 m thick, with the layered series comprising the lowermost 210 m, overlain by 35 m of slightly layered kakortokite and then 40 m of transitional layered kakortokite (Andersen *et al.*, 1981), which has a gradational boundary to the overlying lujavrite.

The layered kakortokite is divided into 29 units, which were distinguished through the recognition of an extremely well developed black-red-white unit, which was numbered '0' by Bohse *et al.* (1971). The underlying and overlying layers were numbered sequentially from -11 to +17 (Bohse *et al.*, 1971). The idealised unit structure is a lower black layer overlain by a red layer and topped by a white layer, although in some units the red layer is poorly developed or missing (Larsen & Sørensen, 1987, Pfaff *et al.*, 2008). The units have a relatively uniform thickness laterally and on average are 7-8 m thick (Larsen & Sørensen, 1987, Pfaff *et al.*, 2008). The black layers have an average thickness of ~1.5 m with a gradational boundary to the overlying red or, when missing, the white layer (Ferguson, 1964). The red layers exhibit thicknesses of <1.5 m, where present, and again have a gradational boundary to the overlying white layers (Ferguson, 1964). The white layers have the greatest thicknesses, up to 12 m (Ferguson, 1964), and typically have a gradational boundary over 5-10 cm to the overlying black layer of the next unit (Ferguson, 1964). Some units however have sharp boundaries (Larsen & Sørensen, 1987). Each unit can be clearly mapped over the entire exposure of the intrusion and the units dip at approximately 10º towards the centre of the intrusion, with this dip increasing sharply at the margin of the complex (Larsen & Sørensen, 1987), where signs of current activity, including trough banding and current bedding, have been observed (Larsen & Sørensen, 1987). These features decrease upwards but reappear in Unit +4, surrounding roof rock autoliths included in Unit +3 (Larsen & Sørensen, 1987). These autoliths are composed of naujaite, augite syenite and foyaite and are conformably enclosed within the layering. They indicate that at least the lower part of the layered kakortokite series was forming coevally with the naujaite (Ferguson, 1970, Sørensen, 1969). Compression of the layered kakortokite below the autoliths was used to infer that the unconsolidated thickness of the kakortokite crystal mush was 15-20 m (Ferguson, 1970).

The kakortokite is modally layered and the most commonly cited process for development of the layering is gravitational settling resulting in density sorting of the minerals (Ferguson, 1964, Larsen & Sørensen, 1987, Sørensen, 1969). More recent work by Pfaff *et al.* (2008) however disputed the effectiveness of gravitational settling. This debate over the significance of gravitational settling during the formation of the kakortokite highlights the complexity of these rocks. Especially as the processes that led to the repetition of the black-red-white units is still controversial within the academic literature. The main hypotheses are as follows:

- Periodic changes in water vapour pressure were suggested by Ferguson (1970). He proposed that periodic decreases in water vapour pressure would both

initiate crystallisation and displace the eutectic of the system, resulting in the early formation of arfvedsonite and aegirine. A subsequent increase in the concentration of volatile elements after the initial water vapour pressure release would increase the density of the magma, enhancing the effectiveness of gravitational settling to generate the modal layering.

- Cyclical variations in the oxygen fugacity have also been invoked as a cause of the repetitive nature of the layering (Ussing, 1912), through the processes described above.
- Intermittent crystallisation was favoured by Sørensen (1969) through crystallisation controlled by thermal or pressure gradients. Increasing temperatures at the magma chamber floor would move the crystallisation front upwards through the magma body. If this crystallisation front reached intervals of high temperatures, crystallisation would cease. Further temperature changes would result in the repetition of the modal layering. Seismic activity could have increased the effectiveness of this process through triggering nucleation of crystals from supersaturated horizons of the magma body.
- Larsen & Sørensen (1987) proposed that the repetitive units formed from a layered magma chamber. Heat loss through the roof rocks initiated a temperature gradient through the magma chamber, which resulted in the development of concentration gradients and compositional stratification of the magma chamber. They further hypothesise that this stratification would have led to the development of double diffusive convection cells within the stratified layers, thus the composition of each layer would remain relatively constant. The lowermost layer would lose heat to the floor cumulates, thus reach the liquidus temperature and start to crystallise. Larsen & Sørensen (1987) suggest arfvedsonite and aegirine could have formed and settled first, but the modal layering developed through density sorting. The abrupt transference to the next layer in the magma chamber would have been accompanied by an increase in volatile elements, resulting in the repetition of the layering. It is important to note that Larsen & Sørensen (1987) do not specify the number of convection cells required, instead they suggest that a range from 1 to 29 convection cells could have formed the observed 29 units.
- As mentioned above Pfaff *et al.* (2008) proposed a theory that argues against density sorting during gravitational settling. They suggest that to generate units with an average thickness of 8 m, a magma body of at least 600 m depth is required for effective density sorting. This would be possible for the lower

kakortokite units, with the suggested 700-800 m depth of the magma chamber, however it would not be possible for the upper kakortokite units. Instead they invoke a volatile pressure release method, as described above, in combination with multiple magmatic replenishment events to generate the 29 units.

2.7.5 Marginal Pegmatite

The marginal pegmatite is 50-100 m wide (Ferguson, 1970) and separates the kakortokite and lujavrite sequences from the augite syenite to the southwest and south of the complex (Fig. 2.9). It also occurs between the lujavrite and the country rocks to the southeast of the complex (Fig. 2.9) (Bohse & Andersen, 1981, Sørensen, 2006) and is locally present at the contact between the naujaite and the country rocks near the roof of the complex in the north (Fig. 2.9) (Sørensen, 2006). The thickness of the unit varies from 100 m (southern shore of Kangerluarsuk) to 25 m (Bohse & Andersen, 1981) and it is inferred to be the first agpaitic rock that crystallised within the lower portions of the complex (Sørensen, 2006, Sørensen *et al.*, 2006). It is interpreted as the contact facies of the kakortokite and locally the naujaite and is composed of complexly intermingled coarse-grained agpaitic nepheline syenites with pegmatitic veins (Sørensen, 2006). These pegmatites are interpreted as developing from spatially constrained volatile-rich melts, while large scale, cross-cutting veins are inferred to have been ‘dykes’ emplaced into joints developed during cooling from volatile-rich melts sourced from the developing kakortokite and lujavrite (Sørensen, 2006).

2.7.6 Lujavrite

The lujavrite is an agpaitic nepheline syenite that is inferred to have crystallised *in* situ in the “sandwich zone” between the underlying kakortokite and overlying naujaite (Larsen & Sørensen, 1987). The lujavrites are mineralogically similar to kakortokite, but are broadly split into two types: a lower aegirine lujavrite, ~225 m thick (Andersen *et al.*, 1981) and an upper arfvedsonite lujavrite, ~150 m thick (Andersen *et al.*, 1981, Ferguson, 1964, Ussing, 1912). The aegirine lujavrite is further subdivided on grain size and lamination into aegirine lujavrite I, ~80 m thick (Andersen *et al.*, 1981) and aegirine lujavrite II, ~145 m thick (Andersen *et al.*, 1981), which is finer grained with a reduced lamination (Bohse & Andersen, 1981).

2.8 Conclusions

The southern portion of Greenland developed during the Palaeoproterozoic accretion and Mesoproterozoic breakup of the supercontinent Nuna. The Ketilidan rocks that host the Ilímaussaq complex formed during the accretion, while extension during the supercontinent break-up led to the development of the Gardar Igneous Province and Ilímaussaq Complex.

The Ilímaussaq Complex was formed through three phases of magmatic activity. The first emplaced the outer augite syenite; the second the peralkaline granite; and the third phase emplaced the agpaitic nepheline syenites. The pulaskite crystallised first, followed by foyaite, sodalite foyaite, naujaite, marginal pegmatite, kakortokite and lastly the lujavrite. Many hypotheses have been developed to account for the layering displayed by the kakortokite, however there is little agreement as which process or series of processes led to the repetitive nature of the layering and the relative importance of gravitational settling vs. *in situ* crystallisation.

2.9 References

Andersen, S., Bohse, H. & Steenfelt, A. (1981). A geological section through the southern part of the Ilímaussaq intrusion. *Rapport Grønlands Geologiske Undersølgelse* **103**, 39-42.

Arzamastsev, A. A., Glaznev, V. N., Raevsky, A. B. & Arzamastseva, L. V. (2000). Morphology and internal structure of the Kola Alkaline intrusions, NE Fennoscandian Shield: 3D density modelling and geological implications. *Journal of Asian Earth Sciences* **18**, 213-228.

Berger, J., Ennih, N., Mercier, J.-C. C., Liégeois, J.-P. & Demaiffe, D. (2009). The role of fractional crystallization and late-stage peralkaline melt segregation in the mineralogical evolution of Cenozoic nephelinites/phonolites from Saghro (SE Morocco). *Mineralogical Magazine* **73**, 59-82.

Bohse, H. & Andersen, S. (1981). Review of the stratigraphic divisions of the kakortokite and lujavrite in southern Ilímaussaq. *Rapport Grønlands Geologiske Undersølgelse* **103**, 53-62.

Bohse, H., Brooks, C. K. & Kunzendorf, H. (1971). Field observations on the kakortokites of the Ilimaussaq intrusion, South Greenland, including mapping and analyses by portable X-ray fluorescence equipment for zirconium and niobium. *Rapport Grønlands Geologiske Undersølgelse* **38**, 43 pp.

Bouabdellah, M., Hoernle, K., Kchit, A., Duggen, S., Hauff, F., Klügel, A., Lowry, D. & Beaudoin, G. (2010). Petrogenesis of the Eocence Tamazert continental carbonatites (Central High Atlas Morocco): Implications for a common source for the Tamazert and Canary and Cape Verde Island carbonatites. *Journal of Petrology* **51**, 1655-1686.

Bowring, S. A., Van Schmus, W. R. & Hoffman, P. F. (1984). U–Pb zircon ages from Athapuscow aulacogen, East Arm of Great Slave Lake, N.W.T., Canada. *Canadian Journal of Earth Sciences* **21**, 1315-1324.

Bussen, I. V. & Sakharov, A. S. (1967). *Geology of Lovozero Tundra*. Leningrad: Nauka.

Cawthorn, R. G. (2005). Pressure fluctuations and the formation of the PGE-rich Merenksy and chromitite reefs, Bushveld Complex. *Mineralium Deposita* **40**, 231-235.

Cawthorn, R. G. (2015). The geometry and emplacement of the Pilanesberg Complex, South Africa. *Geological Magzaine* ***FirstView*** **Article**, 11.

Chadwick, B. & Garde, A. A. (1996). Palaeoproterozoic oblique plate convergence in South Greenland: a reappraisal of the Ketilidian Orogen. *Geological Society London, Special Publications* **112**, 179-196.

Clemmensen, L. B. (1988). Aeolian morphology preserved by lava cover, the Precambrian Mussartût Member, Eriksfjord Formation, South Greenland. *Bulletin of the Geological Society of Denmark* **37**, 105-116.

Conrad, M. E. & Naslund, H. R. (1989). Modally-graded rhythmic layering in the Skaergaard Intrusion. *Journal of Petrology* **30**, 251-269.

Eales, H. V. (2000). Implications of the chromium budget of the Western Limb of the Bushveld Complex. *South African Journal of Geology* **103**, 141-150.

Edgar, A. D. (1974). On the use of the term 'Agpaitic'. *Mineralogical Magazine* **39**, 729-730.

Féménias, O., Coussaert, N., Brassinnes, S. & Demaiffe, D. (2005). Emplacement processes and cooling history of layered cyclic unit II-7 from the Lovozero alkaline massif (Kola Peninsula, Russia). *Lithos* **83**, 371-393.

Ferguson, J. (1964). Geology of the Ilímaussaq alkaline intrusion, South Greenland. Part I. Description of map and structure. *Meddelelser om Grønland* **172**, 1-81.

Ferguson, J. (1970). The significance of the kakortokite in the evolution of the Ilímaussaq intrusion, South Greenland. *Meddelelser om Grønland* **190**, 1-193.

Garde, A. A., Hamilton, M. A., Chadwick, B., Grocott, J. & McCaffrey, K. J. W. (2002). The Ketilidian orogen of South Greenland: geochronology, tectonics, magmatism and fore-arc accretion during Palaeoproterozoic oblique convergence. *Canadian Journal of Earth Sciences* **39**, 756-793.

Geodatastyrelsen. (2013). Den grønlandske Lods, Forklaringer til stednavne.

Halama, R., Wenzel, T., Upton, B. G. J., Siebel, W. & Markl, G. (2003). A geochemical and Sr-Nd-O isotopic study of the Proterozoic Eriksfjord Basalts, Gardar Province, South Greenland: Reconstruction of an OIB signature in crustally contaminated rift-related basalts. *Mineralogical Magazine* **67**, 831-853.

Hoffman, P. F. (1997). Tectonic genealogy of North America. In: van der Pluijim, B. A. & Marshak, S. (eds.) *An Introduction to Structural Geology and Tectonics*. New York: McGraw-Hill, 459-464.

Huppert, H. E. & Sparks, R. S. J. (1980). The fluid dynamics of a basaltic magma chamber replenished by influx of hot, dense ultrabasic magma. *Contributions to Mineralogy and Petrology* **75**, 279-289.

Huppert, H. E. & Sparks, R. S. J. (1984). Double-diffusive convection due to crystallization in magmas. *Annual Review of Earth and Planetary Sciences* **12**, 11-37.

Huppert, H. E. & Turner, J. S. (1981). Double-diffusive convection. *Journal of Fluid Mechanics* **106**, 299-329.

Irvine, T. N. (1975). Crystallisation sequences in the Muskox intrusion and other layered intrusions - II. Origin of chromitite layers and similar deposits of other magmatic ores. *Geochimica et Cosmochimica Acta* **39**.

Irvine, T. N. (1977). Origin of chromitite layers in the Muskox intrusion and other stratiform intrusions: A new interpretation. *Geology* **5**, 273-277.

Irvine, T. N. (1982). Terminology for Layered Intrusions. *Journal of Petrology* **23**, 127-162.

Irvine, T. N. (1987). Processes involved in the formation and development of layered igneous rocks. In: Parsons, I. (ed.) *Origins of Igneous Layering*. Dordrecht: D. Reidel Publishing, 649-656.

Ivanov, N. V. (1960). Distribution of minerals in the rocks of the foyaite-urtite-lujavrite complex of the Lovozero pluton. Problems of geology and mineralogy of the Kola Peninsula. *Vopr. Geol. Mineral. Kol'sk. Polous* **3**.

Kchit, A. (1990). Le Plutonisme alcalin du Tamazeght (Haut Atlas de Midelt, Maroc). Toulouse: Paul Sabatier University.

Kogarko, L. N. (1987). Alkaline rocks of the eastern part of the Baltic Shield (Kola Peninsula). In: Fitton, J. G. & Upton, B. G. J. (eds.) *Alkaline Igneous Rocks*. London: Geological Society, London, Special Publications, 531-611.

Kogarko, L. N. & Khapaev, V. V. (1987). The modelling of formation of apatite deposits of the Khibina massif (Kola Penisula). *NATO ASI series. Series C, Mathematical and physical sciences* **196**, 589-611.

Kogarko, L. N., Lahaye, Y. & Brey, G. P. (2010). Plume-related mantle source of super-large rare metal deposits from the Lovozero and Khibina massifs on the Kola Peninsual, Eastern part of Baltic Shield: Sr, Nd and Hf isotope systematics. *Mineralogy and Petrology* **98**, 197-208.

Kogarko, L. N. & Volkov, V. P. (1963). Physicochemical evolution of the alkaline magma of the differentiated complex of the Lovozero massif in connection to its rhythmic layering. In: Vinogradov, A. P. (ed.) *Chemistry of the Earth's Crust*. Moscow: Khimiya Zemnoy Kory, 140-152.

Kramm, U., Kogarko, L. N., Kononova, V. A. & Vartiainen, H. (1993). The Kola Alkaline Province of the CIS and Finalnd: Precise Rb-Sr ages define 380-360 Ma age range for all magmatism. *Lithos* **30**, 33-44.

Larsen, L. M. (1976). Clinopyroxenes and Coexisting Mafic Minerals from Alkaline Ilimaussaq Intrusion, South Greenland. *Journal of Petrology* **17**, 258-290.

Larsen, L. M. & Sørensen, H. (1987). The Ilímaussaq intrusion - progressive crystallisation and formation of layering in an agpaitic magma. *Geological Society London, Special Publications* **30**, 473-488.

Latypov, R., O'Driscoll, B. & Lavrenchuk, A. (2013). Towards a model for the in situ origin of PGE reefs in layered intrusions: insights from chromitite seams of the Rum Eastern Layered Intrusion, Scotland. *Contributions to Mineralogy and Petrology* **166**, 309-327.

Le Maitre, R. W. (ed.) (2002). *Igneous Rocks A Classification and Glossary of Terms*. Cambridge: Cambridge University Press

Liferovich, R. P. & Mitchell, R. H. (2006). Apatite-group minerals from nepheline syenite, Pilanesberg alkaline complex, South Africa. *Mineralogical Magzine* **70**, 463-484.

Maier, W. D., Barnes, S.-J. & Groves, D. I. (2013). The Bushveld Complex, South Africa: formation of platinum– palladium, chrome- and vanadium-rich layers via hydrodynamic sorting of a mobilized cumulate slurry in a large, relatively slowly cooling, subsiding magma chamber. *Mineralium Deposita* **48**, 1-56.

Markl, G., Marks, M. A. W., Schwinn, G. & Sommer, H. (2001). Phase Equilibrium Constraints on Intensive Crystallization Parameters of the Ilímaussaq Complex, South Greenland. *Journal of Petrology* **42**, 2231-2258.

Marks, M. & Markl, G. (2001). Fractionation and Assimilation Processes in the Alkaline Augite Syenite Unit of the Ilímaussaq Intrusion, South Greenland, as Deduced from Phase Equilibria. *Journal of Petrology* **42**, 1947-1969.

Marks, M. A. W., Coulson, I. M., Schilling, J., Jacob, D. E., Schmitt, A. K. & Markl, G. (2008a). The effect of titanite and other HFSE-rich mineral (Ti-bearing andradite, zircon, eudialyte) fractionation on the geochemical evolution of silicate melts. *Chemical Geology* **257**, 153-172.

Marks, M. A. W., Hettman, K., Schilling, J., Frost, B. R. & Markl, G. (2011). The Mineralogical Diversity of Alkaline Igneous Rocks: Critical Factors for the Transition from Miaskitic to Agpaitic Phase Assemblages. *Journal of Petrology* **52**, 439-455.

Marks, M. A. W., Neukirchen, F., Vennemann, T. & Markl, G. (2009). Textural, chemical, and isotopic effects of late-magmatic carbonatitic fluids in the carbonatite-

syenite Tamazeght complex, High Atlas Mountains. *Mineralogy and Petrology* **97**, 23-42.

Marks, M. A. W., Schilling, J., Coulson, I. M., Wenzel, T. & Markl, G. (2008b). The Alkaline–Peralkaline Tamazeght Complex, High Atlas Mountains, Morocco: Mineral Chemistry and Petrological Constraints for Derivation from a Compositionally Heterogeneous Mantle Source. *Journal of Petrology* **49**, 1097-1131.

Marsh, B. D. (2013). On some fundamentals of igneous petrology. *Contributions to Mineralogy and Petrology* **166**.

Martin, D. & Nokes, R. (1988). Crystal settling in a vigorously convecting magma chamber. *Nature* **332**, 534-536.

McBirney, A. R. (2006). *Igneous Petrology*. London: Jones and Bartlett Publishers.

McBirney, A. R. & Hunter, R. H. (1995). The cumulate paradigm reconsidered. *The Journal of Geology* **103**, 114-122.

McCreath, J. A., Finch, A. A., Simonsen, S. L., Donaldson, C. H. & Armour-Brown, A. (2012). Independent ages of magmatic and hydrothermal activity in alklaine igneous rocks: The Motzfeldt Centre, Gardar Province, South Greenland. *Contributions to Mineralogy and Petrology* **163**, 967-982.

Mitchell, R. H. & Liferovich, R. P. (2004). Ecandrewsite - zincian pyrophanite from luajvrite, Pilanesberg alkaline complex, South Africa. *The Canadian Mineralogist* **42**, 1169-1178.

Mitchell, R. H. & Liferovich, R. P. (2006). Subsolidus deuteric/hydrothermal alteration of eudialyte in lujavrite from the Pilanesberg alkaline complex, South Africa. *Lithos* **91**, 352-372.

Mondal, S. K. & Mathez, E. A. (2007). Origin of the UG2 chromitite layer, Bushveld Complex. *Journal of Petrology* **48**, 495-510.

Naslund, H. R. & McBirney, A. R. (1996). Mechanisms of Formation of Igneous Layering. In: Cawthorn, R. G. (ed.) *Layered Intrusions: Developments in Petrology*. Amsterdam: Elsevier Science B. V.

Nex, P. A. M. (2004). Formation of bifurcating chromitites layers of the UG1 in the Bushveld Igneous Complex, an analogy with sand volcanoes. *Journal of the Geological Society* **161**, 903-909.

O'Driscoll, B., Butcher, A. R. & Latypov, R. (2014). New insights into precious metal enrichment on the Isle of Rum, Scotland. *Geology Today* **30**.

O'Driscoll, B., Emeleus, C. H., Donaldson, C. H. & Daly, J. S. (2010). Cr-spinel Seam Petrogenesis in the Rum Layered Suite, NW Scotland: Cumulate Assimilation and in situ Crystallization in a Deforming Crystal Mush. *Journal of Petrology* **51**, 1171-1201.

Olivio, G. R. & Williams-Jones, A. E. (1999). Hydrothermal REE-rich eudialyte from the Pilanesberg Complex, South Africa. *The Canadian Mineralogist* **37**, 653-663.

Paslick, C. R., Haliday, A. N., Davies, G. R., Mezger, K. & Upton, B. G. J. (1993). Timing of Proterozoic magmatism in the Gardar Province, southern Greenland. *Geological Society of America Bulletin* **105**, 272-278.

Pedersen, J. C. & LeCouteur, P. C. (1991). The Thor Lake beryllium-rare metal deposits, Northwest Territories. In: Padgham, W. A. & Atkinson, D. (eds.) *Mineral deposits of the Slave Province, Northwest Territories (Field Trip 13)*: Geological Survey of Canada, 128-137.

Pfaff, K., Krumrei, T., Marks, M. A. W., Wenzel, T., Rudolf, T. & Markl, G. (2008). Chemical and physical evolution of the 'lowered layered sequence' from the nepheline syenitic Ilímaussaq intrusion, South Greenland: Implications for the origin of magmatic layering in peralkaline felsic liquids. *Lithos* **106**, 280-296.

Pinckston, D. R. & Smith, D. G. W. (1995). Mineralogy of the Lake zone, Thor Lake rare-metals deposit, N.W.T., Canada. *Canadian Journal of Earth Sciences* **32**.

Piper, J. D. A., Thomas, D. N., Share, S. & Rui, Z. Q. (1999). The palaeomagnetism of (Mesoproterozoic) Eriksfjord Group red beds, South Greenland: Multiphase remagnetization during the Gardar and Grenville episodes. *Geophysical Journal International* **136**, 739-756.

SACS. (1980). *Stratigraphy of South Africa Handbook 8. Part 1: Lithostratigraphy of the Republic of South Africa, South West Africa/Namibia and the Republics of Bophuthatswana, Transkei and Venda*. Pretoria: Government Printer.

Salvi, S., Fontan, F. & Monchoux, P. (2000). Hydrothermal Mobilization of High Field Strength Elements in Alkaline Igneous Systems: Evidence from the Tamazeght Complex (Morocco). *Economic Geology* **95**, 559-576.

Schilling, J., Marks, M. A. W., Wenzel, T. & Markl, G. (2009). Reconstruction of magmatic to subsolidus processes in an agpaitic system using eudialyte textures and compostion: A case study from Tamazeght, Morocco. *Canadian Mineralogist* **47**, 351-365.

Sheard, E. R. (2010). Behaviour of zirconium, niobium, yttrium and the rare earth elements in the Thor Lake rare-metal deposit, Northwest Territories, Canada. *Department of Earth and Planetary Sciences*. Montreal: McGill University, 140.

Sheard, E. R., Williams-Jones, A. E., Heiligmann, M., Pederson, C. & Trueman, D. L. (2012). Controls on the Concentration of Zirconium, Niobium, and the Rare Earth Elements in the Thor Lake Rare Metal Deposit, Northwest Territories, Canada. *Economic Geology* **107**, 81-104.

Sørensen, H. (1969). Rythmic igneous layering in peralkaline intrusions: An essay review on Ilímaussaq (Greenland) and Lovozero (Kola, USSR). *Lithos* **2**, 261-283.

Sørensen, H. (1970). Internal structures and geological setting of the three agpaitic intrusions - Khibina and Lovozero of the Kola Peninsula and Ilímaussaq, South Greenland. *Canadian Mineralogist* **10**, 299-334.

Sørensen, H. (1997). The agpaitic rocks - an overview. *Mineralogical Magazine* **61**, 485-498.

Sørensen, H. (2001). Brief introduction to the geology of the Ilímaussaq alkaline complex, South Greenland, and its exploration history. In: Sørensen, H. (ed.) *The Ilímaussaq alkaline complex, South Greenland: status of mineralogical research with new results*. Copenhagen: Geology of Greenland Survey Bulletin.

Sørensen, H. (2006). The Ilímaussaq Alkaline Complex, South Greenland - an overview of 200 yeards of research and an outlook. *Meddeleser om Grønland* **342**, 1-70.

Sørensen, H., Bohse, H. & Bailey, J. C. (2006). The origin and mode of emplacement of lujavrites in the Ilímaussaq alkaline complex, South Greenland. *Lithos* **91**, 286-300.

Spandler, C., Mavrogenes, J. & Arculus, R. (2005). Origin of chromitites in layered intrusions: Evidence from chromite-hosted melt inclusions from the Stillwater Complex. *Geology* **33**, 893-896.

Sparks, R. S. J., Huppert, H. E., Koyaguchi, T. & Hallworth, M. A. (1993). Origin of modal and rhythmic igneous layering by sedimentation in a convecting magma chamber. *Nature* **361**, 246-249.

Streckeisen, A. L. (1967). Classification and Nomenclature of Igneous Rocks, final report of an inquiry. *Neues Jahrbuch Fur Mineralogie-Abhandlungen* **107**, 144-240.

Tait, S. R. & Jaupart, C. (1996). The production of chemically stratified and adcumulate plutonic rocks. *Mineralogical Magazine* **60**, 99-114.

Upton, B. (2013). Tectono-magmatic evolution of the younger Gardar southern rift, South Greenland. *Geological Survey of Denmark and Greenland Bulletin* **29**, 124.

Upton, B., Emeleus, C. H., Heaman, L. M., Goodenough, K. M. & Finch, A. A. (2003). Magmatism of the mid-Proterozoic Gardar Province, South Greenland: chronology, petrogenesis and geological setting. *Lithos* **68**, 43-65.

Ussing, N. V. (1912). Geology of the country around Julianehaab, Greenland. *Medeleser om Grønland* **38**, 1-426.

Vlasov, K. A., Kuzmenko, M. Z. & Eskova, E. M. (1959). *The Lovozero Alkaline Massif*. Moscow: Izd. Acd. Sci.

Waight, T., Baker, J. & Willigers, B. (2002). Rb isotope dilution analyses by MC-ICPMS using Zr to correct for mass fractionation: towards improved Rb-Sr geochronology? *Chemical Geology* **186**, 99-116.

Zhang, S., Li, Z.-X., Evans, D. A. D., Wu, H., Li, H. & Dong, J. (2012). Pre-Rodinia supercontinent Nuna shaping up: A global synthesis with new paleomagnetic results from North China. *Earth and Planetary Science Letters* **353-354**, 145-155.

Zhao, G., Cawood, P. A., Wilde, S. A. & Sun, M. (2002). Review of global 2.1–1.8 Ga orogens: implications for a pre-Rodinia supercontinent. *Earth Science Reviews* **59**, 125-162.

Chapter 3
Fieldwork and Sample Collection

3.1 Introduction

Fieldwork was carried out over a single expedition between 20th July and 20th August 2012. The field area is situated within the TANBREEZ Mining Greenland A/S licence area, which broadly comprises the southern part of the Ilímaussaq Complex (Fig. 3.1). The field area includes the layered kakortokite; the marginal pegmatite; the 'sandwich zone' lujavrite; the naujaite; and the sodalite foyaite, foyaite and pulaskite of the roof zone. Drill cores from the 2010 and 2011 TANBREEZ drilling seasons were examined and sampled to evaluate the layered kakortokite at depth.

The fieldwork aims were (1) to identify the nature of the layering within the exposed kakortokite and observe the textural and mineralogical changes across unit and layer boundaries. (2) To extend these observations to the drill core sequences. (3) To observe the textural and mineralogical changes across the boundary from transitionally layered kakortokite to lujavrite. (4) To observe the textural and mineralogical changes across the boundary from the marginal pegmatite to the layered kakortokite.

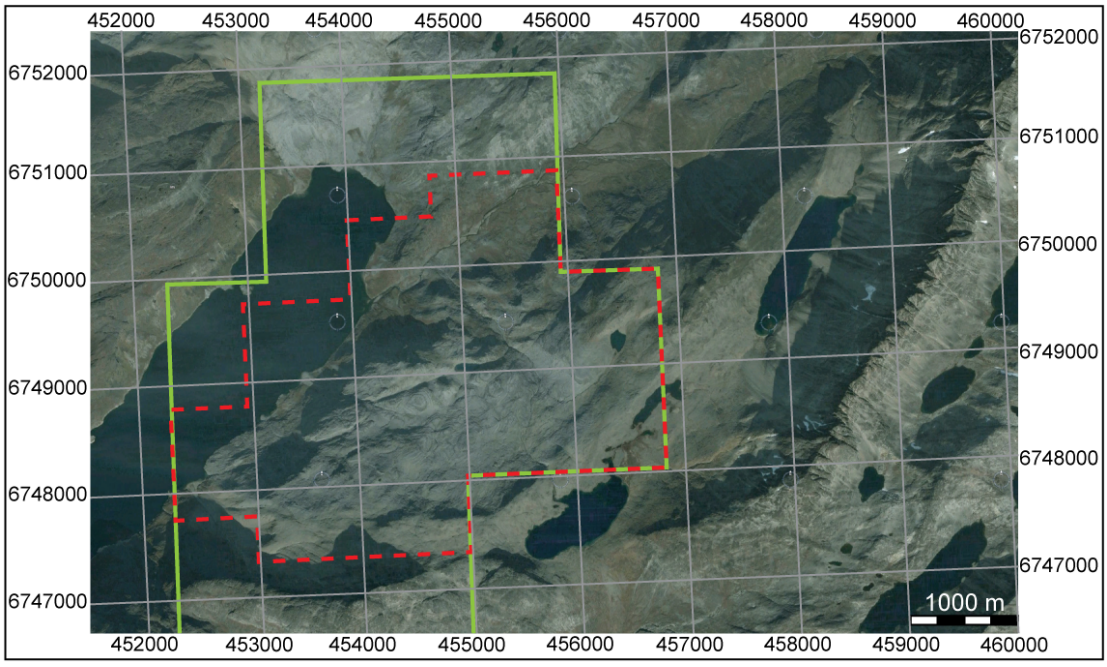

Figure 3.1: TANBREEZ Exploration Licence 2006-04 outlined in green, applied exploitation licence outlined in dashed red. Base map from Google Earth (2011).

3.2 Regional Geography and Geomorphology

The layered kakortokite is exposed in the southern portion of the complex on the south side of Kangerluarsuk Fjord. It is bounded to the north by the fjord and to the north and east by the transition to lujavrite. In the south and west the series is bounded by the marginal pegmatite. The layered series is relatively accessible by boat along Kangerluarsuk Fjord from Narsaq or Qaqortoq, or by foot from Qaqortoq.

The kakortokite outcrops as a vertical cliff face (~60 to 100 m high), sections of which are accessible at the base of the cliffs (Fig. 3.2). Although access is reduced due to large talus slopes, many of which are active and unstable. Sections along the rivers Lakseelv and Lakse-tværelv (Fig 2.9, p.23) provide good accessibility through the layered sequence.

The layered kakortokite forms a plateau, locally called Kringlerne, which is accessible through walking up Lakse-tværelv or by helicopter. Units -11 to -5 crop out at the base of the Kringlerne Cliffs on the south side of Kangerluarsuk Fjord and the western side of the sequence. Units -4 to 0 crop out towards the base of the cliff section within the talus slopes and Lakse-tværelv valley. Units 0 to +13 crop out in the Kringlerne cliff face on the western side of the Layered Series and up Lakse-tværelv in the centre of the Layered Series. Units +9 to +17 are exposed on the plateau. The transitionally layered kakortokite is only exposed on the north side of the Lakseelv valley.

Figure 3.2: Panorama of Kringlerne cliff section, facing southwest.

3.3 Sampling Strategy

Samples were collected for petrographic and chemical analyses from the central portions of layers and boundaries between units. Additional samples of minerals and textures from the kakortokite; a fine-grained, un-layered sequence of rocks within the layered kakortokite, discussed fully in chapter 8 and here referred to as “hybrid/slump” rocks; lujavrite and naujaite were collected. The full list of samples and their localities is in Appendix A and Figure 3.3, which can be correlated with sample numbers referred to within this text. In order to assess lateral variations through the complex, Unit 0, as the marker horizon, was sampled three times across the complex, with samples being collected from the U-1 white kakortokite, U-1/0 boundary and U0 black, red and white varieties. This supplements samples collected by A. Finch in 1999 from Unit 0 consisting of: U-1/0 boundary, U0 black, red and white varieties.

Late-stage veins are present throughout the layered kakortokite, manifesting as either pegmatitic or aegirine-rich veins. Alteration of eudialyte to catapleiite and REE-rich accessory minerals (including nacareniobsite-Ce and britholite) is common throughout the complex. In order to investigate the primary development of the layered kakortokite and assess magma chamber dynamics during their formation, samples were collected from units that did not display extensive alteration or sub-solidus modification. In order to assess the effects of alteration and mobilisation of components with subsequent redistribution and/or import/export, samples of red kakortokite that hosted altered eudialyte crystals were also collected for analysis. As the kakortokite is typically coarse-grained, samples collected for textural and mineral chemical analysis through thin/thick section were fist sized (~0.002 m^3) or larger. Samples of the typically fine/medium grained “hybrid/slump” rocks for whole-rock XRF chemical analysis were up to 2 kg. Samples were always taken from outcrop.

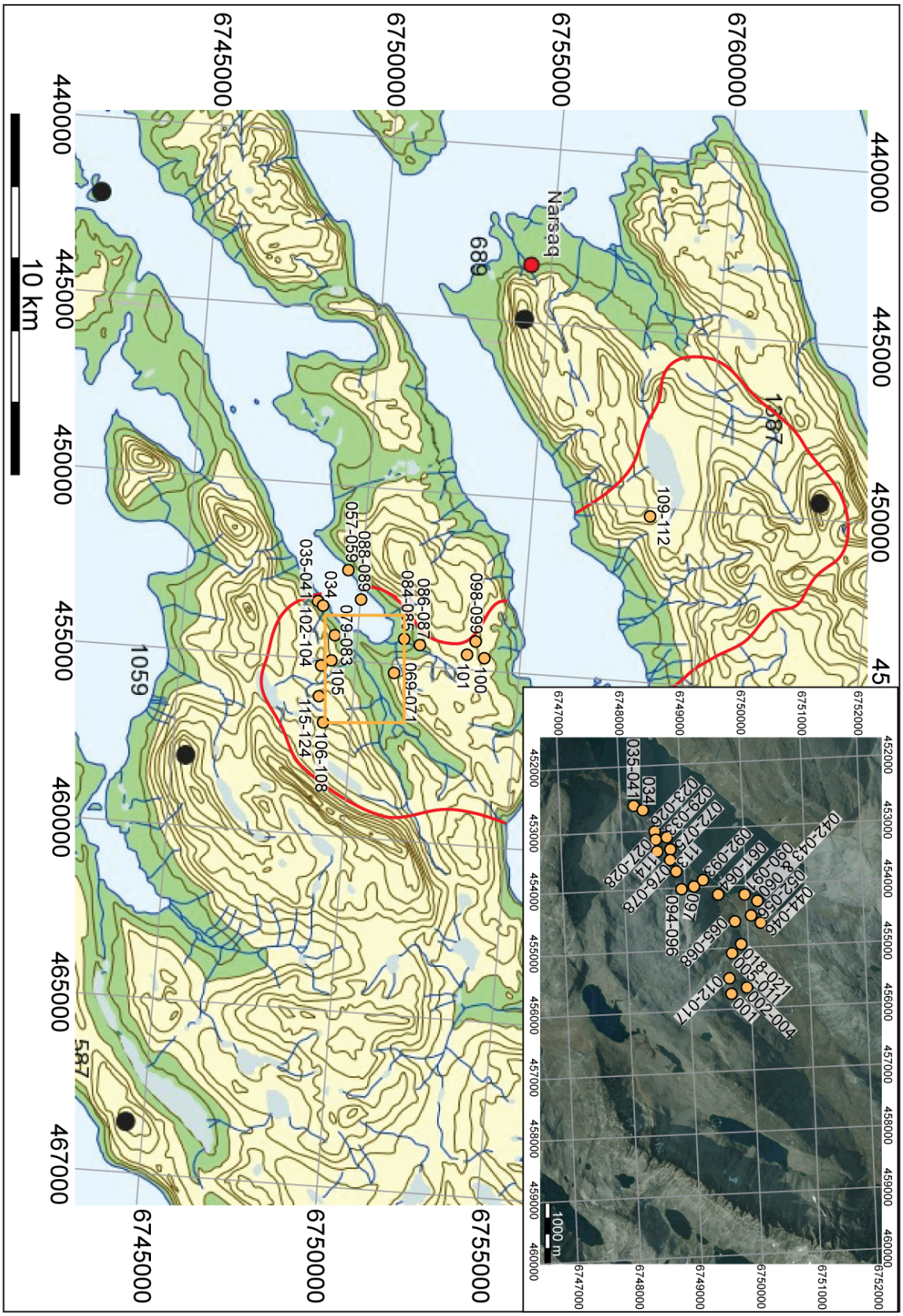

Figure 3.3: Topographic map (Denmarks National Survey) of region indicating sample locations (orange) and enlarged (orange rectangle) on inset map (aerial photo from Google Maps (2011)). Note sample numbers are prefixed by EJH/12/. Boundaries of Ilímaussaq Complex are outlined in red.

3.4 Geological Units

The fieldwork focused on the southern portion of the Ilímaussaq complex, which retains a relatively complete record from the lowermost exposed kakortokite through the lujavrite and naujaite up to the roof zone (Figs. 3.4 & 2.9, p.23).

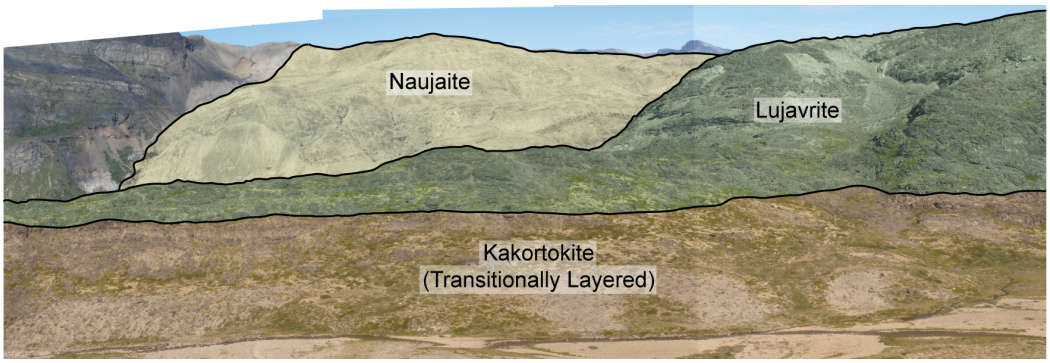

Figure 3.4: View north from layered kakortokite over the transitionally layered kakortokite, north of Lakseelv, to lujavrite and naujaite. Distance across bottom of panorama ~1 km, top of naujaite 490 m ASL.

3.4.1 Roof Zone

The roof zone was studied to the west of Tupersuatsiaat (Fig. 2.9, p.23). Here pulaskite has a distinct boundary to the underlying foyaite (Fig. 3.5). From a distance the pulaskite displays near horizontal layering (Fig 3.5), which becomes less distinct when viewed closely. The foyaite is relatively homogeneous with marked lamination due to numerous platy feldspar crystals.

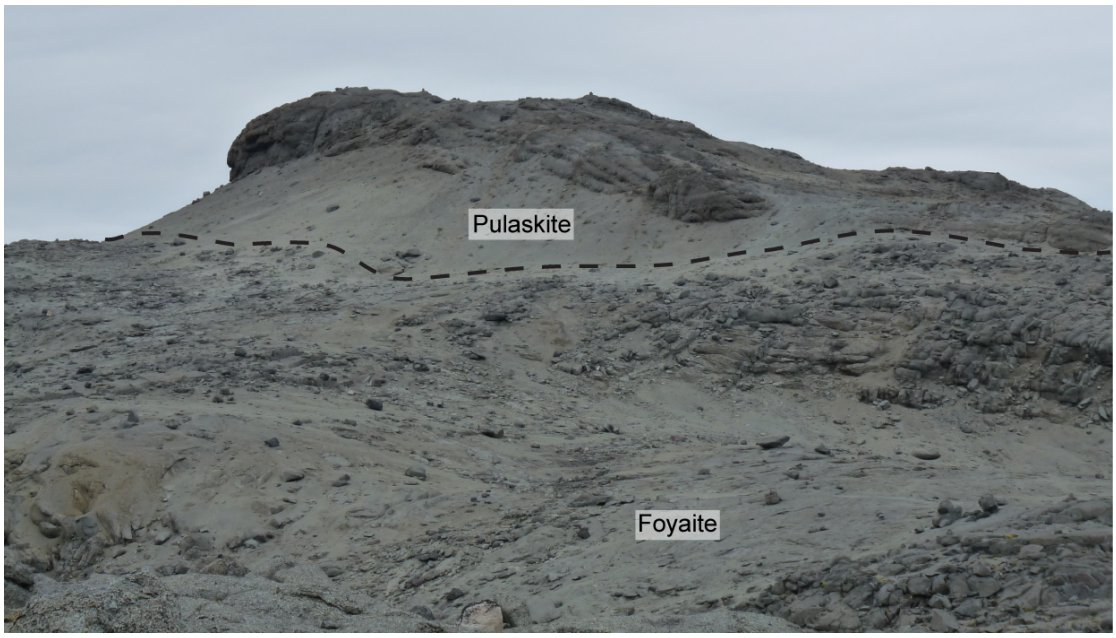

Fig 3.5: Roof zone to west of Tupersuatsiaat, facing northwest. Pulaskite displays ‘inch-scale’ layering above boundary to foyaite. Layered pulaskite outcrop ~2m high.

3.4.2 Naujaite

The naujaite was studied in the Lilleelv valley (Fig. 2.9, p.23), where it overlies and is intruded by lujavrite. It is occasionally weakly layered (Fig. 3.6a), dipping at ~ 13º to the north, however the layering is not laterally continuous at outcrop scale. The texture is poikilitic (Fig 3.6b) with small (0.5 to 1 cm) sodalite crystals ranging in shape from prismatic to polygonal (Fig. 3.6c-d), hosted in larger (6 to 10 cm), oikocrysts of arfvedsonite, eudialyte and alkali feldspar.

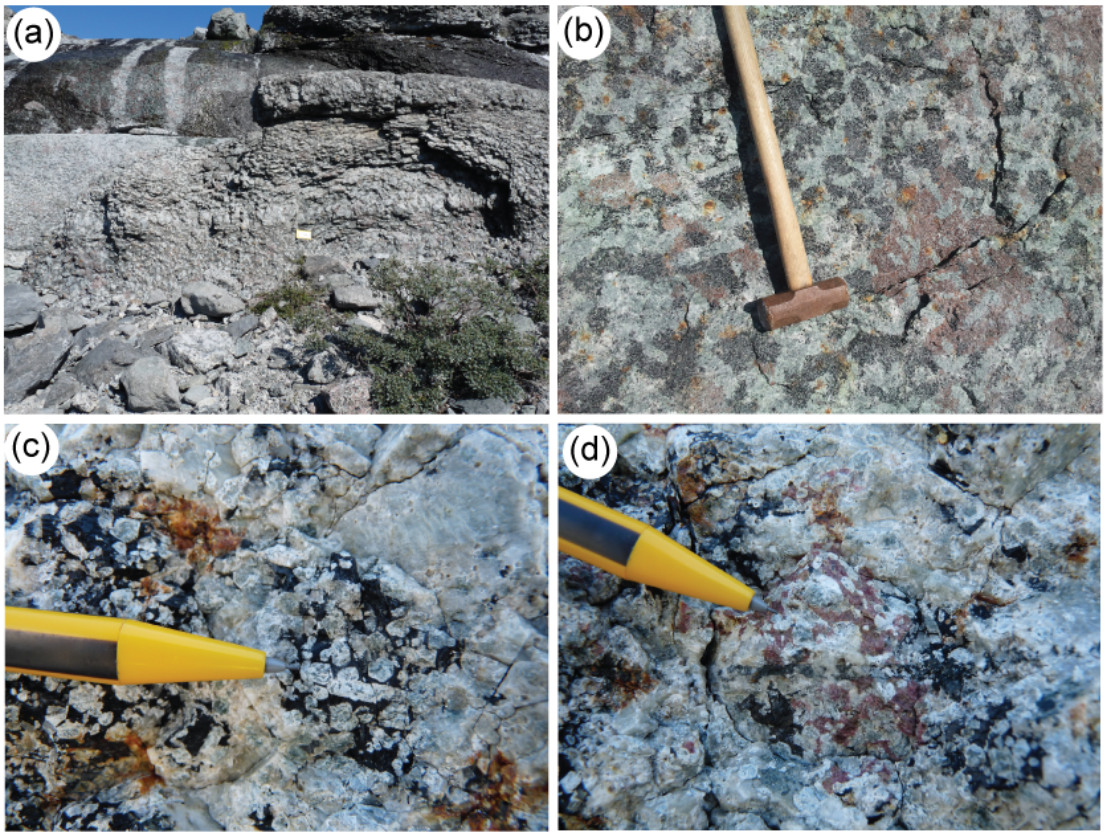

Fig 3.6: Textural and mineralogical features of naujaite. (a) Naujaite in outcrop with poorly developed layering (above notebook, 19 cm in length). (b) Large-scale poikilitic texture in naujaite (hammer head = 15 cm). (c) Oikocrystic arfvedsonite containing hexagonal and prismatic sodalite crystals. (d) Oikocrystic eudialyte containing hexagonal sodalite crystals. Pencil tip = 2 cm.

3.4.3 Layered Kakortokite

The fieldwork studied the layered kakortokite in outcrop in the Kringlerne region (Figs. 2.9 & 3.7a) and additionally from drill core provided by TANBREEZ Mining Greenland A/S (Appendix B). This has allowed the project to extend observations below the exposed kakortokite and recognise an additional eight unexposed units. In accordance with terminology developed by Bohse *et al*. (1971) these units have been named -12 to -19. The lower contact of the kakortokite is against a fine- to medium-grained mesocratic rock that was termed ‘Black Madonna’

during drilling by TANBREEZ (Schonwandt *et al.*, 2014). The contact is gradational and the transition between rock types occurs over 4 to 8 m.

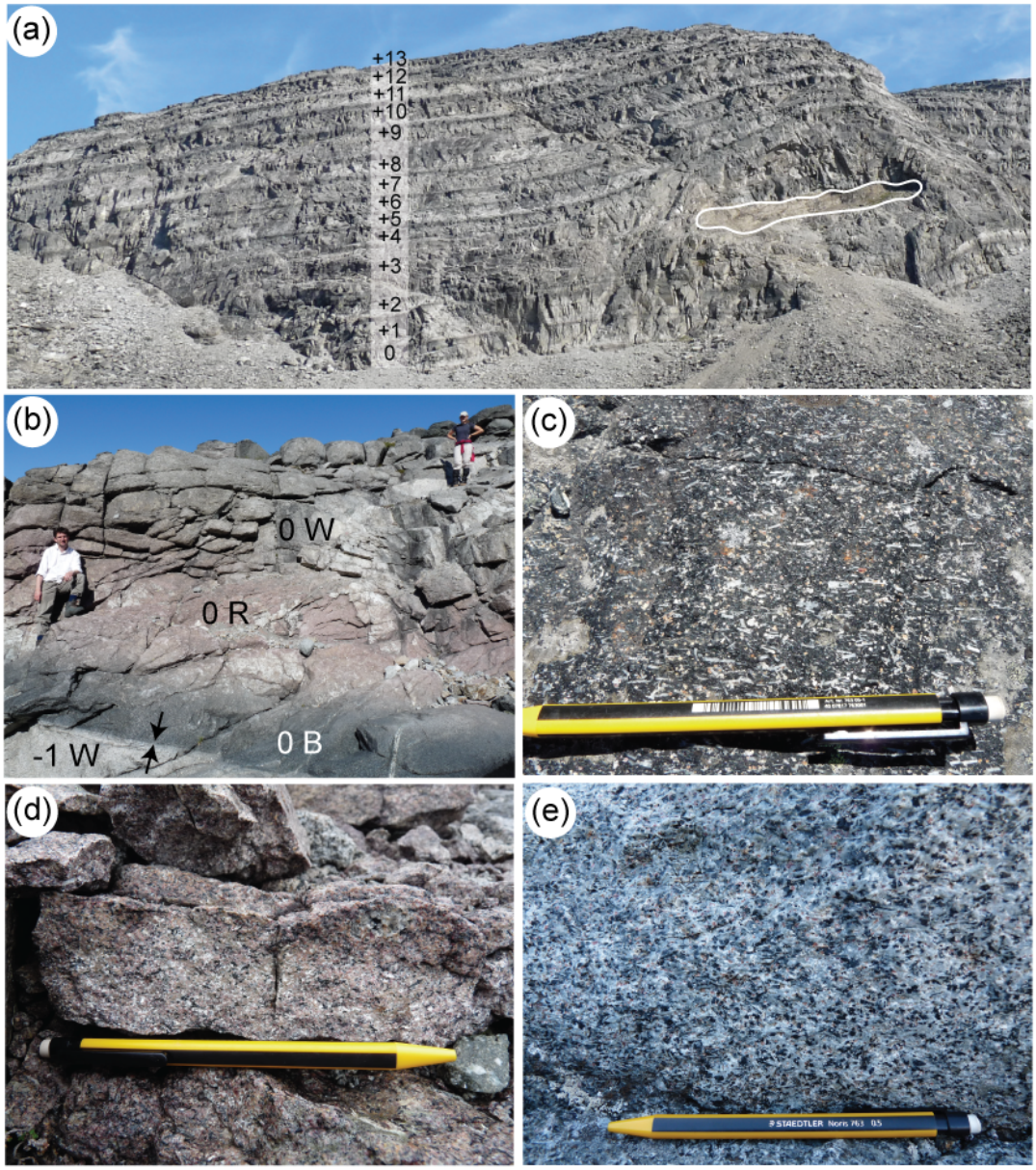

Fig 3.7: (a) Layered kakortokite in the Kringlerne Cliff face, Units 0 to +13 labelled, roof autolith within Unit 3 outlined in white. Height of cliff face ~100 m. (b) Unit -1 white kakortokite to Unit 0 white kakortokite, note sharp boundary from -1 W to 0 B (arrowed) and gradual boundaries between 0 B & 0 R and 0 R & 0 W, A. Finch for scale on left = 1.81 m. (c) Unit 0 black kakortokite. (d) Unit +16 red kakortokite. (e) Unit 0 white kakortokite. B = black kakortokite, R = red kakortokite, W = white kakortokite, pencil = 14 cm long.

Previous workers have suggested that unit boundaries are usually gradational over a few centimetres (Ferguson, 1964, Larsen & Sørensen, 1987); however the present study has found that units typically display sharp boundaries between the lower white kakortokite and overlying black kakortokite (Fig 3.7b). Intra-unit

boundaries between the black, red and white layers are however gradational over 2 to 15 cm (Fig. 3.7b) The mean thickness of the units, measured through drill core, is 7.0 m (range of 2.6 to 17.0 m) and the mean thicknesses of the black, red and white kakortokite layers are 1.1 m (range of 0.2 to 2.6 m), 1.8 m (range of 0.5 to 4.7 m) and 4.1 m (range of 0.9 to 12.6 m) respectively.

The black kakortokite (Fig 3.7c) is typically composed of 50 mod.% arfvedsonite, 15% alkali feldspar, 15% eudialyte and 10% nepheline. It can occasionally have a poor foliation carried by alkali feldspar plates. The red kakortokite is typically saccharoidal (Fig 3.7d) and composed of 40% eudialyte, 20% alkali feldspar, 20% nepheline, 10% arfvedsonite and 10% aegirine. The white kakortokite is commonly foliated, with the fabric defined by alkali feldspar plates (Fig 3.7e) and is typically composed of 40% alkali feldspar, 30% nepheline, 10% eudialyte, 10% aegirine and 10% arfvedsonite. Sodalite can occur in each of the black, red and white kakortokite varieties, and was observed in drill core to form up to 30% of the rock (Appendix B), it was not however typically observed in outcrop.

In addition to the accepted black-red-white unit stratigraphy, Units +10, +5 -4 and -10 contain an additional white layer, thus displaying a black-white-red-white stratigraphy. This subordinate white layer is typically thinner than the upper white layer with a mean thickness of 3.3 m (range 1.5-4.8 m) and is referred to in the present study as ‘Wa’. These ‘Wa’ layers are mineralogically similar to white kakortokite and are typically composed of 30% alkali feldspar, 20% nepheline, 20% aegirine, 15% eudialyte and 15% arfvedsonite.

3.4.4 "Hybrid/Slump" Rocks

This sequence was first noted by Ussing (1912) who referred to these rocks as lujavrite underlying the kakortokite. Ferguson (1970) later described them as hybrid rocks, noting they had a geochemical affinity with the white kakortokite and volumetrically weighted kakortokite average. Bohse *et al.* (1971) mapped this sequence of rocks within the layered kakortokite between Units -6 to -4, and proposed it formed through slumping of unconsolidated kakortokite. The present study has observed the sequence to cut across the layered kakortokite between Units -7 to -2 (Fig 3.8a). The rocks are mesocratic (light to mid grey) and are typically fine- to medium grained (Fig. 3.8). Common textures within the "hybrid/slump" rocks are: net veining (Fig 3.8b) by a leucocratic nepheline syenite; melanocratic schlieren (Fig 3.8c) that are occasionally amphibole-rich; and veins with coarse-grained (up to 1 cm) eudialyte crystals (Fig 3.8d). The genesis of these rocks is explored further in chapter 8.

Fig 3.8: Textural features of "hybrid/slump" rocks. (a) Cross-cutting contact between "hybrid/slump" rocks (above solid line) and Units -7/-6 (boundary = dashed line), A. Finch for scale, 1.81 m. (b) Fine-grained melanocratic "hybrid/slump" rock below Unit -2, containing leucocratic veins (arrowed). (c) "Hybrid/slump" at approx. Unit -2 containing sheared amphibole-rich pods (arrowed). (d) "Hybrid/Slump" at approx. Unit -2 containing coarse-grained eudialyte veins. B = black kakortokite, W = white kakortokite, scale card = 15 cm long, pencil = 14 cm long.

3.4.5 Marginal Pegmatite

The marginal pegmatite is extremely heterogeneous (Fig 3.9a) and is composed of zones of pegmatite in coarse-grained rocks that have a kakortokitic mineralogy. Bohse & Andersen (2006) additionally noted the presence of poikilitic naujaite-type rocks. Although the rocks mineralogically resemble kakortokite, their textures are very different. They contain features of flow banding (Fig 3.9b) and trough banding (Fig 3.9c) reflecting current activity. Irregular layering occurs with alternating concentrations of arfvedsonite, eudialyte and alkali feldspar with nepheline. This layering is typically discontinuous, but increases in thickness and regularity towards the gradational boundary with the layered kakortokite (Fig 3.9d).

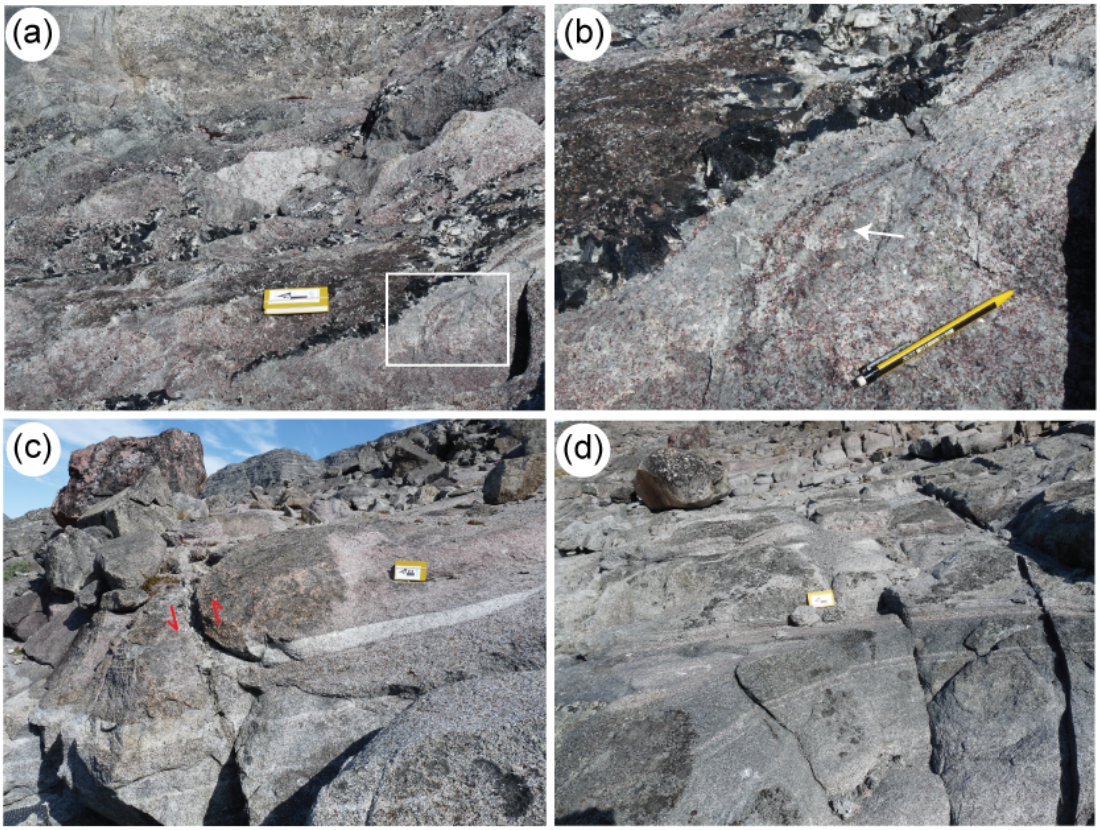

Fig 3.9: (a) N-S trending pegmatite bands within coarse-grained kakortokitic rocks. (b) Enlargement of highlighted square in (a) displaying current banding within coarse-grained kakortokitic rocks (arrowed). (c) Trough banded white kakortokitic rock cut by late stage fault (movement arrowed in red). (d) Thickness of bands within kakortokitic rocks increases with distance away from marginal pegmatite (to east). All photographs facing East, scale card = 15 cm long, pencil = 14 cm long.

3.4.6 Lujavrite

The aegirine lujavrite has a dark green colour associated with a cumulus aegirine matrix. A foliation fabric is present through the rock identified by acicular aegirine and platy alkali feldspar crystals. Above the boundary from the transitionally layered kakortokite, the aegirine lujavrite contains large (up to 2.5 cm) arfvedsonite oikocrysts (Fig 3.10a), which host equant crystals of nepheline, eudialyte and alkali feldspar. Leucocratic veins and xenoliths are present within the aegirine lujavrite (Fig 3.10b) and these are composed of alkali feldspar, nepheline, eudialyte and arfvedsonite. Previous workers have suggested these correspond to recrystallised naujaite autoliths (Bohse & Andersen, 1981).

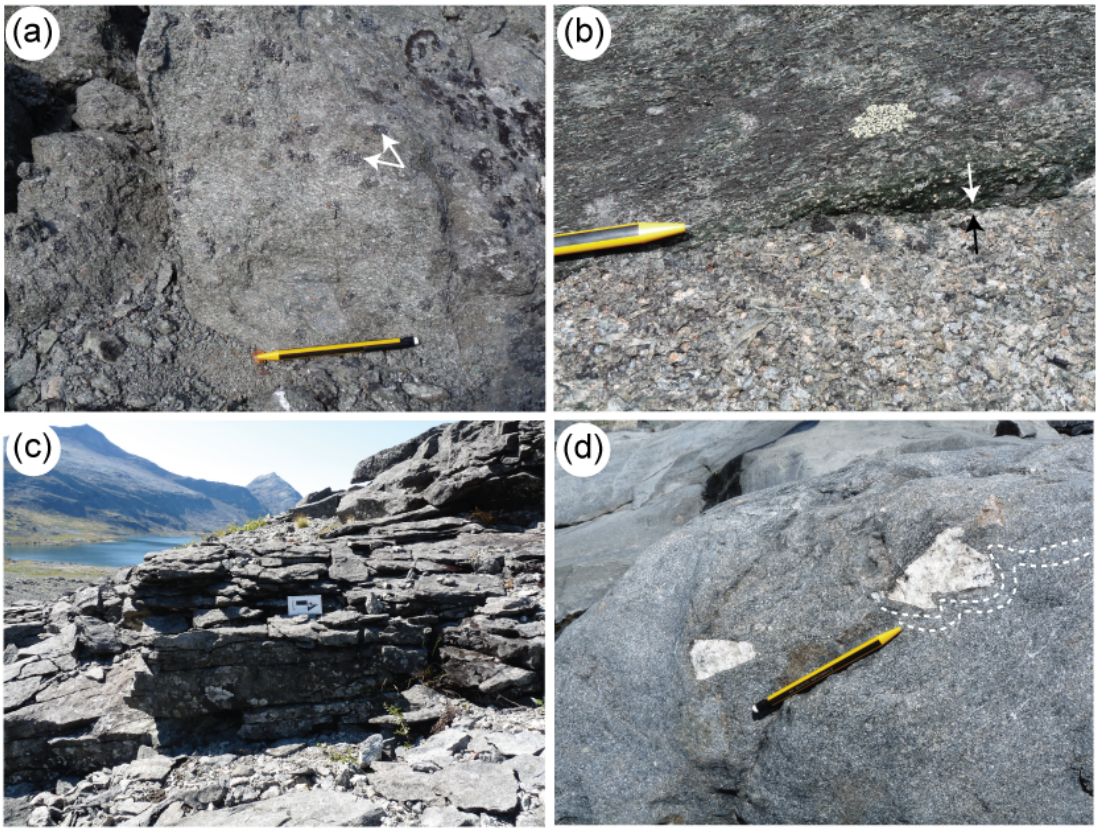

Fig 3.10: (a) Aegirine lujavrite with arfvedsonite oikocrysts (arrowed). (b) Aegirine lujavrite with foliation carried by aegirine needles and alkali feldspar plates, lujavrite cut by leucocratic alkali feldspar- and nepheline-rich rock (contact arrowed). (c) Arfvedsonite lujavrite with notable fissility. (d) Foliated arfvedsonite lujavrite with leucocratic xenoliths, note foliation wraps around xenoliths (dashed white lines). Scale card = 15 cm long, pencil = 14 cm long.

The arfvedsonite lujavrite is dark grey to black coloured and has a cumulus arfvedsonite matrix (Fig 3.10c). Acicular arfvedsonite crystals contribute to the foliation, however the fissility is associated with the alignment of platy alkali feldspar crystals. Leucocratic xenoliths were also noted within the arfvedsonite lujavrite; these

are principally composed of alkali feldspar and nepheline (Fig 3.10d) and again are suggested to correspond to naujaite fragments (Bohse & Andersen, 1981). The foliation within the lujavrite wraps around these xenoliths (Fig 3.10d).

3.5 Conclusions

Fieldwork was focused on the layered kakortokite in both outcrop and drill core with additional observations from the roof rocks, naujaite, lujavrite and marginal pegmatite. Access to drill core allows for the extension of observations to the unexposed layered kakortokite and the present study has recognised an additional eight units below Unit -11, which have been termed Units -12 to -19 downward. Importantly Unit -19 does not mark the base of the complex; instead the layered kakortokite terminates against a fine- to medium-grained, un-layered mesocratic sequence of rocks, which resemble a sequence that crosscuts the layered kakortokite between Units -7 and -2. This sequence of rocks have alternately been hypothesised to represent: lujavrite within the layered kakortokite (Ussing, 1912); hybrid rocks that share chemical similarities with kakortokite (Ferguson, 1970); or slumping of unconsolidated kakortokite (Bohse *et al.*, 1971). These rocks provide an insight into the magma chamber dynamics, as a complex series of processes must have been operating during the development of the layering.

3.6 References

Bohse, H. & Andersen, S. (1981). Review of the stratigraphic divisions of the kakortokite and lujavrite in southern Ilímaussaq. *Rapport Grønlands Geologiske Undersølgelse* **103**, 53-62.

Bohse, H., Brooks, C. K. & Kunzendorf, H. (1971). Field observations on the kakortokites of the Ilimaussaq intrusion, South Greenland, including mapping and analyses by portable X-ray fluorescence equipment for zirconium and niobium. *Rapport Grønlands Geologiske Undersølgelse* **38**, 43 pp.

Ferguson, J. (1964). Geology of the Ilímaussaq alkaline intrusion, South Greenland. Part I. Description of map and structure. *Meddelelser om Grønland* **172**, 1-81.

Ferguson, J. (1970). The significance of the kakortokite in the evolution of the Ilímaussaq intrusion, South Greenland. *Meddelelser om Grønland* **190**, 1-193.

Larsen, L. M. & Sørensen, H. (1987). The Ilímaussaq intrusion - progressive crystallisation and formation of layering in an agpaitic magma. *Geological Society London, Special Publications* **30**, 473-488.

Schonwandt, H. K., Barnes, G. B. & Ulrich, T. (2014). The world-class REE deposit Tanbreez, South Greenland: its size and structure. *ERES2014: 1st European Rare Earth Resources Conference*. Milos.

Sørensen, H., Bohse, H. & Bailey, J. C. (2006). The origin and mode of emplacement of lujavrites in the Ilímaussaq alkaline complex, South Greenland. *Lithos* **91**, 286-300.

Ussing, N. V. (1912). Geology of the country around Julianehaab, Greenland. *Medeleser om Grønland* **38**, 1-426.

Chapter 4
Analytical Techniques and Methods

4.1 Introduction

Three main analytical techniques were applied to study the development of the layered kakortokite: thin section petrography, quantitative textural analysis and mineral chemistry. Whole rock XRF analysis was additionally used to study the development of the fine- to medium-grained, un-layered rock sequence ("hybrid/slump" rocks) hosted within the layered kakortokite. A brief description of each of these techniques follows, with the key parameters used.

4.2 Petrography

Each sample was initially analysed through a petrographic study of the corresponding thin (30 μm) or thick (<60 μm) section with the use of a polarising light microscope. Mineral phases and modal proportions were identified.

4.3 Quantitative Textural Analysis

Quantitative textural analysis was performed through crystal size distribution (CSD) analyses. This is a technique that allows for the quantification of petrographic observations (Higgins, 2006, Marsh, 1998) and provides an insight into the processes of nucleation and growth in a magma. CSD analysis was pioneered through studies of low viscosity basaltic magmas (Cashman & Marsh, 1988, Marsh, 1988b), but the technique is applicable to the Ilímaussaq magmas as they are suggested to have a viscosity between 100 – 900 Pa s, due to their F-rich composition and high volatile contents (Larsen & Sørensen, 1987), i.e. similar to a basalt (Larsen & Sørensen, 1987, Sato, 2005).

4.3.1 CSD Technique

The CSD data were collected through manually tracing crystal outlines from composite photomicrographs of thick/thin sections using Adobe Illustrator and a graphics tablet. An example of the digitising is displayed in Figure 4.1. The sections were photographed in circularly polarised light (CPL) (Higgins, 2010a) using either an optical polarising microscope or the digital Keyence VHX-2000 microscope at the University of St Andrews. CPL was used as this technique ensures that all minerals display their greatest birefringence, and thus the visibility of minerals with a low birefringence is enhanced (Higgins, 2010a). Each mineral phase was processed and analysed separately in order to distinguish the nucleation, crystallisation and growth processes for each mineral phase in the sample.

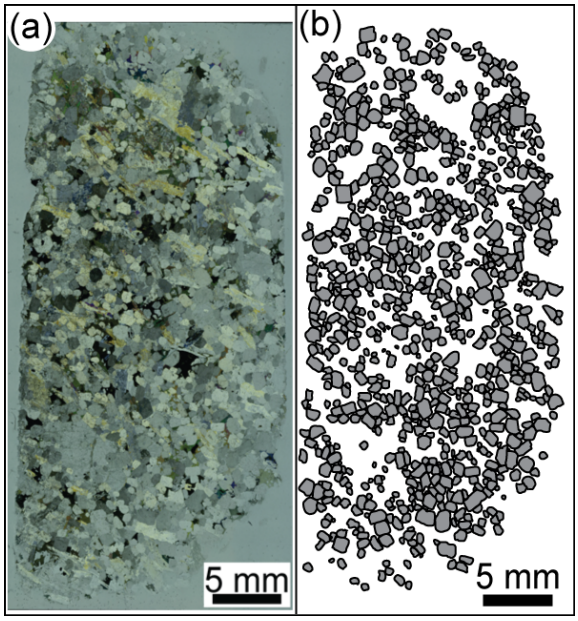

Figure 4.1: (a) Example photomicrograph of sample EJH/12/007, U0 red kakortokite. (b) Digitised eudialyte crystals from sample EJH12/007.

The digitised images were processed using the image analysis software ImageJ (Schneider *et al.*, 2012) to obtain two dimensional crystal shape data. This was input to CSDCorrections (Higgins, 2012) for three dimensional stereological conversion based on crystal size parameters. These crystal size parameters were calculated for each mineral phase studied using the CSDSlice database (Morgan & Jerram, 2006) and are listed in Table 4.1. Where mineral alignment was noted through the petrographic analysis, the igneous fabric was measured and input. Fabric values were calculated though CSDCorrections and the shape preferred orientation measurement software Ellipsoid (Launeau *et al.*, 2010). The data were compared and as the values were consistent, CSDCorrections was used to calculate fabrics throughout the study for standardisation.

Mineral Phase	Aspect Ratio
Aegirine	1 : 1 : 10
Alkali Feldspar	1 : 3.2 : 5.5
Arfvedsonite	1 : 1.4 : 2.3
Eudialyte	1 : 1.15 : 1.5
Nepheline	1 : 1.15 : 1.6

Table 4.1: Crystal aspect ratios calculated using the CSDSlice database.

The resultant data from CSDCorrections are plotted as population density (the logarithmic number of crystals per unit volume), against crystal size (the maximum length). As all the crystals were easily visible in circularly polarised light, as determined through cross-referencing with backscattered electron images, it is inferred that the reported smallest crystal sizes are the lower limit for each sample. CSDCorrections calculates the errors associated with the CSD plots and these are

presented in the raw data (e.g. Fig. 4.2, supplementary materials Appendix C). The greatest uncertainties are associated with smallest and largest sized intervals. The uncertainty associated with the smallest crystal sizes is most likely due to errors in correcting the modal intersection length, this is calculated in CSDCorrections through the contribution of counting errors of other intersection intervals to the total correction of an interval (Higgins, 2000). The uncertainty associated with the largest crystal sizes is most likely due to counting errors, i.e. the square root of the number of sections within an interval, which becomes significant for size intervals with fewer than 20 intersections (Higgins, 2000). Errors can also be associated with the conversion of intermediate (intersection length measurements) and short (intersection width measurements) crystal dimensions to crystal length as errors in the crystal shape can systematically result in errors in both population density and crystal size (Higgins, 2000). The uncertainties were reduced in the present study through only analysing equant crystals that were not overprinted by late-stage alteration. Additionally, when possible, large crystal populations (>200 crystals) were measured.

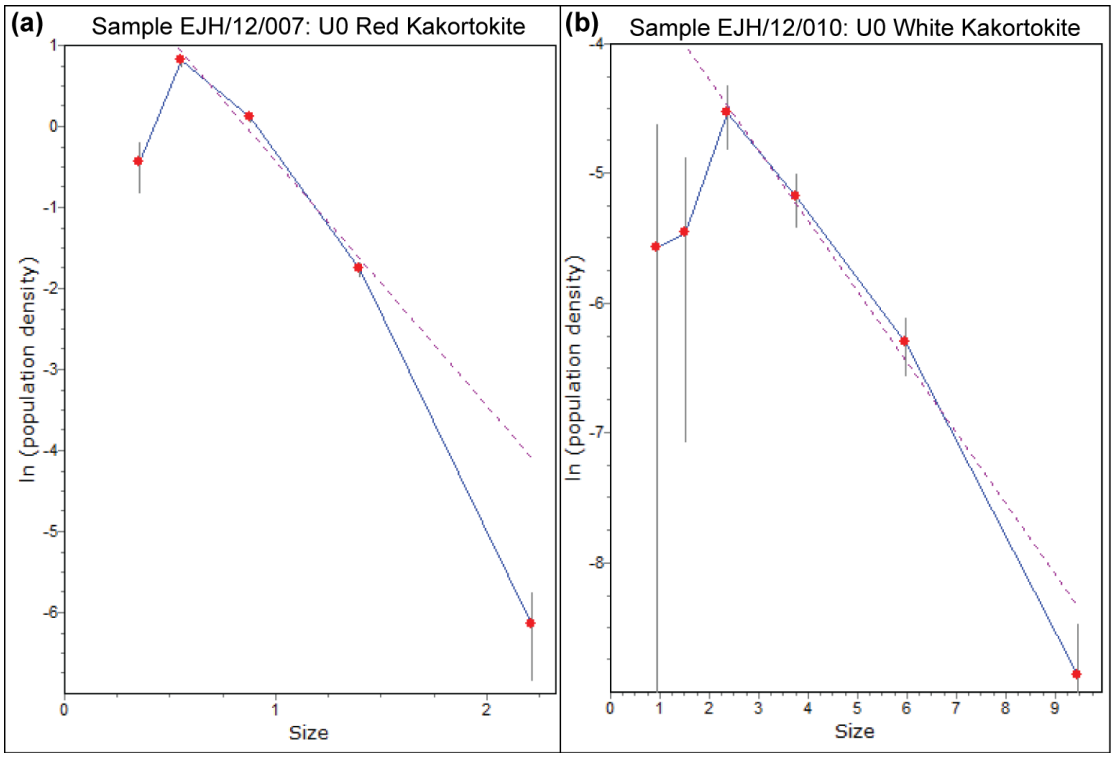

Figure 4.2: Results graphs from CSDCorrections showing vertical error bars associated with each size interval. (a) Sample EJH/12/007, Unit 0 red kakortokite. (b) Sample EJH/12/007, Unit 0 white kakortokite. The solid line represents the CSD plot, dashed line represents the slope of the CSD as calculated by CSDCorrections.

Processes of nucleation, crystallisation and textural development are inferred through plot shapes (Fig. 4.3). Plots that curve upwards at larger crystal sizes are

associated with formation through gravitational settling; log-linear graphs are associated with *in situ* crystallisation; plot shapes that curve downwards at larger crystal sizes are associated with formation through crystal fractionation; and sharp kinks in the plot shape indicate mixing of crystal populations (Boorman *et al.*, 2004, Higgins, 2006, Marsh, 1998). The process of crystal fractionation is the counterpart process to gravitational settling and represents the smaller sized portion of crystals that remain in suspension and were enclosed in the upwards growing crystal mush pile (Marsh, 1988a, Marsh, 1988b). Processes of textural coarsening can also be observed in CSD plots. Key features are downturned slopes at the smallest crystal sizes and fanning of CSD gradients due to progressive coarsening of the larger crystal sizes (Fig. 4.3b) associated with annealing and Ostwald ripening, i.e. the growth of the largest crystals at the expense of the smallest (Higgins, 2010b).

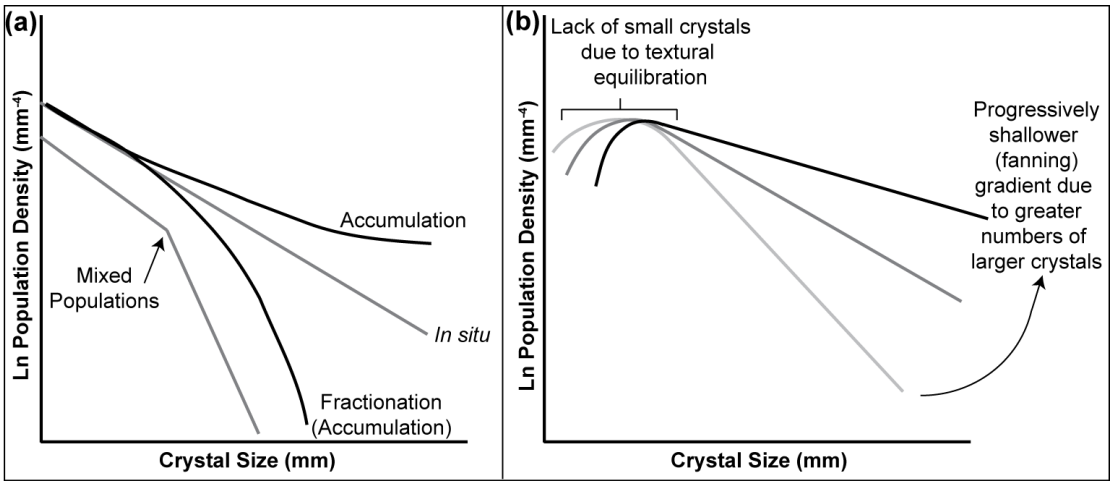

Figure 4.3 (a) Schematic CSD plot indicating range of plot shapes and their associated processes of crystallisation, after Marsh (1988b). (b) Schematic CSD plot indicating plot shapes associated with textural coarsening, adapted from Higgins (1999).

The CSDs can provide further insight into processes of nucleation and growth through the y-axis intercept and slope values; these were used to calculate the final nucleation density (n_{io}) as [exp(y-intercept)] and the characteristic length (C_i) as [-1/slope] (Higgins, 2002). The slopes were calculated through regression lines plotted from the CSD profiles, as the slope values calculated by CSD corrections do not correspond well to the CSD profiles (Fig. 4.2). The crystal size data were used to calculate "Lmax", the mean size of the 4 largest crystals. The volumetric phase proportion (V_i) was calculated for log-linear CSD plots through [$V_i = 6\sigma n_{io} C_i^4$] (Higgins, 2002) and closure was calculated following the methodology outlined in Higgins (2002). These data are used in plots of y-axis intercept vs. characteristic length and Lmax vs. slope.

4.4 Whole Rock Chemistry

Whole rock major element analyses of the “hybrid/slump” rocks were performed through X-ray fluorescence (XRF) at the University of St Andrews using the SPECTRO X-LAB 2000 spectrometer. Samples of unweathered rocks were chosen and cut for analysis. Samples that displayed alteration or separate leucocratic and mesocratic phases were avoided. The rocks were crushed, powdered in a tungsten carbide mill and dried at 105ºC. The analysis was performed on fused beads and all analyses were carried out in Pt/Au (95/5%) crucibles. Calibration was performed using international geological reference samples.

4.5 Mineral Chemistry

Backscattered electron (BSE) imaging and chemical analyses of targeted eudialyte and amphibole crystals were performed at the University of St Andrews through electron probe microanalysis (EPMA) using the JEOL JXA-8600 superprobe in wavelength dispersion mode. Compositions were obtained using the methodology of Pfaff *et al.* (2008) with a defocused beam of 10 μm diameter to measure all elements. Eudialyte, in the form of eudialyte-group minerals (discussed below), was measured using an acceleration voltage of 20 kV and a beam current of 20 nA. Amphibole (arfvedsonite) was measured using an acceleration voltage of 15 kV and a beam current of 15 nA. Count times on peak for major elements were 16 s and 30 to 120 s for minor elements (tables 4.2 & 4.3). Background measurement times were half of the peak times. Na was measured first with a count time of 10 s on peak and 5 s on background, to avoid migration. A combination of natural and synthetic standards were used and corrections were internally performed using PAP (Armstrong, 1991).

Element	Line	BG+	BG-	Crystal	Position	Peak Count (s)	Background count (s)
Si	Kα	6.5	3	TAP	77.57	16	8
Zr	Lα	2	2	PET	194.43	16	8
Hf	Lα	2	2	LiF	109.14	30	15
La	Lα	2	2	LiF	185.36	30	15
Ce	Lα	2	2	LiF	178.12	30	15
Pr	Lα	1.5	1.5	LiF	157.07	30	15
Nd	Lα	0.9	1	LiF	150.68	30	15
Sm	Lβ	9	1.3	LiF	138.94	30	15
Dy	Lβ	0.8	8.4	LiF	118.95	60	30
Yb	Lα	2.5	1.8	LiF	116.26	30	15
Y	Lα	2	2	PET	206.55	30	15
U	Mα	2	3	PET	125.23	60	30
Al	Kα	5	5	TAP	90.60	30	15
Ca	Kα	3	2	PET	107.44	16	8
Fe	Kα	2	2	LiF	134.58	16	8
K	Kα	2	2	PET	119.69	60	30
Mn	Kα	2	2	LiF	146.06	30	15
Na	Kα	4.5	4.5	TAP	129.38	10	5
Ti	Kα	2	2	PET	87.89	120	60
Cl	Kα	2	2	PET	151.33	20	10
Sr	Lα	2	2	PET	290.80	120	60
Ta	Lα	2	2	LiF	105.79	30	15
Nb	Lα	2	2	PET	183.35	30	15

Table 4.2: Eudialyte-group minerals EPMA parameters and counting times for each element studied.

Element	Line	BG+	BG-	Crystal	Position	Peak Count (s)	Background count (s)
Mg	Kα	5	5	TAP	107.44	30	15
Si	Kα	6.5	3	TAP	77.57	16	8
Zr	Lα	2	2	PET	194.43	16	8
Al	Kα	5	5	TAP	90.60	30	15
Ca	Kα	3	2	PET	107.44	16	8
Fe	Kα	2	2	LiF	134.58	16	8
K	Kα	2	2	PET	119.69	60	30
Mn	Kα	2	2	LiF	146.06	30	15
Na	Kα	4.5	4.5	TAP	129.38	10	5
Ti	Kα	2	2	PET	87.89	120	60
Zn	Kα	2	2	LIF	99.87	60	30
Cl	Kα	2	2	PET	151.33	20	10
F	Kα	2	2	TAP	199.14	20	10

Table 4.3: Amphibole EPMA parameters and counting times for each element studied.

The name eudialyte is used in this thesis as a shortened term for the eudialyte-group minerals (EGM). The general formula is:

$$[N(1)N(2)N(3)N(4)N(5)]_3[M(1a)M(1b)]_3M(2)_3M(3)M(4)Z_3[Si_{24}O_{72}]O'_4X_2$$

where *X* = Cl, F, OH or CO3; Z =3 (Johnsen *et al.*, 2003). Common members of the EGM are listed in table 4.4. Their formulae were calculated through normalisation of the sum of the Si+Zr+Ti+Nb+Al+Hf cations to 29 a.p.f.u (Johnsen & Grice, 1999) with site occupancies for the remaining cations calculated following this standardisation. Formulae of the amphiboles were calculated based on 16 cations and 23 oxygens. Li was calculated through the method of Pfaff *et al*. (2008).

Mineral	Formula
Eudialyte	$Na_{15}Ca_6Fe_3Zr_3Si(Si_{25}O_{73})(O,OH,H_2O)_3(Cl,OH)_2$
Kentbrooksite	$Na_{15}Ca_6Mn_3Zr_3Nb(Si_{25}O_{73})(O,OH,H_2O)_3(F,Cl)_2$
Ferrokentbrooksite	$Na_{15}Ca_6Fe_3Zr_3Nb(Si_{25}O_{73})(O,OH,H_2O)_3(F,Cl)_2$
Oneillite	$Na_{15}Ca_3Mn_3Fe_3Zr_3Nb(Si_{25}O_{73})(O,OH,H_2O)_3(OH,Cl)_2$
Zirsilite-(Ce)	$(Na\square_{12})(REE,Na)_3Ca_6Mn_3Zr_3Nb(Si_{25}O_{73})(OH)_3(CO_3)\cdot H_2O$

Table 4.4: Members of the eudialyte-group minerals discussed in this study. Formulae from Johnsen *et al.* (2003).

The uncertainties associated with the EPMA were determined through repeated measurements of a single crystal, which did not display compositional zoning. This was performed for the EGM through 12 measurements on a single crystal from sample EJH/12/007 (table 4.5). The greatest uncertainty is associated with the measurement of Na_2O, which is consistent with migration of Na during analysis. The UO_2 oxide content was below the limit of detection in all analyses. The uncertainty in the EPMA of amphibole was determined through 13 measurements on a single crystal from sample EJH/12/008 (table 4.5). The greatest uncertainties are

associated with the measurements of F. This is interpreted to be associated with highly variable F contents through the single amphibole crystal.

Eudialyte			Amphibole		
Oxide (wt.%)	**Precision (95% Confidence)**	**L.O.D.**	**Oxide (wt.%)**	**Precision (95% Confidence)**	**L.O.D**
Na_2O	0.28	0.42	F	2.57	3.89
Al_2O_3	0.07	0.10	Na_2O	0.53	0.80
SiO_2	0.30	0.45	MgO	0.12	0.18
Cl	0.15	0.23	Al_2O_3	0.15	0.22
K_2O	0.02	0.03	SiO_2	0.66	1.01
CaO	0.16	0.24	Cl	0.02	0.03
TiO_2	0.02	0.04	K_2O	0.09	0.14
MnO	0.07	0.10	CaO	0.28	0.42
FeO	0.17	0.25	TiO_2	0.13	0.19
SrO	0.01	0.01	MnO	0.08	0.13
Y_2O_3	0.16	0.23	FeO	0.81	1.23
ZrO_2	0.42	0.63	ZnO	0.09	0.14
Nb_2O_5	0.25	0.38			
La_2O_3	0.17	0.26			
Ce_2O_3	0.17	0.25			
Pr_2O_3	0.18	0.27			
Nd_2O_3	0.21	0.32			
Sm_2O_3	0.15	0.23			
Dy_2O_3	0.12	0.18			
Yb_2O_3	0.06	0.09			
HfO_2	0.10	0.15			
Ta_2O_5	0.15	0.22			
UO_2	n.d.	n.d.			

Table 4.5: Uncertainty associated with EPMA of eudialyte and amphibole, L.O.D. = limit of detection (3 standard deviations from mean), N.d. = not detected.

4.4.1 Cl Standard

Generic chlorine standards with certificates of analysis at comparable concentrations to those in the EGM were unavailable. Therefore in order to measure the chlorine content of EGM, an internal chlorine standard was created for this project using tugtupite ($Na_4AlBeSi_4O_{12}Cl$) collected during the fieldwork portion of the project.

Tugtupite chips (Fig. 4.4a) collected from a pegmatite vein in lujavrite (60º53'34.8" N, 045º50'40.6 W), were polished and initially examined using energy dispersive x-ray spectroscopy (EDS, Fig. 4.4b) to qualitatively estimate the chemistry. Chemical homogeneity was determined through BSE and cathodoluminescence (CL) imaging (Fig 4.4c-f). A compositionally homogeneous crystal (crystal 1, Fig 4.4a) was selected for use as the standard and the composition was quantitatively measured using the JEOL JCXA733 superprobe at the University of St Andrews and a pure NaCl crystal as a known Cl standard. 25 analyses were performed on the tugtupite crystal (table 4.6) and the mean composition (7.75 wt% Cl) was taken for the standard.

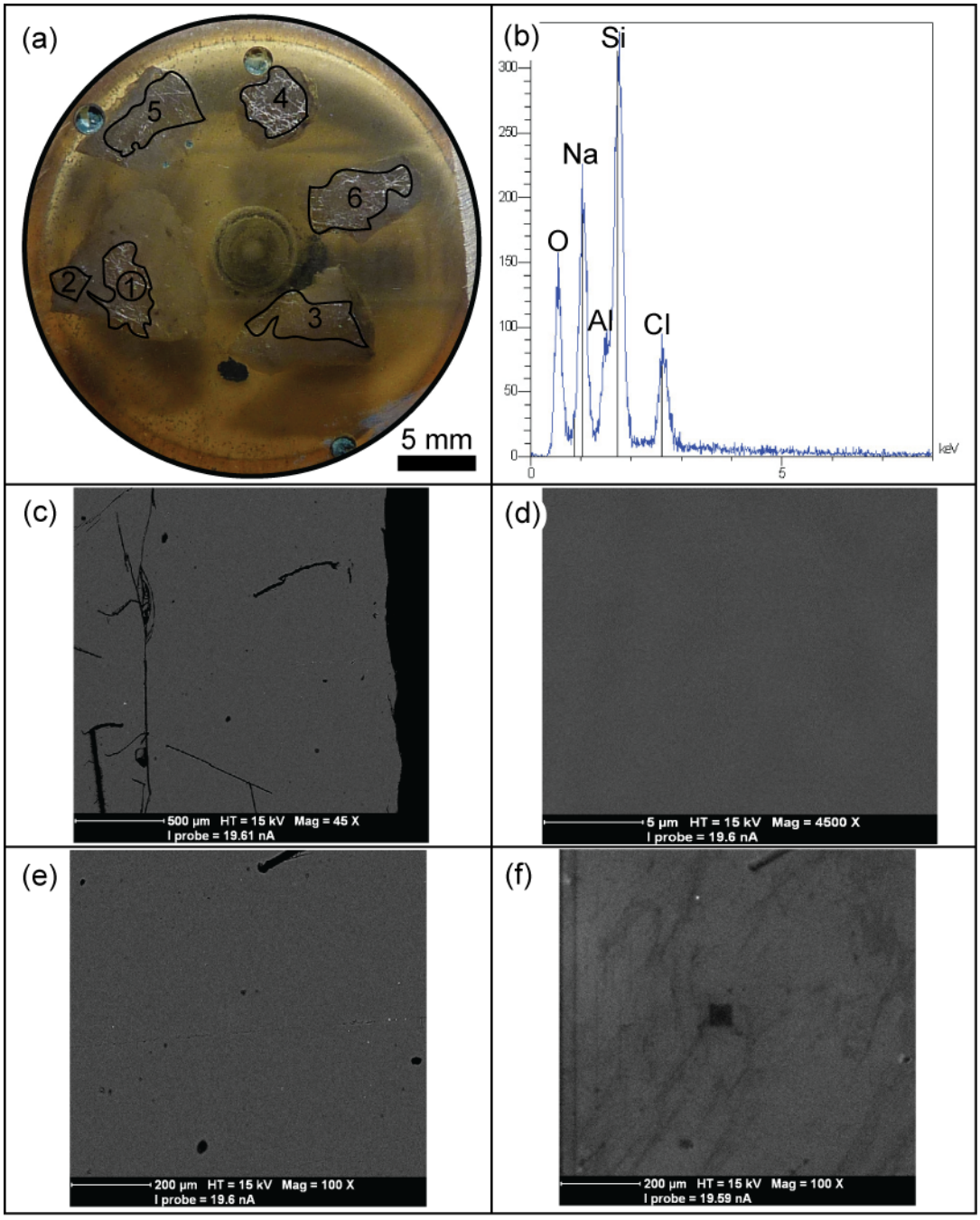

Figure 4.4: (a) Sample block. (b) EDS results indicating Na,Al,Cl,Si, composition. (c) BSE image from crystal 1 at 45x magnification. (d) BSE image from crystal 1, same location as (c) at 4500x magnification indicating homogeneity at a microscale. (e) BSE image from crystal 1 at 100x magnification, same location as (c). (f) CL image from crystal 1 at 100x magnification, same location as (e) showing variations in luminescence that do not correspond to compositional heterogeneities.

	EJH_TUG_6	EJH_TUG_7	EJH_TUG_8	EJH_TUG_9	EJH_TUG_10	EJH_TUG_11	EJH_TUG_12	EJH_TUG_13	EJH_TUG_14
NaO	24.58	24.98	24.88	24.82	24.37	24.25	25.31	24.29	24.58
BeO**	3.09	2.28	2.38	2.93	4.37	3.81	1.37	3.79	2.86
Al_2O_3	11.83	11.93	11.70	11.74	11.74	11.63	11.84	11.66	11.83
SiO_2	52.88	53.00	53.24	52.76	51.71	52.53	53.54	52.48	52.90
Cl	7.62	7.80	7.80	7.75	7.82	7.77	7.95	7.78	7.82
SO_3	0.06	0.06	0.12	0.10	0.09	0.09	0.08	0.13	0.11
ZnO	0.03	0.10	0.09	0.01	0.08	0.06	0.10	0.00	0.06
FeO	0	0	0	0.00	0	0	0.00	0.02	0.03
Cr_2O_3	0	0.01	0	0	0.05	0.01	0	0	0.00
MnO	0	0.00	0	0.01	0	0.00	0	0.01	0
CaO	0	0.02	0.01	0.01	0.01	0.02	0	0	0
TiO	0	0.01	0	0	0.02	0.01	0.00	0.01	0
K_2O	0.01	0	0	0.01	0	0.01	0.01	0.01	0.01
MgO	0	0	0	0	0	0	0	0	0
Total*	95.11	96.00	95.93	95.30	93.99	94.50	96.89	94.50	95.43

Table 4.6: oxide compositions of measurements from crystal 1. *Totals adjusted for Cl_2 = -O. **BeO calculated from [100-total]

	EJH_TUG_15	EJH_TUG_17	EJH_TUG_18	EJH_TUG_19	EJH_TUG_20	EJH_TUG_21	EJH_TUG_22	EJH_TUG_26	EJH_TUG_27
NaO	24.45	23.84	24.43	24.61	24.47	24.28	24.14	24.79	25.12
BeO**	2.64	4.81	4.77	4.43	5.03	5.14	4.77	3.30	3.48
Al_2O_3	11.80	11.67	11.53	11.39	11.34	11.37	11.45	11.54	11.64
SiO_2	53.32	52.05	51.61	51.86	51.33	51.52	51.87	52.64	51.98
Cl	7.78	7.63	7.67	7.70	7.83	7.69	7.77	7.73	7.77
SO_3	0.13	0.10	0.10	0.10	0.05	0.15	0.03	0.08	0.08
ZnO	0.08	0.09	0.08	0.02	0.04	0.07	0.06	0.03	0.03
FeO	0.03	0	0	0.02	0.02	0.06	0	0	0
Cr_2O_3	0	0	0	0.01	0.02	0	0	0.03	0
MnO	0.01	0	0.01	0	0.01	0.01	0.02	0	0
CaO	0	0	0	0	0	0	0	0	0.01
TiO	0	0	0	0	0	0	0.02	0	0
K_2O	0	0	0.01	0	0	0	0.01	0	0
MgO	0	0	0	0	0	0	0	0	0
Total*	95.70	93.52	93.56	93.84	93.23	93.28	93.49	94.93	94.74

Table 4.6 (continued): oxide compositions of measurements from crystal 1. *Totals adjusted for Cl_2 = -O. **BeO calculated from [100-total]

	EJH_TUG_30	EJH_TUG_31	EJH_TUG_32	EJH_TUG_33	EJH_TUG_34	EJH_TUG_35	EJH_TUG_36		Mean Comp.
NaO	24.21	25.11	24.90	24.50	24.41	24.80	24.45		52.39
BeO**	3.95	1.65	3.19	3.32	4.23	3.25	4.96		24.58
Al_2O_3	11.78	11.91	11.81	11.73	11.71	11.94	11.66		11.69
SiO_2	52.29	53.54	52.47	52.67	51.94	52.25	51.35		7.75
Cl	7.77	7.79	7.63	7.79	7.72	7.77	7.58		3.59
SO_3	0.13	0.13	0.09	0.08	0.10	0.09	0.06		0.09
ZnO	0.05	0.10	0.12	0.13	0.08	0.08	0.06		0.07
FeO	0.03	0	0	0	0	0.05	0.01		*n.d.*
Cr_2O_3	0	0	0	0.02	0	0	0		*n.d.*
MnO	0	0.02	0	0	0	0	0		*n.d.*
CaO	0	0.02	0.02	0	0.01	0	0		*n.d.*
TiO	0	0.01	0	0	0	0	0.01		*n.d.*
K_2O	0	0	0	0	0.01	0	0.01		*n.d.*
MgO	0	0	0	0	0	0	0		*n.d.*
Total*	94.37	96.69	95.14	95.01	94.10	95.07	93.33		

Table 4.6 (continued): oxide compositions of measurements from crystal 1 and the mean composition. *N.d.*: elements below detection limits. *Totals adjusted for Cl_2 = -O. **BeO calculated from [100-total]

4.5 References

Armstrong, J. T. (1991). Quantitative elemental analysis of individual microparticles with electron beam instruments. *Electron probe quantitation*: Springer, 261-315.

Boorman, S., Boudreau, A. & Kruger, F. J. (2004). The Lower Zone-Critical Zone Transition of the Bushveld Complex: a Quantitative Textural Study. *Journal of Petrology* **45**, 1209-1235.

Cashman, K. V. & Marsh, B. D. (1988). Crystal size distribution (CSD) in rocks and the kinetics and dynamics of crystallization II: Makaopuhi lava lake. *Contributions to Mineralogy and Petrology* **99**, 292-305.

Higgins, M. D. (1999). Origin of megacrysts in granitoids by textural coarsening: a crystal size distribution (CSD) study of microcline in the Cathedral Peak Granodiorite, Sierra Nevada, California In: Castro, A., Fernández, C. & Vigneresse, J. L. (eds.) *Understanding Granites: Integrating New and Classical Techniques*. London: Geological Society London, Special Publications, 207-219.

Higgins, M. D. (2000). Measurement of crystal size distributions. *American Mineralogist* **85**, 1105-1116.

Higgins, M. D. (2002). Closure in crystal size distributions (CSD), verification of CSD caluclations, and the significance of CSD fans. *American Mineralogist* **87**, 171-175.

Higgins, M. D. (2006). *Quantitative Textural Measurements in Igneous & Metamorphic Petrology*. Cambridge: Cambridge University Press.

Higgins, M. D. (2010a). Imaging birefringent minerals without extinction using circularly polarized light. *The Canadian Mineralogist* **48**, 231-235.

Higgins, M. D. (2010b). Textural coarsening in igneous rocks. *International Geology Review* **1**, 1-23.

Higgins, M. D. (2012). CSDCorrections.

Johnsen, O., Ferraris, G., Gault, R. A., Grice, J. D., Kampf, A. R. & Pekov, I. V. (2003). The Nomenclature of Eudialyte-Group Minerals. *The Canadian Mineralogist* **41**, 785-794.

Johnsen, O. & Grice, J. D. (1999). The crystal chemistry of the eudialyte group. *Canadian Mineralogist* **37**, 865-891.

Larsen, L. M. & Sørensen, H. (1987). The Ilímaussaq intrusion - progressive crystallisation and formation of layering in an agpaitic magma. *Geological Society London, Special Publications* **30**, 473-488.

Launeau, P., Archanjo, C. J., Picard, D., Arbaret, L. & Robin, P.-Y. F. (2010). Two- and three-dimensional shape fabric analysis by the intercept method in grey levels. *Tectonophysics* **492**, 230-239.

Marsh, B. D. (1988a). Crystal capture, sorting, and retention in convecting magma. *Geological Society of America Bulletin* **100**, 1720-1737.

Marsh, B. D. (1988b). Crystal size distribution (CSD) in rocks and the kinetics and dynamics of crystallization I. Theory. *Contributions to Mineralogy and Petrology* **99**, 277-291.

Marsh, B. D. (1998). On the interpretation of crystal size distributions in magmatic systems. *Journal of Petrology* **39**, 553-599.

Morgan, D. J. & Jerram, D. A. (2006). On estimating crystal shape for crystal size distribution analysis. *Journal of Volcanology and Geothermal Research* **154**, 1-7.

Pfaff, K., Krumrei, T., Marks, M. A. W., Wenzel, T., Rudolf, T. & Markl, G. (2008). Chemical and physical evolution of the 'lowered layered sequence' from the nepheline syenitic Ilímaussaq intrusion, South Greenland: Implications for the origin of magmatic layering in peralkaline felsic liquids. *Lithos* **106**, 280-296.

Sato, H. (2005). Viscosity measurement of subliquidus magmas: 1707 basalt of Fuji volcano. *Journal of Mineralogical and Petrological Sciences* **100**, 133-142.

Chapter 5

Introduction to Kakortokite Petrography

5.1 Introduction

Kakortokite is the local name for the layered agpaitic rocks at the base of the Ilímaussaq Complex. These rocks plot as nepheline syenite in QAPF space, although some white kakortokite samples plot as nephelinolite (Fig. 5.1). The outcropping layered kakortokite was mapped by Bohse et al. (1971), who distinguished 29 units (numbered -11 to +17 upwards), typically subdivided into three layers: black kakortokite (arfvedsonite-rich) overlain by red (eudialyte-rich) then white (alkali feldspar- and nepheline-rich) kakortokite. Analysis during the present study indicates that the layering and textures are laterally continuous across the series. Importantly access to drill core (provided by TANBREEZ Mining Greenland A/S, Appendix B) has allowed the first description of the base of the layered series and the identification of an additional eight unexposed units (-12 to -19). This chapter provides an overview of the characteristics of the layered kakortokite and details inconsistencies within the layering. The first full petrographic description of each of the units and their distinguishing characteristics is provided.

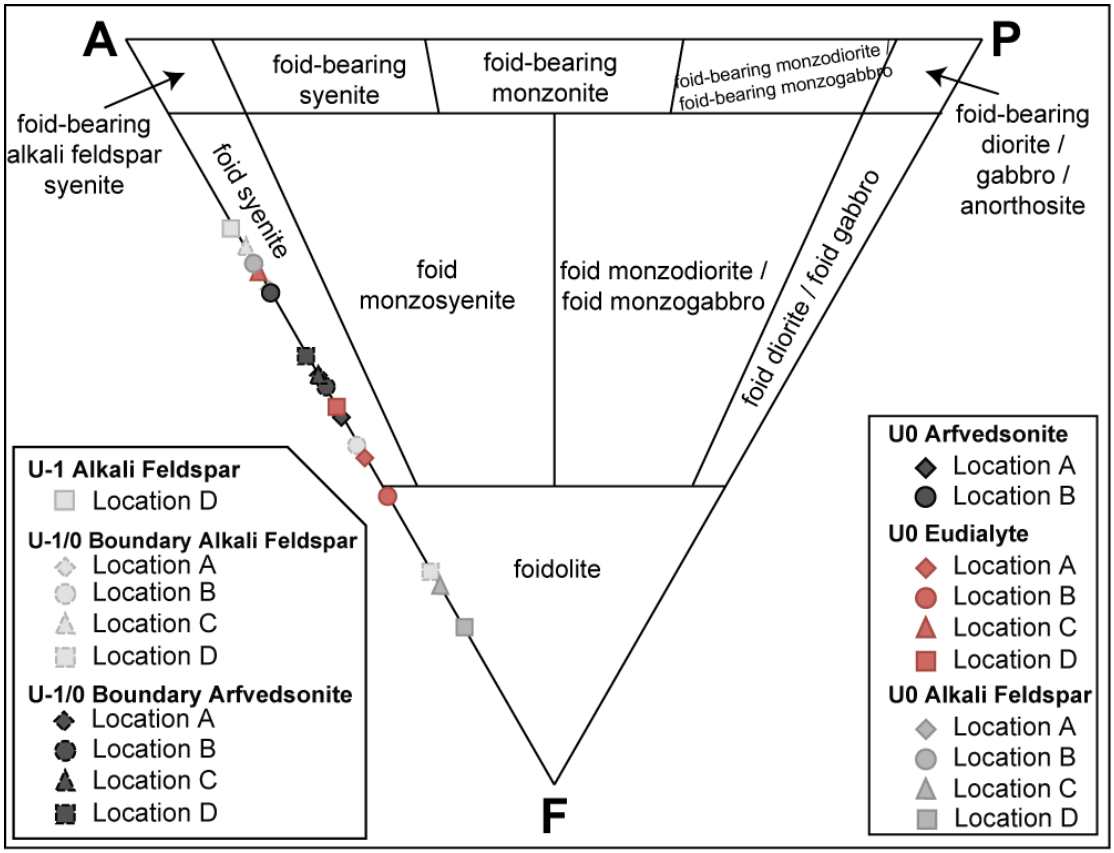

Figure 5.1: APF diagram adapted from Le Maitre (2002) of kakortokite samples from the Unit 0 marker horizon. Data segregated by composition and unit stratigraphy. Most of the samples plot as nepheline syenite, although some white kakortokite samples plot as nephelinolite.

5.2 The Layered Kakortokite

Viewed from a distance (5-10 km) the layering of the kakortokite is strikingly regular (Fig. 5.2a-b), however each unit has unique textural and/or mineralogical characteristics, which allows them to be distinguished through the layered series. Each layer, taken as whole across the complex, is remarkably homogeneous (Fig. 5.2c). The typical unit structure is an arfvedsonite-rich black kakortokite, overlain by eudialyte-rich red kakortokite, followed by alkali feldspar- and nepheline-rich white kakortokite. Previous workers have noted, however, that in some units the red kakortokite is suppressed or missing (Bohse *et al.*, 1971, Larsen & Sørensen, 1987, Pfaff *et al.*, 2008, Sørensen, 1969). The present study has identified portions of each unit that have a relative enrichment in eudialyte, thus distinguishes red kakortokite in each unit, however some are relatively eudialyte-poor (<25% eudialyte) and less striking in field exposure. Units +10, +5, -4 & -10, display an alteration from the typical unit structure as they contain a subordinate alkali feldspar-rich white kakortokite (Fig. 5.3b) between the black and red layers. This subordinate white kakortokite has been termed 'Wa' in the present study.

The boundaries between units are typically distinct and planar and can be traced across the entire outcropping layered series, while all intra-unit boundaries between layers are gradational, typically over 2-15 cm. There is no evidence of scouring or flow indicators, e.g. current bedding or shearing of crystals, except in association with the marginal pegmatite and Unit +3. The marginal pegmatite is heterogeneous with sporadic inch-scale layering developing at the gradational contact (over ~100 m) between the marginal pegmatite and the macrorhythmically layered kakortokite. Unit +3 is associated with numerous roof rock autoliths and inch-scale layering (Fig. 5.2d) is present throughout much of the unit. Features of current bedding were observed around the autoliths in the overlying Unit +4 by Larsen & Sørensen (1987).

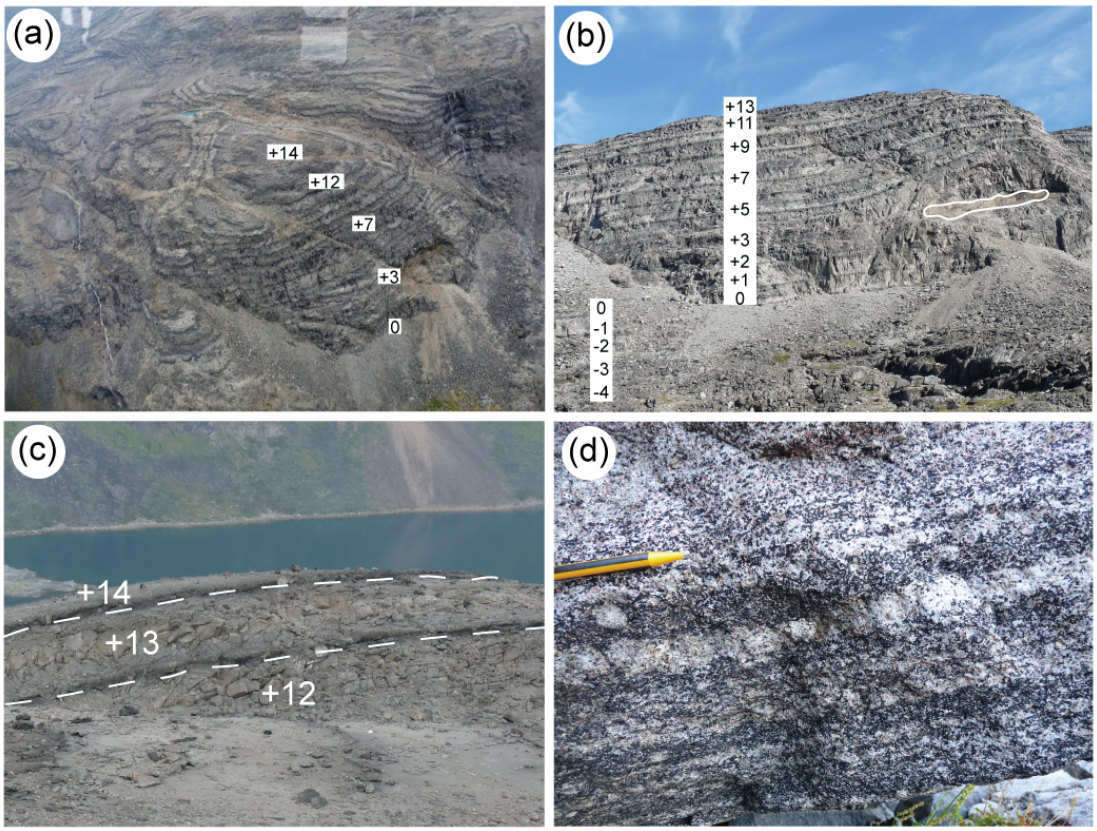

Figure 5.2: (a) Aerial photo of layered kakortokite composing Kringlerne plateau. (b) Layered kakortokite in Kringlerne cliff face, units -4 to +13 are visible, large autolith in Unit +3 is outlined in white. (c) Laterally continuous layering across Kringlerne Plateau, units +12R to +14R, unit boundaries marked by dashed lines. (d) Inch-scale layering of kakortokite in Unit +3. Typical unit thickness = 8 m, yellow pencil tip is 2 cm.

Typical mineralogical compositions of each kakortokite variety are presented in chapter 3.3.4 and Figure 5.3. The black kakortokite is typically massive, but is occasionally foliated, with the fabric identified by acicular arfvedsonite crystals and alkali feldspar plates (e.g. Units +15, +10, -4, -10). Red kakortokite is typically saccharoidal, however it is massive when poorly developed (<25% eudialyte). Occasionally red kakortokite has a foliation fabric, carried by acicular arfvedsonite crystals (e.g. Unit +13). The white kakortokite is typically foliated with the fabric identified by alkali feldspar plates.

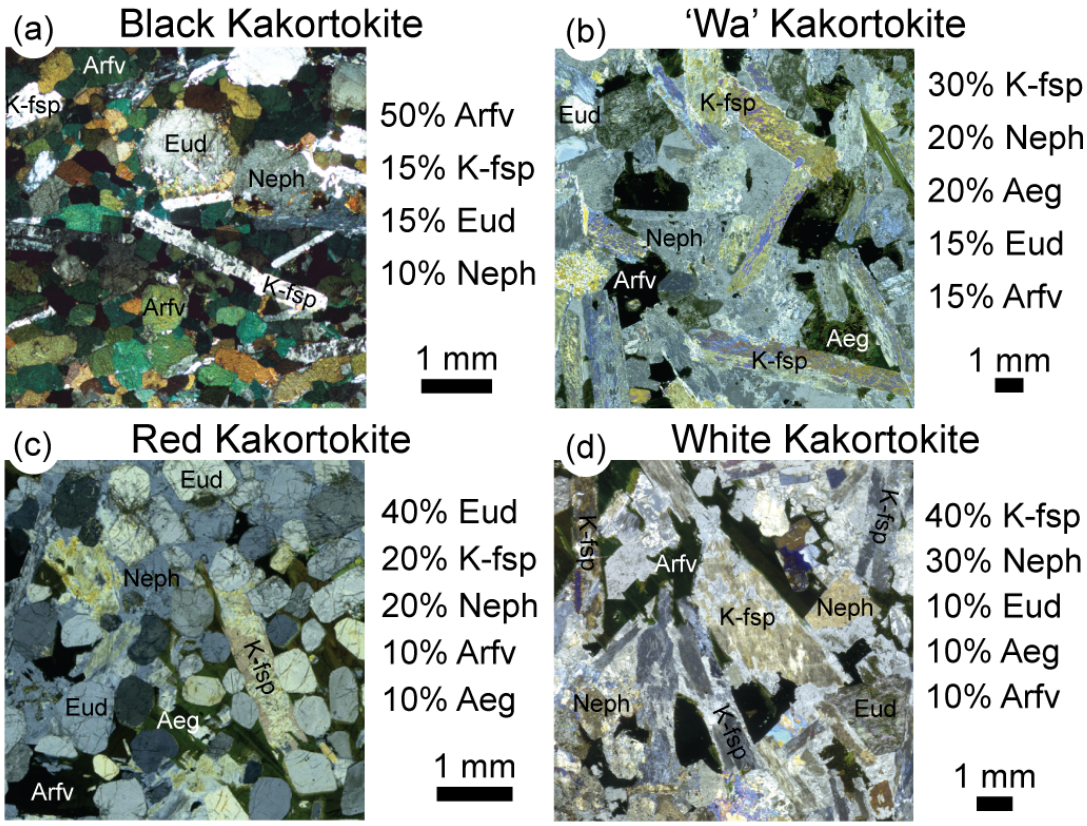

Figure 5.3: Typical kakortokite textures and compositions. (a) Black kakortokite, Unit 0 – sample AF/99/192. (b) Subordinate white kakortokite, Unit -10 – sample EJH/12/219. (c) Red kakortokite, Unit 0 – sample EJH/12/080. (d) White kakortokite, Unit 0 – sample EJH/12/180. (a) = thin section, (b)-(d) polished sections. Aeg: aegirine, Arfv: arfvedsonite, Eud: eudialyte, K-fsp: alkali feldspar, Neph: nepheline.

The layering of the kakortokite is disrupted in some units by rocks with different textures and/or compositions, many of which are traceable across the entire outcropping layered series. The "hybrid" (Ferguson, 1970) or "slump" (Bohse *et al.*, 1971) rocks (Chapter 3.4.4), cut across the layered kakortokite (Fig. 5.4a) and were observed at varying stratigraphic heights between Units -7 and -2. These rocks and their origin are discussed in detail in Chapter 8.

The Units +15/+16 boundary is marked by a sequence of phonolite and pegmatite (Fig. 5.4b) and the Units -1/0 boundary by a vein of cataclastic alteration (Fig. 5.4c), which varies in thickness between 1 and 3.5 mm and a depth of 0.5 to 10 cm below the units boundary.

Minor pegmatitic bodies (Fig. 5.4d) also occur within the layered kakortokite, these are typically small and discontinuous, only affecting portions of a unit or layer. These were observed in Units -7W, -9W and -17W and -18W. Their typical composition is alkali feldspar and aegirine ± eudialyte, arfvedsonite and sodalite. Phonolite bodies occur in Units +3, +1W to +2B and -4W to -3B and are typically aegirine- and alkali feldspar-rich.

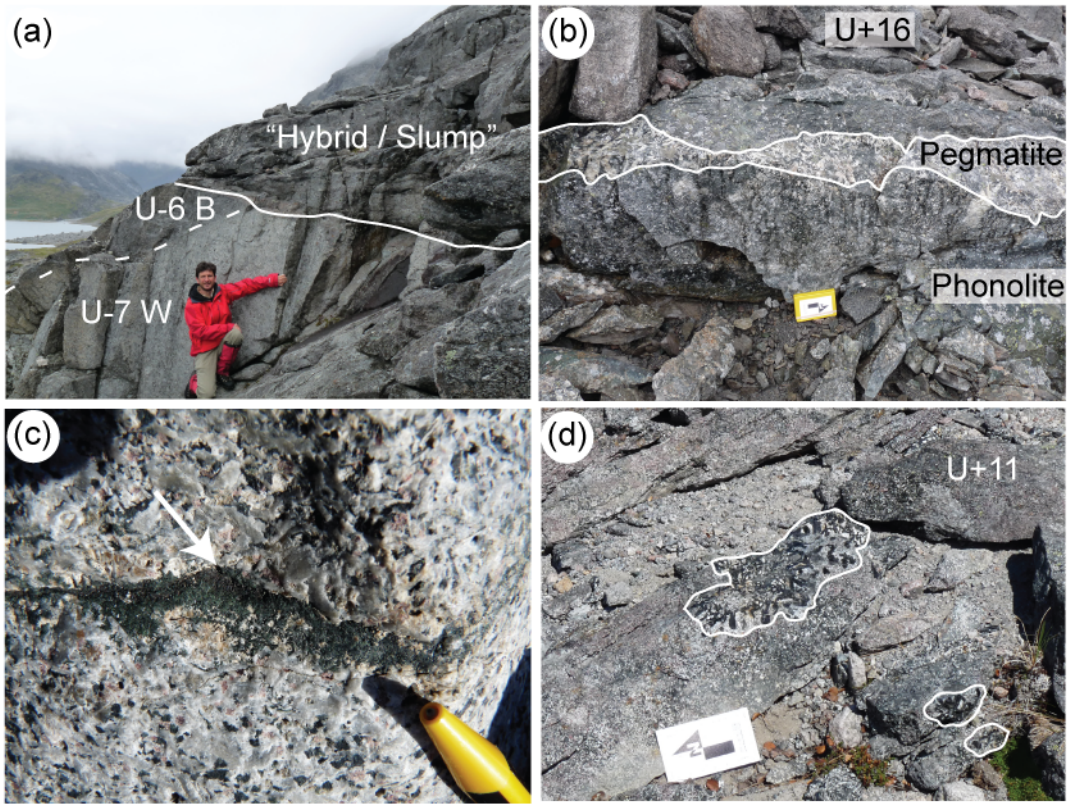

Figure 5.4: (a) "Hybrid/Slump" rocks crosscutting the layered kakortokite at the Units -7/-6 boundary, A Finch for scale = 1.81 m. (b) Pegmatite outlined in white, above phonolite at the Units +15/+16 boundary. (c) Vein of cataclastic alteration, arrowed, below the Units -1/0 boundary. (d) Minor pegmatite bodies, outlined in white, included in Unit +11. Scale card = 15 cm, pencil tip = 2 cm.

Extending the petrographic analysis to drill core allowed for the identification of the lower boundary of the layered kakortokite (Appendix B). It is not a planar contact and is transitional over 4 to 8 m, the depth varies between below Unit -16W in the northeast and below Unit -19B in the southwest. The underlying rock resembles the "hybrid"/"slump" sequence and was termed "Black Madonna" during drilling by TANBREEZ Greenland A/S (Schonwandt *et al.*, 2014). It is a fine- to medium-grained, mesocratic rock with bands of coarser-grained leucocratic material. Analysis of by TANBREEZ indicates it has a tephri-phonolite composition and is composed of aenigmatite, biotite, arfvedsonite, alkali feldspar, nepheline and sodalite (Schonwandt *et al.*, 2014).

Further occurrences of these "hybrid/slump" type rocks were observed in drill core. These rocks are not exposed at the surface but were observed between Units -12B in the southwest and -11W in the northeast in drill core. These rocks are again fine- to medium-grained, mesocratic and contain bands of a coarser-grained leucocratic rock. A 1.3 m thick, coarse-grained leucocratic rock composed of alkali

feldspar, aegirine and fluorite was observed between Units -13 and -14 in drill core. It has been termed a leucocratic lens in the present study.

Alteration of eudialyte is pervasive throughout the layered kakortokite, but is localised and patchy, occurring on a millimetre to metre scale. Crystals may display complete alteration, or alteration at the margins, while the neighbouring crystal is unaffected (Fig. 5.5a). Altered eudialyte is marked by a yellow appearance in hand specimen (Fig 5.5a) and is poly-crystalline in section (Fig 5.5b). The eudialyte is decomposed to a range of minerals including: pectolite, catapleiite, nacareniobsite-(Ce), britholite-(Ce) and zircon. Nepheline and aegirine additionally can occur within the boundaries of the decomposed eudialyte. In drill core the alteration was observed to affect up to 40% of the eudialyte within an individual layer. The processes and products of alteration and decomposition are discussed further in Chapter 6.6.

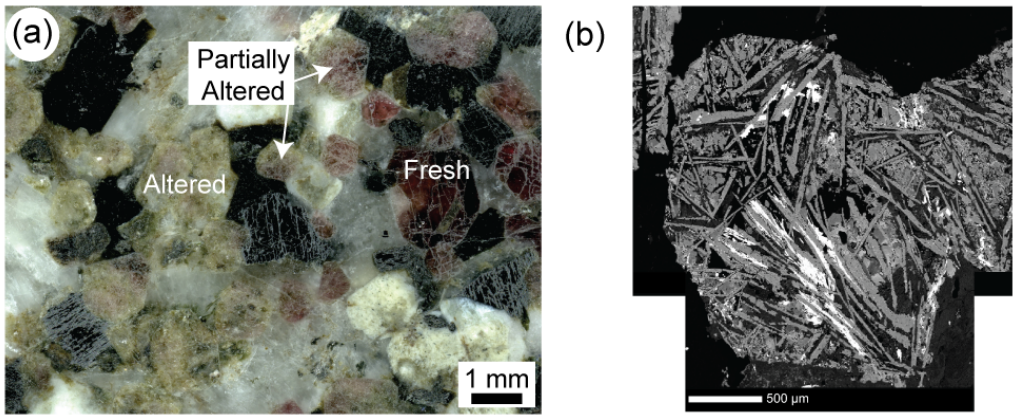

Figure 5.5: (a) Altered eudialyte (Unit -10R) displaying a yellow colour, neighbouring fresh eudialyte. (b) BSE image of completely decomposed eudialyte, Unit -10R.

5.3 Thicknesses of Kakortokite Units

Drill core (provided by TANBREEZ Mining Greenland A/S, Appendix B) was used to determine individual layer thicknesses (Table 5.2) and these were summed to calculate unit thicknesses. Previous studies have measured outcrops, however considerable estimation and calculation was required to provide the reported data (Bohse, 2012). Due to this, analysis of the more complete sections of drill core is a preferable way of determining unit thicknesses. Although errors in these measurements can occur if drilling was not orthogonal to the strike of the units, the measured thicknesses compare well between separate drill cores and units measured from outcrop. It should be noted though that some of the thicknesses presented in this study vary considerably from those published by Bohse *et al*. (1971).

Unit	Black	Wa	Red	White	Total
Mean	*1.0*	*3.0*	*2.9*	*4.0*	*7.0*
16	min. 2.0		ND	ND	2.0
15	1.3		1.6	min 0.1	2.9
14	1.8		2.8	1.3	5.9
13	0.9		0.5	2.6	4.1
12	2.2		3.8	3.2	9.2
11	1.5		0.5	4.2	6.1
10	1.6	4.8	1.2	1.2	8.7
9	1.8		4.7	3.3	9.7
8	1.9		2.2	3.4	7.4
7	0.6		1.4	5.8	7.8
6	1.7		1.2	2.4	5.3
5	1.1	1.5	1.0	0.9	4.5
4	2.6		1.6	3.2	7.4
3	0.5		1.2	0.9	2.6
2	min. 1.4		4.3	10.6	16.3
1	1.2		0.7	min. 4.1	6.0
0	0.7		1.9	5.1	7.8
-1	0.9		0.8	3.3	5.0
-2	1.3		0.6	2.4	4.3
-3	min. 0.5		2.3	7.1	9.9
-4	1.3	min. 4.3	min. 2.9	min. 4.8	13.3
-5	ND		min. 1.9	6.3	8.2
-6	0.4		2.5	1.9	4.8
-7	0.9		2.1	est. 4.7	7.6
-8	0.8		3.5	12.6	17.0
-9	1.1		1.4	est. 4.9	7.4
-10	1.0	3.5	1.3	6.6	12.4
-11	0.5		1.6	est. 7.5	9.5
-12	0.7		0.6	3.5	4.9
-13	0.2		min. 1.5	min. 3.1	4.8
-14	1.2		1.8	3.8	6.9
-15	0.7		2.5	2.5	5.7
-16	1.7		0.5	2.9	5.1
-17	ND		min. 0.6	2.5	3.1
-18	0.3		2.9	2.1	5.3
-19	min. 0.2		0.5	2.9	3.6

Table 5.2: Layer thicknesses measured from drill core during this study. Where boundaries were gradational (section 5.4) the midpoint of the gradational boundary was taken for the unit/layer boundary. Min. = minimum thickness of layer due to contact with pegmatite or phonolite body. Est. = estimated thickness of layer where it contains a pegmatite or phonolite body. N.D. = no data, layer was missing from or not present in drill core.

5.4 Petrological Descriptions of Each Unit

The typical unit, as defined by the Unit 0 marker horizon, forms above a sharp and distinct boundary from the underlying unit and has a black-red-white stratigraphy. However, not all units display this structure as the black and/or red kakortokites can be poorly developed and some units contain a subordinate white kakortokite layer ('Wa') between the black and red kakortokites. These variations throughout the 36 units allow each to be distinguished through the layered series. The main compositional difference throughout the layered kakortokite is the variation in sodalite (observed through shortwave UV fluorescence) between 0 to 30%.
The key mineralogical and textural characteristics of each unit and layer are tabulated in Table 5.3. They were derived from core logs (Appendix B) taken during the present study (cores DX-01 and DDH-07-1 owned by TANBREEZ Mining Greenland A/S) and supplemented with observations from outcrop, hand specimens and thin/polished sections.

Unit	Black	'Wa'	Red	White
+16	Poor foliation carried by K-fsp. 55% arfv, 30% sod, 5% K-fsp, 5% eud, 5% neph. Sharp contact to pegmatite below.		Strong red, saccharoidal, patchy alteration. 40% eud, 20% sod, 15% K-fsp, 10% arfv (euhedral needles), 10% neph, 5% aeg.	Melanocratic and rich in arfv & aeg. Moderate foliation carried by K-fsp and arfv. 25% k-K-fsp, 25% aeg, 25% neph, 15% arfv, 10% eud. No sodalite.
+15	Moderate foliation carried by K-fsp & arfv. 25% aeg, 20% arfv, 20% K-fsp, 10% sod, 10% eud, 10% neph. Sharp contact to +14W.		Dark red layer, poor foliation carried by K-fsp & arfv. Eud altered in patches. 30% eud, 20% aeg, 15% sod, 15% arfv, 15% K-fsp, 5% neph.	Angular contact to phonolite above. Not foliated. 35% K-fsp, 20% neph, 20% eud, 15% aeg, 10% arfv. Relatively sharp boundary to +15R.
+14	Sodalite occurs, moderately foliation (carried by K-fsp & arfv). 25% arfv, 20% aeg, 20% K-fsp, 15% eud, 15% neph, 5% sod.		Spotted texture due to aegirine, no sod. 30% K-fsp, 25% eud, 20% aeg, 15% arfv, 5% neph.	Spotted texture due to aegirine. Poorl foliation identified by K-fsp. Sod increases upwards to +15B. 30% K-fsp, 20% aeg, 20% neph, 15% eud, 5% arfv, 5% sod.

Table 5.3: Textures, modal mineralogy and unit/layer boundary characteristics determined in this study. Unless stated all boundaries were gradational over less than 15 cm. Aeg: aegirine, Arfv: arfvedsonite, Eud: eudialyte, K-fsp: alkali feldspar, Neph: nepheline.

Unit	Black	'Wa'	Red	White
+13	Good black, sod appears 10 cm above +12/+13 boundary. 60% arfv, 15% sod, 10% eud, 10% K-fsp, 5% aeg.		Thin red layer with patchy alteration, eud decreases upwards. 50% eud, 25% arfv (euhedral needles), 10% aeg, 10% K-fsp, 5% sod.	Very poor foliation, sharp boundary to +15B. Sod typically < 5%, 30% K-fsp, 20% neph, 20% aeg, 15% arfv, 10% eud, 5% sod.
+12	Good black. 30% arfv, 25% aeg, 20% K-fsp, 10% eud, 10% neph, 5% sod (patchy, 0-8%). Presumed sharp +11/+12 boundary, core broken with no gradation.		Greatest proportion of eudialyte in centre of layer. Occasional sod crystals. 35% eud, 30% K-fsp, 20% aeg, 10% arfv, 5% neph.	Good white, very leucocratic. Sharp +12/+13 boundary. 40% K-fsp, 15% sod (increases upwards to 13B, 0-20%), 15% aeg, 10% eud, 10% arfv, 5% neph.
+11	Strong black, sod increases upwards to +11R (max. 5%). 70% arfv, 20% K-fsp, 5% eud, 5% aeg.		Eud decreases upwards, saccharoidal at base of layer but foliated at top (carried by K-fsp). Patchy alteration of eud. 40% eud, 30% K-fsp, 20% aeg, 10% arfv, 8% neph, 2% sod.	Dark white, aeg-rich. 35% K-fsp, 30% aeg, 20% neph, 10% eud, 3% arf, 2% sod (patchy, 0-5%).
+10	Good black, foliation carried by K-fsp. 40% arfv, 30% K-fsp, 15% aeg, 10% eud, 5% sod (decreases upwards to 0%).	Dark white, sod-rich. 30% K-fsp, 30% sod, 15% arfv, 15% aeg, 10% eud.	Patchy alteration of eud. Sod-rich. 40% eud, 35% sod, 20% aeg, 5% K-fsp.	Patchy aeg. 40% K-fsp, 20% aeg, 15% eud, 10% sod (decreases upwards to +11B [35-5%]), 5% arfv.
+9	Poor foliation carried by K-fsp, small sodalite crystals (~1 mm), patchy eud alteration. 40% arfv, 20% aeg, 15% sod, 15% K-fsp, 10% eud.		Good red and saccharoidal. Patchy alteration to pink eud, sod decreased in altered patches. 40% eud, 20% sod, 20% aeg, 20% K-fsp.	Good white. 50% K-fsp, 15% neph, 15% arfv, 10% eud, 5% sod (patchy: 0-10%), 5% aeg.
+8	Strong black, no foliation, patches of sodalite throughout. 40% arfv, 20% aeg, 20% K-fsp, 10% neph, 5% eud, 5% sod.		Patchy alteration with one phonolite band. 40% eudialyte, 20% sodalite, 15% K-fsp, 15% aeg, 10% arfv.	Sharp boundary to +9B, marked by K-fsp band. Well-developed white, less sod than +8R. 50% K-fsp, 15% sod, 10% eud, 10% neph, 10% arfv, 5% aeg.
+7	Aeg-rich black. 40% aeg, 30% arfv, 20% K-fsp, 10% eud.		Good red, sharp boundary to +7B below. 50% eud, 20% aeg, 20% K-fsp, 10% neph.	Sharp & distinct +7/+8 boundary. 30% K-fsp, 20% aeg (decreases upwards), 15% sod, 10% eud, 5% arfv.

Table 5.3 (continued): Textures, modal mineralogy and unit/layer boundary characteristics determined in this study. Unless stated all boundaries were gradational over less than 15 cm. Aeg: aegirine, Arfv: arfvedsonite, Eud: eudialyte, K-fsp: alkali feldspar, Neph: nepheline.

Unit	Black	'Wa'	Red	White
+6	Some pegmatite alteration in centre of layer over 30 cm (aeg & K-fsp). 60% aeg, 15% K-fsp, 10% eud, 5% sod.		Altered & aeg-rich. No foliation. 40% eud, 30% aeg, 20% K-fsp, 10% neph.	Moderate foliation carried by K-fsp. 60% K-fsp, 20% aeg, 10% sod, 5% eud, 5% neph.
+5	Strong black. 70% arv, 15% eud, 10% K-fsp, 5% sod.	Aeg-rich. 40% aeg, 20% eud, 20% K-fsp, 10% sod, 10% neph.	Saccharoidal, pink eud. 30% eud, 25% K-fsp, 5% sod, 5% arfv.	Core missing at +5/+6 boundary, presumed sharp contact. Aeg-rich white, non-foliated. 50% K-fsp, 30% aeg, 10% eud, 5% arfv, 5% sod.
+4	Aeg-rich black. 40% aeg, 20% arfv, 20% K-fsp, 10% eud, 5% neph, 5% sod. +3/+4 boundary cut by phonolite.		Patchy aeg, no foliation. 30% aeg, 20% eud, 30% K-fsp, 15% sod, 5% arfv.	Sharp +4/+5 boundary. K-fsp randomly orientated, up to 40% sod. 50% K-fsp, 20% aeg, 10% sod, 10% neph, 10% eud.
+3	Poorly developed black with phonolite patches. 20% arfv, 20% aeg, 20% K-fsp, 20% eud, 15% sod, 5% neph.		Saccharoidal, some eud alteration. 40% eud, 30% K-fsp, 15% sod. 10% aeg, 5% arfv.	Alteration occurs as bands of K-fsp & eud. 40% aeg, 30% K-fsp,15% sod, 10% aeg, 5% arfv.
+2	Poor foliation defined by K-fsp. Dark black layer. 50% arfv, 30% sod, 15% K-fsp, 5% eud.		Non-foliated. 30% eud, 30% sod, 25% aeg, 10% K-fsp, 5% arfv.	+2/+3 boundary indistinct with phonolite patches. Altered with eud-rich phonolite patches. 30% K-fsp, 30% eud, 15% aeg, 15% sod.
+1	Occasional sod crystals, poor foliation defined by K-fsp. 50% arfv, 25% neph, 20% K-fsp, 5% eud.		Patchy alteration. 40% eud, 30% K-fsp, 20% mafic, 10% sod.	Dark white, spotted aeg & arfv. 40% K-fsp, 20% aeg, 15% arf, 15% neph, 10% sod, 5% eud.
0	Strong black, no foliation, <1% sod. 60% arfv, 20% K-fsp, 15% eud, 5% neph.		Strong red, saccharoidal, up to 5% sod, localised patchy alteration. 40% eud, 20% K-fsp, 20% neph, 10% arfv, 10% aeg.	Sharp 0/+1 boundary. 40% K-fsp, 20% neph, 15% sod (increases up from 0R boundary to max 30% then decreases to +1B boundary), 10% arfv, 10% aeg, 5% eud.

Table 5.3 (continued): Textures, modal mineralogy and unit/layer boundary characteristics determined in this study. Unless stated all boundaries were gradational over less than 15 cm. Aeg: aegirine, Arfv: arfvedsonite, Eud: eudialyte, K-fsp: alkali feldspar, Neph: nepheline.

Unit	Black	'Wa'	Red	White
-1	Poor black. 30% aeg, 30% arfv, 25% K-fsp, 10% sod, 10% eud, 5% neph.		Poor red, patchy alteration. 30% eud, 30% sod, 20% arfv, 15% K-fsp, 5% aeg.	Sharp -1/0 boundary. Dark white, poor foliation defined by K-fsp. 40% K-fsp, 30% neph, 20% aeg, 15% arfv, 10% eud, 5% sod (decreases upwards 20-0%).
-2	Strong black, poor foliation defined by K-fsp. 50% arfv, 30% sod, 15% K-fsp, 5% eud.		Strong red, patchy alteration. 40% eud, 25% sod, 20% arfv, 10% K-fsp, 5% neph.	Indistinct -2/-1 boundary. Relatively dark white, large aeg phenocrysts (~1 cm). 40% K-fsp, 20% aeg, 20% neph, 10% arfv, 5% eud, 5% sod (varies from 0 to 5%).
-3	Strong black, no foliation. 50% arfv, 20% neph, 15% sod, 10% K-fsp, 5% eud.		Patchy alteration above contact to -3B, least alteration in centre of layer. Contact to -3W displays arfv oikocrysts. Potentially 3 phases of eud (red, pink & altered yellow). Centre: 50% eud, 30% arfv, 15% K-fsp, 10% neph, 5% sod.	Sharp -3/-2 boundary. Poor foliation defined by K-fsp. 40% K-fsp, 15% sod (increases upwards 0% to 20%), 15% neph, 15% arfv, 10% aeg, 5% eud.
-4	Foliated, defined by K-fsp. 30% arfv, 30% aeg, 20% K-fsp, 10% neph, 10% eud.	Sod varies from 0-10%, some eud-rich bands. Average comp: 40% K-fsp, 20% aeg, 20% neph, 10% sod, 5% arfv, 5% eud.	Moderate foliation defined by K-fsp, patchy alteration of eud. 30% eud, 30% K-fsp, 20% aeg, 10% neph, 5% sod, 5% arfv.	Phonolite present at -3/-4 boundary. Good foliation defined by K-fsp. Sod xtls variable, size varies from <1 mm to >1 cm. 40% K-fsp, 35% aeg, 10% eud, 10% arfv, 5% sod.
-5	Where exposed it is a well-developed, arfv-rich black. In most exposures and in drill core it is replaced by "hybrid/slump" rocks.		Altered at contact to hybrid with large aeg xtls (up to 3 cm). Strong red with oikocrystic arfv. 30% eud, 20% arfv, 20% K-fsp, 20% sod, 10% aeg.	Sharp -5/-4 boundary. Strong K-fsp, no preferred orientation. 50% K-fsp, 15% aeg, 15% sod, 10% neph, 10% eud.

Table 5.3 (continued): Textures, modal mineralogy and unit/layer boundary characteristics determined in this study. Unless stated all boundaries were gradational over less than 15 cm. Aeg: aegirine, Arfv: arfvedsonite, Eud: eudialyte, K-fsp: alkali feldspar, Neph: nepheline.

Unit	Black	'Wa'	Red	White
-6	Aeg-rich black. 30% aeg, 25% arfv, 25% sod, 15% K-fsp, 5% eud.		Very strong & thick red layer, patchy alteration of eud. Aeg coarsens upwards at contact to -6W. 50% eud, 25% aeg, 10% K-fsp, 10% sod. 5% neph.	Good foliation defined by K-fsp.40% K-fsp, 30% aeg, 10% eud, 10% neph, 5% arfv, 5% sod.
-7	Strong black, no foliation, no sodalite. 70% arfv, 15% K-fsp, 10% neph, 5% eud.		Good red, saccharoidal, patchy alteration of eud. 40% eud, 25% K-fsp, 20% aeg, 10% arfv, 5% neph. Patches of sodalite.	Foliated, defined by K-fsp. 40% K-fsp, 20% neph, 20% aeg, 15% sod, 5% eud.
-8	Foliated, defined by K-fsp & arfv. 30% arfv, 30% K-fsp, 15% aeg, 15% eud 10% neph. <5% sod.		Saccharoidal, patchy alteration of eud. 40% eud, 20% sod, 20% K-fsp, 10% arfv, 10% neph.	Sharp -8/-7 boundary. Poor foliation defined by K-fsp, eud very altered. 60% K-fsp, 15% sod (decreases upwards to <5%), 15% eud, 15% neph, 5% aeg, 5% arfv.
-9	Dark black, foliation defined by K-fsp. 50% arfv, 20% aeg, 15% K-fsp, 10% eud, 5% neph. ~1% sod.		Localised sod (0-5%), foliation defined by K-fsp. 40% K-fsp, 30% eud, 20% aeg, 7% neph, 3% arfv.	Strong white. Sharp -9/-8 boundary. 40% K-fsp, 30% neph, 15% arfv, 10% eud, 5% aeg.
-10	Well developed, well foliated, defined by K-fsp. 45% arfv, 25% K-fsp, 20% sod, 5% neph, 5% eud.	Subordinate white layer, transitions from -10B over 5 cm. 30% K-fsp, 20% sod, 20% aeg, 15% eud, 15% arfv.	Poor foliation defined by arfv. Patchy alteration of eud. 40% eudialyte, 30% K-fsp, 15% aeg, 10% neph, 5% aeg. <1% sod.	Sharp -10/-9 boundary. Dark white, poor foliation. 50% K-fsp, 25% neph, 15% eud, 5% aeg, 5% arfv. <1% sod.
-11	Well-developed, very dark, no sod. 70% arfv. 15% neph, 13% K-fsp, 2% eud.		Gradual increase in eud from -11B, no sod, eud in bands not evenly distributed. 15-40% eud. Avg: 35% eud, 30% sod, 15% K-fsp, 15% arfv, 5% aeg.	Becomes more foliated upwards (defined by K-fsp). 50% K-fsp, 20% neph, 10% aeg, 10% eud, 5% sod, 5% aeg. <5% sod.
-12	Well foliated, defined by K-fsp & arfv. 40% arfv, 25% K-fsp, 10% aeg, 10% neph, 10% sod, 5% eud.		30% eud, 30% K-fsp, 15% aeg, 10% neph, 10% sod, 5% arfv.	Sharp -12/-11 boundary. Strong white, moderate foliation defined by K-fsp. 50% K-fsp, 15% eud, 10% neph, 10% sod, 10% aeg, 5% arfv.

Table 5.3 (continued): Textures, modal mineralogy and unit/layer boundary characteristics determined in this study. Unless stated all boundaries were gradational over less than 15 cm. Aeg: aegirine, Arfv: arfvedsonite, Eud: eudialyte, K-fsp: alkali feldspar, Neph: nepheline.

Unit	Black	'Wa'	Red	White
-13	Dark black, poor foliation defined by K-fsp. 60% arfv, 15% K-fsp, 10% eud, 10% neph, 5% sod.		Very eudialyte-rich, saccharoidal. Patchy alteration of eud. 60% eud, 15% sod, 10% aeg, 8% arfv, 7% K-fsp.	Sharp, steeply dipping -13/-12 boundary. Moderate foliation defined by K-fsp. 50% K-fsp, 15% neph, 10% sod, 10% aeg, 10% arfv, 5% eud.
-14	Foliated, defined by K-fsp & arfv. 40% arfv, 25% K-fsp, 10% aeg, 10% eud, 10% neph, 5% sod.		Poor red, foliated (K-fsp). 30% eud, 20% K-fsp, 20% aeg, 10% neph, 10% arfv, 10% sod.	Foliated, defined by K-fsp. 40% K-fsp, 20% aeg, 15% neph, 10% sod, 10% eud, 5% arfv.
-15	Strong black, moderate foliation defined by K-fsp & arfv. 40% arfv, 25% K-fsp, 10% aeg, 10% eud, 10% neph, 5% sod.		Saccharoidal, some K-fsp lathes aligned. Some eud xtls altered at margins. 40% eud, 20% K-fsp, 15% aeg, 10% neph, 10% sod, 5% arfv.	Sharp -15/-14 boundary. Textures vary from oikocrystic (arfv) and foliated (K-fsp). 35% K-fsp, 15% neph, 15% aeg, 10% sod, 10% arfv, 15% eud.
-16	Leucocratic black with patches of eud. 30% arfv, 20% sod, 20% aeg, 20% K-fsp, 10% eud.		Saccharoidal, patchy alteration. 40% eud, 20% K-fsp, 20% sod, 10% aeg, 10% arfv.	Sharp -16/-15 boundary, poor foliation, melanocratic white. 35% K-fsp, 20% neph, 15% aeg, 10% sod, 10% eud, 10% arfv.
-17	Replaced by pegmatite.		Patchy alteration of eud. Saccharoidal, K-fsp defines some foliation. 40% eud, 30% K-fsp, 15% sod, 10% aeg.	Sharp & distinct -17/-16 boundary. Arfv-rich band in centre of layer (alteration?). Foliated, defined by K-fsp. 50% K-fsp, 15% aeg, 15% eud, 10% sod, 10% arfv.
-18	Strong black, foliated (K-fsp lathes). 50% arfv, 30% K-fsp, 10% sod, 10% eud.		Strong red, patchy alteration of eud. 60% eud. 20% sod, 15% arfv, 10% aeg, 10% neph, 5% K-fsp.	Sharp & distinct -18/-17 boundary Foliated, defined by K-fsp & arfv. 40% K-fsp, 20% sod, 15% arfv, 10% aeg, 10% neph, 5% eud.
-19	Thin layer above transition. Strong black, no foliation. 60% arfv, 20% eud, 15% K-fsp, 5% sod.		Thin red layer, foliated (K-fsp lathes). Minor alteration at rims of eud xlts. 40% eud, 30% K-fsp, 20% arfv, 5% sod, 5% aeg.	Sharp & distinct -19/-18 boundary. Melanocratic white. 40% K-fsp, 20% arfv, 15% sod, 10% neph, 10% eud, 5% aeg.

Table 5.3 (continued): Textures, modal mineralogy and unit/layer boundary characteristics determined in this study. Unless stated all boundaries were gradational over less than 15 cm. Aeg: aegirine, Arfv: arfvedsonite, Eud: eudialyte, K-fsp: alkali feldspar, Neph: nepheline.

5.5 Conclusions

The layering of the kakortokite is remarkably homogeneous across the layered series and each layer is laterally consistent. Variations between individual units (Table 5.3) allow each to be distinguished in the layered series. The boundaries between units are typically distinct, planar and can be traced laterally, while the intra-unit boundaries are gradational over 2 to 15 cm. The typical unit structure is black-red-white kakortokite. There are variations as poorly developed black and/or red kakortokite layers were observed and a subordinate white kakortokite ('Wa') was also observed in some units. Minor inclusions of pegmatite and phonolite occur within the layered kakortokite, these are typically small and discontinuous. Occasionally these rocks are thicker and laterally continuous, such as the phonolite and pegmatite below Unit +16 and the "hybrid/slump" sequence. The key observation is that the composition and textures of each layer are laterally continuous across the series.

5.6 References

Bohse, H., Brooks, C. K. & Kunzendorf, H. (1971). Field observations on the kakortokites of the Ilimaussaq intrusion, South Greenland, including mapping and analyses by portable X-ray fluorescence equipment for zirconium and niobium. *Rapport Grønlands Geologiske Undersølgelse* **38**, 43 pp.

Ferguson, J. (1970). The significance of the kakortokite in the evolution of the Ilímaussaq intrusion, South Greenland. *Meddelelser om Grønland* **190**, 1-193.

Larsen, L. M. & Sørensen, H. (1987). The Ilímaussaq intrusion - progressive crystallisation and formation of layering in an agpaitic magma. *Geological Society London, Special Publications* **30**, 473-488.

Le Maitre, R. W. (ed.) (2002). *Igneous Rocks A Classification and Glossary of Terms*. Cambridge: Cambridge University Press

Pfaff, K., Krumrei, T., Marks, M. A. W., Wenzel, T., Rudolf, T. & Markl, G. (2008). Chemical and physical evolution of the 'lowered layered sequence' from the nepheline syenitic Ilímaussaq intrusion, South Greenland: Implications for the origin of magmatic layering in peralkaline felsic liquids. *Lithos* **106**, 280-296.

Schonwandt, H. K., Barnes, G. B. & Ulrich, T. (2014). The world-class REE deposit Tanbreez, South Greenland: its size and structure. *ERES2014: 1st European Rare Earth Resources Conference*. Milos.

Sørensen, H. (1969). Rythmic igneous layering in peralkaline intrusions: An essay review on Ilímaussaq (Greenland) and Lovozero (Kola, USSR). *Lithos* **2**, 261-283.

Chapter 6

Development of the Marker Horizon: Unit 0

6.1 Introduction

Unit 0 is exceptionally well developed, with a relatively arfvedsonite enriched black kakortokite and eudialyte enriched red kakortokite. This allows it to be easily distinguished from a distance (over 5 km) and as such was used by Bohse *et al.* (1971) as their marker horizon for numbering the outcropping kakortokite units. This makes the unit ideal for an initial investigation into the development of layering in the kakortokite. Most hypotheses invoke formation of the layering through gravitational settling and density sorting (Ferguson, 1964, Larsen & Sørensen, 1987, Sørensen & Larsen, 1987). However this was disputed by Pfaff et al. (2008). This chapter presents the results of a combined petrographic, crystal size distribution (CSD) and mineral chemical study of samples from four locations across the layered series (Fig. 6.1). This allows for an assessment of lateral variations and to obtain quantitative insights into nucleation and growth during the formation and solidification of the marker horizon Unit 0. The data are not consistent with formation of the unit purely through gravitational settling and instead a model of ordered nucleation is proposed.

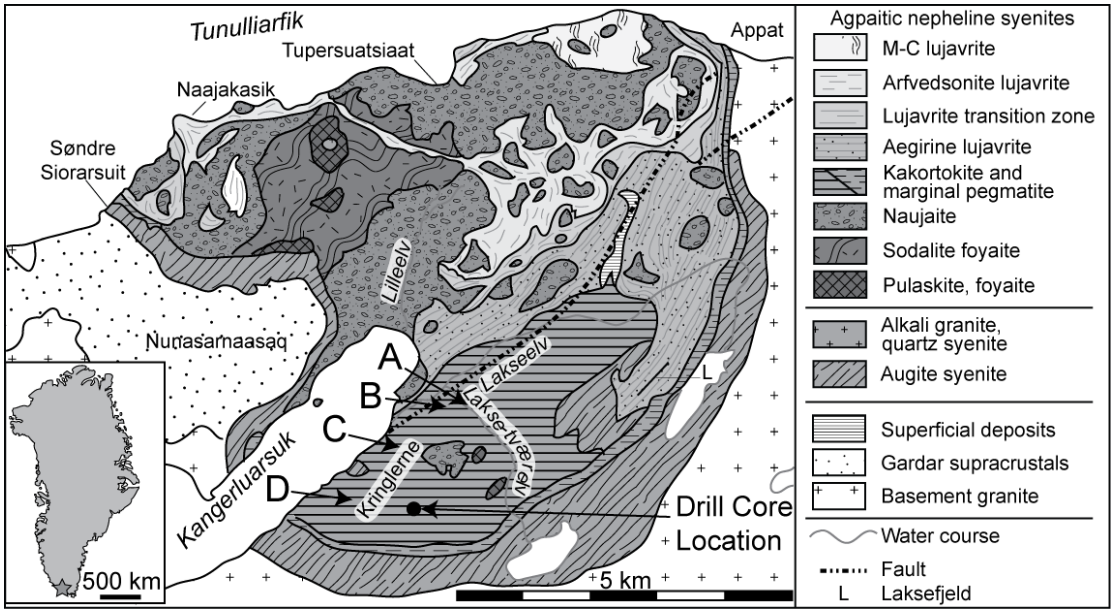

Figure 6.1: Geological sketch map of the southern part of the Ilímaussaq complex displaying sampling locations A-D and the location of the studied drill core (DX-01 from TANBREEZ Mining Greenland A/S).

6.2 Field Characteristics of Unit 0

Unit 0 is laterally continuous and remarkably uniform across the entire outcropping layered series (Fig 6.2a-b) and at all exposures it forms above a distinct, sharp and planar boundary from Unit -1 (Fig 6.2c-d, Fig 6.3a). There is no evidence of scouring or flow indicators, such as shearing of crystals or current bedding, throughout Unit 0. The thickness of the unit is relatively constant, compared across four outcropping locations and drill core (Fig 6.1). It is 7.8 m thick, of which the first 0.7 m is black kakortokite, overlain by 1.9 m of red kakortokite and then 5.1 m of white kakortokite (Fig. 6.2c). The contacts between each layer within Unit 0 are gradational over 2-5 cm (Fig 6.3b-c).

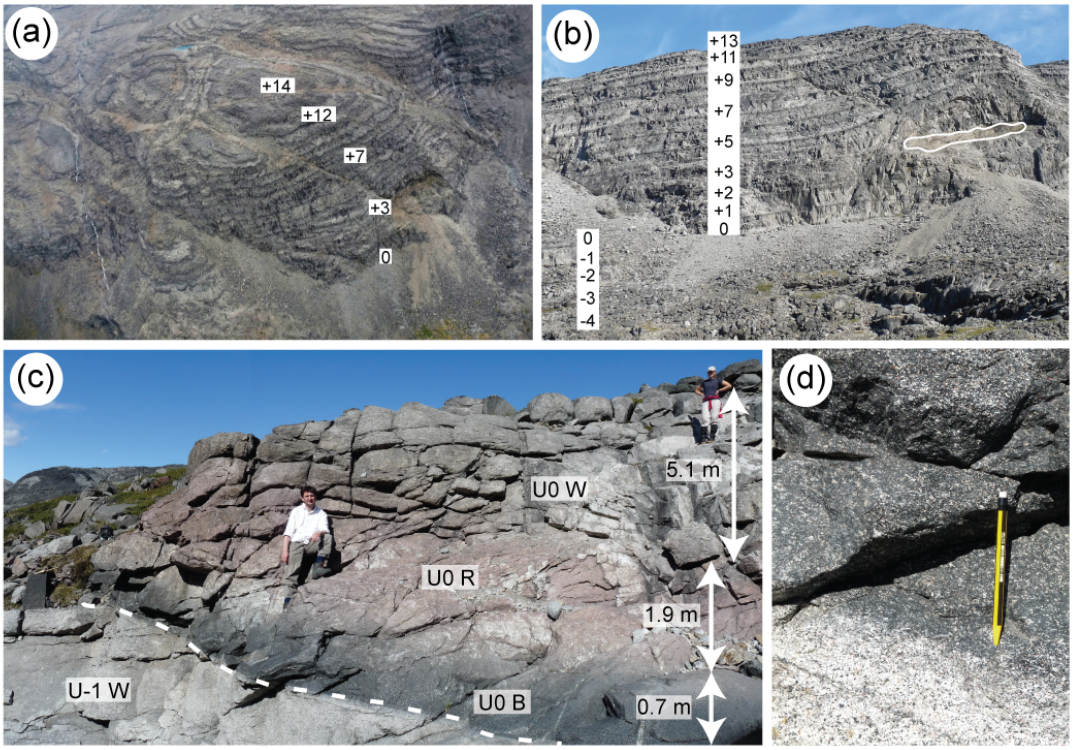

Figure 6.2: (a) Aerial view of layered kakortokite from Unit 0 at base of cliff face to Unit +16, typical unit thickness is 8 m. (b) Units -4 to +13 outcropping in cliff face, white line outlines roof rock autolith in U+3, typical unit thickness is 8 m. (c) Unit 0 outcrop at Location A, dashed white line marks sharp Units -1/0 boundary. A. Finch for scale ~1.8 m. (d) Sharp boundary between Unit -1 white kakortokite and Unit 0 black kakortokite at location A. Note alteration vein ~10 cm below boundary, pencil = 14 cm.

Below the Units -1/0 boundary is a vein of cataclastic alteration (Fig. 6.2d), it is laterally continuous, can be traced for kilometres across outcrop and was also observed in drill core. The depth of the vein below the U-1/0 boundary varies from 10 cm in the centre of the layered series (Location A, Fig 6.2d) to 0.5 cm towards the margin of the series (Location D). The thickness of the vein varies between 1 and 3.5

mm, it has irregular margins and is composed of arfvedsonite, aegirine and alkali feldspar (Fig. 6.3d). The presence of this vein is a useful marker for the U-1/0 boundary, and was used in the present study to identify Unit 0 in outcrop and drill core.

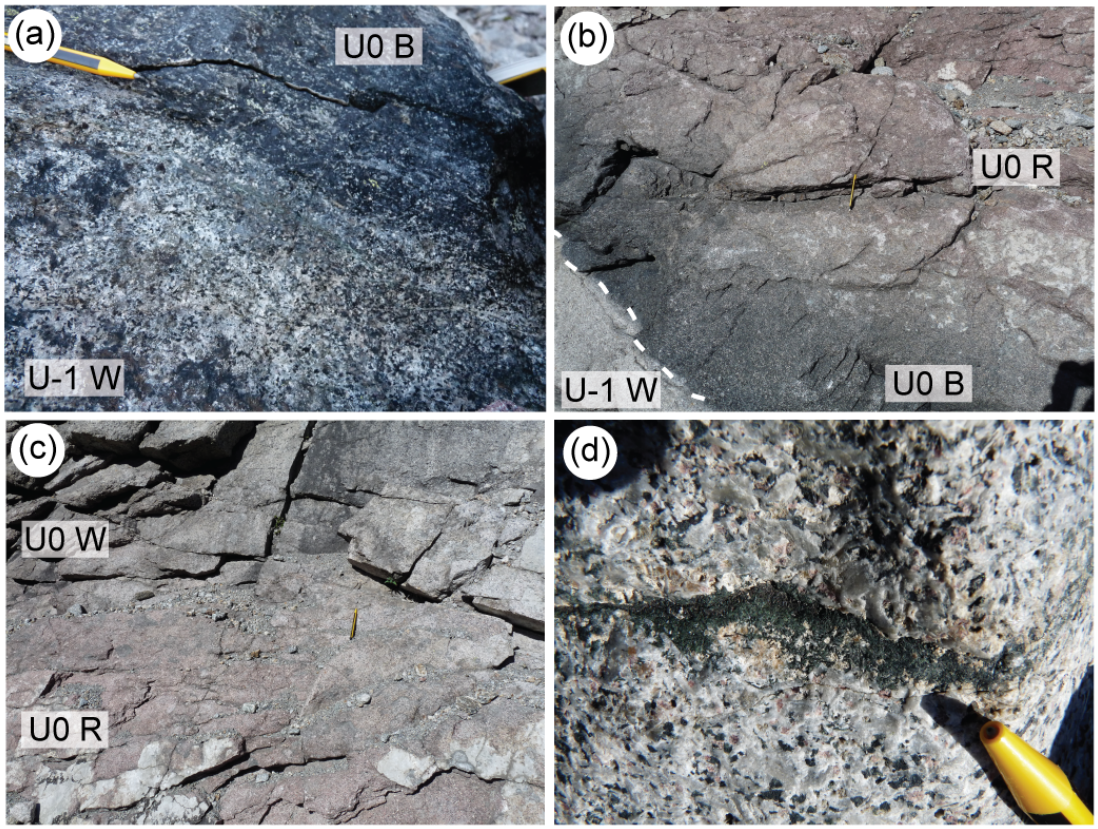

Figure 6.3: (a) Sharp Units -1/0 boundary at Location D. (b) Gradational boundary between Unit 0 black and red kakortokite at Location A with sharp Units -1/0 boundary across left corner, pencil for scale in centre of photo. (c) Gradational boundary between Unit 0 black and red kakortokite at Location A, pencil for scale in centre of photo. (d) Aegirine- and arfvedsonite-rich alteration vein below U-1/0 boundary at Location A. Scale pencil = 14 cm.

Bohse *et al.* (1971) studied Unit 0 in the vicinity of Location A and distinguished 7 sub-layers according to rock textures. An adapted description of these sub-layers is presented in Table 6.1. Although the present study does not subdivide the unit further than the unit boundary, black, red and white layers, Bohse *et al.* (1981) provide a good description of the vertical variations through the unit. Samples in the present study were collected from the equivalent of sublayers i, ii, iii, v, viii and ix.

Unit	Sub-layer	Kakortokite	Description	Height
U-1	i	White	Largely composed of 1 cm X 2.5 cm alkali feldspar crystals defining a marked lamination. Minor amounts of arfvedsonite and eudialyte.	
U-1/0	ii	Boundary	Very sharp, distinct and planar	0 m
U0	iii	Black	Rock composed mainly of arfvedsonite. Feldspar smaller in amount and size than U-1 white.	0-0.3 m
	iv	Black / Red	Very diffuse boundary between U0 black and U0 red.	0.3-0.7 m
	v	Red	Typical red kakortokite with saccharoidal texture due to abundance of equidimensional eudialyte.	0.7-1.2 m
	vi		Appears to be most eudialyte-rich part of red kakortokite	1.2-1.8 m
	vii	Red / White	Decreasing eudialyte content with top transitional to white kakortokite. Arfvedsonite poikilitically encloses eudialyte and nepheline.	1.8-2.9 m
	viii	White	White kakortokite. Alkali feldspar now coarser and similar to that in 'i' described above. Minor amounts of eudialyte, arfvedsonite still poikilitic.	2.9-3.8 m
	ix		White kakortokite very similar to 'i'. Arfvedsonite no longer poikilitic.	3.8-6.5 m

Table 6.1: Descriptions of rock textures through Unit 0 adapted from Bohse *et al.* (1971).

6.3 Petrography

Samples were collected from the Units -1/0 boundary, and Unit 0 black, red and white kakortokite at Locations A and B. At Location C the Units -1/0 boundary and Unit 0 red and white kakortokite were sampled. At Location D the Unit -1 white kakortokite, Units -1/0 boundary and Unit 0 red and poikilitic white kakortokite were sampled. Sample descriptions are located within Table 6.2 and photomicrographs of each sample in Figures 6.4 and 6.5.

The Unit 0 black kakortokite is massive and comprised of 60% arfvedsonite, 20% alkali feldspar (which displays a preferred alignment), 15% nepheline and 5% eudialyte. The arfvedsonite has an apparent bimodal size distribution with large, acicular crystals of arfvedsonite surrounded by a groundmass of equidimensional arfvedsonite crystals (Fig. 6.6a). The red kakortokite is saccharoidal and comprised of 40% eudialyte, 20% alkali feldspar, 20% nepheline, 10% arfvedsonite and 10% aegirine. The white kakortokite is commonly foliated with the fabric identified by alkali feldspar plates. It is typically comprised of 40% alkali feldspar, 20% nepheline, 10% sodalite, 10% arfvedsonite, 10% aegirine and 10% eudialyte. The white kakortokite of Unit 0 displays vertical variation as the base of the layer contains poikilitic arfvedsonite crystals. These decrease upwards and were only observed in the present study to occur in the lower 0.5 m of the unit. Eudialyte crystals in each of three rock types commonly display signs of poly-crystalline alteration. Typically a euhedral crystal outline is preserved while the crystal is pseudomorphed (Fig. 6.6b). The processes and products of this alteration are discussed in detail in section 6.6.

The samples from the Units -1/0 boundary have differing textural characteristics in comparison to the samples from the central portions of the layers. The U-1 white kakortokite samples immediately below (0-25 mm) the boundary typically display embayed alkali feldspar crystals and enclaves of microcrystic alkali feldspars (Fig. 6.6c). Immediately above the U-1/0 boundary (0-25 mm) the U0 black kakortokite contains heavily embayed alkali feldspar crystals, which display greater alteration compared to the portions of the same crystal below the boundary (Fig. 6.6d).

Loc.	Sample No.	Unit	Section Image	Petrography (modal %)
A	EJH/12/009	U-1/0	Figure 6.4b	U-1 White: K-fsp groundmass, 45%, defines foliation, some embayed. 20% neph, 20% arfv, 8% eud, 5% aeg, 2% sod.
				U0 Black: arfv groundmass, 55%, some phenocrysts. 22% K-fsp (commonly embayed, defines foliation), 16% neph, 5% eud, 2% sod.
	EJH/12/008	U0 Black	Figure 6.4f	Arfv groundmass, 48%, some phenocrysts. 23% K-fsp, 22% neph, 5% eud, 2% sod.
	EJH/12/007	U0 Red	Figure 6.5a	Eud groundmass, 59%. 12% K-fsp (defines a foliation fabric), 10% neph, 7% arfv, 7% aeg, 5% sod.
	EJH/12/010	U0 White	Figure 6.5e	K-fsp groundmass, 47%, defines foliation. 25% arfv, 15% neph, 8% eud, 5% sod.
B	AF/99/195	U-1/0	Figure 6.4c	U-1 White: groundmass of K-fsp (34%, defines foliation) and neph (30%). 10% aeg, 10% sod, 8% eud, 8% arfv.
				U0 Black: arfv groundmass, 54%. 20% K-fsp (embayed, defines foliation), 14% neph, 6% eud, 4% sod, 2% aeg.
	AF/99/192	U0 Black	Figure 6.4g	Arfv groundmass, 50%, some phenocrysts. 22% K-fsp, 17% eud, 11% neph, <1% sod.
	AF/99/193	U0 Red	Figure 6.5b	Eud groundmass, 55%, patchy alteration. 15% aeg, 14% neph, 10% K-fsp, 4% arfv, 2% sod.
	AF/99/191	U0 White	Figure 6.5f	K-fsp groundmass, 49%, defines foliation. 20% neph, 19% arfv, 6% aeg, 6% eud, 1% sod.
C	EJH/12/094	U-1/0	Figure 6.4d	U-1 White: K-fsp groundmass, 48%, defines foliation. 18% neph, 16% aeg, 10% eud, 8% arfv
				U0 Black: arfv groundmass, 61%, some phenocrysts. 18% K-fsp (often signs of resorption, defines foliation), 15% nepheline (some altered), 6% altered eud.
	EJH/12/095	U0 Red	Figure 6.5c	Eud groundmass, 50% (80% of which altered at margins. 22% K-fsp, 18% aeg, 10% neph.
	EJH/12/096	U0 White	Figure 6.5g	Neph groundmass, 45%, completely altered. 18% K-fsp (defines foliation), 15% eud, 12% arfv, 6% aeg, 4% sod.
D	EJH/12/081	U-1 White	Figure 6.4a	K-fsp groundmass, 50%, defines foliation. 20% arfv, 15% neph, 8% eud, 5% aeg, 2% sod.
	EJH/12/079	U-1/0	Figure 6.4e	U-1 White: sod groundmass, 42%. 20% K-fsp (defines foliation), 14% aeg, 10% arfv, 8% eud, 6% neph (altered).
				U0 Black: arfv groundmass, 72%. 14% K-fsp (often signs of resorption), 10% neph, 4% eud.
	EJH/12/080	U0 Red	Figure 6.5d	Eud groundmass, 48%, minor alteration at margins. 18% K-fsp, 15% arfv, 12% sod, 5% neph, 3% aeg.
	EJH/12/082	U0 White	Figure 6.5h	Neph groundmass, 55%. 15% K-fsp (defines foliation), 13% arfv (oikocrystic), 8% aeg, 7% eud, 2% sod.

Table 6.2: Description of samples according to locality and brief petrographic descriptions. Alteration refers to late-stage alteration of eudialyte, described in section 6.6. Aeg = aegirine, Arfv = arfvedsonite, Eud = eudialyte, K-fsp = alkali feldspar, Neph = nepheline, Sod = sodalite.

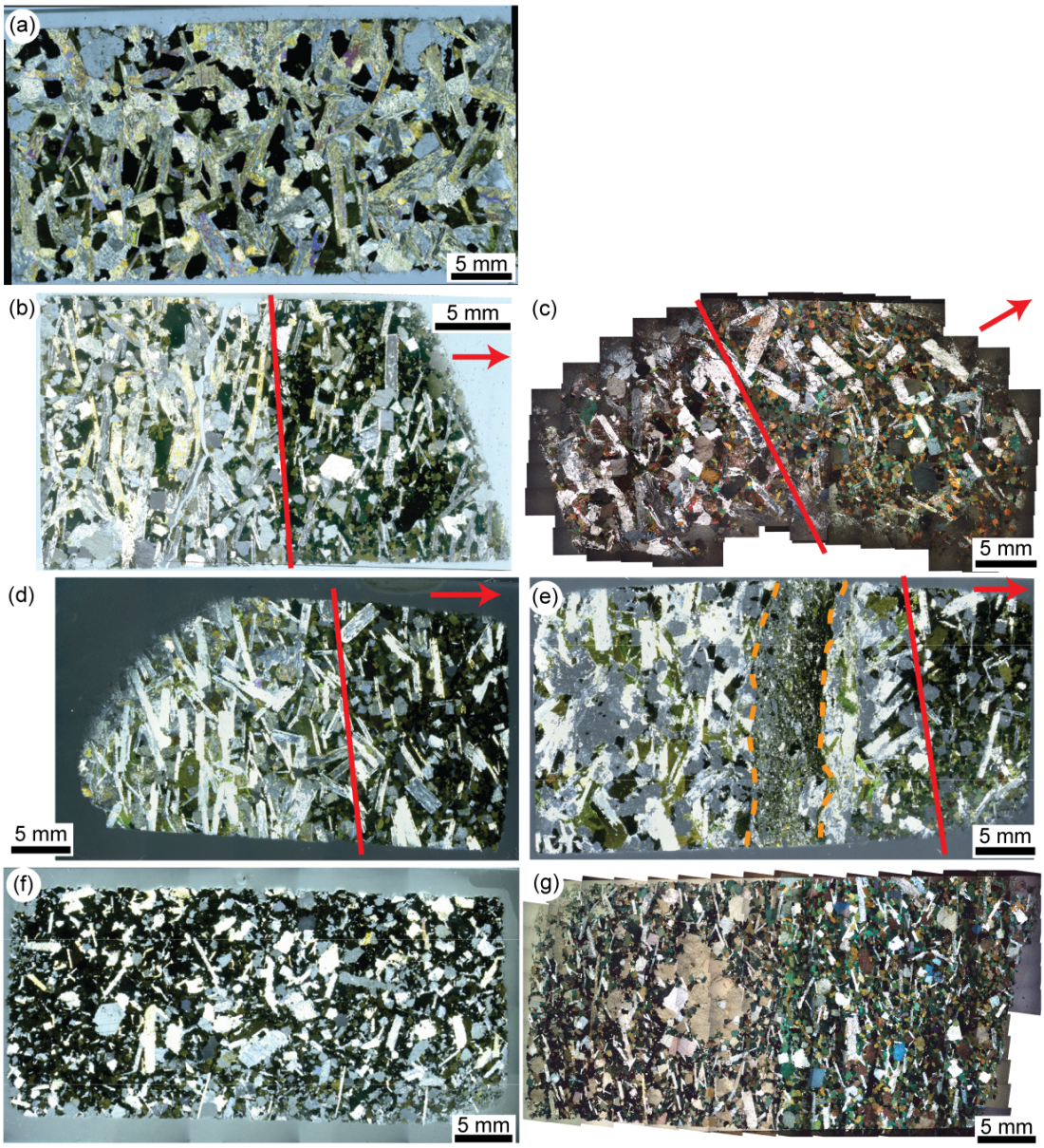

Figure 6. 4: (a) Unit -1 white kakortokite section, location D, sample EJH/12/081. (b) Units -1/0 boundary section, location A, sample EJH/12/009. (c) Units -1/0 boundary section, location B, sample AF/99/195. (d) Units -1/0 boundary section, location C, sample EJH/12/094. (e) Units -1/0 boundary section, location D, sample EJH/12/079, late stage cataclastic alteration band below boundary marked in orange. (f) Unit 0 black kakortokite section, location A, sample EJH/12/008. (h) Unit 0 black kakortokite section, location B, sample AF/99/192. NB all rock sections photographed under circularly polarised light, arfvedsonite can appear opaque in thick section.

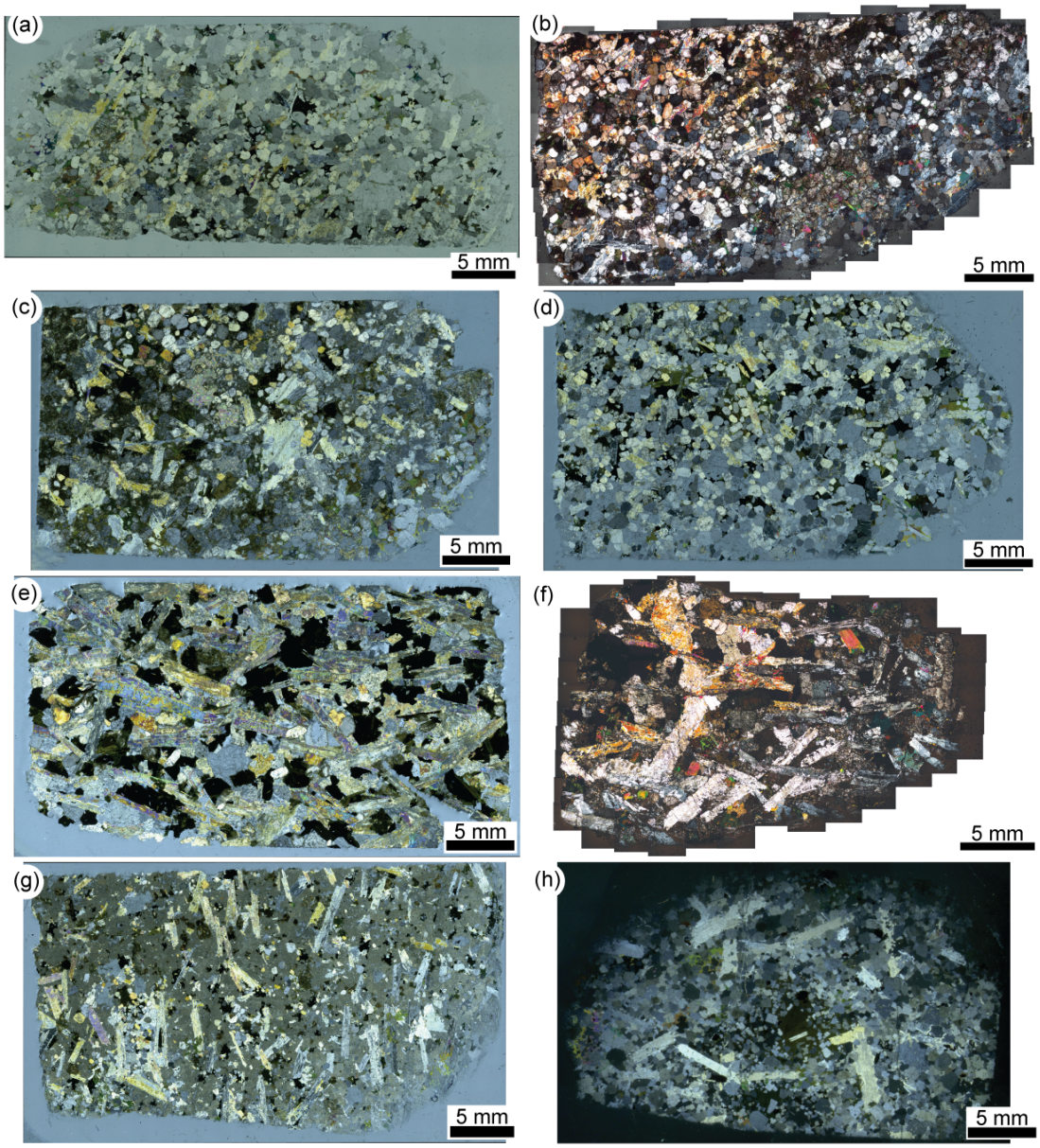

Figure 6.5: (a) Unit 0 red kakortokite section, location A, sample EJH/12/007. (b) Unit 0 red kakortokite section, location B, sample AF/99/193. Unit 0 red kakortokite section, location A, sample EJH/12/007, note patchy alteration of eudialyte. (c) Unit 0 red kakortokite section, location C, sample EJH/12/095, note patchy alteration of eudialyte. (d) Unit 0 red kakortokite section, location D, sample EJH/12/080. (e) Unit 0 white kakortokite section, location A, sample EJH/12/010. (f) Unit 0 white kakortokite section, location B, sample AF/99/191. (g) Unit 0 white kakortokite section, location C, sample EJH/12/096, note alteration of nepheline groundmass. (h) Unit 0 white kakortokite section, location D, sample EJH/12/082, note presence of arfvedsonite oikocrysts at bottom centre of section. NB all rock sections photographed under circularly polarised light, arfvedsonite can appear opaque in thick section.

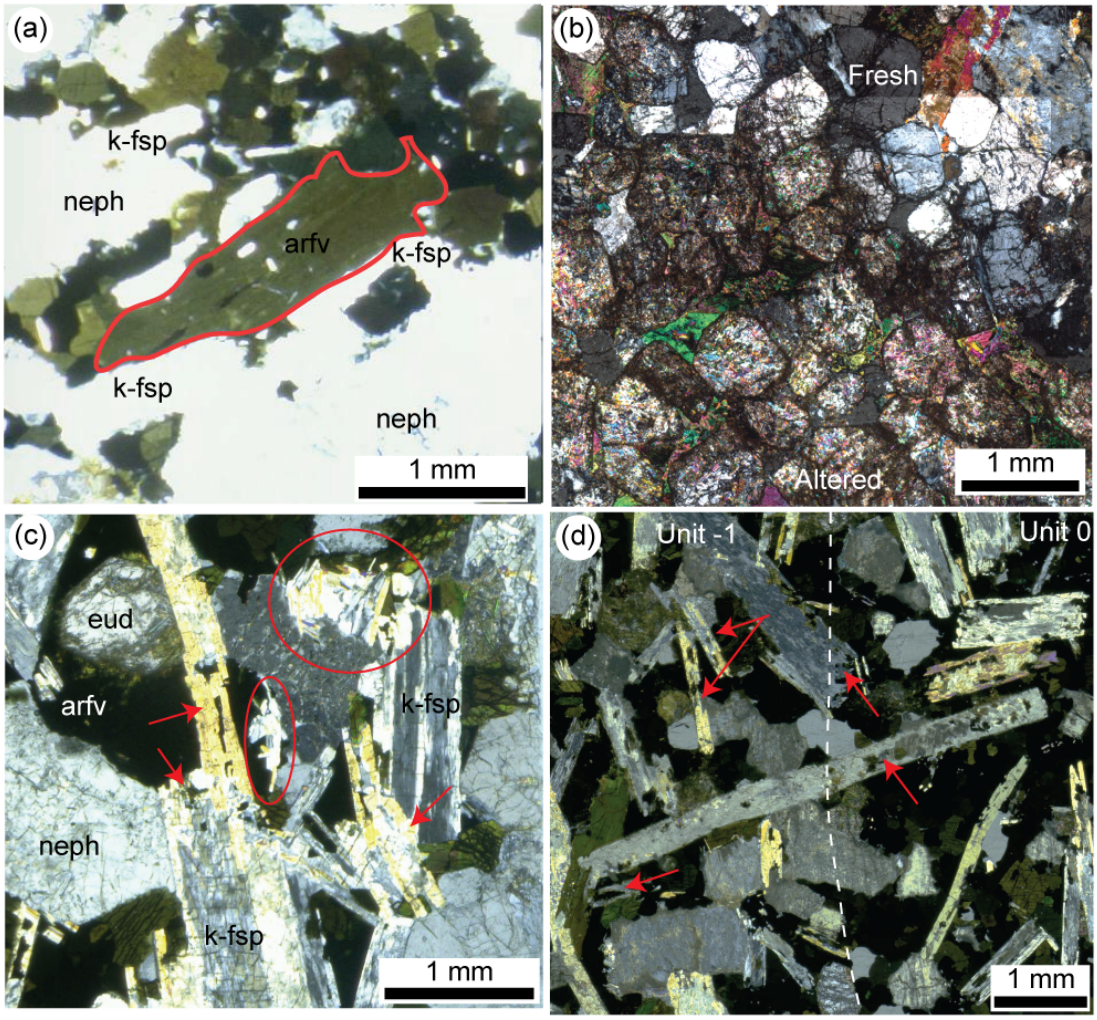

Figure 6.6: (a) Arfvedsonite phenocryst (highlighted in red) surrounded by groundmass of arfvedsonite, nepheline and alkali feldspar in Unit 0 black kakortokite, Location A. (b) Alteration of eudialyte (lower) develops a multi-crystalline (multi-coloured) texture within high relief outlines of relict euhedral eudialyte, from Unit 0 red kakortokite, Location B. (c) Enclaves of microcrystic alkali feldspar (encircled in red) in Unit -1 white kakortokite (Location A) 20 mm below the Units -1/0 boundary, embayed alkali feldspar crystals are marked by red arrows. (b) Units -1/0 boundary (dashed white line) from Location C, embayed alkali feldspar crystals indicated by red arrows. NB all rock sections photographed under circularly polarised light, arfvedsonite can appear opaque in thick section. Abbreviations: arfv – arfvedsonite; eud – eudialyte; k-fsp – alkali feldspar; neph – nepheline.

6.4 Quantitative Textural Analysis

Crystal size distribution analyses were performed on hand digitised crystal outlines (e.g. Fig 6.7) following the methods detailed in Chapter 4.3 for the samples described above. The data are presented in Figure 6.8 and Table 6.3. The raw CSD data are located in the supplementary files in Appendix C.

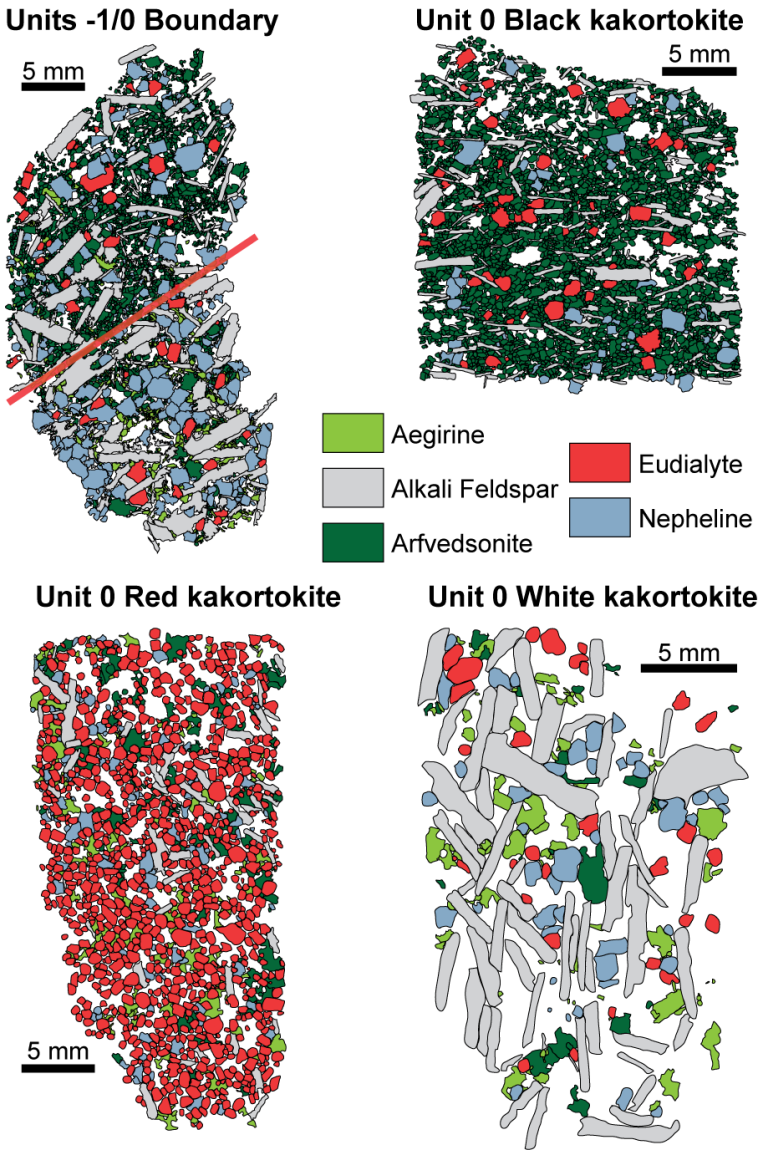

Fig 6.7: Digitised sketch maps of samples from Location B. Units -1/0 boundary, Unit 0 black kakortokite, Unit 0 red kakortokite, Unit 0 white kakortokite. Note blank spaces represent minor phases, e.g. sodalite, fluorite.

Only the characteristic minerals from each layer were investigated across the layered series: arfvedsonite in black, eudialyte in the red and alkali feldspar with nepheline in the white kakortokites. These four minerals were used as they form the bulk of each layer and so are key to identifying layer-forming processes. In addition

use of these characteristic minerals emphasises features of primary crystallisation, while reducing the effects of post-nucleation textural coarsening. To negate the effects of late-stage alteration, which was observed to affect eudialyte and nepheline, relict eudialyte was only included when the original crystal outlines were preserved and identifiable. Nepheline was excluded when altered, as the original crystal outlines were not preserved, thus nepheline data are not presented for all white kakortokite samples.

With the exception of the Unit 0 white kakortokite samples, log-linear slopes are typical of the CSD plots, with minor variations to the slope patterns. Most samples have a downturn in the population density of the smallest crystals. The Units -1/0 white kakortokite alkali feldspar CSDs (0-25 mm below boundary) and the Unit 0 white kakortokite alkali feldspar CSD from location D instead have an increased population density at the smallest crystal sizes.

The Unit -1 white kakortokite CSDs display log-linear plots for both the alkali feldspar and the nepheline crystals, with downturns at the smallest crystal sizes (Fig 6.8a-b). The alkali feldspar crystals range in size from 1.5 to 1.7 mm, and the CSD slope value is -0.62. The nepheline crystal sizes range from 0.6 to 2.3 mm and the slope value is -1.23.

The CSDs for Unit -1 white kakortokite sampled immediately below the Units -1/0 boundary are relatively log-linear. The alkali feldspar crystals from Locations A to C have upward kinks at the smallest crystal sizes, representing an increased population density (Fig. 6.8c). The alkali feldspar crystals from Location D instead display a downturn at the smallest crystal sizes (Fig. 6.8c). Nepheline was only analysed at Location C and the CSD displays a flattening at the smallest crystal sizes (Fig. 6.8d). The alkali feldspar crystal sizes range from 0.01 to 11.3 mm and the CSD slope values range from -0.68 to 0.81. The nepheline crystal sizes range from 0.4 to 2.3 mm and the CSD slope value is -0.81.

The arfvedsonite CSDs for the samples immediately above the Units -1/0 boundary (0-25 mm) have similar slope profiles to the arfvedsonite CSDs from the central portions of the Unit 0 black kakortokite (Fig. 6.8e-f). The arfvedsonite crystal sizes range from 0.1 to 5.0 mm immediately above the boundary and between 0.2 and 5.0 mm in the centre of black layers. The CSDs are relatively log-linear but contain kinks at larger crystal sizes: Locations A (boundary), A (layer), B (boundary) and D (boundary) show kinked plots at 3.18 mm (Fig. 6.8e), 3.17 mm (Fig. 6.8f), 1.27 mm (Fig. 6.8e) and 2.02 mm (Fig. 6.8e), respectively.

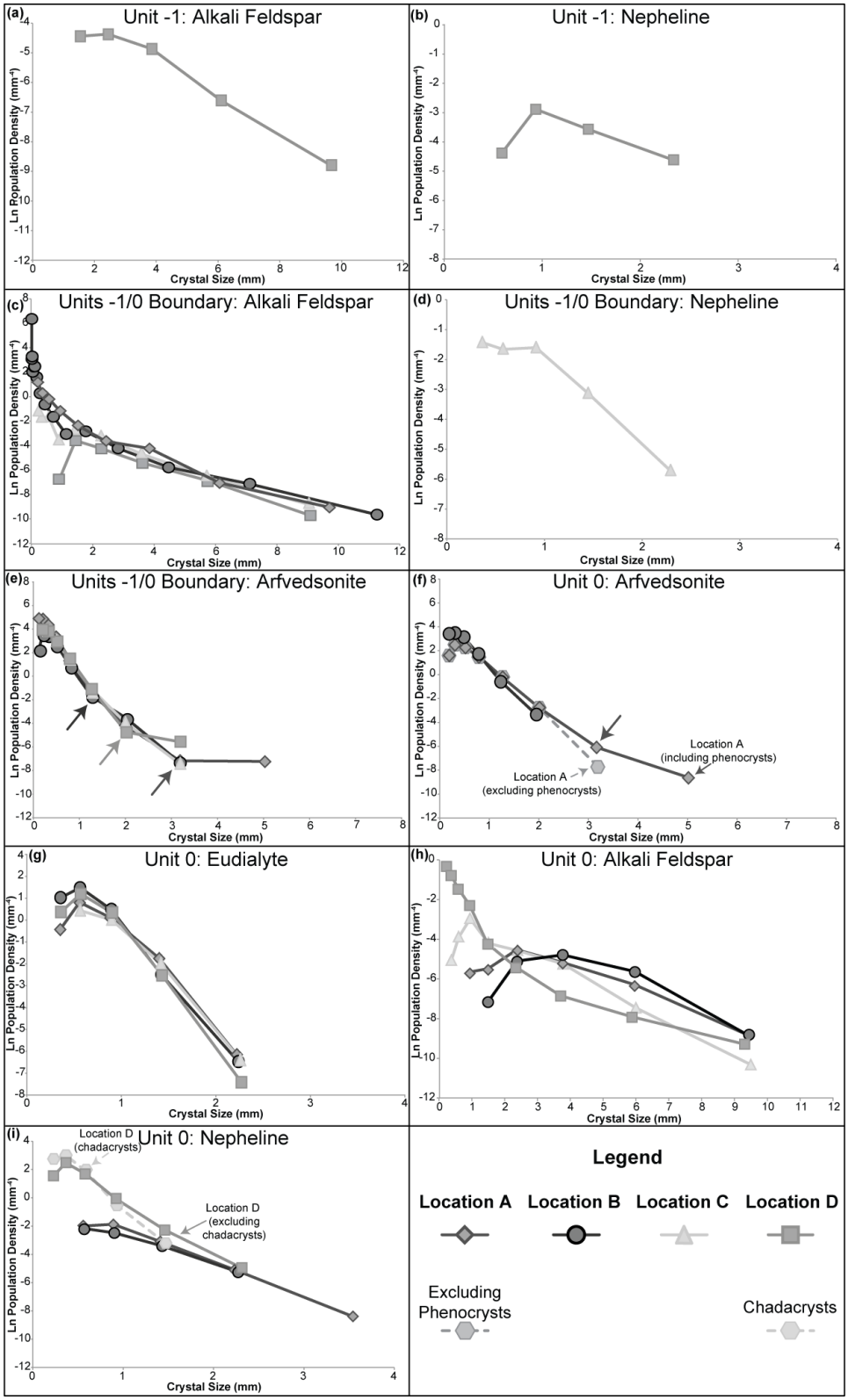

Figure 6.8: CSD Plots (a): U-1 alkali feldspar in white kakortokite at location D. (b) U-1 nepheline in white kakortokite at location D. (c) Alkali feldspar below the unit boundary in U-1 white kakortokite. (d) Nepheline below the unit boundary in U-1 white kakortokite. (e) Arfvedsonite above the unit boundary in U0 black kakortokite. (f) U0 arfvedsonite in black kakortokite. (g) U0 eudialyte in red kakortokite. (h) U0 alkali feldspar in white kakortokite. (i) U0 nepheline in white kakortokite. Boundary samples taken 0-25 mm above/below unit boundary Chadacrysts = euhedral crystals hosted by oikocrysts. NB scales vary to optimise the visibility of each plot.

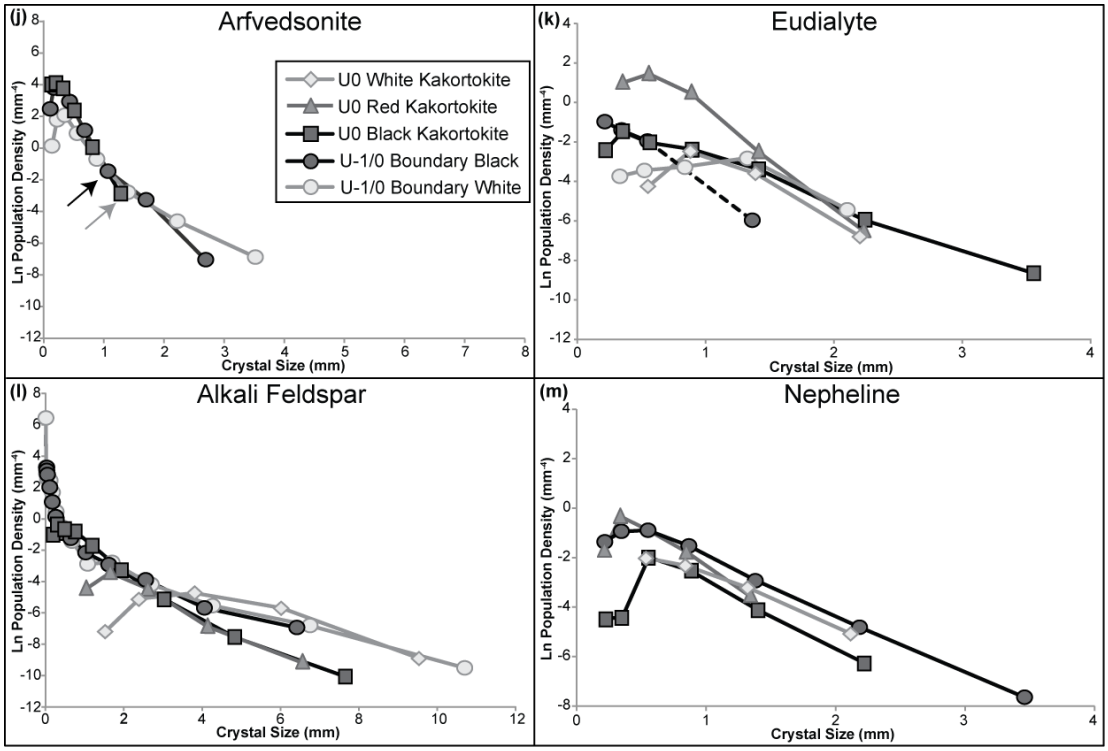

Figure 6.8 (continued): CSD Plots for all mineral species within each kakortokite type, samples from Location B. (j) Arfvedsonite across the U-1/0 boundary and in U0 black kakortokite. (k) Eudialyte across the U-1/0 boundary and in U0 black, red & white kakortokites. (l) Alkali feldspar across the U-1/0 boundary and in U0 black, red & white kakortokites. (m) Nepheline above the U-1/0 boundary and in U0 black, red & white kakortokites. Boundary samples taken 0-25 mm above/below unit boundary. NB scales vary to optimise the visibility of each plot.

The CSDs for the eudialyte in the red kakortokite samples are relatively log-linear and are consistent between locations (Fig. 6.8g). The crystal sizes range from 0.4 to 2.3 mm and the slope values from -4.26 to -5.20.

The Unit 0 white kakortokite alkali feldspar CSDs display a range of slope patterns (Fig. 6.8h). Locations A and C have log-linear slopes, except for downturns at the smallest crystal sizes. Location B displays a concave-downwards profile over the whole range. Location D was sampled from the first 0.5 m of the Unit 0 white kakortokite and displays the oikocrystic texture. Large (up to 12 mm) arfvedsonite oikocrysts host euhedral crystals of nepheline and alkali feldspar (Fig. 6.5h). The CSD plot has a convex-upwards slope over the entire range of crystal sizes and an increased population density at the smallest crystal sizes. Despite the range of patterns, the crystal sizes and CSD slopes are similar between locations. The crystal sizes range from 0.2 to 9.5 mm and the slopes range between -0.61 and -0.79 (Table 6.3). The nepheline data from the Unit 0 white kakortokite have log-linear slopes. The crystal sizes vary between 0.2 and 3.5 mm and the slope values range from -2.04 to -3.87.

To investigate processes of crystallisation of each kakortokite layer, all of the major minerals (Fig. 6.8j-m) were investigated from the samples collected at Location B (Unit 0 white, red and black kakortokites and across the Units -1/0 boundary). Arfvedsonite was investigated from the Unit -1 white kakortokite, immediately below (0-25 mm) the Units -1/0 boundary. This sample has an upwards curvature, starting at 1.4 mm (arrowed, Fig. 6.8j). Crystal sizes are consistent between all measured rock types and range between 0.1 and 3.5 mm (Fig. 6.8j), however the greatest sizes were measured in the sample from immediately below (0-25 mm) the U-1/0 boundary. The slope values increase from this sample to the central portions of the Unit 0 black kakortokite and range between -2.55 to -4.44 (Table 6.3).

Eudialyte crystals were measured in all rock types and the CSDs display a range of slope profiles (Fig. 6.8k). The CSD plots are typically log-linear, excepting the Unit -1 white kakortokite immediately below (0-25 mm) the Units -1/0 boundary, which has an upwards curvature over the entire plot. Crystal sizes range from 0.2 to 3.6 mm and are greatest in the central portions of the Unit 0 black kakortokite. Slope values range between -1.85to -4.88 (Table 6.3).

Alkali feldspar crystals were also measured in all rock types and the CSDs display a range of slope profiles (Fig. 6.8l). The samples from above and below the Units -1/0 boundary have increased numbers of the smallest crystals, followed by slopes that curve upwards at the largest crystal sizes (Fig. 6.8l). The U0 black and red kakortokites also have CSD plots that curve upwards at the largest crystal sizes. The range of crystal sizes is between 0.01 and 10.7 mm, with the greatest crystal sizes in the white kakortokite samples (Fig. 6.8l). The slope values range between -0.68 and -1.38 (Table 6.3)

The CSD plots for nepheline display consistent plot shapes between samples and are relatively log-linear with downturns at the smallest crystal sizes (Fig. 6.8l). Crystal sizes range from 0.2 to 3.5 mm with greatest sizes displayed by the sample from immediately above (0-25 mm) the Units -1/0 boundary. The slope values range from -2.04 and -3.25 (Table 6.3).

Rock	Location	Sample	Crystal %	SPO	Lmax	Y intercept	Y int Error (±)	Characteristic Length	Slope	Slope Error (±)
U-1 White Kakortokite										
Alkali Feldspar	D	EJH/12/081	25.72	0.4	8.11	-2.68	0.020	1.70	-0.62	0.005
Nepheline	D	EJH/12/081	9.67	0.1	2.37	-1.74	0.0004	0.81	-1.23	0.0003
U-1 White Kakortokite Below Boundary (0-25 mm)										
Alkali Feldspar	A	EJH/12/009	35.45	0.5	5.76	-1.69	0.052	1.29	-0.78	0.024
	B	AF/99/195	29.80	0.2	6.74	-2.16	0.052	1.46	-0.68	0.016
	C	EJH/12/094	26.69	0.6	6.53	-1.59	0.010	1.23	-0.81	0.005
	D	EJH/12/079	13.97	0.6	5.64	-2.43	0.004	1.26	-0.79	0.001
Nepheline	C	EJH/12/094	9.15	0.2	1.80	1.16	0.0004	0.33	-3.00	0.001
U0 Black Kakortokite Above Boundary (0-25 mm)										
Arfv	A	EJH/12/009	47.14	0.2	2.44	4.83	0.183	0.25	-4.06	0.154
	B	AF/99/195	26.94	0.1	1.53	4.12	0.101	0.15	-3.74	0.092
	C	EJH/12/094	37.40	-	1.51	4.61	0.076	0.18	-3.96	0.066
	D	EJH/12/079	41.53	-	1.96	5.57	0.004	0.19	-5.15	0.003

Table 6.3: CSD input and output data. Crystal % = percentage of digitised phase. SPO = shape preferred orientation from 0 (no fabric) to 1 (complete alignment). Lmax = mean size of 4 largest crystals. Y-intercept = y-axis intercept of linear regression. Characteristic length = -1/slope. Slope = gradient of linear regression.

Rock	Location	Sample	Crystal %	SPO	Lmax	Y intercept	Y int Error (±)	Characteristic Length	Slope	Slope Error (±)
U0 Black Kakortokite										
Arfvedsonite	A	EJH/12/008	48.58	-	2.42	3.73	0.012	0.34	-3.12	0.010
	A	EJH/12/008 Smaller	46.51	-	1.55	4.12	0.028	0.23	-3.61	0.025
	B	AF/99/192	44.78	0.3	1.23	5.16	0.023	0.20	-4.44	0.019
U0 Red Kakortokite										
Eudialyte	A	EJH/12/007	37.86	-	1.67	3.65	0.087	0.23	-4.26	0.102
	B	AF/99/193	44.43	-	1.64	4.49	0.022	0.20	-4.88	0.024
	C	EJH/12/095	32.95	-	1.62	4.45	0.027	0.21	-4.75	0.029
	D	EJH/12/080	38.53	-	1.54	4.62	0.052	0.22	-5.20	0.059
U0 White Kakortokite										
Alkali Feldspar	A	EJH/12/010	23.87	0.6	7.13	-2.90	0.034	1.63	-0.61	0.007
	B	AF/99/191	51.42	0.5	6.58	-1.71	0.066	1.35	-0.74	0.028
	C	EJH/12/096	12.28	0.6	6.02	-2.70	0.033	1.30	-0.79	0.010
	D	EJH/12/082	36.35	0.5	7.07	-3.94	0.258	1.63	-0.62	0.040
Nepheline	A	EJH/12/010	9.85	0.3	2.26	0.37	0.0001	0.41	-2.46	0.0006
	B	AF/99/191	7.18	-	1.83	-0.58	0.002	0.49	-2.04	0.007
	D	EJH/12/082	45.06	0.1	1.99	3.74	0.033	0.26	-3.87	0.034
	D	EJH/12/082 Chadacrysts	37.90	0.1	1.20	5.10	0.027	0.17	-5.74	0.030

Table 6.3 (continued): CSD input and output data. Crystal % = percentage of digitised phase. SPO = shape preferred orientation from 0, no fabric to 1 complete alignment. Lmax = mean size of 4 largest crystals. Y-intercept = y-axis intercept of linear regression. Characteristic length = -1/slope. Slope = slope of linear regression.

Rock	Location	Sample	Crystal %	SPO	Lmax	Y intercept	Y int Error (±)	Characteristic Length	Slope	Slope Error (±)
Arfvedsonite										
U0 Black	B	AF/99/192	44.78	0.3	1.23	5.16	0.023	0.20	-4.44	0.019
U-1/0 Black		AF/99/195	26.94	0.1	1.53	4.12	0.101	0.15	-3.74	0.092
U-1/0 White		AF/99/195	7.60	0.1	1.59	1.57	0.072	0.15	-2.55	0.118
Eudialyte										
U0 White	B	AF/99/191	4.36	-	1.60	0.66	0.014	0.30	-3.29	0.068
U0 Red		AF/99/193	44.43	-	1.64	4.49	0.022	0.20	-4.88	0.024
U0 Black		AF/99/192	7.48	-	2.17	0.51	0.005	0.44	-2.28	0.021
U-1/0 Black		AF/99/195	5.69	-	1.74	0.20	0.002	0.23	-4.42	0.038
U-1/0 White		AF/99/195	7.17	-	1.58	-1.16	0.322	0.54	-1.85	0.514
Alkali Feldspar										
U0 White	B	AF/99/191	51.42	0.5	6.58	-1.71	0.066	1.35	-0.74	0.028
U0 Red		AF/99/193	6.34	0.3	3.38	-1.60	0.034	0.85	-1.18	0.025
U0 Black		AF/99/192	12.09	0.4	5.38	-0.17	0.151	0.72	-1.38	1.249
U-1/0 Black		AF/99/195	19.66	0.1	4.78	-1.48	0.030	1.11	-0.90	0.018
U-1/0 White		AF/99/195	29.80	0.2	6.74	-2.16	0.052	1.46	-0.68	0.016
Nepheline										
U0 White	B	AF/99/191	7.18	-	1.83	-0.58	0.002	0.49	-2.04	0.007
U0 Red		AF/99/193	5.11	-	1.40	0.84	0.004	0.31	-3.25	0.017
U0 Black		AF/99/192	3.98	-	1.99	-0.39	0.002	0.38	-2.64	0.012
U-1/0 Black		AF/99/195	14.38	-	2.33	0.40	0.0004	0.43	-2.34	0.002

Table 6.3 (continued): CSD input and output data. Crystal % = percentage of digitised phase. SPO = shape preferred orientation from 0, no fabric to 1 complete alignment. Lmax = mean size of 4 largest crystals. Y-intercept = y-axis intercept of linear regression. Characteristic length = -1/slope. Slope = slope of linear regression.

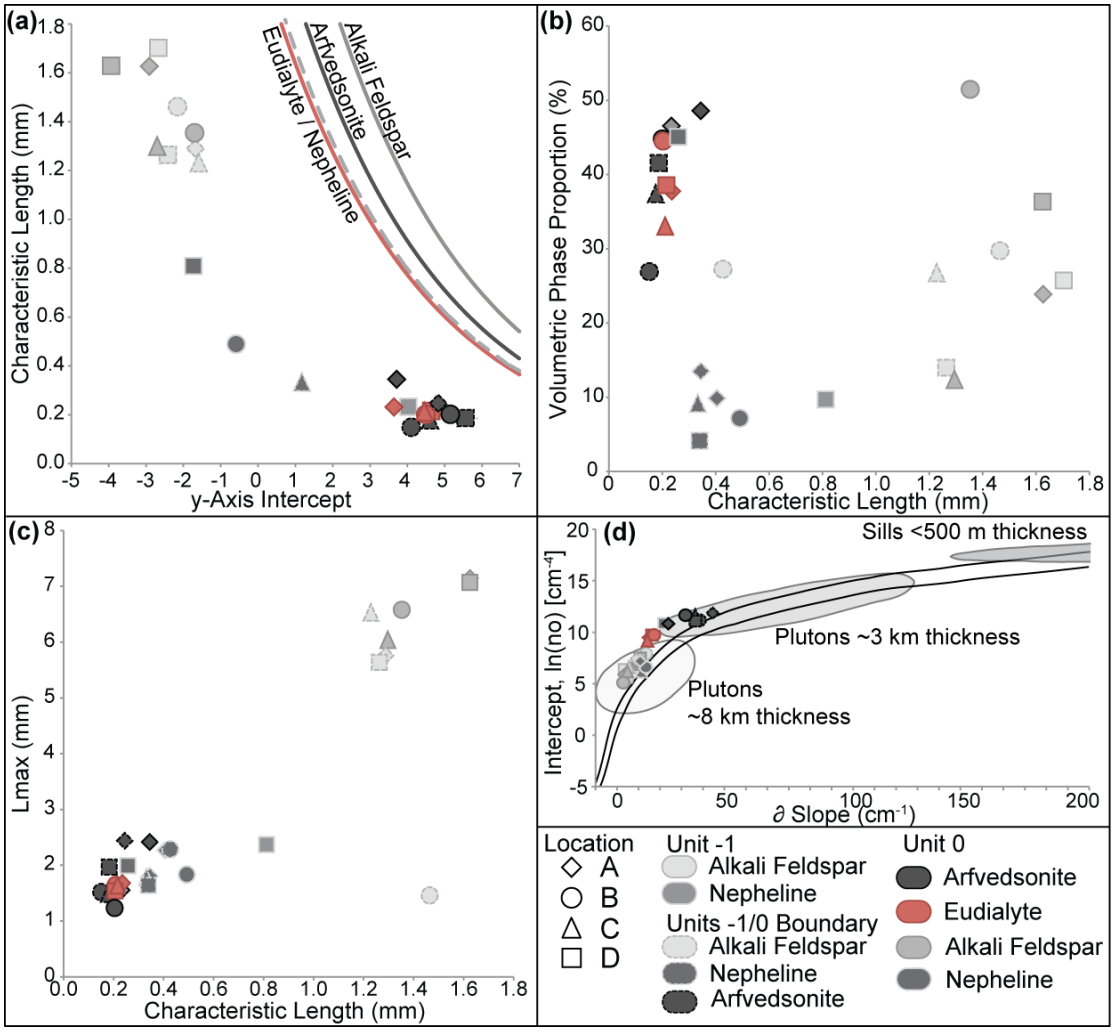

Figure 6.9: (a) Plot of characteristic length vs. y-axis intercept with lines indicating 60% closure limit (indicated by petrography) for each studied mineral, calculated following Higgins (2002a), NB eudialyte and nepheline closure limits overlap, also error bars smaller than symbols. (b) Volumetric phase proportion (measured) vs. characteristic length, no correlation is indicated. (c) Plot of Lmax vs. characteristic length, indicating positive correlation. (d) Plot of calculated intercept vs. slope after Marsh (2013)indicating a variation in size of magma body from which the arfvedsonite, eudialyte, alkali feldspar and nepheline crystallised.

To verify that the calculated CSD data do not exceed the maximum modal percentage for each mineral species, as identified in thin section, closure limits were calculated for 60% crystallinities (Higgins, 2002a). All data plot below their respective limits (Fig. 6.9a), demonstrating no internal inconsistency in the calculated data. The mineral abundance is not related to characteristic length (Fig 6.9b), however there is a positive correlation between the y-axis intercept and characteristic length (Fig. 6.9a). The y-axis intercept has a general negative correlation with the Lmax (Fig. 6.9c). Comparing calculated intercept vs. slope values (Marsh, 2013) indicates a distinction between the arfvedsonite in the black, eudialyte in the red and alkali feldspar plus nepheline in the white kakortokite (Fig. 6.9d).

6.5 Mineral Chemistry

EPMA (Chapter 4.5) was used to determine the composition of the eudialyte-group minerals (EGM) and amphiboles (arfvedsonite) in Unit 0 and across the Units -1/0 boundary. This allows for evaluation of the magmatic evolutionary state during the transition from Unit -1 to Unit 0 and during the crystallisation of Unit 0. The mineral chemical data are located in the supplementary data files in Appendix D.

6.5.1 Eudialyte-Group Minerals

Endmember compositions of the EGM (Fig. 6.10) in Unit 0, the Units -1/0 boundary and the Unit -1 white kakortokite were evaluated using cation site assignments calculated through the methods of Pfaff *et al.* (2010). The compositions range from eudialyte (*s.s.*) to kentbrooksite and ferrokentbrooksite. EGM from each rock type plot in a distinct grouping, from relatively Mn-rich EGM in white kakortokite to relatively Mn-poor EGM in black kakortokite. These data have a similarity to EGM analysed from the Norra Kärr Complex, Sweden (Sjöqvist *et al.*, 2013), as these also grouped according to Mn-contents.

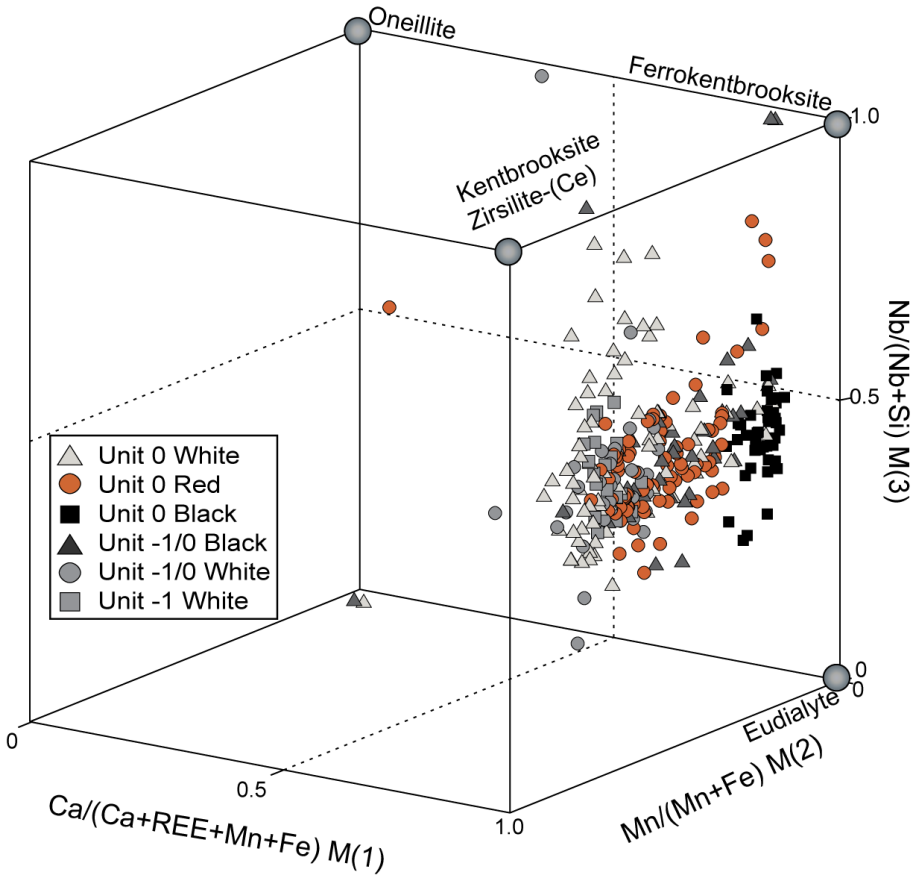

Figure 6.10: 3D scatterplot of Ca/(Ca+REE+Mn+Fe) on the M(1) site vs. Mn/(Mn+Fe) on the M(2) site vs. Nb(Nb+Si) on the M(3) site. Endmember compositions plotted from Sjöqvist *et al.* (2013).

The Fe and Mn content and particularly the $Fe_{(TOT)}$/Mn ratio of EGM is a good indicator of the evolutionary state of the magma during crystallisation (Pfaff *et al.*, 2008, Schilling *et al.*, 2011). Separating the data according to the unit stratigraphy (Fig 6.11) highlights the variation in composition between the black, red and white kakortokites. The EGM in black kakortokite have the greatest $Fe_{(TOT)}$/Mn ratios, between 10.85 and 13.34. The EGM in red kakortokite range from 7.23 and 10.55 and EGM in white kakortokite have the lowest $Fe_{(TOT)}$/Mn ratios between 5.77 and 9.98 (Table 6.4).The EGM from white kakortokite immediately below the boundary (0-25 mm) have similar $Fe_{(TOT)}$/Mn ratios (4.76-9.45) to EGM from the Unit -1 white kakortokite (6.62-0.50, Fig. 6.11, Table 6.4). There is a discontinuity across the Units -1/0 boundary as the EGM from the Unit 0 black kakortokite immediately above the boundary (0-25 mm) have a larger range of, and reduced ratios (7.95-13.18) compared to the EGM in the central portions of the Unit 0 black kakortokite (Fig. 6.11, Table 6.4).

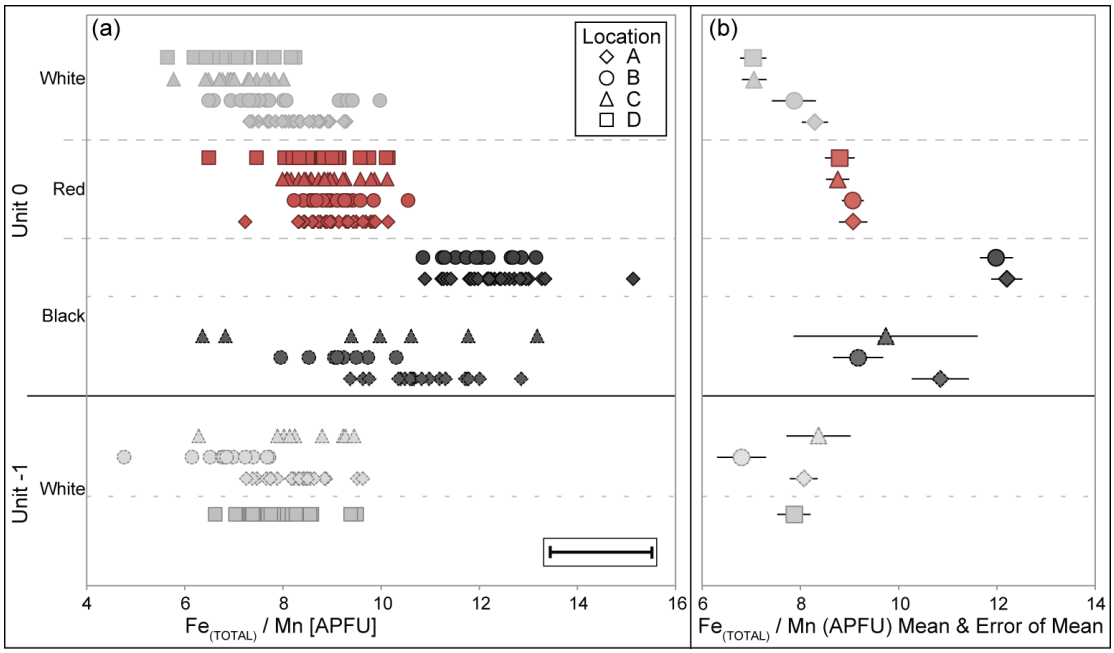

Figure 6.11: EGM Fe_{TOTAL}/Mn measured by EPMA, subdivided according stratigraphy and sample location. (a) Fe_{TOTAL}/Mn ratios. (b) Mean and error of mean to 95% confidence for each dataset. Note outliers are not rejected from mean calculations.

To further interpret the evolutionary state of the magma additional element ratios (Ca/(REE+Y) and Al/Si) were investigated (Pfaff *et al.*, 2008) between the black, red and white layers (Fig. 6.12, Table 6.4). The Cl content of eudialyte can also indicate the fractionation state of the magma as it is suggested to decrease upwards through the Ilímaussaq stratigraphy (Pfaff *et al.*, 2008), associated with a postulated decrease in Cl in the melt during fractionation (Krumrei *et al.*, 2007).

Unit	Rock		$Fe_{(TOT)}/Mn$				Ca/(REE+Y)				Al/Si				Cl (wt.%)			
			Mean	±	Min	Max	Mean	±	Min	Max	Mean	±	Min	Max	Mean	±	Min	Max
U-1	White	D	7.87	0.34	6.62	9.50	11.04	0.63	8.83	14.92	0.005	0.0004	0.003	0.006	1.53	0.04	1.13	1.60
U-1/0 Boundary	White	Mean	7.73	0.35	4.76	9.45	11.05	0.45	8.48	14.71	0.005	0.001	0.003	0.015	1.51	0.04	1.20	1.79
		A	8.07	0.28	7.25	8.85	10.48	0.43	9.49	11.68	0.005	0.0004	0.004	0.006	1.52	0.02	1.43	1.58
		B	6.80	0.50	4.76	7.72	11.05	0.80	8.48	12.77	0.006	0.002	0.003	0.015	1.52	0.09	1.20	1.79
		C	8.37	0.65	6.29	9.45	11.86	0.99	9.99	14.71	0.006	0.002	0.003	0.015	1.48	0.10	1.23	1.67
	Black	Mean	10.33	0.54	7.95	13.18	10.79	0.47	7.81	12.93	0.005	0.0004	0.004	0.007	1.54	0.01	1.48	1.60
		A	10.85	0.58	9.37	12.86	10.48	0.73	7.81	12.15	0.005	0.0004	0.004	0.006	1.54	0.02	1.48	1.60
		B	9.17	0.51	7.95	10.31	11.16	0.56	10.16	12.92	0.006	0.001	0.004	0.007	1.56	0.02	1.52	1.59
		C	11.08	1.73	9.40	13.18	10.96	1.38	9.79	12.93	0.006	0.001	0.004	0.007	1.52	0.04	1.49	1.57
U 0	Black	Mean	12.10	0.23	10.85	13.34	10.67	0.45	8.85	14.32	0.005	0.001	0.0004	0.011	1.52	0.02	1.35	1.62
		A	12.20	0.31	10.89	13.34	10.23	0.55	8.87	13.03	0.003	0.001	0.0004	0.006	1.52	0.03	1.35	1.62
		B	11.99	0.34	10.85	13.16	11.14	0.65	8.85	14.32	0.006	0.001	0.004	0.011	1.52	0.03	1.42	1.61
	Red	Mean	8.93	0.13	7.23	10.55	10.72	0.31	2.09	13.78	0.005	0.0003	0.003	0.014	1.55	0.01	1.43	1.65
		A	9.07	0.29	7.23	10.14	10.37	0.97	2.09	13.78	0.005	0.001	0.003	0.014	1.52	0.02	1.44	1.59
		B	9.07	0.22	8.23	10.55	10.92	0.52	8.63	13.54	0.006	0.001	0.004	0.012	1.57	0.02	1.43	1.65
		C	8.76	0.23	7.99	9.87	11.14	0.32	9.44	12.38	0.005	0.0004	0.003	0.006	1.54	0.02	1.44	1.61
		D	8.80	0.30	7.46	10.15	10.44	0.43	8.96	12.32	0.005	0.0005	0.004	0.009	1.56	0.02	1.49	1.61
	White	Mean	7.59	0.20	5.77	9.98	10.47	0.24	7.31	12.92	0.005	0.0002	0.004	0.008	1.53	0.03	0.97	1.70
		A	8.30	0.27	7.33	9.30	10.83	0.59	7.83	12.74	0.005	0.0003	0.004	0.007	1.47	0.08	0.97	1.66
		B	7.87	0.45	6.49	9.98	10.62	0.44	9.36	12.92	0.006	0.0003	0.005	0.007	1.62	0.02	1.50	1.70
		C	7.06	0.25	5.77	8.01	10.21	0.32	9.29	11.60	0.006	0.0003	0.004	0.006	1.48	0.02	1.41	1.55
		D	7.04	0.27	6.20	8.26	10.15	0.54	7.31	11.95	0.006	0.0004	0.005	0.008	1.58	0.02	1.46	1.65

Table 6.4: Range of $Fe_{(TOT)}/Mn$, Ca/(REE+Y) ad Al/Si ratios and Cl wt.% values according to rock type and sample location. Precision (±) reported to 95% confidence.

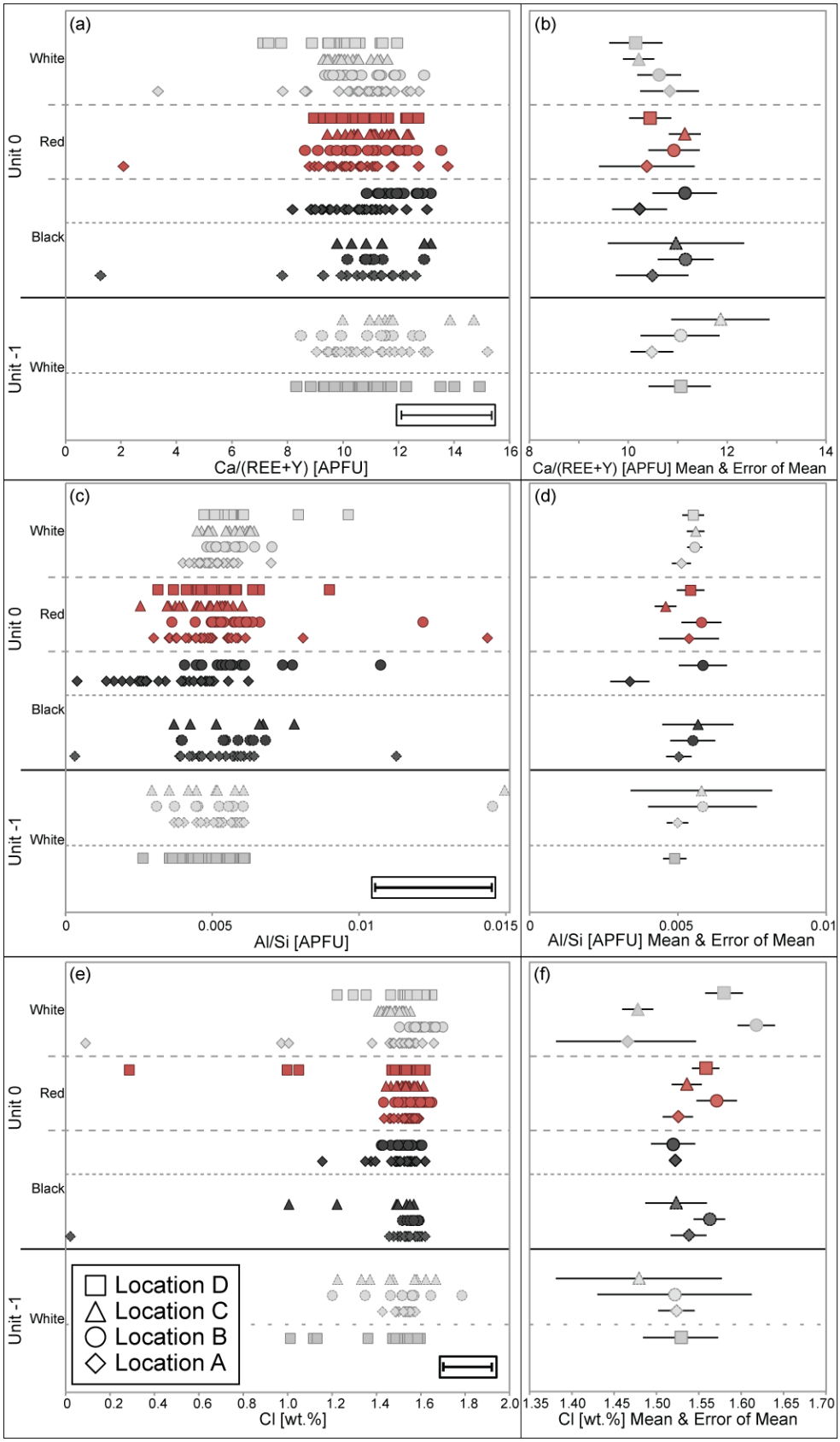

Figure 6.12: EGM chemistry measured by EPMA (a) Ca/(REE+Y). (b) Mean and error of mean for Ca/(REE+Y) data. (c) Al/Si. (d) Mean and error of mean for Al/Si data. (e) Cl. Mean and error of mean to 95% confidence for each dataset. Note outliers are not excluded from mean calculations.

The range of Ca/(REE+Y) ratios display little variation within error through the Units -1/0 boundary and Unit 0 (Fig. 6.12a-b, Table 6.4). There is a general trend of decreasing values upwards through Unit 0 and a discontinuity occurs across the Units -1/0 boundary. The outlying low values are associated with EGM crystals that were identified during the petrographic analysis to be partially altered. The Al/Si follow the same trend of the highest range of values being associated with EGM in the black kakortokite and the lowest in the EGM in the white kakortokite (Fig. 6.12c-d, Table 6.4).

The EGM display a general decrease in Cl content upwards through Unit 0 (Fig. 6.12e-f, Table 6.4). There is a discontinuity at the Units -1/0 boundary as the EGM in the U-1 white kakortokite have lower Cl contents than the EGM in the overlying black kakortokite of U0. The EGM in the Unit 0 white kakortokite have the greatest variation between locations.

6.5.2 Amphibole

Amphibole compositions were measured from the black kakortokite immediately above (0-25 mm) the U-1/0 boundary at all locations and from the central portions of the black kakortokite layers from Locations A and B. Additionally amphiboles were measured at Location A from the U-1 white kakortokite immediately below the U-1/0 boundary and the red and white kakortokite layers from U0. The amphiboles range towards the sodic end-members, from katophorite to arfvedsonite (Fig. 6.13).

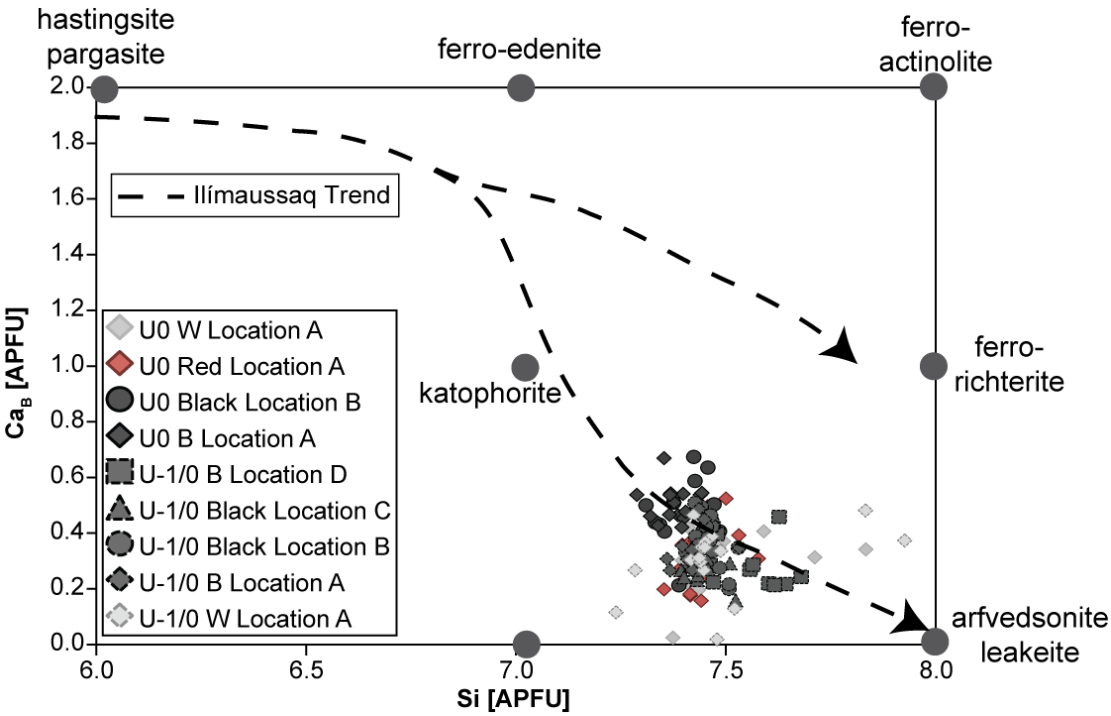

Figure 6.13: Plot of Ca_B vs. Si (APFU) in amphibole plotted according to location and unit. Plot adapted from Marks *et al.* (2004), data follow their bimodal Ilímaussaq trend.

Two geochemical ratios were measured from the Unit 0 amphiboles, the Ca/(Na+K) and X_{Fe} (Fe^{2+}/[Fe^{2+}+Mn+Mg]) ratios (Table 6.5, Fig 6.14). The Ca/(Na+K) ratio systematically decreases during evolution of the melt (Pfaff *et al.*, 2008). This is associated with crystallographic preferences Na & K on the A-site & Ca and Na on the B-site (Pfaff *et al.*, 2008). The X_{Fe} ratio is controlled by the Fe-Mn composition of the melt and indicates melt evolution as it reflects either amphibole-dominated crystallisation (lower-Fe) or pyroxene-dominated crystallisation (higher-Fe). Thus the higher the X_{Fe} ratio, the more evolved the melt from which the amphibole crystallised (Pfaff *et al.*, 2008). This ratio can be affected by structural effects or intensive parameters (e.g. f(H_2O)) as it uses Fe^{2+} contents (Di Carlo *et al.*, 2010), however the data presented here reflect the trends observed in the EGM.

Unit	Rock	Location	Ca/(Na+K)				X_{Fe}			
			Mean	±	Min	Max	Mean	±	Min	Max
U-1/0 Boundary	White	A	0.12	0.02	0.04	0.16	0.90	0.06	0.71	0.99
	Black	Mean	0.12	0.01	0.05	0.21	0.87	0.04	0.38	0.95
		A	0.13	0.02	0.10	0.20	0.91	0.01	0.88	0.94
		B	0.14	0.02	0.07	0.21	0.93	0.003	0.92	0.94
		C	0.11	0.02	0.05	0.18	0.83	0.08	0.38	0.93
		D	0.11	0.03	0.07	0.18	0.80	0.12	0.44	0.95
U 0	Black	Mean	0.20	0.01	0.15	0.30	0.91	0.003	0.89	0.92
		A	0.21	0.02	0.16	0.30	0.91	0.005	0.90	0.92
		B	0.19	0.02	0.15	0.30	0.91	0.005	0.89	0.92
	Red	A	0.11	0.02	0.06	0.20	0.93	0.01	0.90	0.95
	White	A	0.11	0.03	0.01	0.16	0.93	0.01	0.90	0.95

Table 6.5: Amphibole ratios. $X_{Fe} = Fe^{2+}/[Fe^{2+}+Mn+Mg]$. Precision (±) reported to 95% confidence.

The Ca/(Na+K) ratios have a similar compositional pattern to the $Fe_{(TOT)}/Mn$ compositions in the EGM. The ratios are the greatest in the U0 black kakortokite and decrease upwards through the remainder of U0 (Fig 6.14a-b, Table 6.5). The Ca/(Na+K) ratios display a marked discontinuity above the Units -1/0 boundary as the values increase upwards from the amphiboles measured immediately above the boundary and compared to those below the boundary. The greatest values are displayed by the amphiboles in the U0 black kakortokite.

The X_{Fe} ratios display little variation throughout Unit 0 (Fig. 6.14c-d, Table 6.5). The Location C and D samples from immediately above the U-1/0 boundary display a wide range of values.

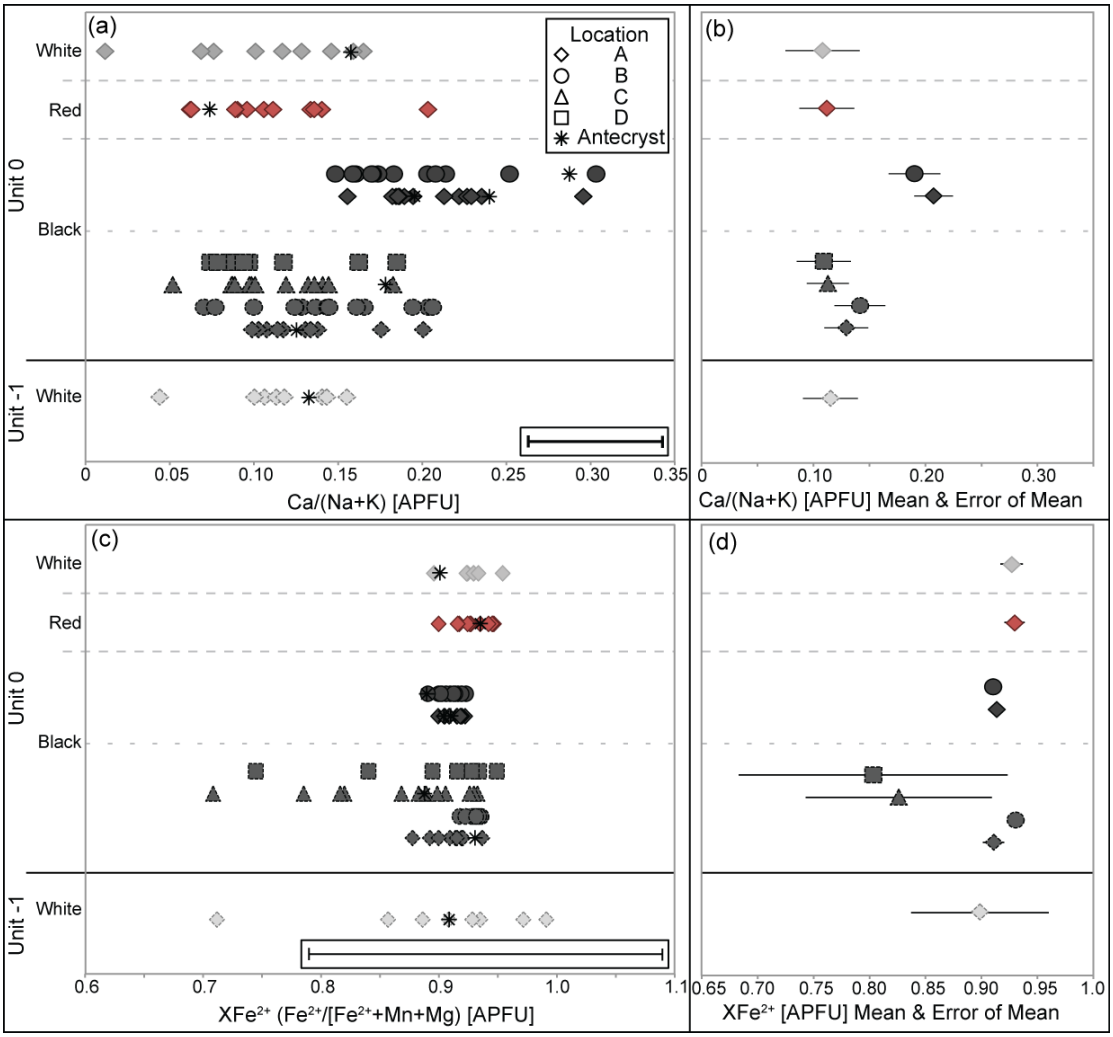

Figure 6.14: Amphibole Ca/(Na+K) ratios measured by EPMA. (a) Ca/(Na+K) ratios, error bar bottom right. (b) Mean and error of mean of Ca/(Na+K) ratios. (c) X_{Fe} ratio ($Fe^{2+}/[Fe^{2+}+Mn+Mg]$), error bar bottom left. (d) Mean and error of mean of X_{Fe} ratios. Mean and error of mean to 95% confidence for each dataset. Note outliers are not excluded from mean calculations.

6.6 Eudialyte Alteration: Process and Products

Alteration of eudialyte in the Ilímaussaq Complex was first described by Ussing (1912) and was noted by the present study to be widespread throughout the complex. There is no spatial pattern to the alteration, but in drill core it can affect up to 40% of the EGM in a single kakortokite layer. The alteration has developed a range of minerals within relict euhedral crystals. These have been described in detail by Karup-Møller *et al.* (2010) who distinguished two types of alteration. (1) A catapleiite-type, represented by decomposition of eudialyte to a fine-grained crystalline aggregrate of catapleiite ± aegirine, analcime, fluorite (minor), Y-fergusonite, apatite, monazite, nacareniobsite-(Ce), thorianite and neptunite. (2) A zircon-type, represented by decomposition of eudialyte into a fine-grained crystalline aggregate of zircon, K-feldspar, albite, aegirine, fluorite and grossularite. The non-uniform nature of the alteration, combined with the fine-grain size of the multi-phase crystalline aggregates poses a challenge for REE extraction from the kakortokite. Therefore a greater understanding of the products and styles of alteration is required to fully understand the economic potential of the kakortokite.

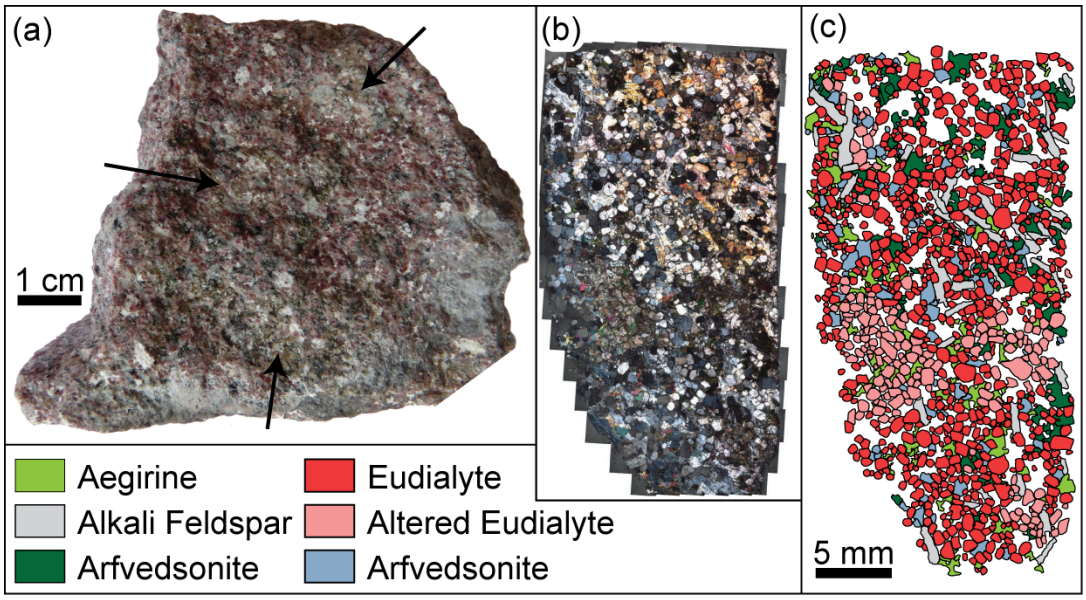

Figure 6.15: Alteration of eudialyte in Sample AF/99/193. (a) Patchy alteration in hand specimen marked by yellow colour of crystals (arrowed). (b) Probe section of sample with alteration marked by multicrystalline appearance. (c) Digitisation of (b) indicating altered crystals.

The alteration is not spatially restricted or contained, and patches of alteration were observed in all of the kakortokite units. The alteration is marked in hand specimen by a dull yellow appearance to the altered eudialyte crystals (Fig. 6.15a). The patchy nature of the alteration is best observed at the micro-scale, where the

poly-crystalline nature of the alteration can be detected (Fig. 6.15b) in discrete patches (Fig. 6.15c).

The alteration can either partially or wholly affect a eudialyte crystal and is best observed through BSE imaging (Fig. 6.16a,c), where the individual phases comprising the alteration can be distinguished. In the present study the catapleiite-type alteration was observed to comprise of aegirine, britholite, catapeliite, Nacareniobsite-(Ce), nepheline and pectolite (Fig. 6.16b). This type of alteration has developed a pronounced orientation of the alteration minerals (Fig. 6.16a-b). The zircon-type alteration was only observed to partially affect eudialyte crystals, with decomposition to aegirine, britholite, fluorite, nepheline, pectolite and zircon (Fig. 6.16d). Unaltered eudialyte commonly comprises most of the crystal with the alteration concentrated at the margins (Fig. 6.16c-d).

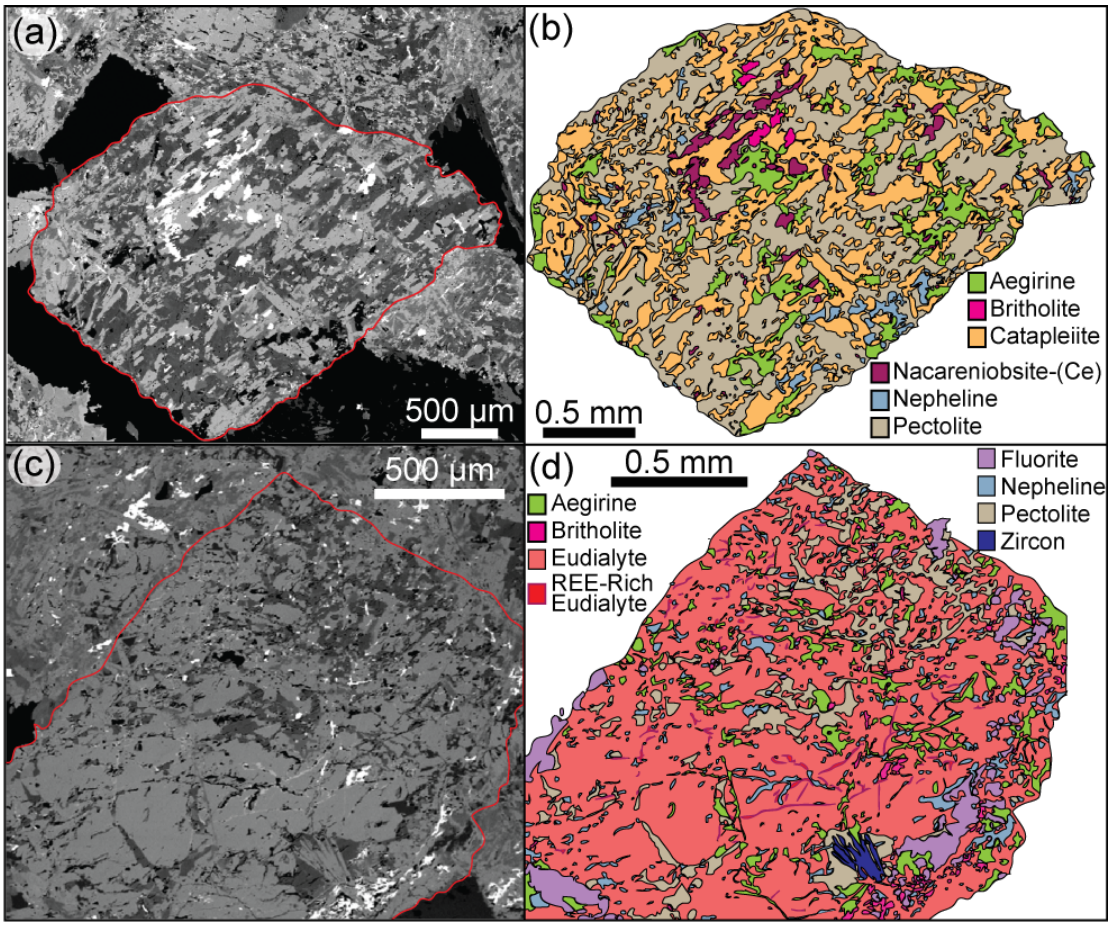

Figure 6.16: Types of alteration. (a) BSE image of catapleiite-type alteration. (b) Digitised crystal in (a) indicating products of decomposition. (c) BSE image of zircon-type alteration. (d) Digitised crystal in (c) indicating products of decomposition.

Catapleiite will only crystallise in agpaitic to hyperagpaitic aqueous fluids (Mitchell & Liferovich, 2006), zircon is unstable at these alkalinities and instead forms in more acidic, miaskitic fluids (Mitchell & Liferovich, 2006). The composition of the

fluids that altered the eudialyte were investigated in the present study through stoichiometrically balanced conceptual equations for each type of alteration, using texturally determined proportions of the alteration products:

Catapleiite-type:

1 eudialyte + from the fluid

$(Na,REE)_{15}Ca_6(Fe,REE)_3(Zr,Nb)_3Si(Si_{25}O_{73})(O,OH,H_2O)_3(Cl,OH)_2 + 3F^- + 4Ca^{2+} + 2Na^+ + 2PO_4^{3-} + 4H_2O$

→

2 catapleiite + 3 pectolite + 1 Nacareniobsite-(Ce) + 1 britholite

$2[Na_2ZrSi_3O_8{\cdot}nH_2O] + 3[NaCa_2Si_3O_8(OH)] + Na_3Ca_3REENb(Si_2O_7)_2OF_3 + CaREE_9(SiO_4)_4(PO_4)2O_2 + 3Si^{4+} + 5H^+$

+ to the fluid

Zircon-type:

1 eudialyte + from the fluid

$(Na,REE)_{15}Ca_6(Fe,REE)_3(Zr,Nb)_3Si(Si_{25}O_{73})(O,OH,H_2O)_3(Cl,OH)_2 + 2PO_4^{3-} + 7Ca^{2+} + 3F^- + 2H^+$

→

1 zircon + 5 pectolite + 2 fluorite + 1 britholite. + to the fluid

$Zr_3REEPO_2Si_4O_{16} + 5[NaCa_2Si_3O_8(OH)] + 2[CaF_2] + CaREE_9(SiO_4)_4(PO_4)2O_2 + 3Na^+ + 3Si^{4+} + H_2O$

This analysis indicates that the fluids that formed the alteration products of each type of alteration were calcium-, fluorine- and phosphorous-bearing aqueous fluids.

6.7 Development of Unit 0

6.7.1 Formation of Unit 0

The log-linear slopes associated with most of the characteristic minerals from the layers (Fig. 6.8) are consistent with *in situ* crystallisation at steady rates of nucleation and undercooling (Marsh, 1988). The exception of the Unit 0 white kakortokite samples is discussed later. In all samples there is evidence of modification of primary CSDs. The downturn at small crystal sizes displayed by all minerals reflects textural coarsening (Higgins, 1999, Higgins, 2010), while the upward trends at small crystal sizes for some alkali feldspar and nepheline CSDs is indicative of secondary nucleation.

The effects of textural coarsening can be further identified from the location D Unit 0 white kakortokite sample with the oikocrystic texture (Fig. 6.5h). Growth of an arfvedsonite oikocryst will terminate the growth of the crystals it hosts, thus preserving a record of their sizes before solidification was complete. Only nepheline crystals were present in sufficient numbers to generate a CSD (Fig. 6.8i). This has a log-linear slope but a downturn at the smallest crystal sizes indicates the nepheline crystals were affected by textural coarsening (Higgins, 1999, Higgins, 2002b, Marsh, 1998). Thus the nepheline crystals had time to grow and undergo textural equilibration before enclosure by the arfvedsonite oikocrysts.

The kinked slopes displayed by the arfvedsonite CSDs represent mixing of two crystal populations with differing histories of textural coarsening (Boorman *et al.*, 2004, Higgins, 2002b, Marsh, 1988, Marsh, 1998). All black kakortokite samples from the present study contain large arfvedsonite crystals (euhedral and markedly larger than the arfvedsonite groundmass, Fig. 6.6c). Their effect on the CSD patterns was investigated by plotting a second CSD for the Unit 0 location A black kakortokite, which excludes the large crystals (Fig. 6.8f). This CSD has a log-linear plot (indicating *in situ* crystallisation), whereas the combined CSD for the large crystals and groundmass has a concave-upwards plot. Although this plot shape is typically associated with formation through the process of gravitational settling (Boorman *et al.*, 2004, Marsh, 1988), it can also indicate the addition of two log-linear CSDs (Higgins, 2002b). As the CSD that excludes the largest crystals is log-linear, the latter hypothesis is accepted to have developed the plot shape.

Unit 0 white kakortokite alkali feldspar CSDs display a range of patterns (Fig. 6.8h). Samples from locations A and C have log-linear slopes with downturns at the smallest crystal sizes, this is associated with *in* situ crystallisation followed by textural coarsening. The location B sample has a concave-downwards slope over the entire

range of crystal sizes, pointing to formation by crystal fractionation only (Boorman *et al.*, 2004, Marsh, 1988). The location D sample curves upwards towards the larger crystal sizes. This is interpreted to reflect gravitational settling (Boorman *et al.*, 2004, Marsh, 1988), rather than a mixed population, as the sample does not contain crystals of alkali feldspar that are distinctly larger than the groundmass, i.e. there is a continuous range of crystal sizes. The CSD indicates show an increased population of small crystals (Fig. 6.8h) with an upward kink at 1.5 mm, indicating postcumulus modification through secondary crystallisation.

Ussing (1912) originally investigated crystal sizes of each of the major minerals (arfvedsonite, eudialyte and alkali feldspar) throughout entire units and noted that each mineral species had similar crystal sizes in each of the black, red and white kakortokite layers. The present study investigated crystal sizes of arfvedsonite (Fig. 6.8j), eudialyte (Fig. 6.8k), alkali feldspar (Fig. 6.8l), and nepheline (Fig. 6.8m) in each layer of Unit 0 at Location B. The results indicate that arfvedsonite crystal sizes are greatest in the Units -1/0 boundary samples and smaller in the central portion of the black kakortokite layer. While the arfvedsonite in the black kakortokite samples is indicated to have formed through *in situ* crystallisation, the arfvedsonite from immediately below the Units -1/0 boundary in the white kakortokite has a CSD plot that is more reflective of gravitational settling (Fig. 6.8j). The downturn at small crystal sizes reflects late stage textural coarsening. Eudialyte displays similar crystal sizes in most samples (0.2 to 2.2 mm), excepting the Unit 0 black kakortokite, which has much greater crystal sizes (up to 3.6 mm, Fig 6.8k). The eudialyte plot shapes typically reflect *in situ* crystallisation, although the samples from immediately below (0-25 mm) the Units -1/0 boundary in the white kakortokite has a shape that is more reflective of fractionation, i.e. enclosure of suspended crystals in the upwards growing crystal mush pile. The alkali feldspar crystals increase in size from the black and red layers (0.3 to 7.7 mm) to the white layer (0.1 to 10.7 mm, Fig 6.8l). Similar to the U0 white kakortokite layer, the CSD plot shapes indicate a range of processes including *in situ* crystallisation, gravitational settling and fractionation. The downturn at small crystal sizes for the samples from the central portions of black, red and white layers reflects late stage textural coarsening. The upturn at small crystal sizes in the samples from immediately above/below (0-25 mm) the Units -1/0 boundary is indicative of secondary nucleation. The nepheline crystals also display a range of crystal sizes, being smallest in the red layer (0.2 to 1.3 mm), then white layer (0.5 to 2.1 mm) and largest in the black layer (0.2 to 3.5 mm). All plot shapes are log-linear (Fig 6.8m) indicating formation through *in situ* crystallisation. The downturn at small crystal sizes

reflects late stage textural coarsening. These data are an indicator of varying crystal sizes throughout Unit 0, however due to the small number of crystals measured when the mineral species is not forming the groundmass of the layer (Table 6.3), the statistical viability of the CSD plots is questionable, thus care should be taken when interpreting these plots.

Although textural coarsening modifies the CSDs, I suggest that primary crystallisation features are still preserved in the slopes. The CSDs reflect formation of groundmass arfvedsonite (black kakortokite), groundmass eudialyte (red kakortokite) and groundmass nepheline (white kakortokite) through *in situ* crystallisation, while groundmass alkali feldspar (white kakortokite) formed through a variety of processes, including gravitational settling, *in situ* crystallisation and fractional crystallisation. Hence, formation of the tripartite layering purely through density sorting of the crystals is untenable.

Alteration was observed to affect the kakortokite through the widespread, but not spatially constrained, alteration of the eudialyte (EGM) through either catapleiite-type or zircon-type alteration. The alteration is patchy and can wholly affect one crystal while the neighbouring crystal is unaffected. The products of catapleiite-type alteration are aligned, indicating a fabric control on the alteration, associated with either fractures or cleavage planes. This indicates that the orientation of individual eudialyte crystals is a control on whether the eudialyte underwent complete alteration, partial alteration or was unaffected.

Not all the minerals contained in the decomposed eudialyte crystals could have formed through hydrothermal alteration. Aegirine and nepheline, which are magmatic phases, occur in the relict eudialyte crystals. It is interpreted to be a continuous process through the solidus to hydrothermal alteration. The bulk of the preserved mineral assemblage is interpreted to have formed during hydrothermal alteration, by calcium-, fluorine- and phosphorous-bearing aqueous fluids.

The REE were mobilised during the alteration. In the catapleiite-type, Ce and Nd were concentrated up to 42 wt.% and 11 wt.%, respectively in britholite. The zircon-type alteration displays lower concentrations of REEs with up to 21 wt.% of Ce and 12 wt.% of Nd in britholite. The zircon-type additionally formed a REE-rich EGM (up to 7 wt.% total REE), which contains over double the concentation of REEs compared to the unaltered EGM (~3 wt.%). However comparing the total REE content of the proportionally determined alteration products to the original EGM composition does not indicate any additional REE input. Instead the REE were translated from the crystal undergoing alteration and concentrated in britholite and Nacareniobsite-(Ce).

The two types of alteration can be achieved by Ca, F, and PO_4 bearing fluids, however alkalinity must have been a key control to form either catapleiite or zircon. The catapleiite-type alteration would require agpaitic to hyper-agpaitic (extremely alkaline) fluids to crystallise the phases present (Mitchell & Liferovich, 2006), while the zircon-type alteration would require much more acidic, i.e. miaskitic, fluids to crystallise (Mitchell & Liferovich, 2006). The presence of both of these alteration types in a single sample (AF/99/193, U0 Red kakortokite) indicates that local and/or temporal controls on the alkalinity of the late-stage hydrothermal fluids were important in determining the type of alteration products.

6.7.2 Magma Chamber Processes

Models for development of the 3-layered units typically invoke density sorting during gravitational settling (c.f. Upton, 2013). A recent model by Bons *et al.* (2015) applied an adaptation of Burgers' equation to invoke interactions between rising or sinking crystals, which locally slow the movement of crystals, resulting in the development of 'crystal mats' in low viscosity magmas. This process acts to develop separated layers of magma from the main body, which act as barriers to settling/flotation but are porous enough to allow for the migration of melt during late stage equilibration and/or compaction. Bons *et al.* (2015) envisage the layered kakortokite forming through small density perturbations developed during cooling of the chamber, which allows for the development of several 'mats' that consist of relatively dense minerals (i.e. arfvedsonite) with the more buoyant, less dense minerals (i.e. alkali feldspar and nepheline) trapped below the 'mat' and potentially a sandwich horizon of melt in between the trapped buoyant layer and underlying 'mat'. The requirements of this model are a relatively low viscosity magma and conditions that allow for crystals to sink or float a significant distance before they become trapped, with the process of gravitational settling being key (Bons *et al.*, 2015). However the CSD data from the present study are inconsistent with formation of the tripartite unit through gravitational settling alone.

Fieldwork in the present study found little direct evidence for magma flow, i.e. pseudosedimentary indicators were lacking, except at the contact with the marginal pegmatite and around the roof rock autolith in Unit +3 (Fig. 6.1b), thus it is inferred that the magma chamber was quiescent throughout the development of the layered series, excepting during the roof collapse event. Instead an ordered crystallisation model is proposed and we adopt a modified model (Larsen & Sørensen, 1987) for control on the order of nucleation through an oscillating volatile element

concentration and degree of undercooling. Like them I propose nucleation in a bottom layer of crystal-poor magma, between the resident magma and a sharp lower contact to a semi-rigid crystal mush corresponding to the Unit -1 white kakortokite. This is a similar model to the one proposed by Bailey *et al.* (2006) for development of microrhythmic layering in arfvedsonite lujavrite. They propose crystallisation in a stagnant bottom layer with alternate crystallisation of a dark layer (arfvedsonite-, nepheline-, sodalite- and microcline-rich) and a light urtite (sodalite free and microcline-poor) controlled by variations in volatile concentrations and activities. I follow Marsh's (2013) magmatic principles and apply them to Ilímaussaq to infer that the layered series was unlikely to have formed through a single emplacement event. There is textural evidence of resorption of the largest alkali feldspar crystals (Table 6.2, Fi. 6.6a-b) in Unit -1 white kakortokite boundary samples (0-25 mm below Unit 0), demonstrating a change in the thermal and/or chemical regime. Additionally the upturned kink in all alkali feldspar CSDs, except location D (Fig. 6.8c), is indicative of secondary nucleation (Figure 6.6a). At locations B and C, there is a small downturned kink between 1.8 to 1.1 mm and 1.4 to 0.9 mm, respectively; indicating this secondary nucleation overprints and postdates the textural coarsening. I attribute this resorption and secondary nucleation to a melt associated with a replenishment event, which infiltrated the crystal mush to a depth of a few centimetres.

The chemical data presented in section 6.5 corroborate this hypothesis as the $Fe_{(TOT)}$/Mn ratios in the EGM display a sharp discontinuity across the Units -1/0 boundary (Fig 6.11). The $Fe_{(TOT)}$/Mn ratios increase from the U-1 white kakortokite across the Units -1/0 boundary to a maximum in the black kakortokite samples from the central portions of the layer (Fig. 6.11, Table 6.4). Low $Fe_{(TOT)}$/Mn ratios in EGM reflect formation from relatively evolved magmas, while high $Fe_{(TOT)}$/Mn ratios reflect formation from relatively primitive magmas (Pfaff *et al.*, 2008, Schilling *et al.*, 2011). This indicates that the EGM in the Unit 0 black kakortokite crystallised from more primitive magmas than the EGM in the underlying Unit -1 white kakortokite, indicating a change in magma composition at the Units -1/0 boundary. Within Unit 0 the $Fe_{(TOT)}$/Mn ratios display a continuous decrease upwards through Unit 0, reflecting crystallisation from a progressively evolving magma.

The additional chemical data from the EGM are supportive of an injection of a relatively primitive magma that was volatile-rich. The Ca/(REE+Y) and Al/Si ratios and Cl contents decrease during melt evolution (Pfaff *et al.*, 2008) and all data display a discontinuity at the Units -1/0 boundary with the highest ratios in the black kakortokite. The values then decrease upwards through Unit 0 (Fig. 6.12). The same

trend is displayed by the amphibole data (Fig. 6.14) where the investigated ratios also decrease during melt evolution (Pfaff *et al.*, 2008).

Injection of this primitive magma would form the bottom magma layer in the model, due to compositional differences between it and the non-convecting resident magma. The sharp boundary between Unit -1 and Unit 0 formed from combined thermal and chemical erosion of the crystal mush as evidenced by the embayed alkali feldspar crystals at the units boundary. The initial high volatile element concentration, as indicated by the Cl-enriched EGM (Fig. 6.12e-f), has the effect of inhibiting nucleation of all mineral phases, resulting in supersaturation of each mineral phase in the magma. As the bottom layer of magma cools, due to thermal equilibration, arfvedsonite is the first phase to break through the inhibition on nucleation (Fig. 6.17) as can crystallise at higher volatile element concentrations than the other phases (Sørensen, 1969). It crystallised *in situ* above the boundary, most likely through the process of epitaxy, this is the process of crystal growth onto a crystalline substrate that acts to control the orientation of the growing crystals. Subordinate crystallisation of the minor phases formed the black kakortokite layer of Unit 0.

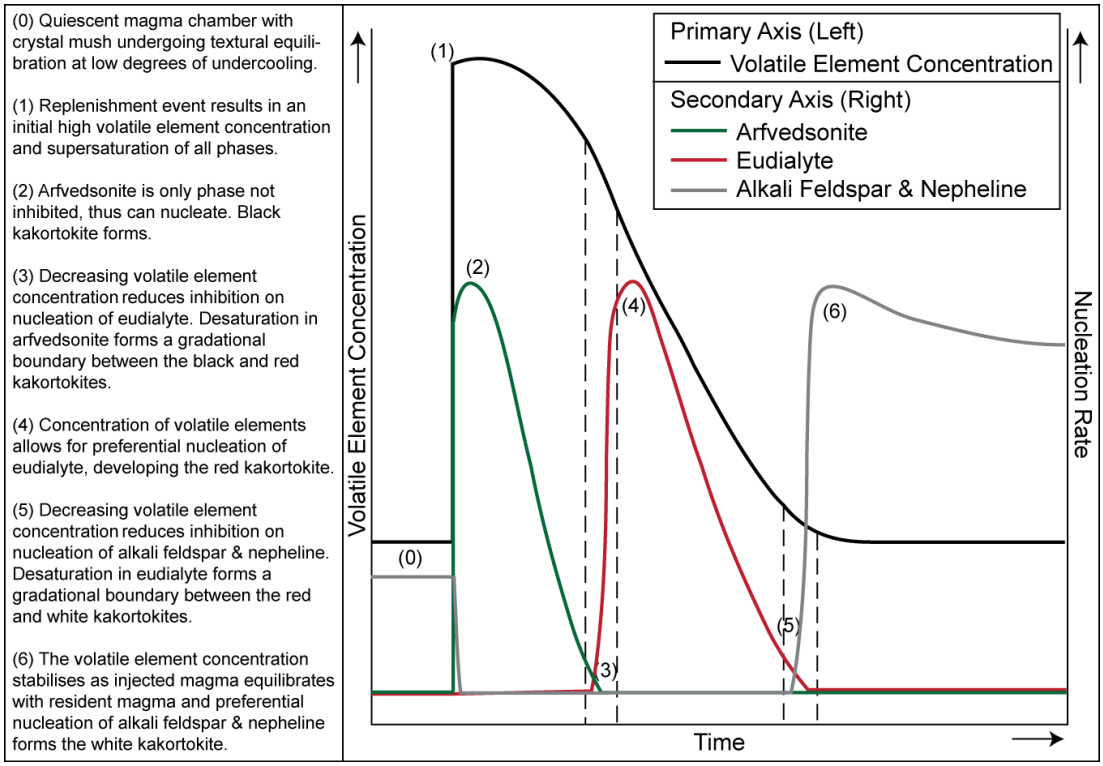

Figure 6.17: Speculative kinematic model indicating effects of varying volatile element concentrations on the nucleation of arfvedsonite, eudialyte, alkali feldspar and nepheline.

Crystallisation of the black kakortokite results in a decrease in the volatile element concentration of the bottom magma layer, as crystallisation of arfvedsonite will take up F from the magma during crystallisation. Minor processes of upwards loss of volatile elements along concentration gradients develops as a result of the quiescent state of the magma and the coeval crystallisation of the roof rocks (Larsen & Sørensen, 1987), would also reduce the volatile element concentration. This would lessen the inhibition on the nucleation of eudialyte (Fig. 6.17) and allow it to nucleate *in situ*. A continuous change in volatile element concentration and desaturation in arfvedsonite developed the gradational boundary between the black and red kakortokites (Fig. 6.17). Large-scale crystallisation of eudialyte through epitaxy and minor crystallisation of the other phases developed the red kakortokite.

The volatile element concentration is envisioned to continue decreasing throughout the formation of the red kakortokite. This is due to gradual equilibration of the bottom magma layer with the resident magma; loss of volatile elements due to crystallisation of the Cl-rich eudialyte and minor upward loss along a concentration gradient associated with the sodalite crystallisation at the roof of the chamber. This, combined with desaturation of the melt in eudialyte would allow alkali feldspar (Fig. 6.17) and nepheline to nucleate in a relatively halogen-poor magma, developing the white kakortokite above a gradational boundary.

The range of CSD profiles for the alkali feldspar in the Unit 0 white kakortokite (Fig. 6.8h) indicates that it crystallised through a range of processes: *in situ* crystallisation at the crystal mush – magma interface; gravitational settling of crystals onto the crystal mush; and enclosure of crystals suspended in the magma by the growing crystal mush pile (crystal fractionation). The calculated slope and intercept data from CSDs indicate the arfvedsonite in the black kakortokite and eudialyte in the red kakortokite crystallised from a thinner magma body than the alkali feldspar and nepheline in the white kakortokite (Fig. 6.9d). This is indicative of crystallisation of the arfvedsonite in the black and eudialyte in the red kakortokite from the bottom layer of the magma and crystallisation of the alkali feldspar and nepheline in the white kakortokite as the bottom layer of magma equilibrates with the resident magma body.

The control on the order of nucleation may be more directly related to the halogen content of the magma. High concentrations of halogens can depolymerise silicate melts, reducing the length of the silicate chains that can crystallise (e.g. Dingwell *et al.*, 1985) Arfvedsonite has a chain structure (Hawthorne, 1976); eudialyte a ring structure (Johnsen & Grice, 1999); while alkali feldspar and nepheline have three-dimensional frameworks of SiO_4 tetrahedra (Colville & Ribbe, 1968, Tait *et al.*, 2003), thus the structural complexity increases upwards through the

unit. As arfvedsonite has the simplest structure it can crystallise first at relatively high concentrations of halogens, while the other phases are inhibited. Reducing the halogen concentrations would allow eudialyte and then alkali feldspar and nepheline to nucleate.

Conditions in the crystal mush changed after the crystallisation of Unit 0 to allow for the postcumulus textural coarsening observed in the CSDs. Textural coarsening requires a low degree of undercooling (Higgins, 1999) for both crystal growth and diffusion. Thus undercooling must have decreased between the crystallisation of the Unit 0 white kakortokite and the textural coarsening, either from the latent heat of crystallisation from the ~5 m thick white kakortokite layer and/or due to increasing volatile element concentration associated with a later replenishment event. This reduction in the degree of undercooling inhibited nucleation in Unit 0 and increased the potential for crystal growth, allowing for the extensive postcumulus textural coarsening. Foliation fabrics are common in the black and white kakortokites, with the fabric defined by arfvedsonite and/or alkali feldspar crystals. The preferred orientation of these is likely associated with epitaxy during the development of the layers. The platy shape of the alkali feldspar crystals and compaction of the crystal mush before solidification of the layer may have enhanced the fabric. It is not interpreted to be associated with magmatic flow as there are no flow indicators throughout Unit 0. Alkali feldspar crystals with long aspect ratios cross the Units -1/0 boundary (Fig. 6.6b) and these would not have been preserved during magmatic flow.

The large arfvedsonite crystals in black kakortokite could be associated with either of two processes: (1) an antecrystic (i.e. crystals that formed from a progenitor magma (Larrea *et al.*, 2013)) origin, due to the replenishing magma entraining arfvedsonite crystals formed at depth in a sub-chamber within the plumbing system, i.e. Marsh's 'Tramp Crystals'; or (2) an *in situ* origin, due to textural coarsening in the presence of intercumulus fluids (2013), which would allow for much greater rates of diffusion. Circulation of intercumulus fluids through the crystal mush during the sub-liquidus stage is credible as there is evidence of late-stage magmatic to hydrothermal alteration of eudialyte. However, there is no extensive alteration in association with the large arfvedsonite crystals, thus this proposition is inconsistent with the observations from the present study. This present study indicates the bulk of nucleation occurred within the Ilímaussaq magma chamber, as the petrography and CSDs do not reflect crystal emplacement in slurries. The high-energy emplacement of a crystal-bearing slurry would not have preserved the aforementioned delicate, large alkali feldspar crystals (Fig. 6.6c). The compositions of the cores of the large

arfvedsonite crystals are within the range of the groundmass arfvedsonite (Fig. 6.14), however the compositions are typically towards the primitive end of the compositional ranges as they have relatively high Ca/(Na+K) ratios. Thus the entrainment of some arfvedsonite antecrysts from a deeper level magma body, i.e. the 'Tramp Crystal' hypothesis followed by chemical equilibration, is the only mechanism consistent with the data.

6.8 Conclusions

The CSD data indicate that the bulk of the unit formed through *in situ* crystallisation with processes of gravitational settling and fractional crystallisation being minor contributors. The key control on unit development was an oscillating volatile element concentration, which gradually decreased during the development of a unit and sharply increased at the boundary to the next, in combination with variations in undercooling. An open-system model is proposed whereby a replenishment event formed Unit 0. An initial high volatile element concentration allowed for the formation of the black kakortokite. Crystallisation and the minor processes of equilibration of the of bottom magma layer with the resident magma and upwards loss of volatiles along concentration gradients to the roof decreased the volatile element concentration. This allowed for development of the red and then white kakortokite above gradational boundaries from the underlying layer. Late-stage reduction in magma undercooling promoted the pervasive textural coarsening that is preserved in the CSDs. Although Unit 0 is particularly well developed, the model developed in this chapter is believed to generally applicable to the entire sequence of layered kakortokite. It will however be further tested in the following chapter on the lowest exposed kakortokite units.

6.9 References

Andersen, S., Bohse, H. & Steenfelt, A. (1981). A geological section through the southern part of the Ilímaussaq intrusion. *Rapport Grønlands Geologiske Undersølgelse* **103**, 39-42.

Bailey, J. C., Sørensen, H., Anderson, T., Kogarko, L. N. & Rose-Hansen, J. (2006). On the origin of microrhythmic layering in arfvedsonite lujavrite from the Ilímaussaq alkaline complex, South Greenland. *Lithos* **91**, 301-318.

Bohse, H., Brooks, C. K. & Kunzendorf, H. (1971). Field observations on the kakortokites of the Ilimaussaq intrusion, South Greenland, including mapping and analyses by portable X-ray fluorescence equipment for zirconium and niobium. *Rapport Grønlands Geologiske Undersølgelse* **38**, 43 pp.

Bons, P. D., Baur, A., Elburg, M. A., Lindhuber, M. J., Marks, M. A. W., Soesoo, A., van Milligen, B. P. & Walte, N. P. (2015). Layered intrusions and traffic jams. *Geology* **43**, 71-74.

Boorman, S., Boudreau, A. & Kruger, F. J. (2004). The Lower Zone-Critical Zone Transition of the Bushveld Complex: a Quantitative Textural Study. *Journal of Petrology* **45**, 1209-1235.

Colville, A. A. & Ribbe, P. H. (1968). The crystal structure of an adularia and a refinement of the structure of orthoclase. *The American Mineralogist* **53**, 25-37.

Di Carlo, I., Rotolo, S. G., Scaillet, B., Vincenzo, B. & Pichavant, M. (2010). Phase Equilibrium Constraints on Pre-eruptive Conditions of Recent Felsic Explosive Volcanism at Pantelleria Island, Italy. *Journal of Petrology* **51**, 2245-2276.

Dingwell, D. B., Scarfe, C. M. & Cronin, D. J. (1985). The effect of fluorine on viscosities in the system Na2O-Al2O3-SiO2: implications for phonolites, trachytes and rhyolites. *American Mineralogist* **70**, 80-87.

Ferguson, J. (1964). Geology of the Ilímaussaq alkaline intrusion, South Greenland. Part I. Description of map and structure. *Meddelelser om Grønland* **172**, 1-81.

Hawthorne, F. C. (1976). The crystal chemistry of the amphiboles: V. The structure and chemistry of arfvedsonite. *Candian Mineralogist* **14**, 346-356.

Higgins, M. D. (1999). Origin of megacrysts in granitoids by textural coarsening: a crystal size distribution (CSD) study of microcline in the Cathedral Peak Granodiorite, Sierra Nevada, California In: Castro, A., Fernández, C. & Vigneresse, J. L. (eds.) *Understanding Granites: Integrating New and Classical Techniques*. London: Geological Society London, Special Publications, 207-219.

Higgins, M. D. (2002a). Closure in crystal size distributions (CSD), verification of CSD caluclations, and the significance of CSD fans. *American Mineralogist* **87**, 171-175.

Higgins, M. D. (2002b). A crystal size-distribution study of the Kiglapait layered mafic intrusion, Labrador, Canada: evidence for textural coarsening. *Contributions to Mineralogy and Petrology* **144**, 314-330.

Higgins, M. D. (2010). Textural coarsening in igneous rocks. *International Geology Review* **1**, 1-23.

Johnsen, O. & Grice, J. D. (1999). The crystal chemistry of the eudialyte group. *Canadian Mineralogist* **37**, 865-891.

Karup-Møller, S., Rose-Hansen, J. & Sørensen, H. (2010). Eudialyte decomposition minerals with new hitherto undescribed phases from the Ilimaussaq complex, South Greenland. *Bulletin of the Geological Society of Denmark* **58**, 75-88.

Krumrei, T. V., Pernicka, E., Kaliwoda, M. & Markl, G. (2007). Volatiles in a peralkaline system: Abiogenic hydrocarbons and F-Cl-Br systematics in the naujaite of the Ilímaussaq intrusion, South Greenland. *Lithos* **95**, 298-314.

Larrea, P., França, Z., Lago, M., Galé, C. & Ubide, T. (2013). Magmatic Processes and the Role of Antecrysts in the Genesis of Corvo Island (Azores Archipelago, Portugal). *Journal of Petrology* **54**, 769-793.

Larsen, L. M. & Sørensen, H. (1987). The Ilímaussaq intrusion - progressive crystallisation and formation of layering in an agpaitic magma. *Geological Society London, Special Publications* **30**, 473-488.

Marks, M., Halama, R., Wenzel, T. & Markl, G. (2004). Trace element variations in clinopyroxene and amphibole from alkaline to peralkaline syenites and granites: implications for mineral-melt trace-element partitioning. *Chemical Geology* **211**, 185-215.

Marsh, B. D. (1988). Crystal size distribution (CSD) in rocks and the kinetics and dynamics of crystallization I. Theory. *Contributions to Mineralogy and Petrology* **99**, 277-291.

Marsh, B. D. (1998). On the interpretation of crystal size distributions in magmatic systems. *Journal of Petrology* **39**, 553-599.

Marsh, B. D. (2013). On some fundamentals of igneous petrology. *Contributions to Mineralogy and Petrology* **166**.

Mitchell, R. H. & Liferovich, R. P. (2006). Subsolidus deuteric/hydrothermal alteration of eudialyte in lujavrite from the Pilanesberg alkaline complex, South Africa. *Lithos* **91**, 352-372.

Pfaff, K., Krumrei, T., Marks, M. A. W., Wenzel, T., Rudolf, T. & Markl, G. (2008). Chemical and physical evolution of the 'lowered layered sequence' from the nepheline syenitic Ilímaussaq intrusion, South Greenland: Implications for the origin of magmatic layering in peralkaline felsic liquids. *Lithos* **106**, 280-296.

Pfaff, K., Wenzel, T., Schilling, J., Marks, M. A. W. & Markl, G. (2010). A fast and easy-to-use approach to cation site assignment for eudialyte-group minerals. *Neues Jahrbuch Fur Mineralogie-Abhandlungen* **187**, 69-81.

Schilling, J., Wu, F.-Y., McCammon, C., Wenzel, T., Marks, M. A. W., Pfaff, K., Jacob, D. E. & Markl, G. (2011). The compositional variability of eudialyte-group minerals. *Mineralogical Magzine* **75**, 87-115.

Sjöqvist, A. S. L., Cornell, D. H., Andersen, T., Erambert, M., Ek, M. & Leijd, M. (2013). Three Compositional Varieties of Rare-Earth Element Ore: Eudialyte-Group Minerals from the Norra Kärr Alkaline Complex, Southern Sweden. *Minerals* **3**, 94-120.

Sørensen, H. (1969). Rythmic igneous layering in peralkaline intrusions: An essay review on Ilímaussaq (Greenland) and Lovozero (Kola, USSR). *Lithos* **2**, 261-283.

Sørensen, H. & Larsen, L. M. (1987). Layering in the Ilimaussaq alkaline intrusion, South Greenland. In: Parsons, I. (ed.) *Origins of Igneous Layering*. Dordrecht: D. Reidel Publishing, 1-28.

Tait, K. T., Sokolova, E. & Hawthorne, F. C. (2003). The crystal chemistry of nepheline. *The Canadian Mineralogist* **41**, 61-70.

Upton, B. (2013). Tectono-magmatic evolution of the younger Gardar southern rift, South Greenland. *Geological Survey of Denmark and Greenland Bulletin* **29**, 124.

Ussing, N. V. (1912). Geology of the country around Julianehaab, Greenland. *Medeleser om Grønland* **38**, 1-426.

Chapter 7

Development of the Lowest Exposed Units

7.1 Introduction

The lowest exposed layered kakortokite (Units -11 to -8) is important in the magmatic history of the Ilímaussaq Complex as these rocks are commonly interpreted as forming at the same time as the naujaite (sodalite syenite) at the roof of the magma chamber. The naujaite is inferred to have formed as a flotation cumulate from sodalite crystals that rose to the roof, due to their light density, while the kakortokite formed through gravitational settling and density sorting (Engell, 1973, Ferguson, 1964, Ferguson, 1970, Larsen & Sørensen, 1987, Sørensen, 1969, Sørensen, 2006, Upton, 2013). There are problems in detail with this model as Unit -10 contains a subordinate white kakortokite, termed in the present study 'Wa' (Chapter 5.2), between denser layers of black kakortokite and red kakortokite. This is hard to envision forming through density sorting during gravitational settling. An ordered nucleation model, controlled by oscillating volatile concentrations between units in combination with variations in undercooling, was developed in Chapter 6 to account for the formation of Unit 0. To determine if this model is applicable to the other units across the layered series, the combined petrographic, textural and mineral chemical analysis was applied to the lowest exposed units (Fig. 7.1). This chapter provides an insight into the magma chamber dynamics operating at the base of the chamber during the coeval formation of the naujaite at the roof.

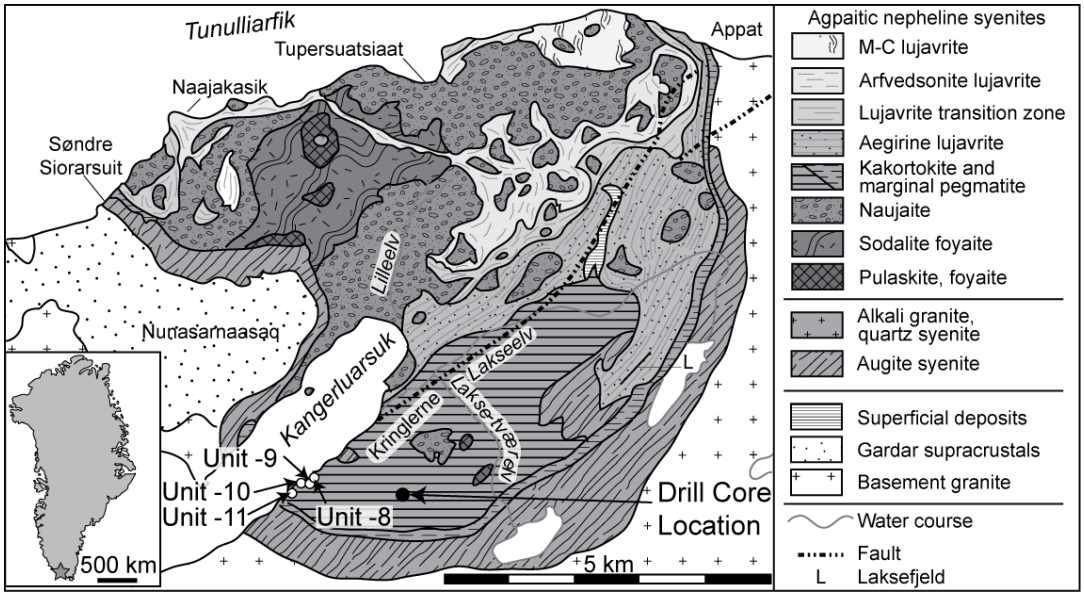

Figure 7.1: Map of southern part of complex, locations of studied units and drill core are arrowed.

7.2 Field relationships

The lowest outcropping units (-11 to -8) display distinct, planar layering, which is laterally continuous and homogeneous at the metre scale. There are no indicators of grading or current activity (e.g. cross-lamination, current bedding or apparent erosive features).

The lowest exposed rock is the Unit -11 white kakortokite, which is leucocratic and alkali feldspar-rich. The red and black kakortokites of U-11 are not exposed at the surface. The boundary between the Units -11 and -10 is sharp and planar (Fig. 7.2a-b), but becomes less distinct when viewed close up (Fig. 7.2c). Although the boundary between the units is definable, the concentration of arfvedsonite increases upwards to a maximum, at 0.5 m above the boundary. These features were not observed in the Unit 0 marker horizon, but are common throughout the remainder of the layered series. The black kakortokite of Unit -10 is melanocratic and displays a foyaitic texture defined by platy alkali feldspar crystals. Immediately above the boundary from the U-11 white kakortokite, the U-10 black kakortokite contains discrete veins of analcime and alkali feldspar, which occur wholly within U-10 without sharp boundaries to the kakortokite (Fig. 7.2d).

The U-10 black kakortokite is overlain by a leucocratic, alkali feldspar-rich rock, which forms above a gradational boundary (over 10-15 cm) from the black kakortokite (Fig. 7.2a,e). This rock has been described in Chapter 5.2 and is termed in the present study ‘Wa’ as it resembles a subordinate white kakortokite layer. It is enriched in eudialyte in patches with some areas resembling a eudialyte-poor red kakortokite; the unit however typically contains less than 10% eudialyte.

The ‘Wa’ layer is overlain by a red kakortokite (Fig. 7.2a), which forms above a boundary that is gradational over 10-15 cm. The U-10 red kakortokite has the typical saccharoidal texture but also contains acicular amphibole and platy alkali feldspar crystals (Fig. 7.2f).

The U-10 white kakortokite forms above a gradational boundary (over 5-10 cm) from the red kakortokite. It has a poorly developed foliation fabric defined by platy alkali feldspar crystals (Fig. 7.2g).

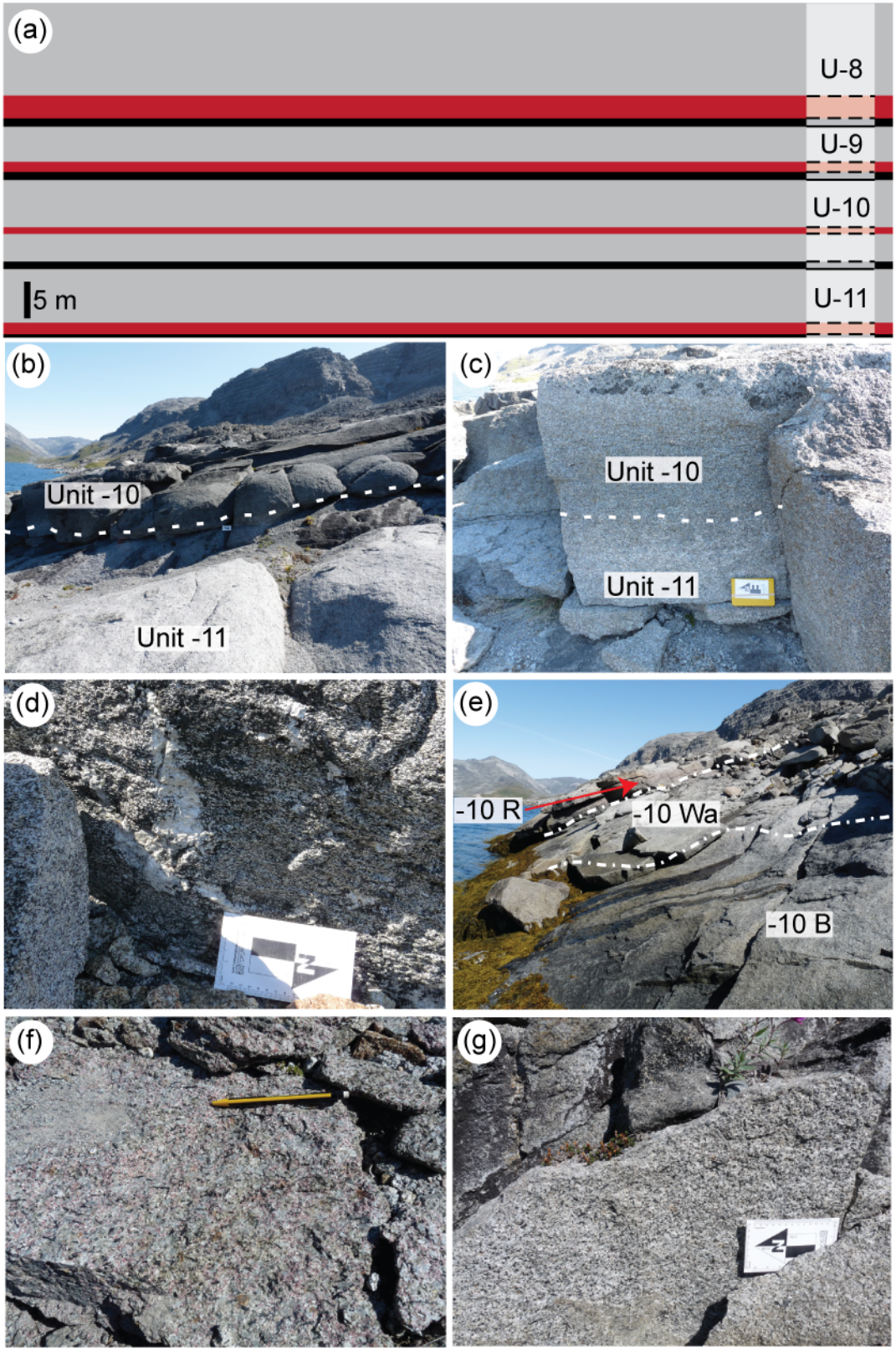

Figure 7.2: (a) Schematic stratigraphy of Units -11 to -8, solid lines indicate sharp boundaries, dashed = gradational. (b) Sharp boundary between Unit -11 white and Unit -10 black kakortokite. (c) Units -11/-10 boundary is less distinct when viewed closer. (d) Unit -10 black kakortokite with white (analcime) veins. (e) Unit -10: black kakortokite (B) overlain by white ('Wa') then red kakortokite (R), height of loose block in foreground = 0.5 m. (f) Unit -10 red kakortokite with acicular arfvedsonite needles. (g) Unit -10 white kakortokite. Scale card = 15 cm long, pencil = 14 cm long.

Unit -9 forms above a sharp boundary from Unit -10 (Fig. 7.3a). Similar to the U-10 black kakortokite, the concentration of arfvedsonite increases to a maximum concentration 0.3 m above the distinct boundary. The U-9 black kakortokite is arfvedsonite-rich and does not have a foliation fabric. The U-9 red kakortokite forms above a gradational boundary (over ~0.3 m) from the black kakortokite (Fig. 7.2a). It is relatively eudialyte-poor and avoids the typical saccharoidal texture (Fig. 7.3b). The U-9 white kakortokite occurs above a gradational boundary (5-10 cm) from the red kakortokite (Fig. 7.2a). It is leucocratic with a very poor foliation fabric identified by platy alkali feldspar crystals.

Unit -8 overlies a sharp boundary from the Unit -9 white kakortokite (Figs 7.2a, 7.3c). Unlike the Units -11/-10 boundary the Units -9/-8 boundary is relatively distinct when viewed closer. Above this boundary the concentration of arfvedsonite increases to a maximum over 0.9 m. The U-8 black kakortokite is arfvedsonite-rich and has a foliation fabric identified by platy alkali feldspar crystals.

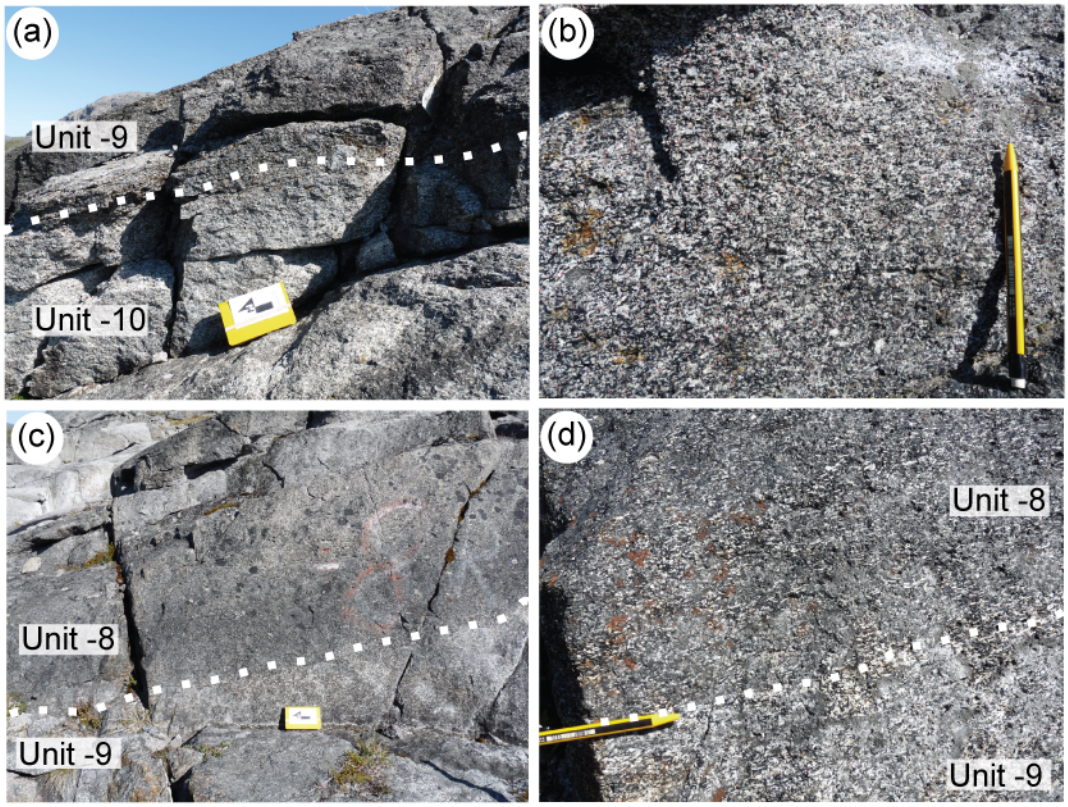

Figure 7.3: Field photos of the lowest layered kakortokite. (a) Sharp boundary between Unit -10 white kakortokite and Unit -9 black kakortokite, card for scale. (b) Unit -9 red kakortokite, it is eudialyte-poor but marks a distinct increase in eudialyte compared to the remainder of the unit. (c) Sharp boundary between Unit -9 white and Unit-8 black kakortokites. (d) Units -9/-8 boundary is relatively distinct when viewed closer. Scale card = 15 cm long, pencil = 14 cm long.

7.3 Petrography

Samples were collected from the locations indicated in Fig 7.1. Samples of U-11 white kakortokite; U-11/-10 boundary; U-10 black, red & white layers; U-10/-9 boundary; U-9 black, red & white layers; and U-8 black kakortokite were collected from outcrop. The U-10 'Wa' layer (EJH/12/219) was sampled from the DX-01 drill core. Petrographic descriptions of each sample are in Table 7.1.

Sample No.	Unit	Section Image	Petrography (modal %)	Sample Height
EJH/12/032	U-8 Black	Figure 7.5f	50% arfv, 25% k-fsp, 15% neph, 10% eud.	1 m above boundary
EJH/12/033	U-9 White	Figure 7.5e	35% k-fsp, 20% neph, 20% arfv, 15% aeg, 10% eud.	2 m above boundary
EJH/12/031	U-9 Red	Figure 7.5d	30% k-fsp, 25% eud (of which 50% is altered), 20% neph, 20% arfv, 5% sod.	0.8 m above boundary
EJH/12/029	U-9 Black	Figure 7.5c	45% arfv, 20% neph, 15% eud, 15% k-fsp, 5% sod.	0.5 m above boundary
EJH/12/030	U-10/-9 Boundary	Figure 7.5b	U-9 Black: 30% arfv, 30% k-fsp, 20% neph, 20% eud.	0-25 mm above boundary
		Figure 7.5a	U-10 White: 35% k-fsp (carries moderate foliation), 20% neph, 20%, eud, 15% arfv, 10% aeg.	0-25 mm below boundary
EJH/12/028	U-10 White	Figure 7.4f	50% k-fsp, 25% neph, 15% eud (mostly altered), 5% arfv, 5% aeg.	2 m above boundary
EJH/12/027	U-10 Red	Figure 7.4e	40% eudialyte (alteration to 50% of crystals), 20% k-fsp, 20% neph, 15% arfv, 5% aeg.	0.8 m above boundary
EJH/12/219	U-10 'Wa'	Figure 7.4d	30% k-fsp (carries moderate foliation fabric), 20% sod, 20% aeg, 15% eud (of which 60% is altered), 15% arfv.	1.2 m above boundary
EJH/12/024	U-10 Black	Figure 7.4c	50% arfv, 30% k-fsp (carries a strong foliation fabric), 15% neph, 5% eud.	0.9 m above boundary
EJH/12/023	U-11/10 Boundary	Figure 7.4b	U-10 Black: 35% k-fsp, 30% arfv 20% neph, 15% eud.	0-25 mm above boundary
			U-11 White: 45% k-fsp, 15% neph, 15% eud, 10% aeg, 10% sod, 5% arfv.	0-25 mm below boundary
EJH/12/025	U-11 White	Figure 7.4a	40% k-fsp, carries a strong foliation fabric; 25% neph, 15% aeg, 10% arfv, 10% eud.	2 m below boundary

Table 7.1: Petrographical descriptions of samples. Alteration refers to hydrothermal alteration of eudialyte to nacareniobsite-Ce, catapleiite, pectolite and britholite (Chapter 6.6). Abbreviations: Aeg – aegirine, arfv – arfvedsonite, eud – eudialyte, K-fsp – alkali feldspar, neph – nepheline, sod – sodalite.

The samples taken from the unit boundaries have differing mineral proportions to the white or black kakortokite layers. The observed increase in arfvedsonite above the unit boundaries in outcrop is confirmed in thin section. The U-10 black kakortokite immediately above (0-10 mm) the Units -11/-10 boundary contains 30% arfvedsonite, which increases to 45% over 1m (Fig. 7.4b-c).

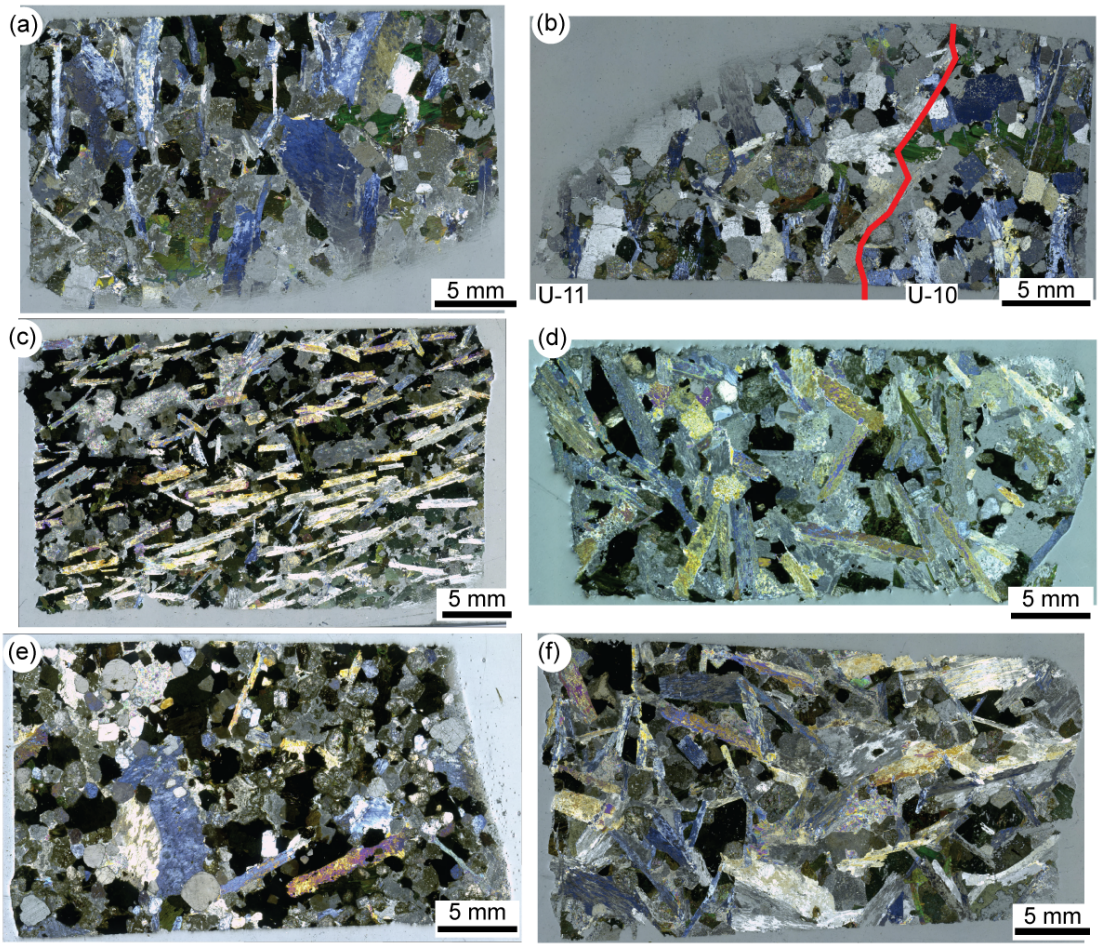

Figure 7.4: Probe sections of samples from Unit -11 to Unit -10, all photographed under circularly polarised light. (a) U-11 white kakortokite. (b) Boundary (red) between Unit -11 white and Unit -10 black. (c) U-10 black, note it is much richer in arfvedsonite above the unit boundary. (d) U-10 'Wa', it is enriched in alkali feldspar and poor in eudialyte. (e) U-10 red, it is greatly enriched in eudialyte compared to the underlying 'Wa' layer. (f) U-10 white.

The variations in arfvedsonite concentration are also seen in the white kakortokite samples below the unit boundaries. Relatively increased arfvedsonite concentrations are observed immediately below the unit boundaries. For example at the Units -10/-9 boundary, the arfvedsonite concentration in the U-10 white kakortokite increases from 5% in the centre of the layer to 15% at the upper boundary (Fig. 7.5a-b).

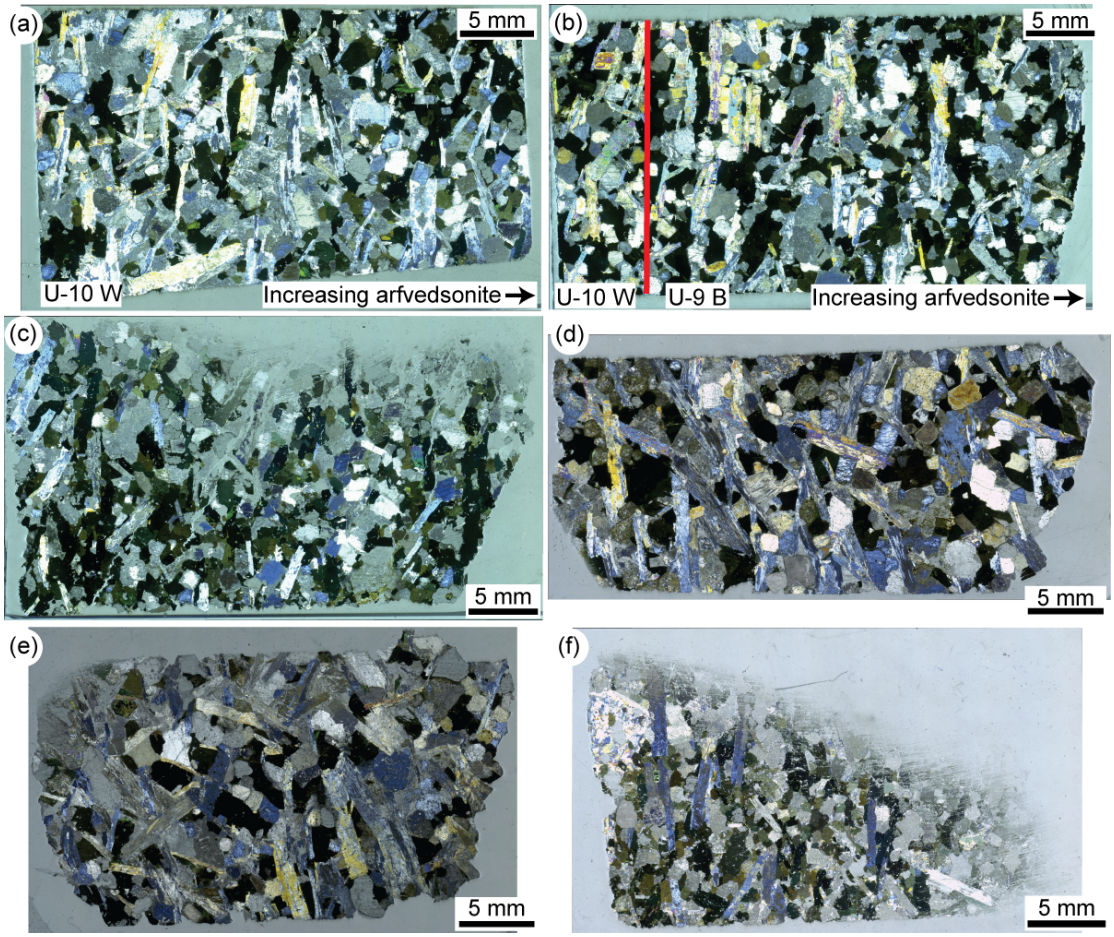

Figure 7.5: Probe sections of samples from Units -10/-9 boundary to Unit -8, all photographed under circularly polarised light. (a) Unit -10 white kakortokite immediately below Units -10/-9 boundary. (b) Units -10/-9 boundary (red), section continues from (a). Note increasing arfvedsonite content from (a) through to top of (b). (c) Unit -9 black kakortokite, note relative enrichment in arfvedsonite compared to (b). (d) Unit -9 red kakortokite, it is relatively eudialyte poor compared to U-10 red. (e) Unit -9 white kakortokite. (f) Unit -8 black kakortokite.

7.4 Quantitative Textural Analysis

Crystal size distribution analyses were performed on hand digitised crystal outlines following the methods detailed in Chapter 4.3. All the samples described above were analysed, apart from U-11/-10 black kakortokite due to lack of sufficient arfvedsonite crystals immediately above the boundary for an accurate analysis. Arfvedsonite was measured from the black, eudialyte from the red and alkali feldspar from the white kakortokites. The data are presented in Fig. 7.6 and Table 7.2, for ease of analysis the plots are separated according to rock type: black, red white and two unit boundary plots for white and black kakortokite. The raw CSD data are located in the supplementary data files in Appendix C.

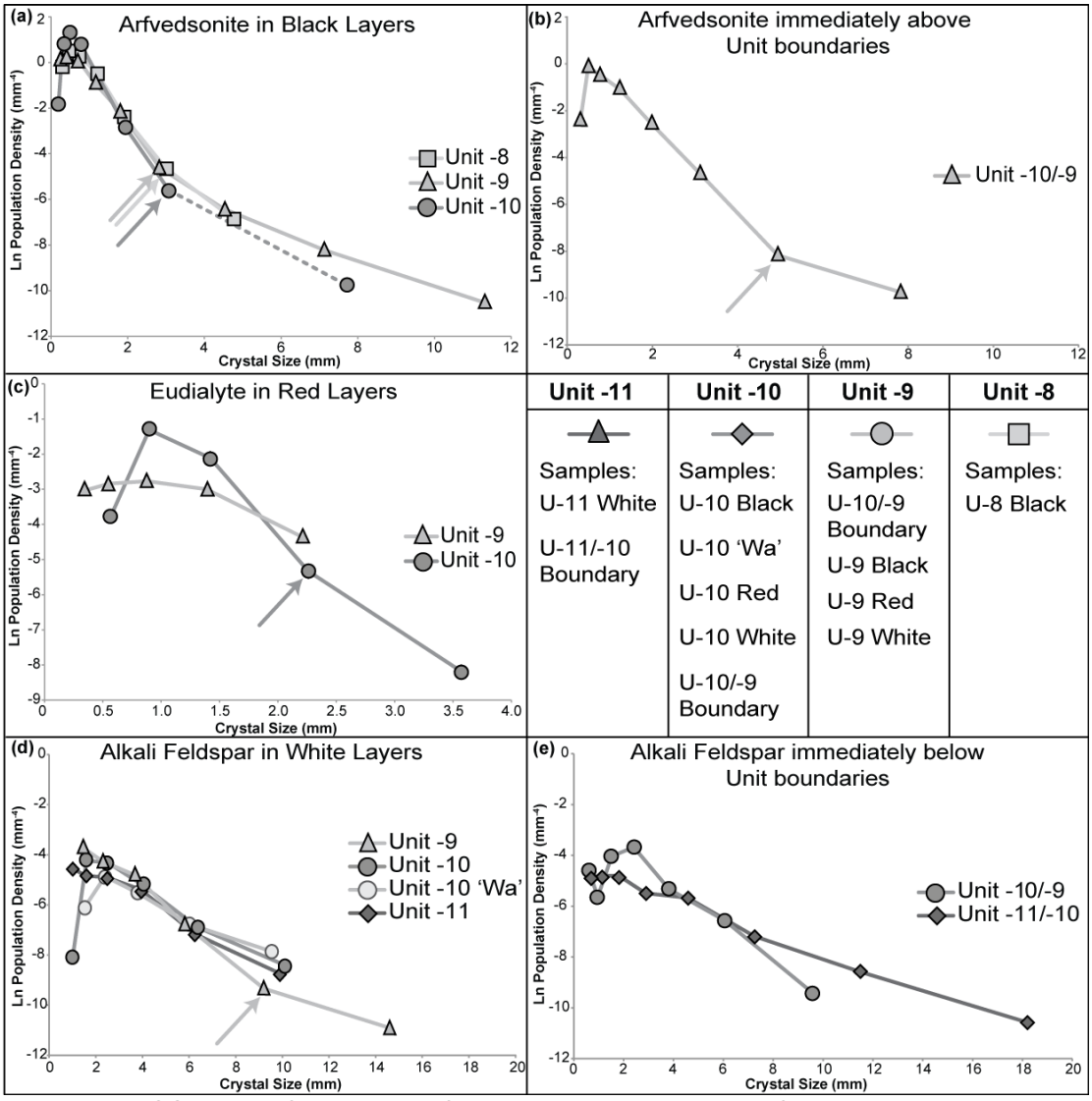

Figure 7.6: CSD plots for samples from Units -11 to -8. (a) Arfvedsonite in black kakortokite. (b) Arfvedsonite in black kakortokite immediately above (0-25 mm) the unit boundaries. (c) Eudialyte in red kakortokite. (d) Alkali feldspar in white kakortokite. (e) Alkali feldspar in white kakortokite immediately below (0-25 mm) the unit boundaries.

Arfvedsonite crystal sizes range from 0.2 to 11.3 mm in the central portions of the black kakortokite layers (Fig. 7.6a). In comparison the black kakortokite sample from immediately above (0-25 mm) the Units -10/-9 boundary displays smaller crystal sizes between 0.3 and 7.8 mm (Fig. 7.6b) The slope values are much steeper for the arfvedsonite crystals in the black kakortokite from the central portions of the layer (-2.13 to -2.75) compared to the sample from U-10/-9 (-1.84). The plots for all arfvedsonite samples have kinks (arrowed on Fig 7.6 a-b), similar to the arfvedsonite analyses from Unit 0 (Chapter 6.4). Unit -10 is kinked at 3.1 mm, U-9 at 2.8 mm, U-8 at 3.0 mm and the U-10/-9 boundary at 4.9 mm. The main portions of the CSDs are log-linear, although all samples display a downturn at the smallest crystal sizes, representing a reduction in the population density of the smallest crystals.

The eudialyte crystal sizes range from 0.4 to 3.6 mm and the slope values vary between -1.24 and -2.68. The plot shapes differ between units (Fig. 7.6c). The U-10 red kakortokite has a relatively log-linear plot, with a minor kink at 2.3 mm and a downturn at the smallest crystal sizes. The U-9 eudialyte-poor red kakortokite displays a flattened CSD profile, with a slight upwards curvature over the entire range of crystal sizes.

The alkali feldspar crystal sizes range from 0.1 to 14.6 mm in the central portions of white kakortokite layers. The samples from the boundaries U-11/-10 and U-10/-9 display a larger range of crystal sizes (0.6 to 18.2 mm). The slope values for the white kakortokites range from -0.42 to -0.74 while the boundary samples have a larger range between -0.35 and -0.77. The plot shapes are relatively log-linear (Fig. 7.6d-e) and all samples have a downturn at the smallest crystal sizes. The Unit -9 white kakortokite has a kink at the larger crystal sizes (at 9.2 mm), after which the slope is flattened. The U-10 ‘Wa’ layer has a similar plot shape and crystal sizes compared to the white kakortokite layers (Fig. 7.6d).

Sample	Unit	Mineral	Crystal %	SPO	Lmax (mm)	Y intercept	Y int Error (±)	Characteristic Length	Slope	Slope Error (±)
EJH/12/025	-11 W	K-Fsp	20.0	0.7	7.2	-3.89	0.09	2.1	-0.49	0.01
EJH/12/023	-11/-10 W	K-Fsp	49.4	0.4	5.9	-4.41	0.05	2.9	-0.35	0.004
EJH/12/024	-10 B	Arfvedsonite	29.5	0.3	3.0	2.74	0.01	0.4	-2.75	0.01
EJH/12/0219	-10 Wa	K-Fsp	28.9	0.5	8.3	-3.95	0.08	2.4	-0.42	0.01
EJH/12/027	-10 R	Eudialyte	19.8	-	2.1	1.23	0.02	0.4	-2.68	0.05
EJH/12/028	-10 W	K-Fsp	29.2	0.1	8.5	-3.23	0.05	1.9	-0.52	0.01
EJH/12/030	-10/-9 W	K-Fsp	22.0	0.4	7.0	-2.04	0.02	1.3	-0.77	0.01
EJH/12/030	10/-9 B	Arfvedsonite	28.6	0.2	3.3	0.99	0.002	0.5	-1.84	0.004
EJH/12/029	-9 B	Arfvedsonite	38.3	0.3	5.3	1.69	0.003	0.5	-2.20	0.004
EJH/12/031	-9 R	Eudialyte	12.6	-	2.2	-1.53	0.10	0.8	-1.24	0.08
EJH/12/033	-9 W	K-Fsp	23.5	0.4	8.0	-2.48	0.02	1.4	-0.74	0.01
EJH/12/032	-8 B	Arfvedsonite	35.5	0.3	2.7	1.78	0.02	0.5	-2.13	0.02

Table 7.2: CSD input and output data. Crystal % = percentage of digitised phase. SPO = shape preferred orientation from 0 (no fabric) to 1 (complete alignment). Lmax = mean size of 4 largest crystals. Y-intercept = y-axis intercept of linear regression. Characteristic length = -1/slope. Slope = gradient of linear regression. K-Fsp = alkali feldspar.

To verify that the calculated CSD data do not exceed the maximum modal percentage for each mineral species, as identified in thin section, closure limits were calculated (Higgins, 2002a) at 60% crystallinities for each mineral species. The characteristic length vs. y-axis intercept data all plot below their respective closure limits, demonstrating no internal inconsistency in the calculated data (Fig. 7.7a). There is no relationship between the volumetric phase proportion of each analysed sample and the characteristic length (Fig. 7.7b). There is a general positive correlation between the Lmax and the characteristic length (Fig. 7.7c) although the alkali feldspar, arfvedsonite and eudialyte plot in separate groups.

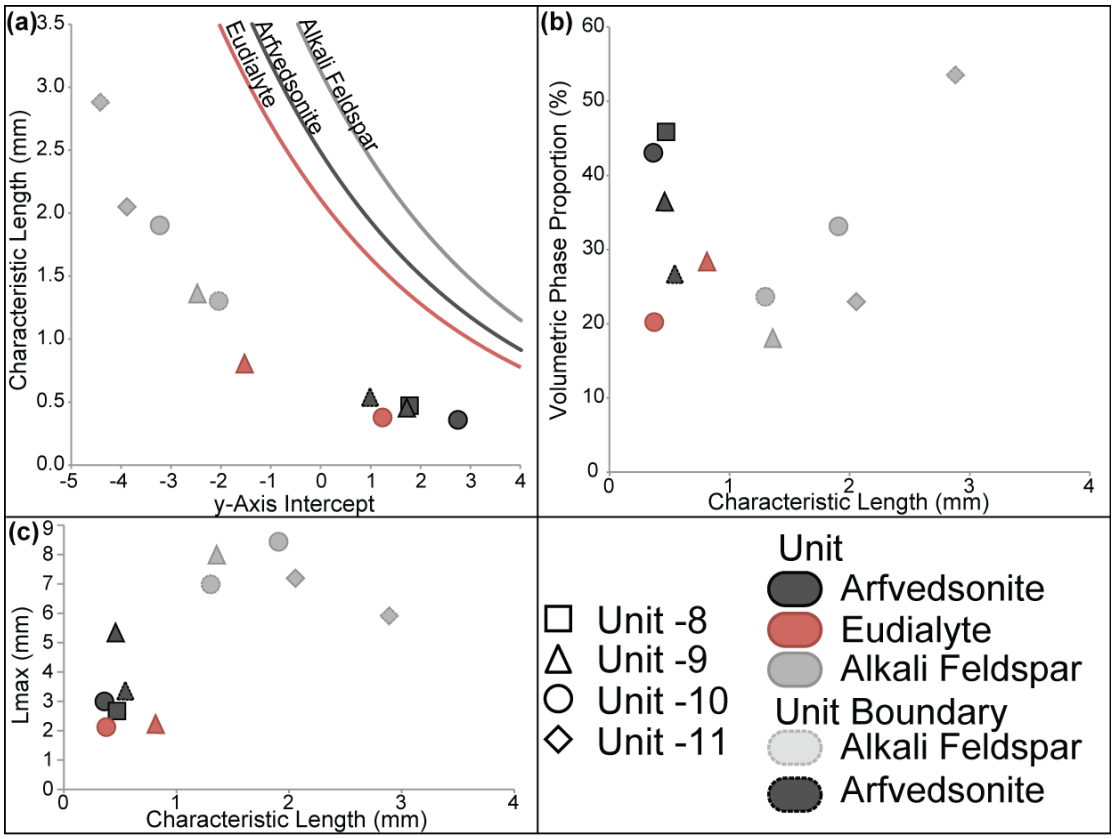

Figure 7.7: (a) plot of characteristic length vs. y-Axis intercept, all samples plot below their calculated crystallinity limits. (b) plot of characteristic length vs. volumetric phase abundance. (c) plot of y-Axis intercept vs. Lmax, displaying a general decrease in y-axis intercept with Lmax.

7.5 Mineral Chemistry

EPMA (Chapter 4.5) was used to evaluate the composition of the eudialyte-group minerals (EGM) and amphibole (arfvedsonite) within the lowest exposed units (-11 to -8). The mineral chemical data are located in the supplementary data files in Appendix D.

7.5.1 Eudialyte-Group Minerals

EGM are present in all of the analysed samples in varying concentrations (Table 7.1). The $Fe_{(TOT)}$/Mn ratios (Fig. 7.8, Table 7.3) are used as an indicator of the relative evolutionary state of the melt at time of the EGM crystallisation, as relatively primitive melts crystallise Fe-rich EGM, while more evolved melts crystallise Mn-rich EGM (Pfaff *et al.*, 2008, Schilling *et al.*, 2011).

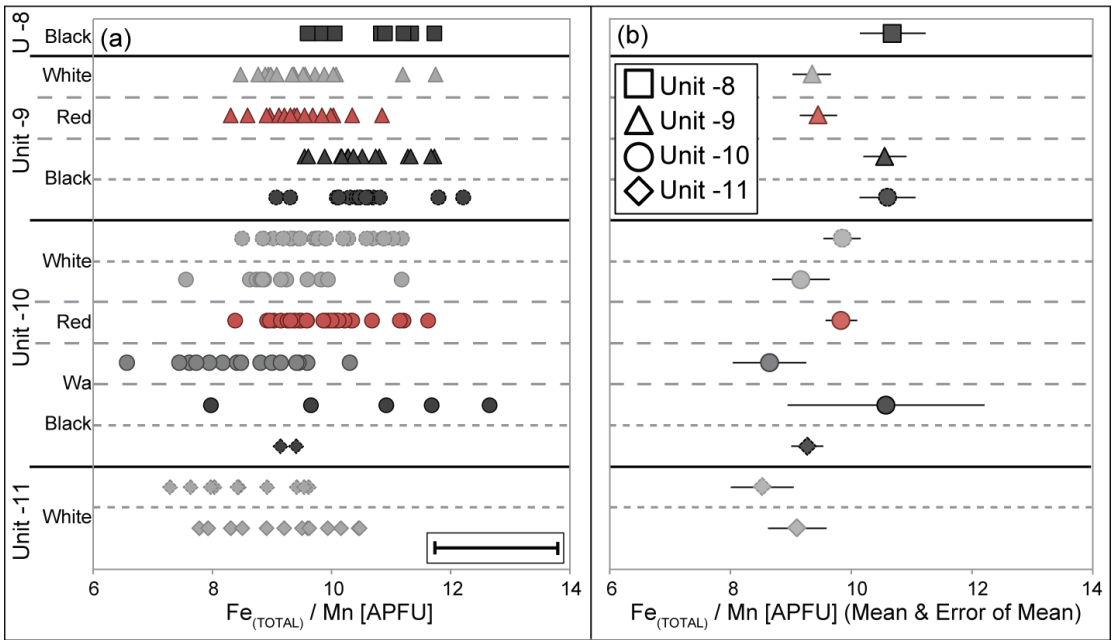

Figure 7.8: EGM Fe_{TOTAL}/Mn ratios through EPMA, separated according to unit stratigraphy. (a) Data for the range of textures, error bar on individual analyses bottom right. (b) Mean and error of mean to 95% confidence for each dataset. Note outliers are not excluded from mean calculations.

The $Fe_{(TOT)}$/Mn ratio plots (Fig. 7.8) display a contrast between the black, red and white kakortokite data (Table 7.3). The EGM in the black kakortokite from the central portions of the layers have the greatest $Fe_{(TOT)}$/Mn ratios, with a mean value of 10.60±0.46, (ranging between 7.97 and 12.65). The black kakortokite samples from the central portions of the layers have a higher range of values than the black kakortokite sampled immediately above (0-25 mm) unit boundaries (mean, 10.46±0.36, range 9.07 to 12.21). The red kakortokite samples have intermediate compositions, with a mean of 9.70±0.21 and range from 8.31 to 11.62.

Unit	Rock	$Fe_{(TOT)}/Mn$				Ca/REE+Y				Al/Si				Cl (wt.%)			
		Mean	±	Min	Max	Mean	±	Min	Max	Mean	±	Min	Max	Mean	±	Min	Max
-8	Black	10.69	0.54	9.62	11.73	12.11	0.61	10.77	13.35	0.005	0.0004	0.004	0.006	1.61	0.05	1.46	1.69
-9	White	9.34	0.32	8.47	10.08	12.31	0.70	10.14	14.00	0.006	0.0004	0.030	0.007	1.63	0.03	1.53	1.69
	Red	9.46	0.31	8.31	10.85	11.43	0.51	9.00	13.02	0.007	0.0018	0.005	0.020	1.58	0.03	1.39	1.66
	Black	10.56	0.36	9.55	11.72	11.98	0.65	10.04	14.53	0.005	0.0003	0.004	0.006	1.54	0.05	1.24	1.60
-10/-9 Boundary	Black	10.60	0.46	9.07	12.21	12.13	0.56	10.53	14.08	0.005	0.0003	0.004	0.006	1.53	0.06	1.23	1.65
	White	9.85	0.31	8.50	11.18	12.31	0.46	10.54	15.46	0.006	0.0003	0.004	0.007	1.60	0.02	1.48	1.68
-10	White	9.17	0.47	7.55	11.18	11.68	0.79	9.63	15.27	0.005	0.0003	0.005	0.007	1.63	0.04	1.44	1.70
	Red	9.84	0.26	8.38	11.62	12.19	0.41	9.85	14.64	0.005	0.0003	0.004	0.008	1.63	0.02	1.54	1.71
	'Wa'	8.64	0.61	6.57	10.31	12.21	0.74	10.25	14.43	0.005	0.0005	0.004	0.007	1.55	0.03	1.45	1.64
	Black	10.58	1.63	7.97	12.65	12.24	1.16	10.20	13.39	0.008	0.0040	0.005	0.066	1.44	0.07	1.31	1.49
-11/-10 Boundary	Black	9.27	0.26	9.14	9.40	12.40	0.30	12.25	12.55	0.005	0.0005	0.004	0.005	1.42	0.23	1.31	1.53
	White	8.53	0.52	7.29	9.62	12.11	0.98	10.41	15.86	0.006	0.0004	0.005	0.006	1.56	0.04	1.44	1.63
-11	White	9.11	0.49	7.78	10.47	11.73	9.56	9.41	13.60	0.006	0.0004	0.004	0.007	1.60	0.49	1.29	1.68
Mean Compositions and Ranges																	
Boundary Black		10.46	0.46	9.07	12.21	12.16	0.50	10.53	14.08	0.005	0.0003	0.004	0.006	1.52	0.06	1.23	1.65
Black		10.60	0.36	7.97	12.65	12.07	0.43	10.04	14.53	0.008	0.0043	0.004	0.066	1.54	0.04	1.24	1.69
Red		9.70	0.21	8.31	11.62	11.92	0.33	9.00	14.64	0.006	0.0007	0.004	0.020	1.62	0.02	1.39	1.71
White		9.19	0.26	7.55	11.18	11.88	0.39	9.41	15.27	0.006	0.0002	0.004	0.007	1.62	0.02	1.29	1.70
Boundary White		9.46	0.33	7.29	11.18	12.25	0.43	10.41	15.86	0.006	0.0002	0.004	0.007	1.59	0.02	1.44	1.68

Table 7.3: Mean, Minimum and Maximum values for geochemical ratios measured in EGM from the black, red, white and boundary samples from Units -11 to -8. Precision (±) to 95% confidence.

The white kakortokite samples have some of the lowest $Fe_{(TOT)}$/Mn ratios. The central portions of the white kakortokite layers have a mean $Fe_{(TOT)}$/Mn ratio of 9.19±0.26, ranging between 7.55 and 11.18. The white kakortokite immediately below (0-25 mm) unit boundaries has slightly increased ratios (mean of 9.46±0.33, range of 7.29 to 11.18) while the U-10 'Wa' layer has the lowest ratios (mean of 8.64±0.61, range of 6.57 to 10.31).

To investigate further the relative evolutionary state of the magma during crystallisation Ca/(REE+Y) and Al/Si ratios were analysed. The Ca/(REE+Y) ratio reflects the evolutionary state of the magma, as the (REE+Y) content increases as the magma evolves, thus lower ratios indicate more evolved magmas (Pfaff *et al.*, 2008). The range of values do not display much variation through the analysed layers (Fig 7.9a), however there are discontinuities across the unit boundaries as the EGM in the black kakortokite have lower values than the EGM in the underlying white kakortokite (Fig 7.9a-b, Table 7.3). There is a general trend of increasing Ca/(REE+Y) ratios upwards through each unit (Fig. 7.9a-b, Table 7.3). The U-10 'Wa' layer has a composition intermediate between that of the underlying black and overlying red kakortokite (Fig. 7.9a-b, Table 7.3)

The Al/Si ratio is suggested to increase as the magma from which the EGM crystallised evolves (Pfaff *et al.*, 2008). Similar to the Ca/(REE+Y) ratios, there is little variation between the layers. The ratios are greatest in the black kakortokite and decrease upwards through each unit (Fig. 7.9c-d, Table 7.3). The U-10 'Wa' layer has a similar range of ratios (0.004 to 0.007) to the white kakortokite samples (0.004 to 0.007), although these have a slightly higher mean (0.006±0.0002) compared to the 'Wa' layer (0.005±0.0005; Fig. 7.9c-d, Table 7.3).

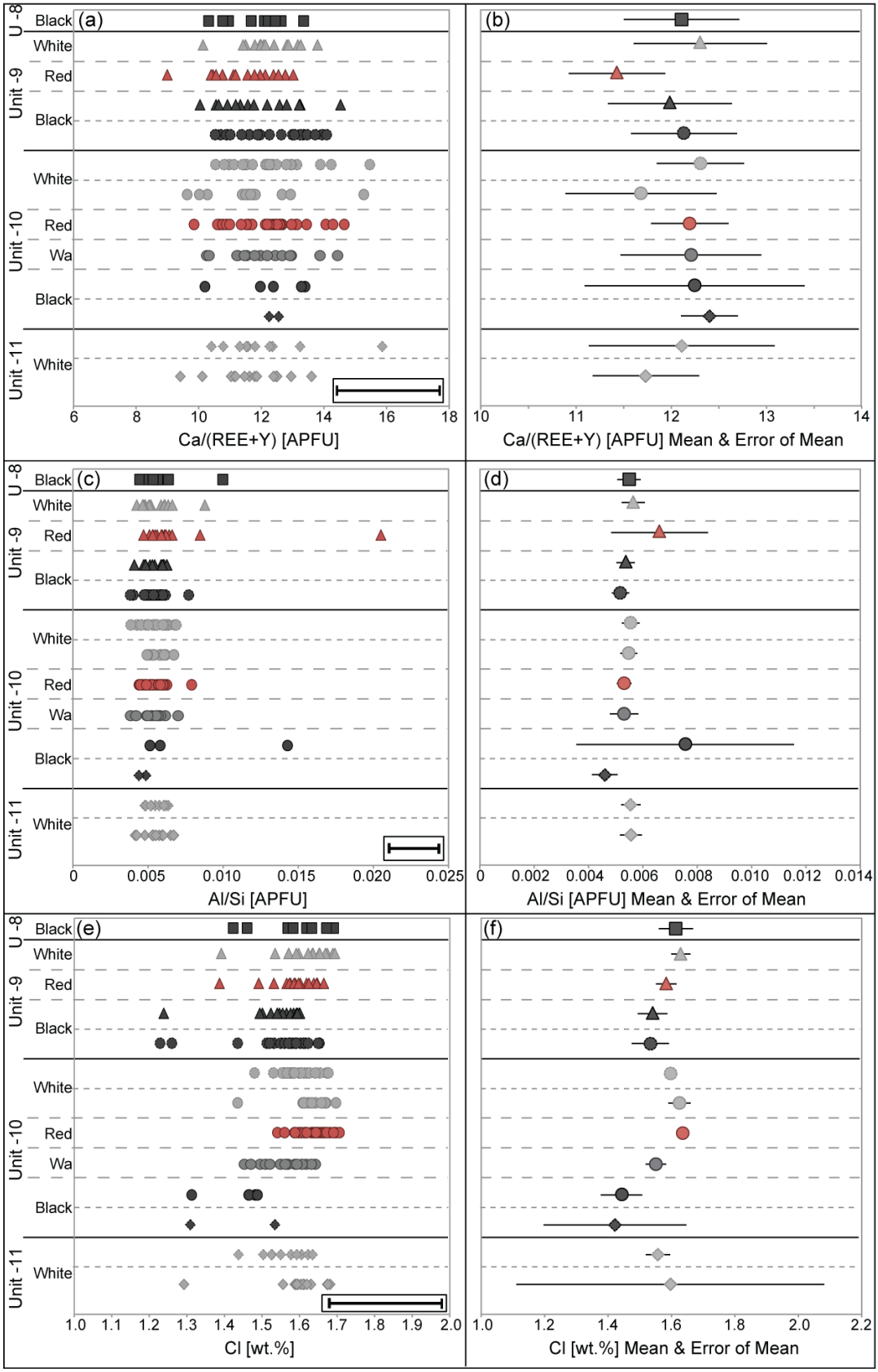

Figure 7.9: EGM chemistry through EPMA, error bar for individual analyses at bottom right of plots. (a) Ca/(REE+Y). (b) Mean and error of mean for Ca/(REE+Y) data. (c) Al/Si. (d) Mean and error of mean for Al/Si data. (e) Cl. (f) Mean and error of mean for Cl data. Note outliers are not excluded from mean calculations.

The Cl content of eudialyte was also investigated as this is suggested to decrease upwards through the Ilímaussaq stratigraphy (Pfaff *et al.*, 2008), due to decreasing Cl in the melt during fractionation (Krumrei *et al.*, 2007). Discontinuities occur at unit boundaries with the black kakortokite from immediately above the boundaries (mean = 1.52±0.04 wt.%, 1.23-1.65 wt.%) and from the central portions of the layers (mean = 1.54±0.04 wt.%, 1.23-1.69 wt.%) having lower Cl contents (Fig. 7.9e-f, Table 7.3) than the white kakortokite underlying the unit boundaries (mean = 1.59±0.02 wt.%, 1.44-1.68 wt.%). The EGM from the red kakortokite samples have an intermediate composition in comparison to the other rock types (Fig. 7.9e-f, Table 7.3), with a range between 1.39 and 1.71 wt.% and a mean composition of 1.62±0.02 wt.% Cl. The EGM in the central portions of the white kakortokite samples have the lowest range of Cl contents (mean = 1.62±0.02 wt.%wt.%, 1.29-1.70 wt.%, Fig. 7.9e-f, Table 7.3). In comparison the EGM in the subordinate 'Wa' layer have a greater similarity (mean = 1.55±0.03 wt.%, 1.45-1.64 wt.%) to the black and red kakortokite layers of Unit -10 (Fig. 7.9e-f, Table 7.3).

7.5.2 Amphibole

The amphibole compositions from Units -11 to -8 range towards the sodic end-members, between katophorite and arfvedsonite (Fig. 7.10).

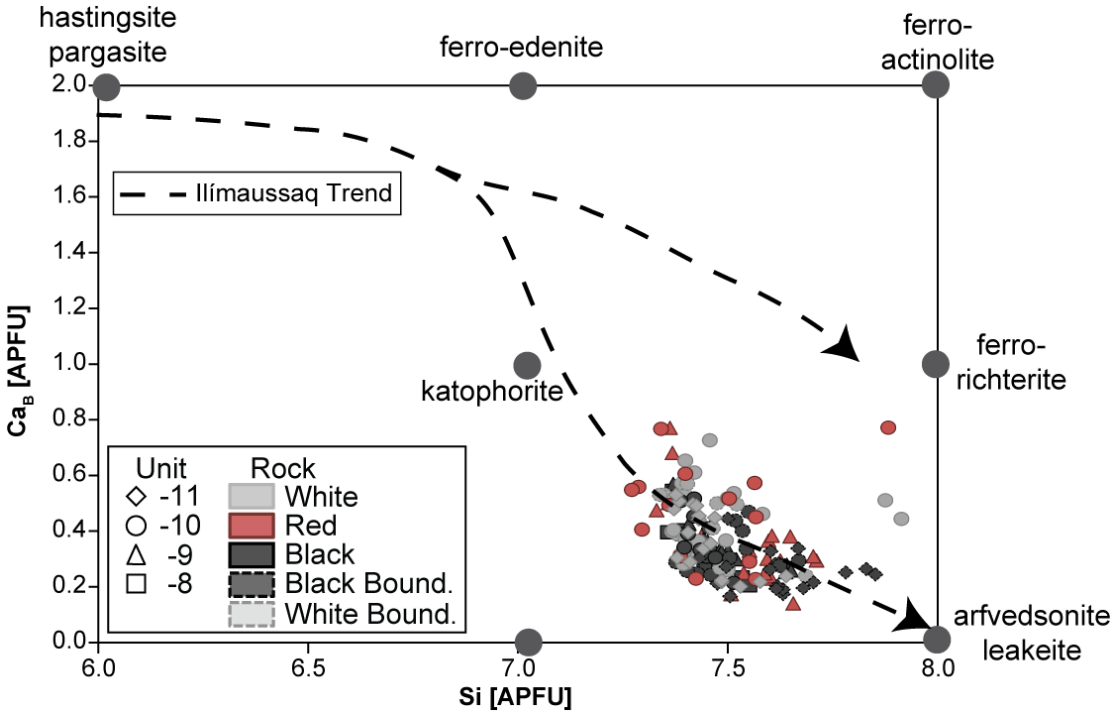

Figure 7.10: Plot of Ca_B vs. Si (APFU) in amphibole. Data subdivided according to unit stratigraphy. Plot adapted from Marks *et al.* (2004), data follow their bimodal Ilímaussaq trend.

Two chemical ratios were used to investigate the amphibole chemistries, the Ca/(Na+K) and $X_{Fe(TOT)}$ ($Fe_{(TOT)}$/[$Fe_{(TOT)}$+Mn+Mg]). Ca/(Na+K) should systematically decrease as the melt from which amphibole crystallises evolves (Pfaff et al., 2008). This is an effect of the crystallographic preferences of Na & K on the A-site & Ca and Na on the B-site (Pfaff et al., 2008). The $X_{Fe(TOT)}$ ratio was used as it is not affected by structural effects or intensive parameters (Di Carlo et al., 2010), while the X_{Fe} ratio (Fe^{2+}/[Fe^{2+}+Mn+Mg]), which can be affected, did not correlate between rock types or with variations in the Ca/(Na+K) ratio. Similar to the X_{Fe} ratio, the $X_{Fe(TOT)}$ ratio should reflect either amphibole-dominated crystallisation (lower-Fe) or pyroxene-dominated crystallisation (higher-Fe) (Pfaff et al., 2008). Thus a high $X_{Fe(TOT)}$ ratio typically reflects crystallisation from a more evolved melt.

Unit	Rock	Ca/(Na+K)				XFe(TOT)			
		Mean	±	Min	Max	Mean	±	Min	Max
-8	Black	0.13	0.02	0.07	0.22	0.95	0.002	0.94	0.95
-9	White	0.13	0.13	0.08	0.33	0.93	0.004	0.91	0.95
	Red	0.15	0.02	0.08	0.33	0.95	0.010	0.92	0.99
	Black	0.22	0.01	0.09	0.22	0.94	0.003	0.93	0.96
-10/-9 Boundary	Black	0.16	0.02	0.09	0.18	0.93	0.003	0.93	0.95
	White	0.16	0.02	0.09	0.24	0.93	0.002	0.93	0.94
-10	White	0.17	0.03	0.10	0.31	0.94	0.009	0.91	0.98
	Red	0.18	0.04	0.08	0.33	0.94	0.009	0.92	0.98
	Black	0.15	0.03	0.08	0.33	0.93	0.003	0.92	0.94
-11/-10 Boundary	Black	0.09	0.01	0.06	0.17	0.91	0.004	0.90	0.94
-11	White	0.14	0.02	0.86	0.92	0.93	0.001	0.93	0.94
Mean Compositions and Ranges									
Boundary Black		0.11	0.01	0.06	0.18	0.93	0.005	0.90	0.95
Black		0.13	0.01	0.07	0.22	0.94	0.002	0.92	0.96
Red		0.16	0.02	0.08	0.33	0.94	0.007	0.92	0.99
White		0.15	0.02	0.04	0.34	0.93	0.003	0.91	0.98
Boundary White		0.16	0.02	0.09	0.24	0.93	0.002	0.93	0.94

Table 7.4: Mean, Minimum and Maximum values for geochemical ratios measured in amphiboles from the black, red, white and boundary samples from Units -11 to -8. Precision (±) to 95% confidence.

The Ca/(Na+K) ratios are lowest in the black kakortokite (Fig. 7.11a-b, Table 7.4), ranging between 0.07 and 0.22, with a mean of 0.13±0.01. The black kakortokite sampled immediately above (0-25mm) the unit boundaries has the lowest ratios between 0.06 and 0.18 and a mean of 0.11±0.01. The amphiboles in red kakortokite samples have intermediate compositions (Fig. 7.11a-b, Table 7.4), with Ca/(Na+K) ratios between 0.08 and 0.33, and a mean of 0.16±0.02. The white kakortokite has Ca/(Na+K) ratios (Fig. 7.11a-b, Table 7.4), ranging between 0.04 and 0.34, and a mean of 0.15±0.02. The highest Ca/(Na+K) ratios are observed in the white kakortokite samples immediately below (0-25 mm) the unit boundaries. These ratios range between 0.09 and 0.24, with a mean of 0.16±0.02.

The range of $X_{Fe(TOT)}$ ratios has little variation across the studied layers (Table 7.4), however individual units do show contrasts (Fig. 7.11c-d) and discontinuities occur across unit boundaries.

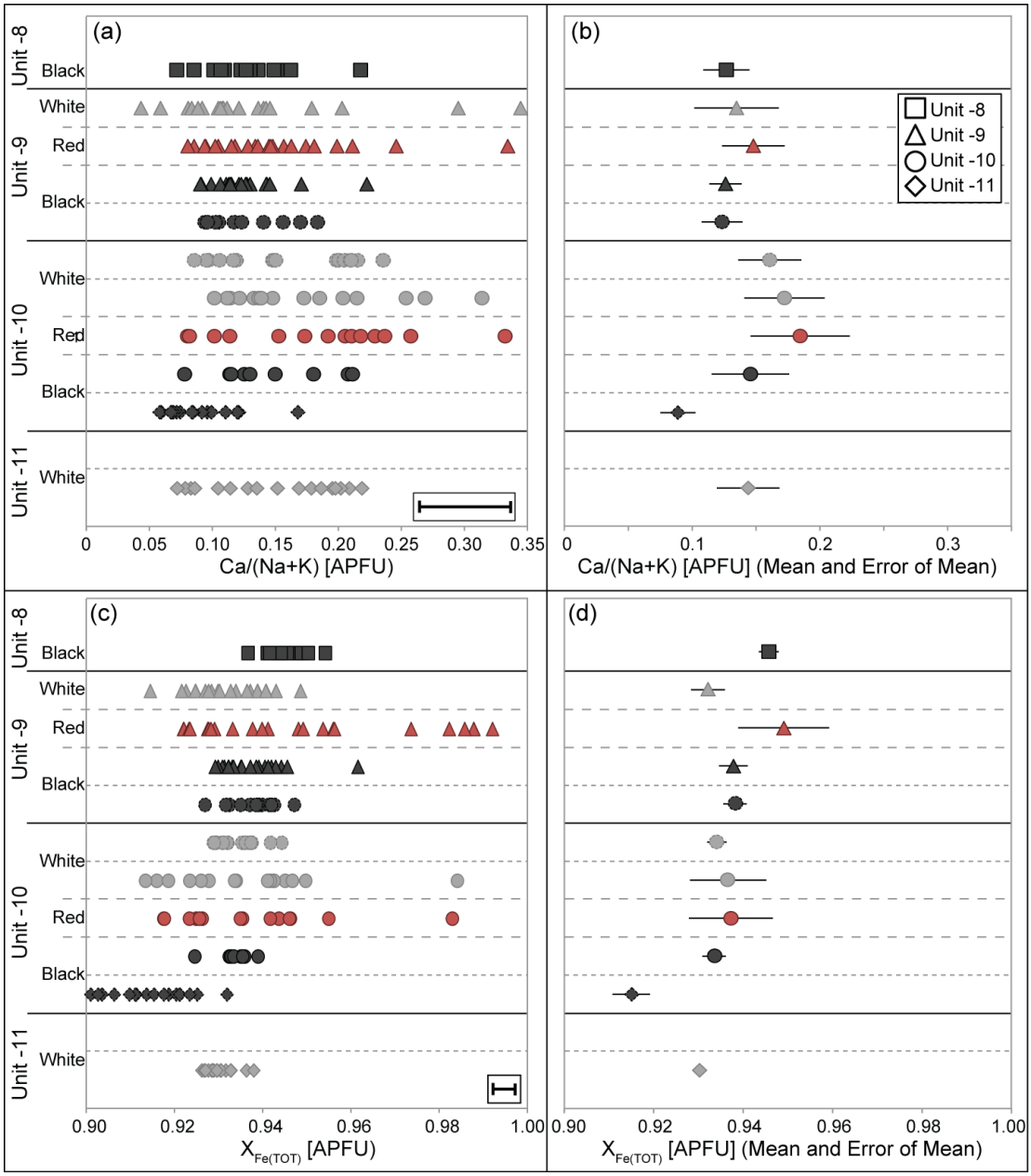

Figure 7.11: Amphibole compositions measured by EPMA, all data subdivided according to unit stratigraphy. Note Unit-10 Wa was not analysed. (a) Ca/(Na+K) ratios, error bar on individual analyses bottom right. (b) Mean and error of mean of Ca/(Na+K) ratios. (c) $X_{Fe(TOT)}$ ratio ($Fe_{(TOT)}$/[$Fe_{(TOT)}$+Mn+Mg]), error bar bottom right. (d) Mean and error of mean of $X_{Fe(TOT)}$ ratios. Note outliers are not excluded from mean calculations.

7.6 Development of Units -11 to -8.

The lowest outcropping units (-11 to -8) have regular, planar layering, which is laterally continuous and homogeneous on a metre scale. There are no indicators of current activity. Each unit is marked by sharp upper and lower boundaries (Figs. 7.2a-b, 7.3a-b) although these can be less distinct when viewed closer due to a gradational increase in arfvedsonite upwards from the marked boundaries. The unit boundaries are considered in the present study to be sharp as there is an abrupt increase in the concentration of arfvedsonite from 10 mod.% in the white kakortokite to 30% in the black kakortokite. The concentration of arfvedsonite then increases to a maximum (45-50%) upwards through the first 0.3 to 0.9 m of the black layer. The internal boundaries between layers are always gradational over 0.1 to 0.3 m (Fig. 7.2d). There are variations between the units, for example the subordinate white kakortokite, termed 'Wa', in between the black and red layers of Unit -10; and the eudialyte-poor red kakortokite in Unit -9.

Despite the differences in volume of arfvedsonite, the CSD profiles immediately above the unit boundary (0-25 mm) and the central portions of the layers are similar (Fig. 7.6a-b). The profiles are broadly log-linear, indicating *in situ* crystallisation of the bulk of the groundmass at the crystal mush – magma interface (Marsh, 1988). Minor kinks occur in the plot shapes at larger crystal sizes (Fig 7.6a-b), similar to the Unit 0 black kakortokites (Fig. 6.8), reflecting mixing of crystal populations (Marsh, 1988). In Unit 0 these kinks were interpreted as two populations of arfvedsonite: where the groundmass crystals nucleated and grew *in situ* to form the bulk of the black kakortokite, while the large crystals are antecrysts sourced from the plumbing system below the magma chamber and entrained in the replenishing magma. The arfvedsonite crystals in the lowest exposed units (-11 to -8) have bimodal crystal populations, which is exemplified by the CSD for the arfvedsonite in the Unit -10 black kakortokite (Fig. 7.6a). The range of crystal sizes is not continuous between the smaller size fractions (>3 mm) and the larger size fractions (up to 7.7 mm), marked by the dashed line on the CSD plot (Fig. 7.6a). The bimodal range of crystal sizes is consistent with an antecrystic origin for the large crystals, similar to Unit 0.

The CSD plot for the eudialyte in the U-10 red kakortokite is broadly log-linear, reflecting *in situ* crystallisation at the crystal mush – magma interface (Marsh, 1988). There is a kink at 2.3 mm, which indicates mixed crystal populations (Marsh, 1988). Unlike arfvedsonite, the eudialyte data from U-10 do not have a bimodal range of crystal sizes, but rather represent a continuous range of sizes, suggesting a

different history. The kink in the U-10 eudialyte data is thus interpreted to be associated with differing extents of textural coarsening (Higgins, 2002b), with the largest eudialyte crystals in this sample having undergone textural coarsening to a greater extent. The Unit -9 red kakortokite is relatively eudialyte-poor, containing 25% eudialyte in comparison to 40% in U-10. The plot profile is relatively flattened, with a small upwards curvature over the entire range of crystal sizes. This plot shape is associated with crystal fractionation (Marsh, 1988), envisioned here as the process of suspended eudialyte crystals being enclosed in the upwards growing crystal mush. The lack of current indicators in the layered kakortokite indicates a stable and quiescent magma body, thus suspension of eudialyte crystals could be sustained. This mode of crystallisation of eudialyte is reflected by the relative lack of eudialyte in the U-9 red kakortokite.

The CSDs for the alkali feldspar in the white kakortokite are typically log-linear, reflecting *in situ* nucleation of alkali feldspar at the crystal mush – magma interface (Marsh, 1988). The slopes of the CSDs for the white kakortokite layers are consistent (Table 7.2), excepting Unit -9. This sample has the largest crystal sizes and the plot is kinked at 9.2 mm. Similar to the U-10 eudialyte data from the red kakortokites, this kink is interpreted to have formed through varying degrees of textural coarsening (Higgins, 2002b) across the sample, as a relatively continuous range of crystal sizes was observed. The CSD for the alkali feldspar in the 'Wa' layer from U-10 compares well to the white kakortokite CSD plots (Fig. 7.6d) thus similar processes developed this layer. The CSDs for alkali feldspar from white kakortokites immediately below (0-25 mm) the unit boundaries have slopes that compare well to the CSDs from the central portions of the units (Table 7.2). The slopes are log-linear, reflecting *in situ* nucleation at the crystal mush – magma interface (Marsh, 1988). The slope profiles are more complex at the smaller crystal sizes as the plots have an upturn, reflecting an increased population density, followed by a downturn at the smallest crystal sizes (Fig. 7.6e). Similar to the Units -1/0 samples this is interpreted as secondary nucleation followed by textural coarsening.

All the CSDs indicate modification through textural coarsening, from the downturns in the profiles at the smallest crystal sizes. This represents growth of the largest crystals at the expense of the smaller crystals through Ostwald ripening and coalescence of smaller crystals to form a single large crystal (Higgins, 2010). The primary processes of nucleation and crystallisation can however still be inferred from the CSDs and the dominant process is through *in situ* nucleation and growth at the crystal mush – magma interface.

Therefore layer formation through eutectic crystallisation of all phases, and subsequent density segregation through gravitational sorting (cf. Upton, 2013) is inconsistent with the data. Gravitational settling also cannot account for the presence of the subordinate white kakortokite ('Wa' layer), principally comprised of low-density alkali feldspar, with an overlying layer that is principally comprised of denser eudialyte. Instead the model of ordered nucleation proposed in chapter 6 is applied to the data.

The textural and chemical similarities between the lowest exposed units (-11 to -8) and Unit 0 (chapter 6), indicates formation of each of the units through similar processes. The ordered crystallisation model invokes repeated replenishment by a volatile-rich magma, which forms a crystal-poor boundary layer between the crystal mush and the overlying resident magma in a quiescent chamber. Nucleation of each phase is controlled by variations in the concentration of volatile elements, an initial high volatile element concentration acts to inhibit nucleation of all phases, excepting arfvedsonite, which can crystallise at high concentrations of volatile elements (Sørensen, 1969). The arfvedsonite nucleates *in situ* at the crystal mush – magma interface, through the process of epitaxy, to develop the black kakortokite.

Crystallisation of arfvedsonite reduces the F content of the magma, decreasing the volatile element concentration; in combination with the minor processes of progressive equilibration of the bottom magma layer with the resident magma body and the upwards loss of volatile elements along a concentration gradient, due to the crystallisation of the sodalite-rich roof rocks (Sørensen & Larsen, 1987). Combining this with desaturation in arfvedsonite allows for the next phase (eudialyte) to nucleate. The eudialyte crystallises *in situ* at the crystal mush – magma interface, again through epitaxy, with minor nucleation of the other mineral phases to form the red kakortokite. The volatile element concentration continues to decrease due to crystallisation of eudialyte, which reduces the Cl content of the magma, which combined with the minor processes described above, allows for the nucleation of alkali feldspar and nepheline thus developing the white kakortokite. After a period of time, a further replenishment event occurs, increasing the volatile element concentration and initiating the formation of a new unit. If the chemical and thermal characteristics of the injected magma substantially differ from the crystal mush, a sharp unit boundary, e.g. Units -9/-8, will form due to chemical and/or thermal erosion. If the chemical and thermal characteristics of the magma are less pronounced or if the crystal mush is relatively unconsolidated, then a less distinct boundary will form, e.g. Units -11/-10 and -10/-9.

The mineral chemical data from the EGM are consistent with a replenishment model. The $Fe_{(TOT)}$/Mn data display marked discontinuities across the unit boundaries (Fig. 7.8). The ratios increase from the white kakortokite in the underlying unit to the black kakortokite in the overlying unit. Indicating crystallisation from more primitive melts above the unit boundaries (Pfaff *et al.*, 2008, Schilling *et al.*, 2011). This is not indicative of closed system crystallisation; instead it reflects open system, replenishment events. Further evidence is provided by the EGM Ca/(REE+Y) ratios, which decrease with melt evolution (Pfaff *et al.*, 2008). The Ca/(REE+Y) ratios display the same pattern with discontinuities at unit boundaries and the black kakortokite samples have the highest ratios. The Ca/(REE+Y) ratios then progressively decrease upwards through the unit to the overlying boundary (Fig. 7.9 a-b) again indicating more primitive compositions above the unit boundaries (Pfaff *et al.*, 2008).

These discontinuities at unit boundaries are highlighted by compositional differences in the EGM immediately above/below the boundary in comparison to those in the central portions of the same layer (Fig. 7.8, 7.9). The EGM in the white kakortokite immediately below the boundaries (0-25 mm) have ratios (Fe_{TOT}/Mn and Ca/(REE+Y)) that are higher and thus more primitive than the EGM in the white kakortokite in the central portions of the layer. The EGM in the black kakortokite immediately above (0-25 mm) the boundaries have higher and thus more evolved ratios than the EGM in the black kakortokite in the central portions of the layer. This reflects mixing between the injected magma and a melt derived from small amounts of partial melting of the uppermost (few centimetres) crystal mush, as evidenced by the increased number of small crystals immediately below (0-25 mm) unit boundaries (Fig. 7.6e) which reflect secondary nucleation. This partial melting is associated with thermal and/or chemical disequilibrium associated with the replenishment event. The observed secondary nucleation of alkali feldspar in the white kakortokite immediately below (0-25 mm) the unit boundaries is associated with this partial melting and subsequent recrystallisation. The mixing is also displayed by the amphibole data, as the lowest and relatively primitive (Pfaff *et al.*, 2008) Ca/(Na+K) ratios are displayed by the amphiboles in the red kakortokite, while the amphiboles in the black kakortokite represent mixed compositions. The progressive increase in arfvedsonite in the black kakortokite from immediately above the boundary to a maximum concentration in the first metre of the black kakortokite layer also reflects this interaction between the crystal mush and the relatively primitive replenishing magma.

The model proposed in chapter 6 involves a volatile-rich magma which controls the order of nucleation and provides the conditions for initial crystallisation of

arfvedsonite while the other phases are inhibited (Sørensen, 1969). The primary volatile compounds in the Ilímaussaq magmas include HF and HCl, (Bailey *et al.*, 2001) and Pfaff et al. (2008) propose a reduction in volatile elements, specifically Cl, upwards through the layered kakortokites due to magmatic evolution. The data from Units -11 to -8 however do not fit this trend, as the most primitive EGM, according to the $Fe_{(TOT)}$/Mn and Ca/(REE+Y) ratios, have the lowest Cl contents (Fig, 7.9, Table 7.3). The Cl contents of the EGM from the lowest exposed units also vary in Cl contents in comparison to Unit 0. The EGM in the Units -11 to -8 black kakortokite layers (1.54±0.04) are similar to the U0 black kakortokite (1.52±0.02) although the red (1.62±0.02) and white (1.62±0.02) of Units -11 to -8 have much higher Cl contents compared to Unit 0 (red = 1.55±0.01, white = 1.53±0.03). This is interpreted to reflect initial injection of a volatile-rich magma, which mixes with the uppermost portions of the crystal mush, as described above, thus decreasing the concentration of Cl, although the volatile element concentration is still great enough to inhibit crystallisation of all phases apart from arfvedsonite. An initial high volatile element concentration is inferred from the presence of sodalite in the black kakortokites of Unit -10. The progressive increase in Cl upwards through the EGM is related to the progressive equilibration of the boundary layer magma, generated by the replenishment event, with the resident magma. The nucleation of sodalite is gradually supressed due to a decrease in the saturation of Cl in the melt. This combination of processes would increase the availability of Cl during the crystallisation of EGM at the top of each unit.

The data do not disprove the model proposed in chapter 6, however the ‘Wa’ layer in Unit -10 must be considered. The layered syenites from the Klokken Complex (Gardar Igneous Province) are proposed to have formed through a similar model (Parsons, 1979) to the one developed in the present study for the layered kakortokite. The layered sequence at Klokken is interrupted by laterally discontinuous sheets of granular syenite, that are suggested to have settled as rafts after crystallisation at the roof (Parsons & Butterfield, 1981). Irregular lower contacts and pseudo-sedimentary features of lobate contacts and flame structures have been used to provide evidence for settling of these rafts onto the inversely graded layers (Parsons, 1979, Parsons & Butterfield, 1981).

The subordinate ‘Wa’ kakortokite layers however do not resemble the granular syenites from the Klokken as the ‘Wa’ layers are laterally continuous and were observed in both outcrop and drill core. They also do not contain pseudo-sedimentary indicators and display gradational contacts to the underlying black kakortokite and overlying red kakortokite. The textural analysis indicates that the Unit

-10 ‘Wa’ layer formed *in situ* above the black layer, through similar processes to the white kakortokite.

The $Fe_{(TOT)}$/Mn ratios reflect relatively evolved compositions for the EGM in the ‘Wa’ layer compared to the remainder of the unit, however the Ca/(REE+Y) ratios indicate a composition intermediate between the EGM in the black and red layers of Unit -10. $Fe_{(TOT)}$/Mn ratios can be affected by hydrothermal alteration, as EGM formed in the presence of hydrothermal fluids are relatively enriched in Mn (Schilling *et al.*, 2011). Although care was taken during the analysis to sample only unaltered crystal cores, up 60% of the EGM in the U-10 ‘Wa’ layer displayed partial or complete alteration. Therefore the relatively high Mn contents of the EGM indicate late-stage hydrothermal alteration and/or chemical equilibration. Due to this the Ca/(REE+Y) ratios are interpreted to be more reflective of the primary magmatic compositions. Similar to the textural data they reflect formation of the ‘Wa’ layer after the black kakortokite and before the red kakortokite.

This would require a relatively rapid reduction in the volatile element concentration during the formation of the Unit -10 black kakortokite. This could be achieved by large-scale crystallisation of sodalite, which forms 20% of the ‘Wa’ layer. Although sodalite is not present in the U-10 black kakortokite samples taken from outcrop, it does form 20% of the black kakortokite layer in drill core (DX-01, Appendix B). Sodalite is not present in the U-10 red or white kakortokites in either outcrop or drill core, indicating comparatively decreased volatile element concentrations during the formation of these layers. The chlorine is instead taken up by the EGM in the red and white layers, which display a marked increase in Cl contents (mean values of 1.63±0.02 wt.% in the red and 1.63±0.04 wt.% in the white) compared to the ‘Wa’ (1.53±0.03 wt.%) and black (1.44±0.07 wt.%) layers. Thus the development of the ‘Wa’ layer in Unit -10 can be explained by a nucleation of sodalite, which reduced the availability of Cl to eudialyte, thus developing a ‘Wa’ layer through nucleation of alkali feldspar and nepheline under relatively reduced volatile element concentrations. This follows the work by Bailey *et al.* (2006) who suggest that the repetitive changes between nepheline-, sodalite- and microcline-bearing dark layers and sodalite-free, microcline-poor uritic layers in the arfvedsonite lujavrite is related to the NaCl and silica activities. They infer that crystallisation of sodalite exhausts the NaCl component, resulting in a shift towards crystallisation of nepheline, thus developing the overlying nepheline-rich urtite layer. Following this I suggest that once the boundary layer crystallising the kakortokite was desaturated in sodalite, the inhibition on the nucleation of eudialyte would be lifted, thus allowing development of the red

kakortokite. Desaturation in eudialyte during the development of the red kakortokite would allow for crystallisation of the overlying Unit -10 white kakortokite.

The data from the lowest exposed layered units (-11 to -8) are important for understanding the processes operating during the early stages of agpaitic magmatism in the Ilímaussaq magma chamber. The effects of the crystallisation of sodalite on the development of the layered kakortokites may also provide an insight into the processes operating at the roof of the chamber. The present study indicates formation of the layering through gravitational settling alone is untenable, thus formation of the naujaite at the roof through flotation of sodalite crystallised in the resident magma is unlikely. Instead the formation of the naujaite may also be controlled by replenishment events. Injection of melts that are richer in volatile elements than those inferred to have formed the kakortokite would likely be less dense and thus would rise to the roof. It is speculated that injections of these melts could initiate crystallisation at the roof, with the initial high volatile element concentrations favouring the nucleation of sodalite. Once the volatile element concentration decreased the interstitial phases would not be inhibited and could nucleate. While the present study has not collected data from naujaite to support this hypothesis, the insights gained from the present analysis of the kakortokite may be key to understanding the development of the naujaite.

7.7 Conclusions

The lowest exposed units (-11 to -8) have received relatively little attention as most recent studies have focused on Unit 0 and the overlying units. The inclusion of a subordinate white kakortokite ('Wa') between the black and red layers of Unit -10 indicates that formation of these purely through density sorting and gravitational settling is implausible. Instead another mode of formation should be invoked. The model developed in chapter 6 of ordered nucleation controlled by an oscillating volatile element concentration, was applied to Units -11 to -8. The textural and chemical data fit the model, indicating *in situ* crystallisation within a boundary layer, while chemical discontinuities at unit boundaries reflect replenishment events by relatively primitive magmas. The key insight gained through this analysis is the variation in Cl contents of EGM through these units. The relatively low concentrations in the EGM in the black and red layers could only have formed if the Cl was taken up by another mineral. The model proposed in chapter 6 is extended to include the coeval crystallisation of sodalite. This provides an important insight, not only into the development of the layered kakortokite, but also into the development of the naujaite.

7.8 References

Bailey, J. C., Gwozdz, R., Rose-Hansen, J. & Sørensen, H. (2001). Geochemical overview of the Ilímaussaq alkaline complex, South Greenland. *Geology of Greenland Survey Bulletin* **190**, 35-53.

Bailey, J. C., Sørensen, H., Anderson, T., Kogarko, L. N. & Rose-Hansen, J. (2006). On the origin of microrhythmic layering in arfvedsonite lujavrite from the Ilímaussaq alkaline complex, South Greenland. *Lithos* **91**, 301-318.

Di Carlo, I., Rotolo, S. G., Scaillet, B., Vincenzo, B. & Pichavant, M. (2010). Phase Equilibrium Constraints on Pre-eruptive Conditions of Recent Felsic Explosive Volcanism at Pantelleria Island, Italy. *Journal of Petrology* **51**, 2245-2276.

Engell, J. (1973). A closed system crystal-fractionation model for the agpaitic Ilímaussaq Intrusion, South Greenland with special reference to the lujavrites. *Bulletin of the Geological Society of Denmark* **22**, 334-362.

Ferguson, J. (1964). Geology of the Ilímaussaq alkaline intrusion, South Greenland. Part I. Description of map and structure. *Meddelelser om Grønland* **172**, 1-81.

Ferguson, J. (1970). The differentiation of agpaitic magmas; the Ilímaussaq intrusion, south Greenland. *Canadian Mineralogist* **10**, 335-349.

Higgins, M. D. (2002a). Closure in crystal size distributions (CSD), verification of CSD caluclations, and the significance of CSD fans. *American Mineralogist* **87**, 171-175.

Higgins, M. D. (2002b). A crystal size-distribution study of the Kiglapait layered mafic intrusion, Labrador, Canada: evidence for textural coarsening. *Contributions to Mineralogy and Petrology* **144**, 314-330.

Higgins, M. D. (2010). Textural coarsening in igneous rocks. *International Geology Review* **1**, 1-23.

Krumrei, T. V., Pernicka, E., Kaliwoda, M. & Markl, G. (2007). Volatiles in a peralkaline system: Abiogenic hydrocarbons and F-Cl-Br systematics in the naujaite of the Ilímaussaq intrusion, South Greenland. *Lithos* **95**, 298-314.

Larsen, L. M. & Sørensen, H. (1987). The Ilímaussaq intrusion - progressive crystallisation and formation of layering in an agpaitic magma. *Geological Society London, Special Publications* **30**, 473-488.

Marks, M., Halama, R., Wenzel, T. & Markl, G. (2004). Trace element variations in clinopyroxene and amphibole from alkaline to peralkaline syenites and granites: implications for mineral-melt trace-element partitioning. *Chemical Geology* **211**, 185-215.

Marsh, B. D. (1988). Crystal size distribution (CSD) in rocks and the kinetics and dynamics of crystallization I. Theory. *Contributions to Mineralogy and Petrology* **99**, 277-291.

Parsons, I. (1979). The Klokken Gabbro-Syenite Complex, South Greenland: Cryptic Variation and Origin of Inversely Graded Layering. *Journal of Petrology* **20**, 653-694.

Parsons, I. & Butterfield, A. W. (1981). Sedimentary features of the Nunarssuit and Klokken syenites, S Greenland. *Journal of the Geological Society* **138**, 289-306.

Pfaff, K., Krumrei, T., Marks, M. A. W., Wenzel, T., Rudolf, T. & Markl, G. (2008). Chemical and physical evolution of the 'lowered layered sequence' from the nepheline syenitic Ilímaussaq intrusion, South Greenland: Implications for the origin of magmatic layering in peralkaline felsic liquids. *Lithos* **106**, 280-296.

Schilling, J., Wu, F.-Y., McCammon, C., Wenzel, T., Marks, M. A. W., Pfaff, K., Jacob, D. E. & Markl, G. (2011). The compositional variability of eudialyte-group minerals. *Mineralogical Magzine* **75**, 87-115.

Sørensen, H. (1969). Rythmic igneous layering in peralkaline intrusions: An essay review on Ilímaussaq (Greenland) and Lovozero (Kola, USSR). *Lithos* **2**, 261-283.

Sørensen, H. (2006). The Ilímaussaq Alkaline Complex, South Greenland - an overview of 200 yeards of research and an outlook. *Meddeleser om Grønland* **342**, 1-70.

Sørensen, H. & Larsen, L. M. (1987). Layering in the Ilimaussaq alkaline intrusion, South Greenland. In: Parsons, I. (ed.) *Origins of Igneous Layering*. Dordrecht: D. Reidel Publishing, 1-28.

Upton, B. (2013). Tectono-magmatic evolution of the younger Gardar southern rift, South Greenland. *Geological Survey of Denmark and Greenland Bulletin* **29**, 124.

Chapter 8

Magma Mingling and Mixing in the Layered Kakortokite Series

8.1 Introduction

The layered kakortokite is interrupted by a sequence of rocks that are unlayered and do not physically resemble kakortokite. These rocks have received comparatively little study compared to the rest of the Ilímaussaq Complex and their genesis has not previously been fully explored. They were first described by Ussing (1912) who considered them to be lujavrite within the kakortokite. Ferguson (1970) provided data that indicated these rocks have closer textural, compositional and chemical similarities with kakortokite, rather than lujavrite. Due to the lack of layering however, he suggested the rock sequence should be referred to as a "hybrid". Bohse *et al.* (1971) mapped these rocks between Units -6 to -3, but could not determine their thickness due to lack of exposure. They suggested the sequence formed from slumping of unconsolidated kakortokite mush and hence termed them a "slumped zone".

The present study observed a range of textures within these rocks, including pillows with crenulated margins and net veining. These are not wholly consistent with the formation of the sequence through slumping and instead are more reminiscent of magma mingling textures (e.g. Vernon *et al.*, 1988). The genesis of these rocks is investigated in this chapter through a detailed field, petrographic, textural and chemical study.

An understanding of these rocks is important as drill core (access from TANBREEZ Greenland A/S) analysis during the present study, has revealed that this rock sequence occurs multiple times within the layered kakortokite (Core logs located in Appendix B). A second sequence occurs at depth and the layered kakortokite terminates against rocks that have an apparent affinity to these "hybrid" or "slump" rocks. Thus understanding the processes that formed these rocks is vital to understanding the magma chamber dynamics during the formation of the layered kakortokite.

8.2 Field Relationships

This unlayered rock sequence outcrops in the lower layered kakortokite (below Unit 0). The lowest observed occurrence of these rocks is in the southwest (Fig. 8.1a), where they crosscut the Units -7/-6 boundary (Fig. 8.1b). Due to lack of exposure and erosion, a complete vertical profile of the sequence cannot be observed in outcrop. However, incomplete sections of the sequence outcrop at varying stratigraphic levels in the lower layered kakortokite. The uppermost-observed occurrence is in the northeast (Fig. 8.1a), where the unlayered rocks outcrop at the

approximate height of Unit -2. Here, rafts of coarse-grained white (Fig. 8.1c) and red (Fig. 8.1d) kakortokite are included.

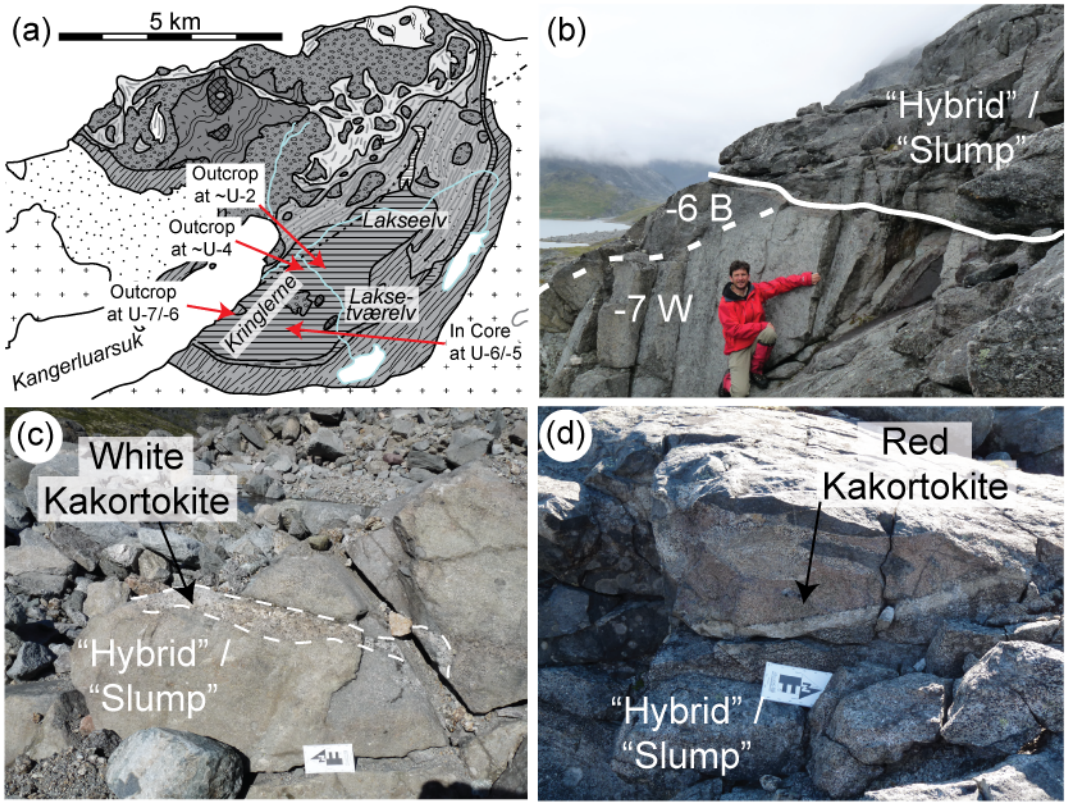

Fig. 8.1: (a) Sketch map of southern part of Ilímaussaq complex indicating varying stratigraphic height of "hybrid/slump" rocks. (b) The sequence crosscuts the layered kakortokite, person (1.8m) for scale. (c) Raft of white kakortokite (outlined) enclosed within the "hybrid/slump" sequence. (d) Eudialyte-rich red kakortokite enclosed within the "hybrid/slump" sequence.

Access to drill core in the present study allowed for analysis of a complete vertical section through these unlayered rocks. In drill core DX-01 the sequence occurs between Units -6 and -5 (Fig. 8.1a); and it is 21.3 m thick. The lower contact truncates the Unit -6 white kakortokite, which has a reduced thickness of 1.9 m, in comparison to the typical 4 m thickness. Above this contact the unlayered rocks contain light-coloured bands, the thickness and frequency of which decrease upwards. At approximately 6 m vertically up through the sequence, a 0.7 m thick arfvedsonite-rich band occurs. Above this, the remaining 15 m contains light and dark banding. At outcrop scale these bands are discontinuous on a metre scale, thus the drill core is not interpreted to display layering.

The banding is composed of three rock varieties, distinguished by grain size and colour index. (1) A fine-grained (<1 mm crystals) mesocratic (colour index from 35-70) rock that plots in the foid syenite field in APF space (Fig. 8.2). Due to the fine grain size, the present study refers to this rock type as a phonolite. (2) A medium-

grained (1-3 mm crystals), mesocratic (colour index from 35-70) rock that plots across the foid syenite and foidolite fields in APF space (Fig. 8.2). As most of the rocks plot in the foidolite field, the present study refers to this rock type as a micro-nephelinolite (micro-ijolite). (3) A coarse-grained (>3 mm crystals), leucocratic (colour index from 10-25) rock that plots in the foid syenite field in APF space (Fig. 8.2), the present study refers to this rock type as a nepheline syenite.

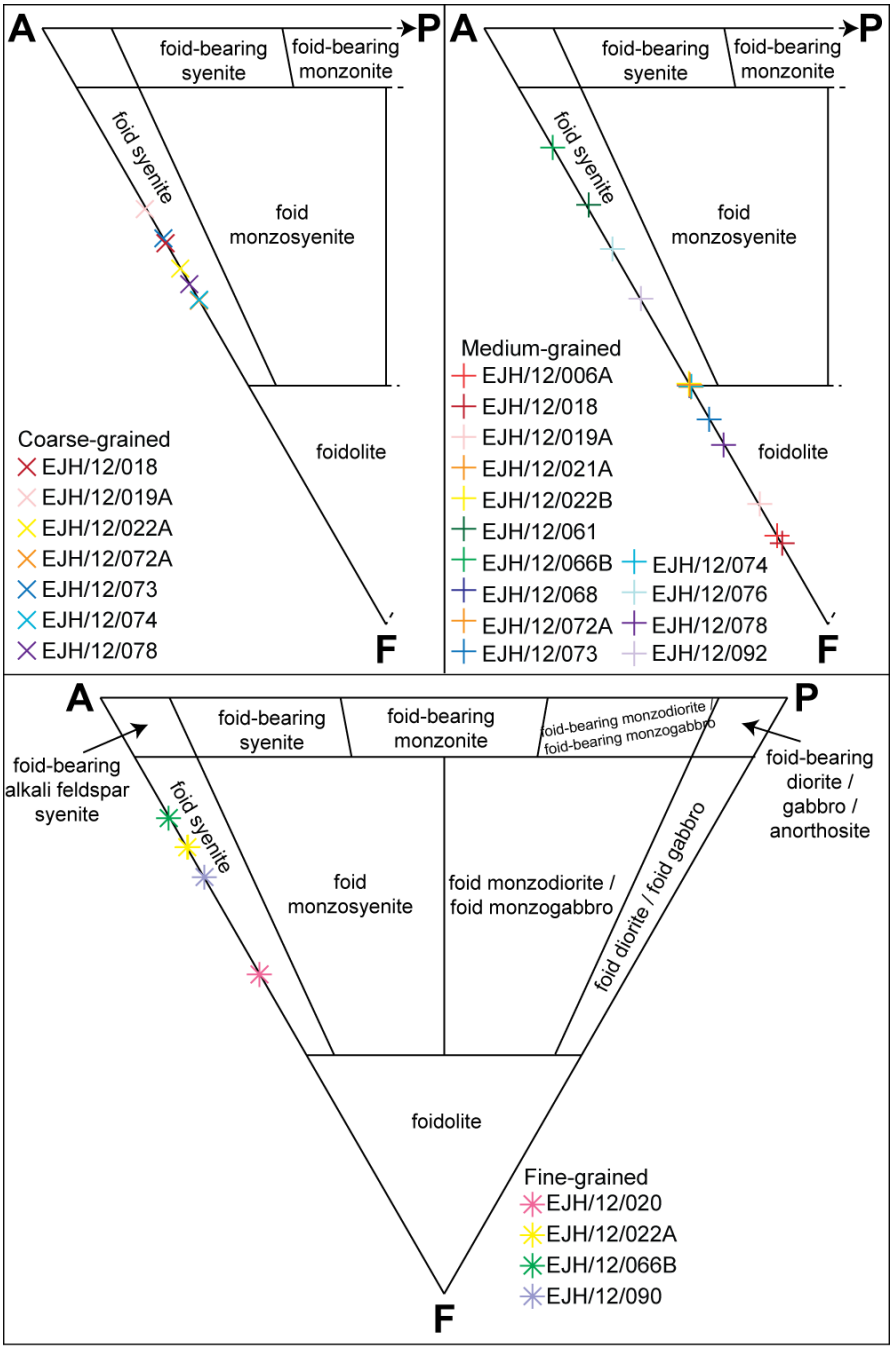

Figure 8.2: APF diagrams adapted from Le Maitre (2002). Data segregated according to coarse-grained, medium-grained and fine-grained textures.

Interactions of these 3 rock types produce a range of textures at the macro (outcrop) to micro (thin section) scale. In outcrop, textures such as net veining (Fig 8.3a) and pillows with either crenulate margins (Fig. 8.3b), or margins marked by decreased grain sizes (Fig. 8.3c-d) are formed by nepheline syenite in phonolite or micro-nephelinolite. Less commonly schlieren of phonolite or micro-nephelinolite are included within nepheline syenite (Fig. 8.3e-f), these typically display rounded contacts. Rarely arfvedsonite- and eudialyte-rich pods are included within the phonolite and micro-nephelinolite (Fig. 8.2g); these are typically comprised of >70% arfvedsonite with coarse-grained eudialyte crystals (up to 1 cm in diameter). At the smallest scale, a foliation fabric, identified by platy alkali feldspar crystals, can occur in all three of the rock types. In some instances this fabric was observed to cross from one rock type to another, across the contact (Fig. 8.2h).

Figure 8.3 (overleaf): (a) Net veins of nepheline syenite within micro-nephelinolite. (b) Pillows of nepheline syenite with crenulated margins. (c) Block of nepheline syenite within micro-nephelinolite, fracture displays 3D structure of block. (d) Enlargement of (c) indicating finer-grained nepheline microsyenite margin and arfvedsonite-rich rim to micro-nephelinolite. (e) Micro-phonolite schlieren with rounded margins in nepheline syenite. (f) Enlargement of (Fig. 8.1d) showing complex mingling of red and white kakortokite with pods of micro-nephelinolite. (g) Arfvedsonite- and eudialyte-rich pod in micro-nephelinolite with vein extension to lower left of image. (h) Contact between micro-nephelinolite and nepheline syenite. Platy alkali feldspar crystals in both rocks display a preferred orientation, marked by white/black lines. Scale card ~15 cm, pencil ~14 cm.

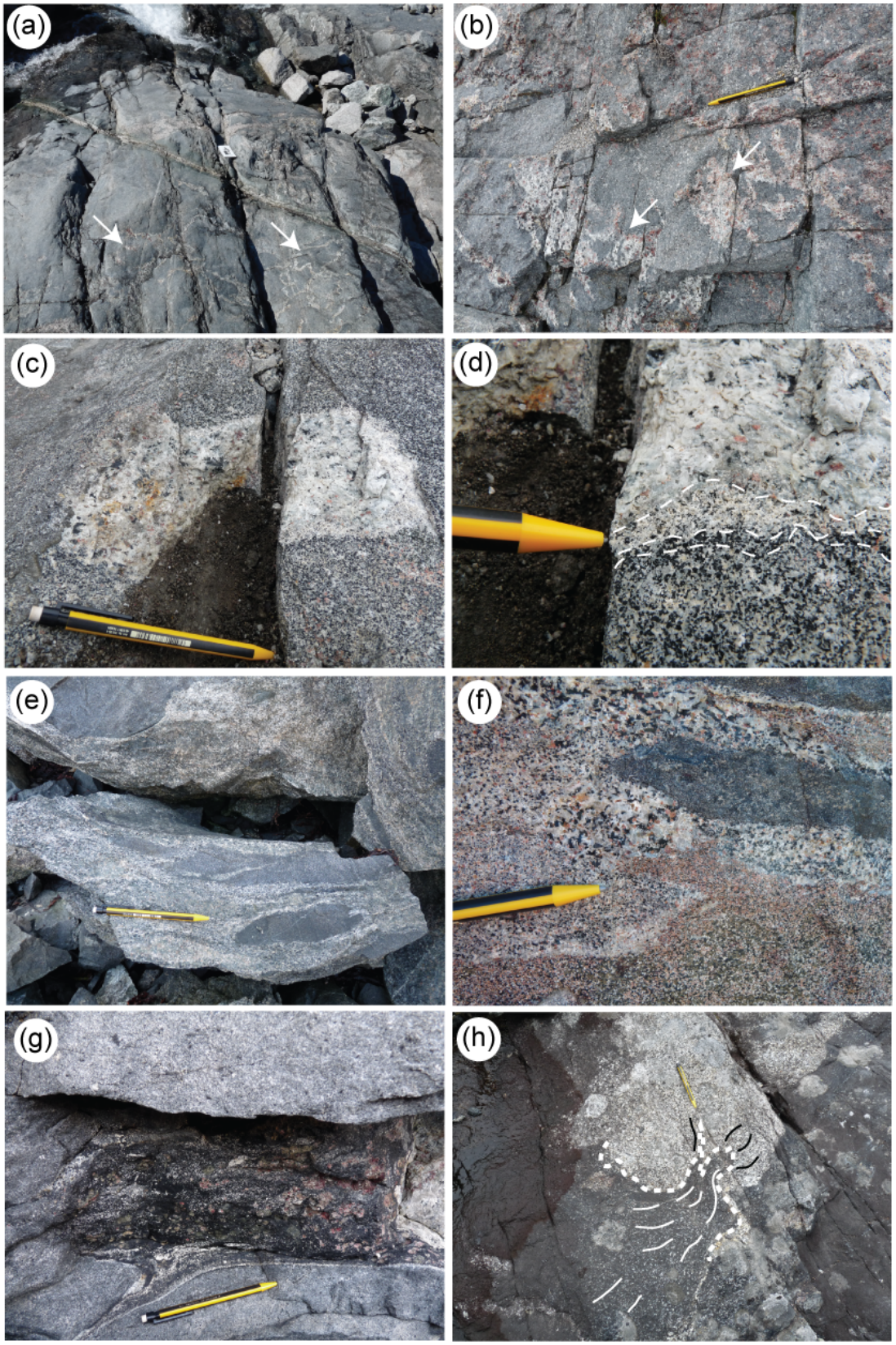
(a)
(b)
(c)
(d)
(e)
(f)
(g)
(h)

8.3 Petrography

Samples from the wide range of the textures described previously were collected for detailed study. They were obtained from the southwest of the layered series along the Kangerluarsuk shoreline towards the centre of the layered series (Lakse-tværelv valley, Fig. 8.4).

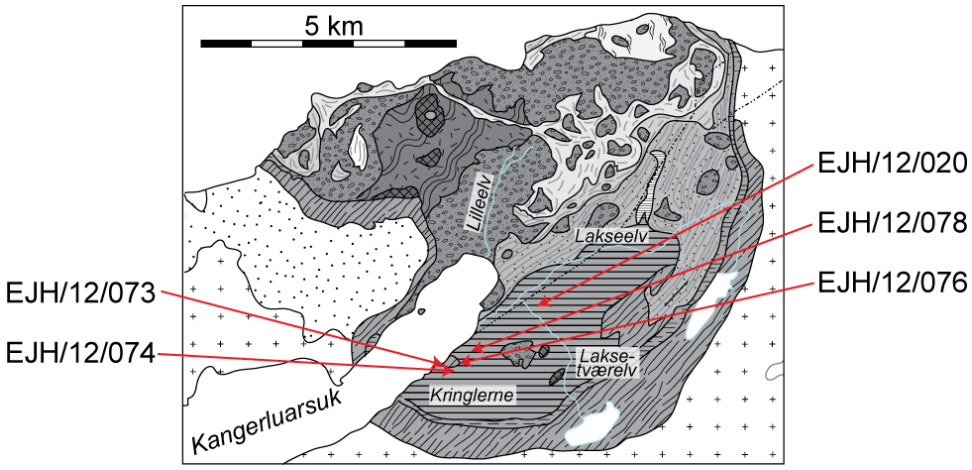

Figure 8.4: Sketch map of southern part of Ilímaussaq complex with sample locations arrowed in red.

The phonolite has a typical composition of: 50% mafic minerals (arfvedsonite ± aenigmatite (Fig. 8.5a) ± augite (Fig. 8.5b)); 35% alkali feldspar; 10% nepheline and 5% sodalite. Eudialyte is uncommon and when present does not form euhedral crystals. Iron sulphides are accessory (~1%) minerals in some samples.

The micro-nephelinolite has a typical composition of: 50% mafic minerals (arfvedsonite ± aenigmatite, Fig. 8.5a); 20% nepheline; 20% alkali feldspar; and 10% sodalite. Similar to the phonolite, eudialyte is uncommon and iron sulphides are accessory (~1%) minerals in some samples.

The nepheline syenite is typically composed of: 40% alkali feldspar, 20% arfvedsonite, 20% nepheline, 15% eudialyte and 5% sodalite.

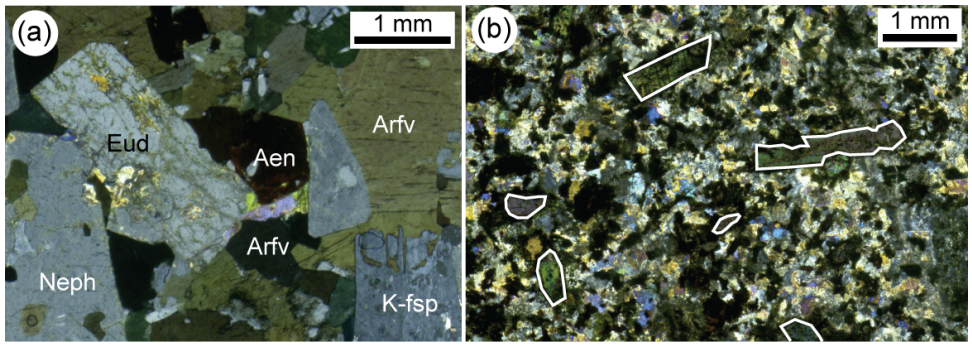

Figure 8.5: (a) Aenigmatite in sample EJH/12/067. Aeg – aenigmatite, Arfv – arfvedsonite, Eud – eudialyte, K-fsp – alkali feldspar, Neph – nepheline. (b) Augite phenocrysts (outlined) in sample EJH/12/090.

EJH/12/020 was sampled from the Laskse-tværelv valley at the approximate stratigraphic height of Unit -3 (Fig 8.4). The phonolite in this location is fissile, mesocratic and has a range of grain sizes (Fig 8.6a) associated with intermingled coarser- and finer-grained textures. The fine-grained (≤1 mm) portions of the rock are phonolitic and rich in mafic minerals (arfvedsonite + augite). The coarser-grained portions have crystal sizes between 1-3 mm. It is a nepheline microsyenite (grouped in this study with the micro-nephelinolite), composed of 35% alkali feldspar, 30% nepheline, 15% arfvedsonite, 15% aenigmatite and 5% eudialyte (Fig 8.6b). The eudialyte typically occurs as clots, surrounded by alkali feldspar crystals.

EJH/12/073 was collected on the south side of Kangerluarsuk Fjord at the approximate stratigraphic height of the Units -7/-6 boundary. The outcrop displays apparent loading of micro-nephelinolite on to sheared kakortokite-like rocks. The micro-nephelinolite is medium-grained (1-3 mm) and contains anastomosing vein networks of coarse-grained (3-6 mm) nepheline syenite (Fig 8.6c). The micro-nephelinolite is comprised of 40% arfvedsonite, 30% nepheline, 20% alkali feldspar, 9% sodalite, 1% eudialyte and <1% iron sulphides. The nepheline syenite has a typical composition of 37% alkali feldspar, 20% nepheline, 20% arfvedsonite, 18% eudialyte, 5% sodalite and <1% iron sulphides. Eudialyte is not evenly distributed through the syenite, instead it occurs in clots (Fig 8.6d), where large, unaltered crystals occur (up to 6 mm).

EJH/12/074 was sampled on the south side of Kangerluarsuk Fjord at the approximate stratigraphic height of Unit -6 (Fig. 8.4), ~1 m above the contact between micro-nephelinolite and kakortokite. Similar to sample EJH/12/073 it displays anastomosing vein networks of nepheline syenite. Platy alkali feldspar crystals within both the micro-nephelinolite and nepheline syenite display a preferred alignment (Fig 8.6e). The micro-nephelinolite is medium-grained (1 to 3 mm) and is composed of 30% nepheline, 25% aenigmatite, 23% arfvedsonite, 20% alkali feldspar and 2% eudialyte. The eudialyte is commonly altered and is typically anhedral (Fig 8.6f). The nepheline syenite is coarse-grained (2-5 mm) and composed of 30% alkali feldspar, 25% nepheline 20% eudialyte, 15% arfvedsonite and 10% aenigmatite. The crystals are typically fresh, however the alkali feldspar crystals have a bimodal range of crystal sizes. The smallest are typically <1 mm in width (short axis) and the largest between 2-3 mm in width. The smallest alkali feldspar crystals in the nepheline syenite are aligned towards the boundary with the micro-nephelinolite.

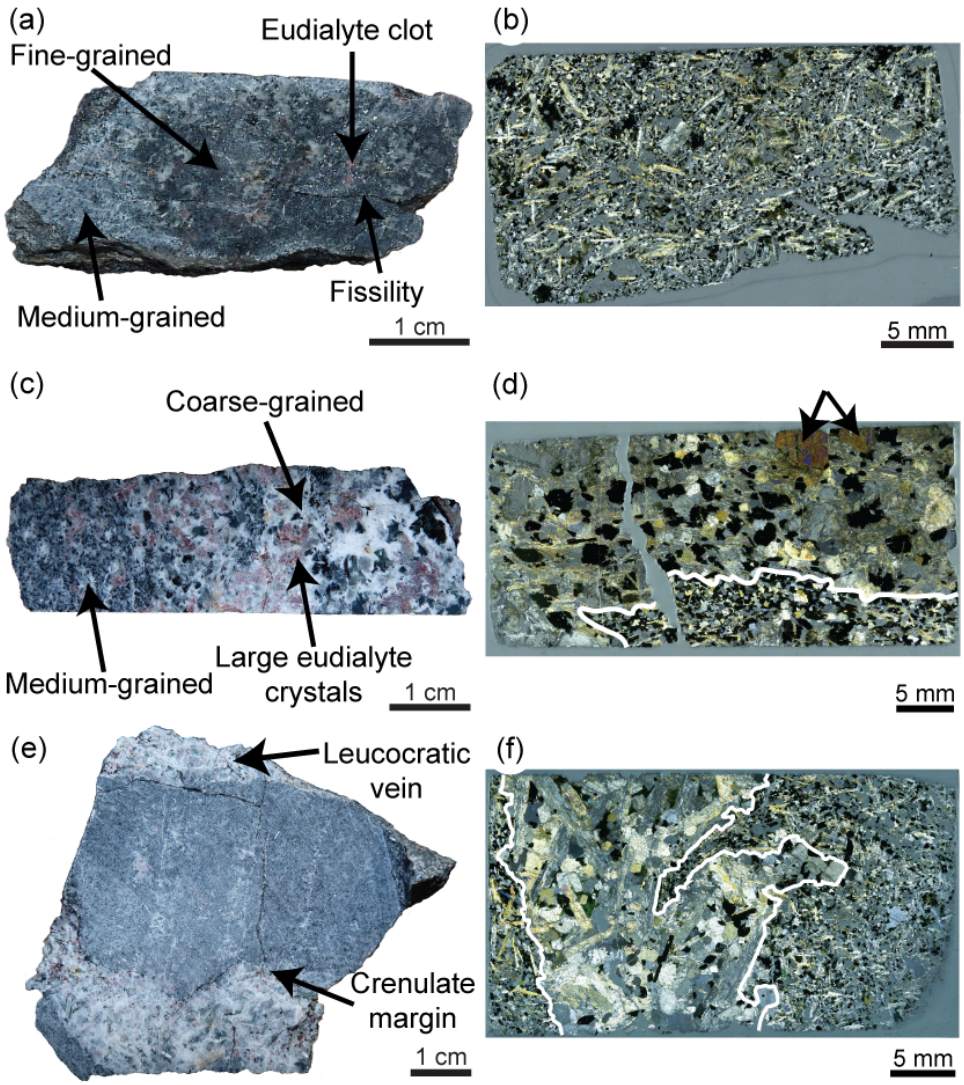

Figure 8.6: (a) Hand specimen of EJH/12/020 displaying a fissility and variation between a lighter medium-grained and darker fine-grained material. (b). Polished section of EJH/12/020 displaying general orientation of alkali feldspar. (c) Hand specimen of EJH/12/073 with banding of dark fine-grained micro-nephelinolite and light coarse-grained nepheline syenite that incorporates large eudialyte crystals. (d) Polished section of EJH/12/073 displaying sharp boundary (white) between medium- and coarse-grained, large eudialyte crystals are arrowed. (e) Hand specimen of EJH/12/074 with anastomosing veins of nepheline syenite (arrowed). (f) Contact (white line) between medium- and coarse-grained in polished section (EJH/12/074).

Sample EJH/12/076 is a lens of a black arfvedsonite-rich rock (Fig. 8.7a) incorporated within micro-nephelinolite. It was sampled on the south side of Kangerluarsuk Fjord at the approximate stratigraphic height of the Units -6/-5 boundary (Fig 8.3). It is medium grained, with a typical crystal size of 1-3 mm, and is composed of 70% arfvedsonite, 17% alkali feldspar, 10% nepheline and 3% eudialyte, indicating it is a nepheline microsyenite. The hand specimen does not have an altered appearance, though in section the nepheline and eudialyte display some alteration (Fig 8.7b).

EJH/12/078 is one of the leucocratic veins (Fig. 8.7c) through the micro-nephelinolite, sampled from the south side of Kangerluarsuk at the approximate stratigraphic height of Unit -5 (Fig. 8.4). It is a nepheline syenite, coarse-grained (3-5 mm), and comprised of 40% alkali feldspar, 30% nepheline, 20% arfvedsonite and 10% eudialyte. The contact between the vein and the micro-nephelinolite is marked by an increase in arfvedsonite crystals in the micro-nephelinolite up to 2 mm from the seam. The micro-nephelinolite is fine- to medium-grained (≤1 to 2 mm) and composed of 35% nepheline, 30% aenigmatite, 19% arfvedsonite, 15% alkali feldspar and 1% eudialyte (Fig. 8.7d). The eudialyte is typically anhedral.

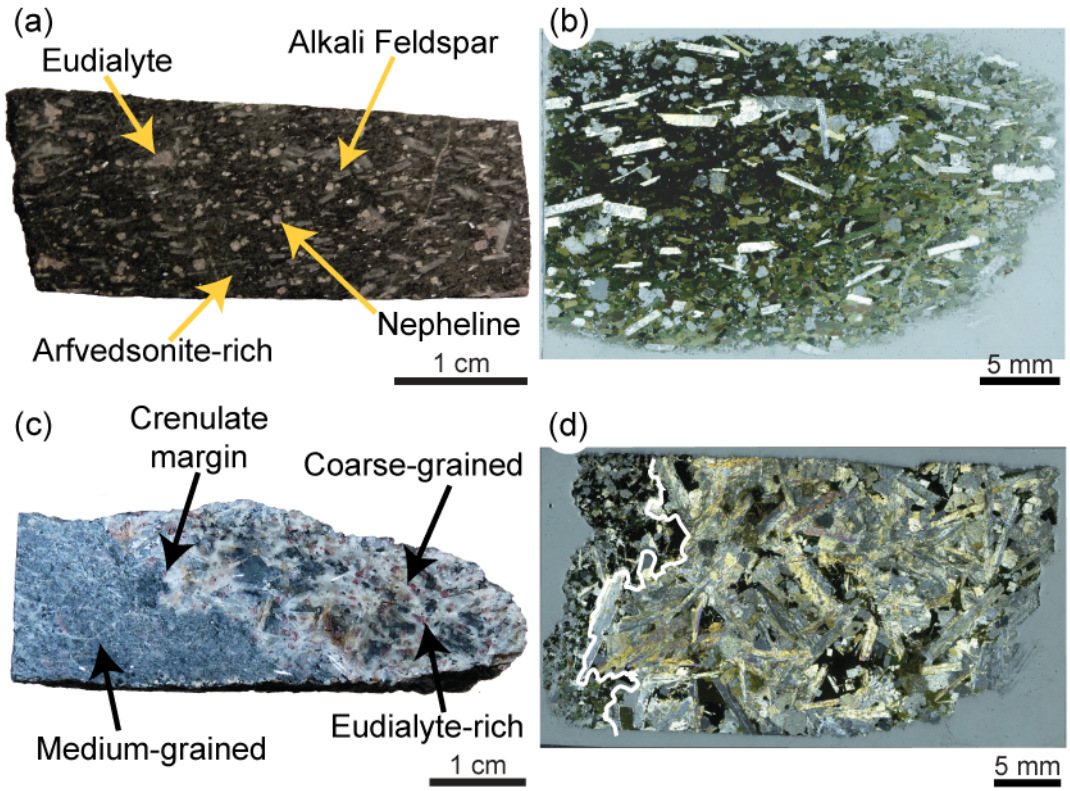

Figure 8.7: (a) Dark coloured, arfvedsonite-rich hand specimen of EJH/12/076. (b) Polished section of EJH/12/076 highlighting arfvedsonite groundmass. (c) Crenulate contact between medium-grained micro-nephelinolite and nepheline syenite in hand specimen and (d) polished section (EJH/12/078).

8.4 Quantitative Textural Analysis

Crystal size distribution analyses were performed on hand digitised crystal outlines (e.g. Fig 8.8) for the samples described above (EJH/12/020, 073, 074, 076, 078) following the methods outlined in Chapter 4.3. To most effectively map textural variations between phonolite, micro-nephelinolite, nepheline syenite and layered kakortokite, three mineral species were chosen: alkali feldspar, arfvedsonite and eudialyte. The data are presented in Table 8.1 and Figure 8.9; the raw CSD data are location in the supplementary data files in Appendix C. For ease of viewing each mineral species is displayed on a separate plot and compared to relevant CSD plots from Unit 0.

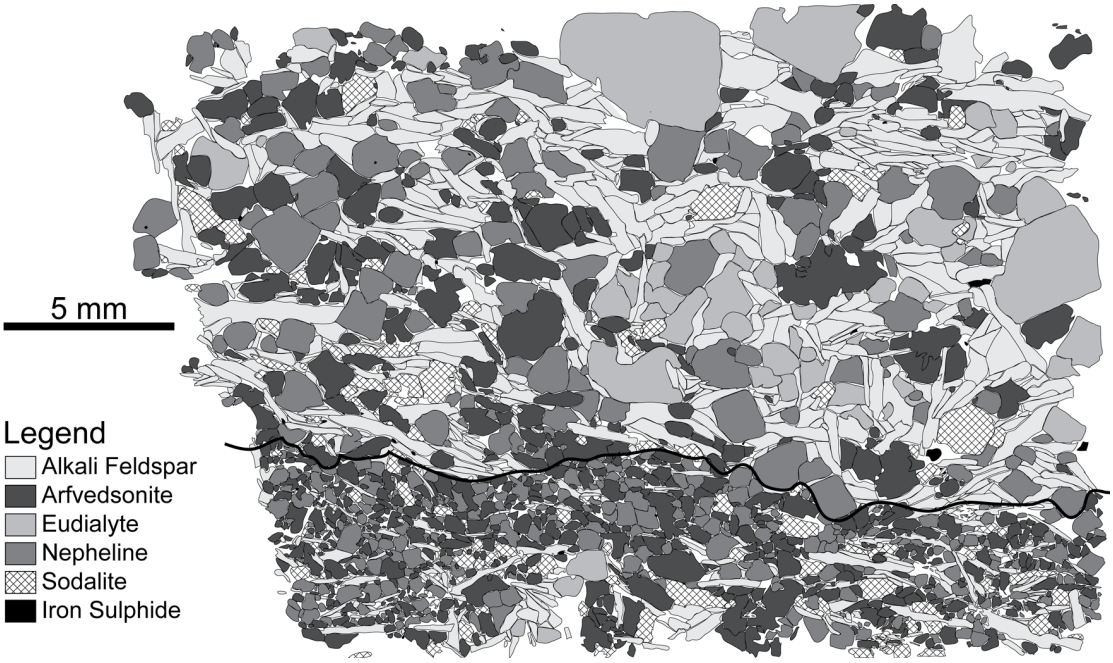

Fig 8.8: Digitised sketch map of sample EJH/12/073. Black line demarcates boundary between coarse-grained nepheline syenite and medium-grained micro-nephelinolite.

Coarse-grained (up to 10 mm, long axis) alkali feldspar crystals in nepheline syenite were measured from samples EJH/12/073, 074 and 078. Finer-grained (typically <6 mm, long axis) alkali feldspar crystals in phonolite and micro-nephelinolite were measured from samples EJH/12/020, 073 and 074. Coarse-grained (>3 mm) arfvedsonite crystals in syenite were measured from samples EJH/12/073 and 076. Finer-grained (<3 mm) arfvedsonite crystals in micro-nephelinolite were measured from Sample EJH/12/073. Eudialyte crystals in nepheline syenite were measured from samples EJH/12/073, 074 and 078.

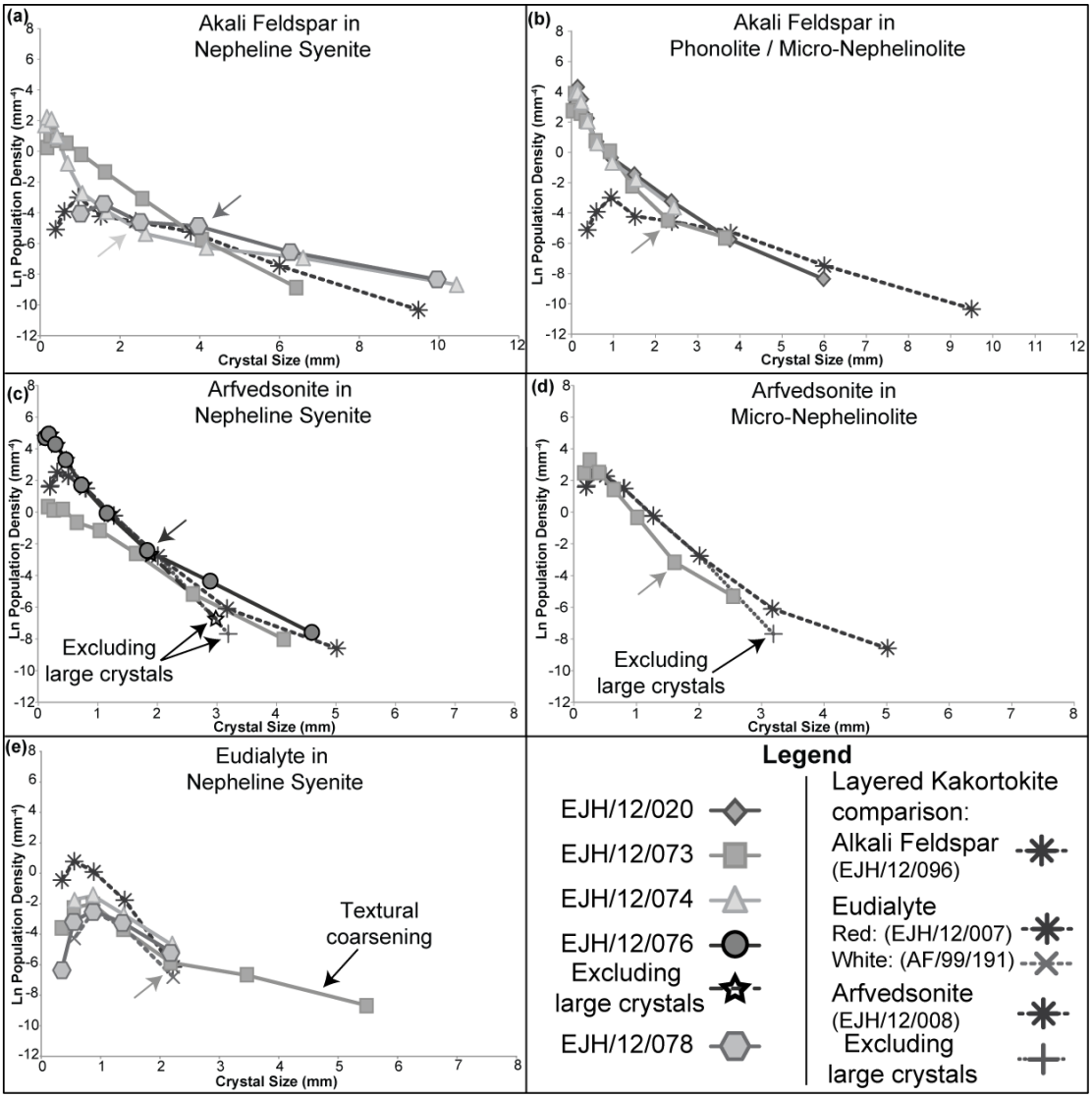

Figure 8.9: CSD Plots (a) Alkali feldspar in nepheline syenite, kinks in plots indicated by arrows. Unit 0 alkali feldspar in white kakortokite (EJH/12/096) plotted for comparison. (b) Alkali feldspar in phonolite/micro-nephelinolite, kink in plot for EJH/12/073 indicated by an arrow. Unit 0 alkali feldspar in white kakortokite (EJH/12/096) plotted for comparison. (c) Arfvedsonite in nepheline syenite, kink in plot for EJH/12/076 indicated by an arrow. Secondary plots excluding large crystal size fraction are labelled. Unit 0 arfvedsonite in black kakortokite (EJH/12/008) plotted for comparison. (d) Arfvedsonite in micro-nephelinolite, kink in plot for EJH/12/073 indicated by an arrow. Unit 0 arfvedsonite in black kakortokite (EJH/12/008) plotted for comparison, a secondary plot excluding the large crystal size fraction is labelled. (e) Eudialyte in nepheline syenite: kink in plot and enlarged grain sizes for EJH/12/073 arrowed. Unit 0 eudialyte in red kakortokite (EJH/12/096) and white kakortokite (AF/99/191) plotted for comparison.

The syenitic alkali feldspars display a greater range of crystal sizes (0.1 to 10.5 mm) in comparison to those in phonolite and micro-nephelinolite (0.1 to 6 mm). The slope values for alkali feldspars in phonolite and micro-nephelinolite are much steeper (1.68 to 3.14) in comparison to those for the alkali feldspar in nepheline syenite (0.41 to 1.65). The slopes for alkali feldspar in layered kakortokite are also

shallower (0.62 to 0.80) than the slopes for the alkali feldspar crystals in phonolite and micro-nephelinolite. The nepheline syenite alkali feldspar plots display a range of plot shapes (Fig. 8.9a); samples EJH/12/073 and 074 have a high population density at the smallest crystal sizes. EJH/12/073 displays a log-linear slope while EJH/12/074 has a slope that curves at the largest crystal sizes (arrowed, Fig. 8.9a). Sample EJH/12/078 has a lower population density, similar to alkali feldspar in layered white kakortokite. Minor kinks occur (arrowed, Fig. 8.8a) but overall the plot shape is log-linear. The plots for finer-grained alkali feldspar in phonolite and micro-nephelinolite are consistent. All display a high population density of the finest grained crystals and relatively log-linear slopes, excepting sample EJH/12/073, which has a sharp kink at 2.3 mm (arrowed, Fig. 8.8b). All plots are dissimilar to alkali feldspar from layered white kakortokite (Fig. 8.8b).

Arfvedsonite in nepheline syenite displays a greater range of crystal sizes (0.1 to 4.6 mm) in comparison those in micro-nephelinolite (0.2 to 2.6 mm). The arfvedsonite CSDs display similar slope values for both the micro-nephelinolite (4.73) and the nepheline syenite samples (2.20 to 5.16). The profiles for the arfvedsonite crystals in nepheline syenite share similarities with arfvedsonite from layered black kakortokite (sample EJH/12/076, Fig. 8.9c). Similar to black kakortokite the arfvedsonite crystal sizes are bimodal and this is indicated in the plot for sample EJH/12/076, by the kink (1.8 mm, arrowed). Like the black kakortokite, the CSD has a log-linear shape when the large crystal size fraction is not included (Fig. 8.9c). Sample EJH/12/073 has a log-linear plot for the crystals from syenite and a kinked plot (1.6 mm, arrowed) for the crystals from micro-nephelinolite (Fig. 8.9d).

The eudialyte crystals range in size from 0.3 to 5.5 mm and have much shallower slope values (0.86 to 2.44) in comparison to eudialyte in layered red kakortokite (4.26 to 5.2) and layered white kakortokite (3.29). The plot shapes are similar at the left hand side, with a downturn towards the smallest crystal sizes (Fig. 8.9e). Samples EJH/12/074 and EJH/12/078 have log-linear slopes for the right hand portions. Sample EJH/12/073 has the greatest crystal size range and displays a strong kink at 1.4 mm (arrowed, Fig. 8.8e), after which the slope profile is relatively flat.

Sample	Crystal %	SPO	Lmax	Lmax Error (±)	Y intercept	Y int Error (±)	Characteristic Length	Slope	Slope Error (±)
Alkali Feldspar (Phonolite / Micro-nephelinolite)									
EJH/12/020	22.2	0.3	3.77	0.79	1.18	0.02	0.60	-1.68	0.03
EJH/12/073	12.6	0.5	2.69	0.88	2.66	0.03	0.32	-3.14	0.03
EJH/12/074	14.2	0.2	2.16	0.08	1.79	0.03	0.44	-2.26	0.03
Alkali Feldspar (Nepheline Syenite)									
EJH/12/073	29.5	0.4	3.61	1.20	1.39	0.01	0.61	-1.65	0.01
EJH/12/074	24.4	0	6.71	1.02	-4.38	0.04	2.44	-0.41	3.92E-03
EJH/12/078	33.9	0.2	7.85	1.38	-3.10	0.06	1.90	-0.53	0.01
Arfvedsonite (Phonolite / Micro-nephelinolite)									
EJH/12/073	28.9	0.3	1.62	0.29	4.45	4.45E-04	0.21	-4.73	4.73E-04
EJH/12/076	58.2	0.3	2.55	0.90	5.72	0.04	0.19	-5.16	0.04
EJH/12/076	53.3	0.3	1.52	0.27	5.21	0.04	0.24	-4.11	0.03
Arfvedsonite (Nepheline Syenite)									
EJH/12/073	16.8	0.3	2.29	1.06	0.90	0.01	0.45	-2.20	0.01
Eudialyte (Nepheline Syenite)									
EJH/12/073	13.5	0.3	3.61	1.83	-3.87	0.04	1.16	-0.86	0.01
EJH/12/074	14.2	0	2.07	0.26	0.66	6.62E-06	0.41	-2.44	2.44E-05
EJH/12/078	7.6	0	2.07	0.34	-0.55	0.01	0.48	-2.08	0.02

Table 8.1: CSD input and output data. Crystal % = percentage of digitised phase. SPO = shape preferred orientation from 0 (no fabric) to 1 (complete alignment). Lmax = mean size of 4 largest crystals. Y-intercept = y-axis intercept of linear regression. Characteristic length = -1/slope. Slope = gradient of linear regression.

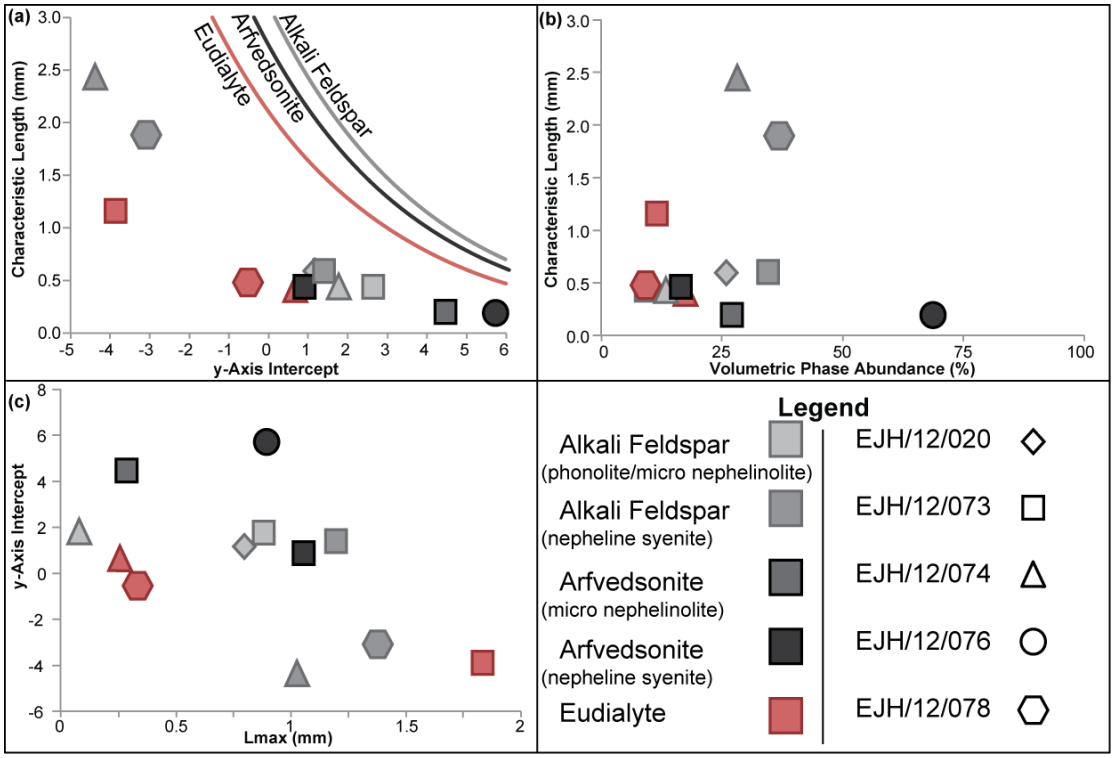

Figure 8.10: (a) plot of characteristic length vs. y-Axis intercept, all samples plot below their calculated crystallinity limits. (b) plot of characteristic length vs. volumetric phase abundance. (c) plot of y-Axis intercept vs. Lmax, displaying a generalised decrease in y-axis intercept with Lmax.

To verify that the calculated CSD data do not exceed the maximum modal percentage for each mineral species, as identified in thin section, closure limits were calculated for 40% alkali feldspar, 70% arfvedsonite and 20% eudialyte crystallinities (Higgins, 2002a). In a plot of characteristic length (-1/slope) vs. y-Axis intercept all data plot below their respective limits, demonstrating no internal inconsistency in the calculated data (Fig. 8.10a). Volumetric phase abundances were calculated (Higgins, 2002a) for each dataset and correspond to the petrographically determined modal abundances (Table 8.2). The mineral abundance is not related to characteristic length (Fig 8.10b). There is a correspondence between the y-axis intercept and characteristic length (Fig. 8.10a) as the samples with largest characteristic lengths have the lowest y-axis intercepts. The y-axis intercept has a general correspondence with Lmax (the mean size of the four largest crystals) as the samples containing the largest crystals have lower y-axis intercepts (Fig 8.10c).

Sample	Modal Abundance (%)	Volumetric Phase Abundance (%)
Alkali Feldspar (Phonolite / Micro-nephelinolite)		
EJH/12/020	35	26.0
EJH/12/073	20	9.3
EJH/12/074	20	14.5
Alkali Feldspar (Nepheline Syenite)		
EJH/12/073	37	34.5
EJH/12/074	30	28.3
EJH/12/078	40	36.9
Arfvedsonite (Micro-nephelinolite)		
EJH/12/073	40	27.2
EJH/12/076	70	68.8
Arfvedsonite (Nepheline Syenite)		
EJH/12/073	20	16.7
Eudialyte (Nepheline Syenite)		
EJH/12/073	18	11.5
EJH/12/074	20	16.9
EJH/12/078	10	9.5

Table 8.2: petrographically determined modal abundance and calculated volumetric phase abundance.

8.5 Whole Rock Chemistry

Whole rock chemistry (see Chap 4.4) was performed on samples of phonolite and micro-nephelinolite to compare their chemistries with Ilímaussaq rocks. Samples were selected to cover the range of textures from fine-grained phonolite to medium-grained micro-nephelinolite (Fig. 8.11). The data (Table 8.3) from these samples were compared to whole rock data from layered kakortokite (Bailey *et al.*, 2001), lujavrite (Bailey *et al.*, 2001), and "micro-kakortokite" from a peralkaline dyke that is suggested to be closely related to the complex (Larsen & Steenfelt, 1974) (Table 8.4).

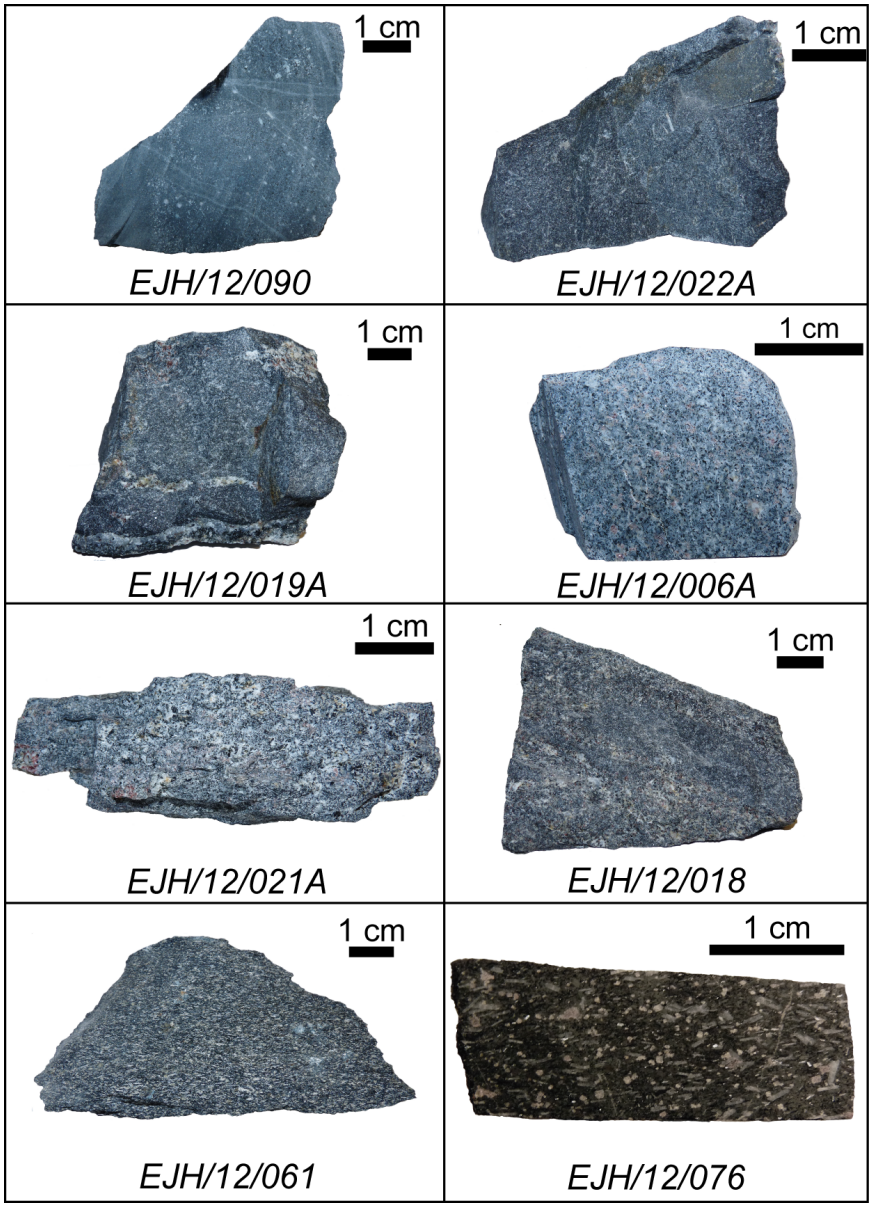

Figure 8.11: photos of the whole rock samples analysed for XRF, arranged (left to right, top to bottom) from finest- to coarsest-grained.

	EJH/12/090	EJH/12/022B	EJH/12/019A	EJH/12/006A
	Phonolite	Phonolite	Micro-nephelinolite	Micro-nephelinolite
SiO_2	54.29	55.97	53.01	53.18
TiO_2	1.34	0.68	0.49	0.45
Al_2O_3	16.45	16.97	18.88	17.95
Fe_2O_3	10.62	9.89	9.46	9.92
MnO	0.26	0.21	0.18	0.21
MgO	1.37	0.48	0.17	0.15
CaO	5.34	2.39	2.57	2.53
Na_2O	4.85	7.43	8.73	9.14
K_2O	2.68	4.04	4.17	4.26
P_2O_5	0.50	0.26	0.09	0.09
Total	99.84	99.49	99.10	99.19
P.I.	0.66	0.98	1.00	1.09
	EJH/12/021A	EJH/12/018	EJH/12/061	EJH/12/076
	Micro-nephelinolite	Micro-nephelinolite	Micro-nephelinolite	Micro-nephelinolite
SiO_2	52.72	51.50	51.57	50.22
TiO_2	0.49	0.39	0.37	0.78
Al_2O_3	17.70	17.63	8.98	7.37
Fe_2O_3	9.63	9.76	24.56	27.87
MnO	0.20	0.22	0.47	0.54
MgO	0.14	0.18	0.26	1.06
CaO	2.55	2.50	3.19	3.89
Na_2O	9.60	10.42	7.74	6.14
K_2O	4.57	5.19	2.22	2.31
P_2O_5	0.13	0.14	0.02	0.02
Total	99.13	99.18	99.93	99.80
P.I.	1.17	1.29	1.69	1.71

Table 8.3: Whole rock comparison data for phonolite and micro-nephelinolite. Total Fe content reported as Fe_2O_3. P.I. = peralkalinity index (molar $[Na_2O*K_2O]/Al_2O$).

GGU No.	Black Kakortokite 154335	Red Kakortokite 154326	White Kakortokite 154314	Bulk Kakortokite Calc. Mean	Aegirine Lujavrite 57033	Arfvedsonite Lujavrite 154358
SiO_2	48.06	52.20	53.30	52.23	53.24	53.06
TiO_2	0.57	0.68	0.16	0.35	0.17	0.15
Al_2O_3	8.16	10.51	13.40	11.88	15.08	14.29
Fe_2O_3	7.17	6.04	7.90	7.32	8.83	2.89
FeO	17.08	6.90	3.42	6.37	2.20	7.75
MnO	0.48	0.41	0.31	0.36	0.21	0.44
MgO	0.58	0.28	0.23	0.30	0.19	0.14
CaO	4.39	3.58	2.10	2.82	0.79	0.38
Na_2O	6.95	9.26	8.84	8.66	11.53	9.84
K_2O	2.79	3.39	4.04	3.69	3.32	3.42
P_2O_5	0.01	0.04	0.04	0.04	0.03	0.54
Total	100.02	99.35	99.47	99.52	99.36	99.62
P.I.	1.77	1.80	1.41	1.53	1.51	1.39

GGU No.	M-C Lujavrite 154399	Micro-kakortokite 1 150766	Micro-kakortokite 2 42506	Micro-kakortokite 3 42508	Phonolite Mean	Micro-nephelinolite Mean
SiO_2	53.87	53.51	52.96	57.41	55.13	52.03
TiO_2	0.43	0.50	0.52	0.56	1.01	0.49
Al_2O_3	12.94	14.62	15.09	13.29	16.71	14.75
Fe_2O_3	3.48	13.35	9.44	8.62	10.25	15.20
FeO	8.29	5.04	3.62	4.36	-	-
MnO	0.61	0.28	0.34	0.50	0.24	0.30
MgO	0.10	0.43	0.16	0.18	0.92	0.33
CaO	0.29	0.95	2.75	2.73	3.86	2.87
Na_2O	7.91	6.13	7.75	7.65	6.14	8.63
K_2O	5.34	4.89	5.05	3.38	3.36	3.79
P_2O_5	0.47	0.11	0.12	0.12	0.38	0.08
Total	99.19	100.13	99.09	99.12	100.25	99.39
P.I.	1.45	1.05	1.21	1.57	0.82	1.33

Table 8.4: Whole rock comparison data. Kakortokite and lujavrite data from Bailey et al. (2001). Mean kakortokite composition calculated from the bulk composition of the layered kakortokite - black (15.2%), red (25.0%) and white (59.8%) - using compositional data from (Bailey *et al.*, 2001). Micro-kakortokite from Larsen & Steenfelt (1974), low-alkalinity micro-kakortokite. Mean phonolite and micro-nephelinolite compositions calculated from data from present study, note total Fe content reported as Fe_2O_3. P.I. = peralkalinity index (molar $[Na_2O*K_2O]/Al_2O$).

Most of the samples do not share chemical similarities with the layered kakortokite or lujavrite (Tables 8.3 & 8.4). The peralkalinity indices (0.66-1.29, Fig. 8.12a) are much lower than layered kakortokite (1.41-1.77) and lujavrite (1.39-1.51), while the TiO_2 (0.34-0.94 wt.%, Fig. 8.12b) and Al_2O_3 (16.45-18.88 wt.%) contents are higher than layered kakortokite (TiO_2 = 0.16-0.57 wt.%, Al_2O_3 = 8.16-13.40 wt.%) and lujavrite (TiO_2 = 0.17-0.43 wt.%, Al_2O_3 = 12.94-15.08 wt.%). The phonolite and micro-nephelinolite samples do however share chemical similarities with the micro-kakortokite (peralkalinitiy index = 1.05-1.57 and TiO_2 = 0.50-0.56 wt.%, Al_2O_3 = 13.29-15.09 wt.%).

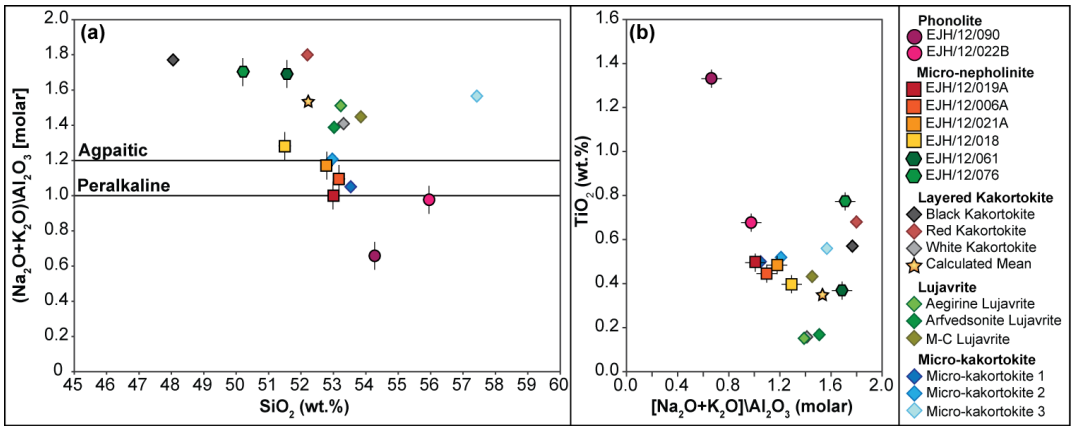

Figure 8.12: (a) plot of peralkalinity index vs. SiO2 indicating range of hybrid compositions from agpaitic, through to peralkaline and non-peralkaline. (b) plot of TiO2 vs. peralkalinity index displaying a range of compositions from relatively Ti-poor layered kakortokite to relatively Ti-rich hybrid rocks that contain augite. Kakortokite and lujavrite data from Bailey *et al.* (2001); mean calculated using measured kakortokite unit/layer thickness from present study and data from Bailey *et al.* (2001); micro-kakortokite data from Larsen & Steenfelt (1974).

The variation in chemical composition has a link to grain size. The finest-grained samples (phonolite) have the lowest peralkalinity indices (0.66-0.98) and highest TiO_2 contents (0.68-1.34 wt.%). The peralkalinity increases with grain size through the micro-nephelinolite samples (1.00-1.71) and TiO_2 contents are reduced (0.37-0.78).

These chemical differences with grain size are highlighted by the two coarsest-grained micro-nephelinolite samples (EJH/12/076 and EJH/12/061). Unlike the other micro-nephelinolite and phonolite samples, these chemically compare well to layered kakortokite (Fig. 8.12). Their whole rock compositions are similar to black kakortokite (Tables 8.3 & 8.4), e.g. peralkalinity index (1.69-1.71 compared to 1.77, Fig. 8.12a); TiO_2 (0.37-0.78 wt.% compared to 0.57 wt.%, Fig. 8.12b); Al_2O_3 (7.4-9.0 wt.% compared to 8.2 wt.%).

8.6 Mineral Chemistry

EPMA (Chapter 4.5) was used to compare the composition of the eudialyte (micro-nephelinolite and nepheline syenite) and amphibole (phonolite, micro-nephelinolite and nepheline syenite) to the same minerals in the layered kakortokite. The data are located in the supplementary files, Appendix D.

8.6.1 Eudialyte-Group Minerals

EGM are uncommon in the phonolite and in most of the micro-nephelinolite samples. However, it was analysed from three micro-nephelinolite (EJH/12/022A, 068, 092) samples and the arfvedsonite-rich micro-nephelinolite that has chemical similarities with black kakortokite (Chap 8.5). Additionally it was measured in the nepheline syenite that displayed unusually large eudialyte crystals (texturally coarsened, EJH/12/073) and a further three nepheline syenite samples (EJH/12/072A, 074, 078). Similar to the layered kakortokite the $Fe_{(TOTAL)}$/Mn ratio is an indicator of the evolutionary state of the magma that the eudialyte crystallised from (Pfaff *et al.*, 2008). In the nepheline syenite this ratio ranges from 5.54 to 13.45, a similar range (Fig. 8.13) to the layered kakortokite (5.77 to 13.45). The sample that chemically resembles layered kakortokite (EJH/12/076) has a $Fe_{(TOTAL)}$/Mn ratio between 9.24 to 12.76, similar to the composition of black kakortokite (10.85-13.34, Fig. 8.13).

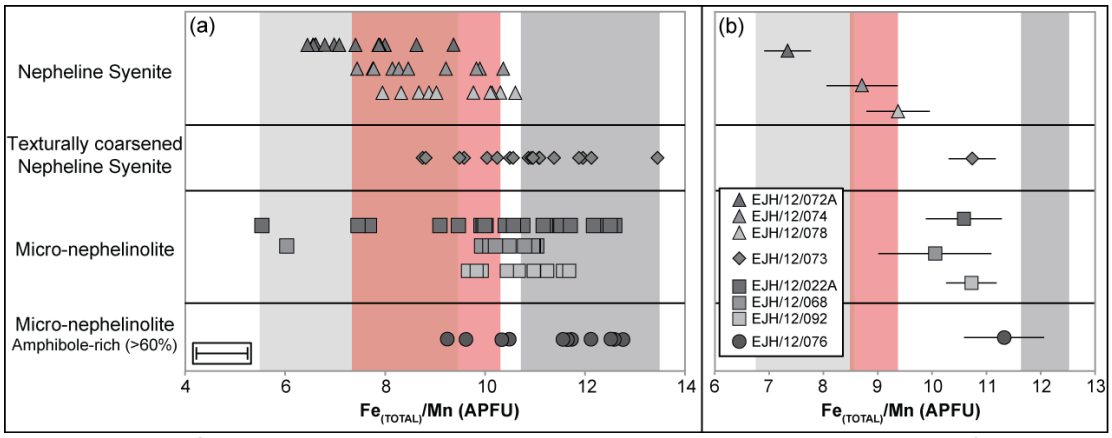

Figure 8.13: EGM Fe_{TOTAL}/Mn measured through EPMA compared to data from Unit 0 layered kakortokite (black = dark grey band, red = red band, white = light grey band). (a) Data for the range of textures. (b) Mean and error of mean for each dataset. Note outliers are not excluded from mean calculations.

The EGM in the micro-nephelinolite has $Fe_{(TOTAL)}$/Mn ratios between 5.54 to 12.59, which extend into the range of red (7.23-10.55) and white (5.77-9.98) kakortokite compositions. The mean values, however, are between the compositions of eudialyte from red and black kakortokite (Fig 8.13b, Table 8.5).

The EGM from the texturally coarsened nepheline syenite (EJH/12/073) has a similar range of $Fe_{(TOTAL)}$/Mn ratios (8.75-13.45) to the micro-nephelinolite. The eudialyte compositions mostly correspond to EGM in black and red kakortokites (Fig. 8.13a, Table 8.5) with the mean of the dataset falling between red and black compositions (Fig. 8.13b, Table 8.5).

The EGM in the nepheline syenite has a range of $Fe_{(TOTAL)}$/Mn ratios between 6.45 to 10.61, which compare to compositions between white (5.77 to 9.98) and red (7.23-10.55) kakortokite (Fig. 8.14a, Table 8.5). The mean of the datasets ranges between red to white compositions (Fig. 8.14b, Table 8.5).

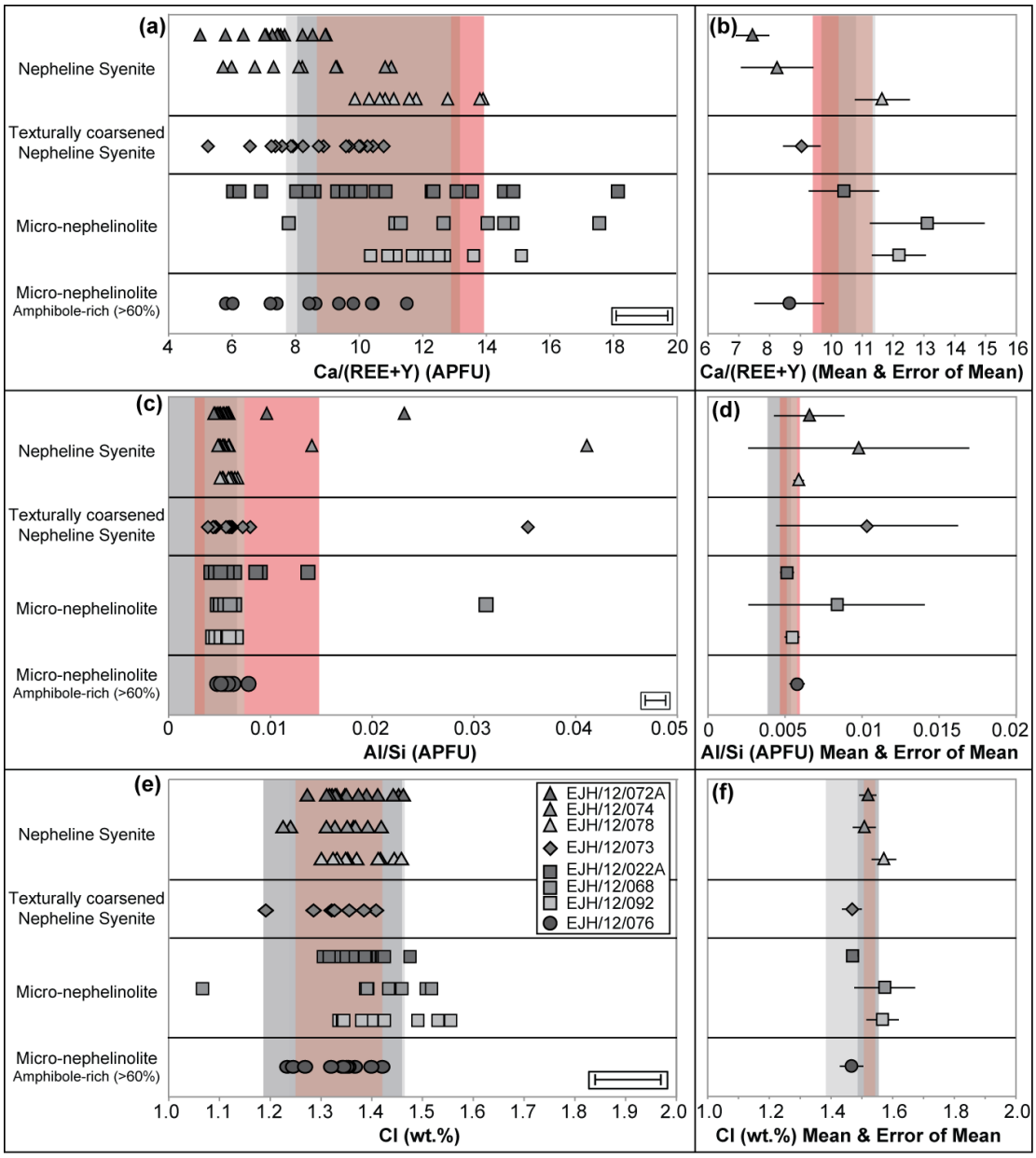

Figure 8.14: EGM chemistry through EPMA for 'hybrid' textures compared to data from Unit 0 layered black (dark grey), red (red) and white (light grey) kakortokites. (a)-(b) Ca/(REE+Y) data. (c)-(d) Al/Si data. (e)-(f) Cl data. Errors calculated to 95% confidence. Note outliers are not excluded from mean calculations.

Rock	Sample	Fe/Mn				Ca/(REE+Y)				Al/Si				Cl			
		Mean	±	Min	Max	Mean	±	Min	Max	Mean	±	Min	Max	Mean	±	Min	Max
Amphibole-rich	EJH/12/076	11.33	0.74	9.24	12.76	8.63	1.13	5.81	11.50	0.006	0.0005	0.005	0.008	1.47	0.04	1.36	1.55
Micro-nephelinolite	EJH/12/022A	10.72	0.47	9.65	11.68	12.19	0.88	10.33	15.09	0.005	0.0005	0.004	0.007	1.57	0.05	1.45	1.72
	EJH/12/068	10.05	1.04	6.03	11.03	13.11	1.86	7.79	17.54	0.008	0.0057	0.005	0.031	1.57	0.10	1.21	1.71
	EJH/12/092	10.58	0.70	5.54	12.59	10.41	1.14	6.04	18.13	0.005	0.0005	0.004	0.009	1.47	0.01	1.41	1.50
Texturally Coarsened	EJH/12/073	10.74	0.43	8.28	13.45	9.04	0.61	5.23	12.57	0.010	0.0059	0.004	0.081	1.47	0.03	1.18	1.57
Nepheline Syenite	EJH/12/072A	9.38	0.58	7.95	10.61	11.66	0.89	9.87	13.89	0.006	0.0003	0.005	0.007	1.57	0.04	1.48	1.66
	EJH/12/074	8.71	0.65	7.44	10.36	8.24	1.18	5.70	11.00	0.010	0.0072	0.005	0.041	1.51	0.04	1.41	1.59
	EJH/12/078	7.34	0.43	6.45	9.37	7.44	0.55	4.99	8.96	0.007	0.0023	0.004	0.023	1.52	0.03	1.40	1.60
Compositional Ranges																	
Micro-nephelinolite		10.51	0.46	5.54	12.59	11.36	0.84	6.04	18.13	0.006	0.0013	0.004	0.031	1.52	0.03	1.21	1.72
Nepheline Syenite		8.29	0.42	6.45	10.61	8.84	0.76	4.99	13.89	0.007	0.0022	0.004	0.041	1.53	0.02	1.40	1.66

Table 8.5: Mean, Minimum and Maximum values for geochemical ratios measured in EGM from the phonolite, micro-nephelinolite and syenite samples. Precision (±) to 95% confidence.

Additional element ratios Ca/(REE+Y) and (Al/Si) were analysed as these can reflect the evolutionary state of the magma during orthomagmatic crystallisation, (Pfaff *et al.*, 2008). The Cl content of eudialyte was also investigated as this is suggested to decrease upwards through the Ilímaussaq stratigraphy (Pfaff *et al.*, 2008), due to the decrease in Cl in the melt during fractionation (Krumrei *et al.*, 2007). The Ca/(REE+Y) ratio range is highly variable between textures: the kakortokitic sample (EJH/12/076) has a lower range of values (5.81-11.5) than the layered kakortokite (7.31-14.32; Fig 8.14a,b, Table 8.5). The micro-nephelinolite samples have the greatest range of values from 6.04 to 18.13 (Fig. 8.14a, Table 8.5), with the mean of one sample (EJH/12/022A) approaching the composition of the layered kakortokite (Fig. 8.14b, Table 8.5). The texturally coarsened nepheline syenite sample has a range of values (6.55-10.76) similar to those of white kakortokite (7.31-12.92, Fig. 8.14a, Table 8.5). The nepheline syenite samples have a wide range of values and the lowest ratios (4.99-13.89, Fig. 8.14a, Table 8.5), but a greater range than the layered kakortokite (Fig. 8.14b, Table 8.5).

The Al/Si ratio of the samples typically falls into the layered kakortokite range (Fig. 8.14c, Table 8.5), however outliers increase the compositional ranges (Fig. 8.14d, Table 8.5). The Al/Si ratio of the kakortokitic sample (EJH/12/076, 0.005-0.008) falls in the range of white kakortokite (0.0004-0.008, Fig. 8.14c,d, Table 8.5). The micro-nephelinolite samples are also typically in the range (0.004-0.014, Table 8.5) of red to white layered kakortokite (0.003-0.014, Table 8.5) with one outlier (Fig. 8.14c) increasing the range of sample EJH/12/068 (Fig. 8.14d). The texturally coarsened nepheline syenite sample has an outlier at 0.035, however the range of the other data points is 0.004 to 0.007, similar to white kakortokite (Fig 8.14c, Table 8.5). The nepheline syenite again has outliers with relatively increased Al/Si values up to 0.041 (Fig. 8.14c,d, Table 8.5) but the typical ranges are similar to white kakortokite (Fig. 8.14c, Table 8.5).

The Cl contents for the samples are typically in the range of layered kakortokite compositions (Fig. 8.14e). The kakortokitic sample (EJH/12/076) has a range of 1.23-1.42, very similar to the range of Cl in eudialyte in black kakortokite (1.20-1.45, Fig. 8.14e, Table 8.5). The ranges in the micro-nephelinolite are slightly higher (1.07-1.56) compared to layered kakortokite (0.85-1.45); the texturally coarsened nepheline syenite is similar to kakortokite ranging from 1.19-1.41 (Fig. 8.14e, Table 8.5). The coarse-grained nepheline syenite is also in the range of layered kakortokite, ranging from 1.23 to 1.46 (Fig. 8.14e, Table 8.5).

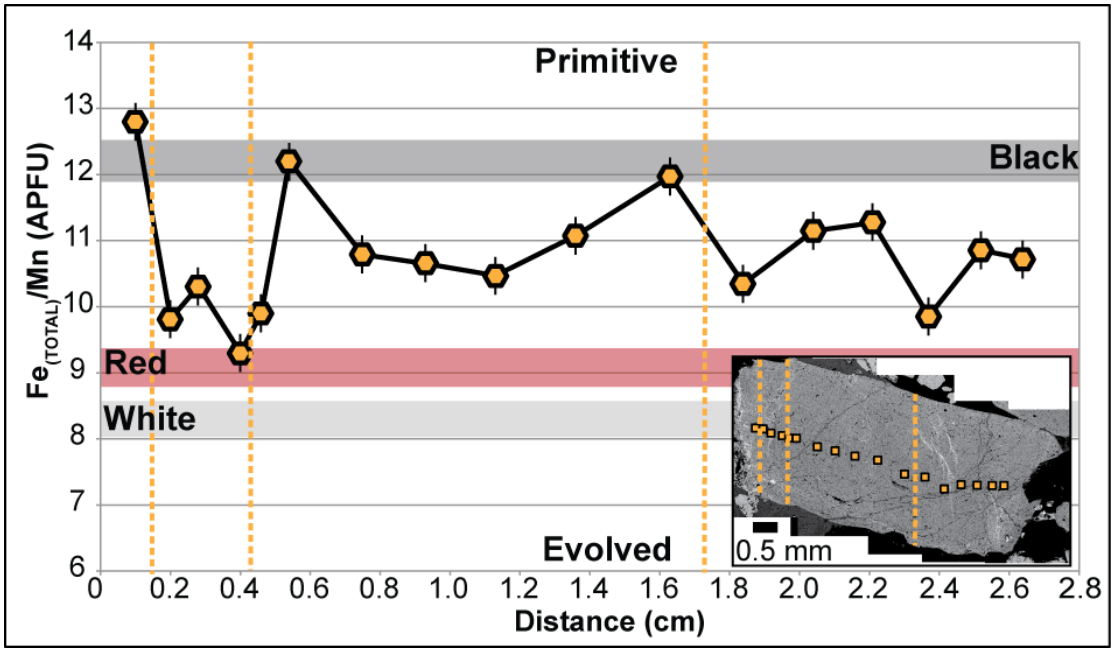

Figure 8.15: EPMA traverse across large, texturally coarsened, eudialyte crystal (insert) from sample EJH/12/068, measuring $Fe_{(TOTAL)}$/Mn ratios. Orange lines mark compositional zones. Coloured bars represent Unit 0 black, red and white ratios.

A traverse across a texturally coarsened EGM crystal (sample EJH/12/068) was performed to investigate the magmatic compositions during textural coarsening. The $Fe_{(TOTAL)}$/Mn ratio was used as the best indicator of magmatic evolutionary state and the data fall in the range between black and red kakortokitic compositions (9.31-12.80, Fig. 8.15). The core has a mean $Fe_{(TOTAL)}$/Mn ratio of 11.19±1.04 (10.47-12.20) with the rim having a lower range (9.31-11.27, Fig. 8.15).

8.6.2 Amphibole

Amphibole is a common mafic mineral in all three of the rock types and major element compositions were measured through EPMA. The amphibole compositions range towards the sodic end-members, from katophorite and ferro-richterite to arfvedsonite (Fig. 8.16).

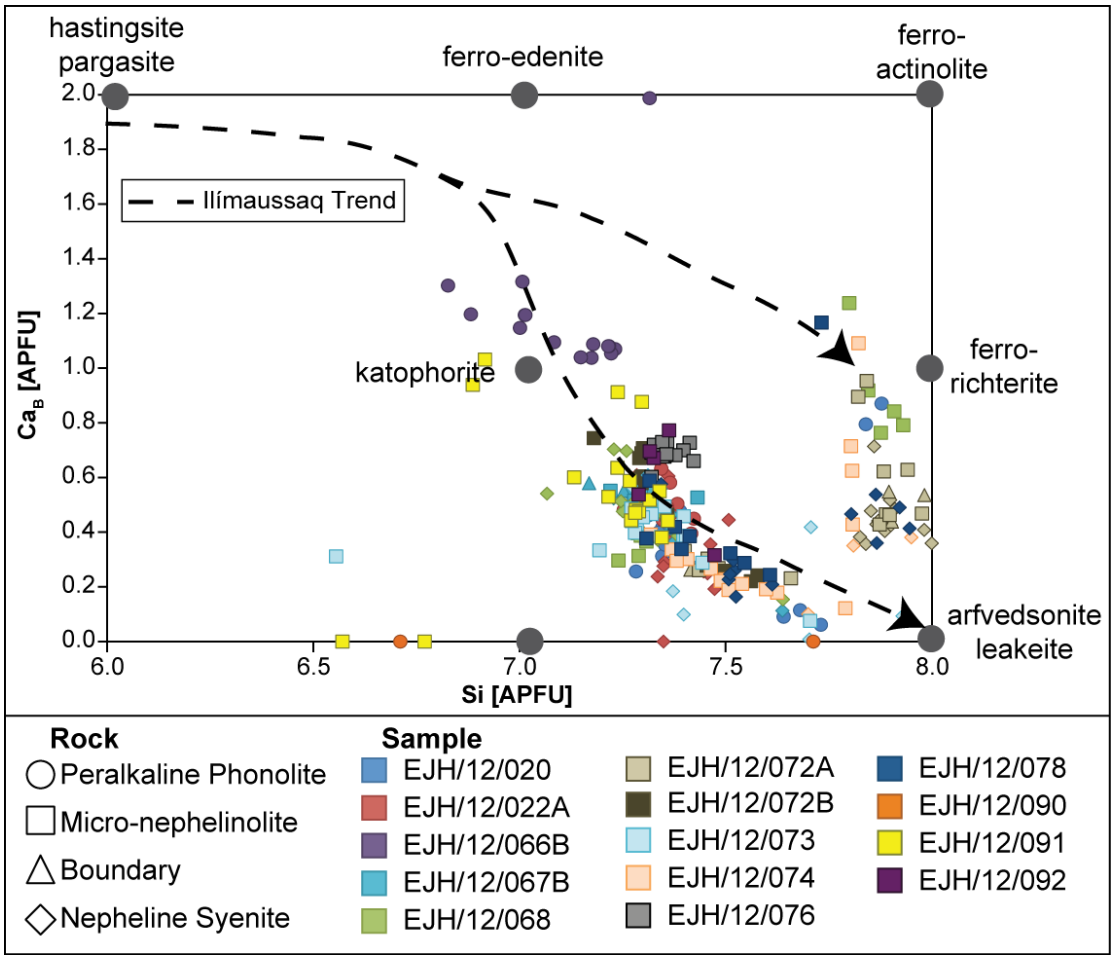

Figure 8.16: Plot of Ca_B vs. Si (APFU) in amphibole plotted according to texture – coarse: syenite, boundary: syenite-phonolite contact, fine: phonolite. Plot adapted from Marks *et al.* (2004), data follow their bimodal Ilímaussaq trend.

Two chemical ratios were used to investigate the amphibole chemistries, the Ca/(Na+K) and X_{Fe} (Fe^{2+}/[Fe^{2+}+Mn+Mg]). Ca/(Na+K) should systematically decrease as the melt from which amphibole crystallises evolves (Pfaff *et al.*, 2008). This is an effect of the crystallographic preferences of Na & K on the A-site & Ca and Na on the B-site (Pfaff *et al.*, 2008).

The Ca/(Na+K) ratio indicates an overall decrease from the amphiboles in fine-grained phonolite (0.03-1.52); to the micro-nephelinolite (0.002-0.44), the crystals at the boundary (over 5 mm) between micro-nephelinolite and syenite (0.1-0.32); to the lowest values for amphiboles in nepheline syenite (0.003-0.31). It is best displayed by single samples, e.g. EJH/12/067B (Fig. 8.17a, Table 8.6):

micro-nephelinolite – 0.21-0.32, boundary – 0.21-0.32, nepheline syenite – 0.05-0.24. The ratios have a similar range to the amphiboles in layered kakortokite (0.01-0.3). The finest-grained amphiboles have ratios similar to those of amphiboles in black kakortokite (0.15-0.3). The coarser-grained amphiboles in nepheline syenite have ratios that compare better to amphiboles in red (0.06-0.20) and white (0.01-0.16) kakortokites (Fig. 8.17 a&b, Table 8.6).

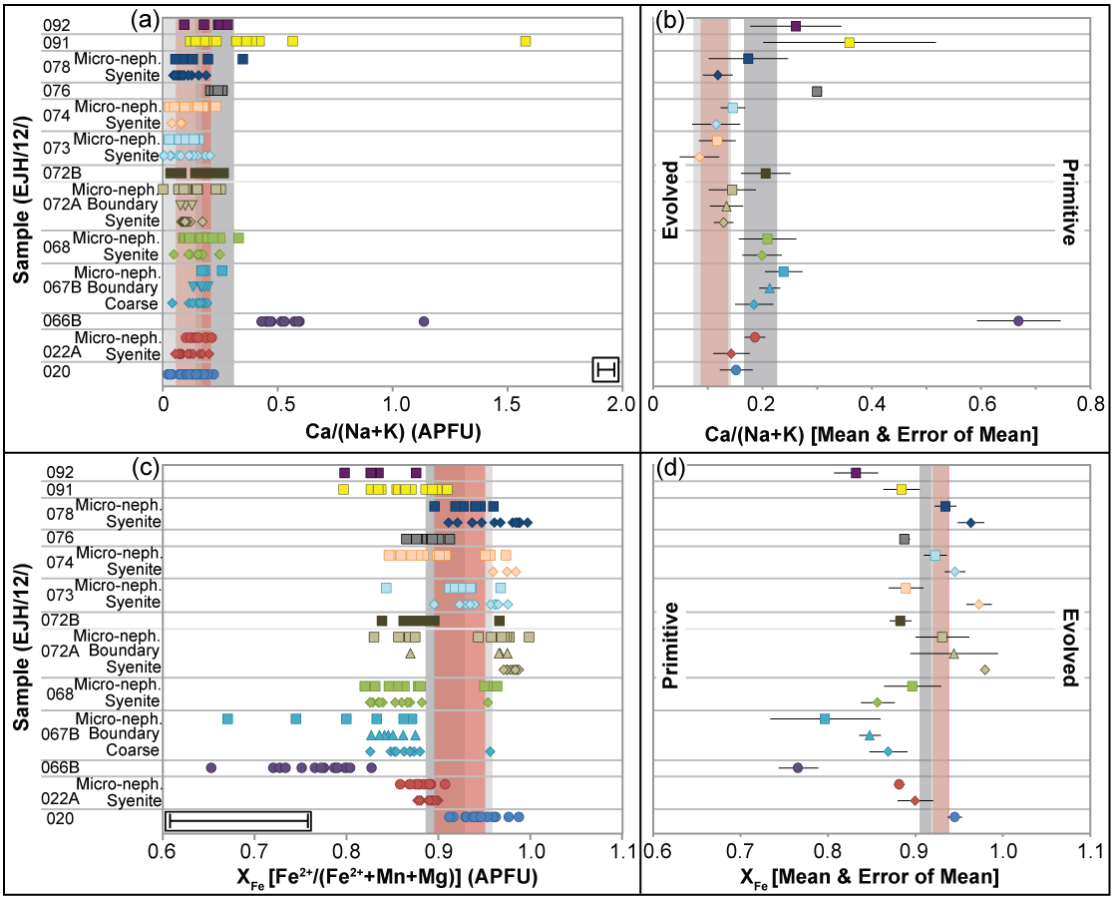

Figure 8.17: Amphibole Ca/(Na+K) ratios measured through EPMA, all data subdivided by sample number and texture. Coloured bars represent amphibole compositions in Unit 0 black (dark grey), red (red) and white (light grey) kakortokites. (a) Ca/(Na+K) ratios, error bar bottom right. (b) Mean and error of mean of Ca/(Na+K) ratios. (c) X_{Fe} ratio ($Fe^{2+}/[Fe^{2+}+Mn+Mg]$), error bar bottom left. (d) Mean and error of mean of X_{Fe} ratios. Note outliers are not excluded from mean calculations.

The X_{Fe} ratio is controlled by the Fe-Mn composition of the melt, which modally reflects amphibole-dominated crystallisation (lower-Fe) or pyroxene-dominated crystallisation (higher-Fe). Thus a high X_{Fe} ratio typically reflects crystallisation from more evolved melts (Pfaff *et al.*, 2008). The ratio can be affected by both structural effects and intensive parameters (e.g. $f(H_2O)$ (Di Carlo *et al.*, 2010)), however as the X_{Fe} ratio correlates with variations in the Ca/(Na+K) ratio, it is inferred to reflect magmatic evolution.

The X_{Fe} ratio progressively increases from the amphiboles in fine-grained phonolite (0.65-0.99), in micro-nephelinolite (0.67-1.00), crystals at the boundary (over 5 mm) between micro-nephelinolite and syenite (0.83-0.87) to the highest values for amphiboles in nepheline syenite (0.83-1.00). Again this progressive increase is best exemplified in the single samples (Fig. 8.17 c&d, Table 8.6), e.g. Sample EJH/12/067B: micro-nephelinolite – 0.67-0.87, boundary – 0.83-0.87, nepheline syenite – 0.83-0.96.

The X_{Fe} ratios have a much greater range (0.67-1.00, Table 8.6) compared to those for amphiboles in layered kakortokite (0.89-0.95). In samples EJH/12/067B, 068 and 072 A&B, there is a gap in composition over the range of layered kakortokite ratios (Fig. 8.17c). Excepting this unusual feature, the X_{Fe} ratios over the range of amphibole textures do not correspond to the ratios in layered kakortokite (black: 0.89-0.92 or red and white 0.90-0.95; Fig. 8.17 a&b, Table 8.6).

Sample	Rock	Ca/(Na+K)				XFe^{2+}			
		Mean	±	Min	Max	Mean	±	Min	Max
EJH/12/020	Phonolite	0.15	0.03	0.03	0.28	0.95	0.01	0.91	0.99
EJH/12/022A	Micro-nephelinolite	0.19	0.02	0.13	0.27	0.88	0.01	0.86	0.91
EJH/12/022A	Nepheline Syenite	0.14	0.03	0.07	0.25	0.88	0.01	0.88	0.90
EJH/12/066B	Phonolite	0.67	0.11	0.54	1.42	0.77	0.02	0.65	0.83
EJH/12/067B	Micro-nephelinolite	0.24	0.03	0.21	0.32	0.80	0.06	0.67	0.87
EJH/12/067B	Boundary	0.21	0.02	0.17	0.25	0.85	0.01	0.83	0.87
EJH/12/067B	Nepheline Syenite	0.18	0.03	0.05	0.24	0.87	0.02	0.83	0.96
EJH/12/068	Micro-nephelinolite	0.21	0.05	0.11	0.41	0.86	0.02	0.82	0.96
EJH/12/068	Nepheline Syenite	0.20	0.04	0.06	0.31	0.86	0.02	0.83	0.95
EJH/12/072A	Micro-nephelinolite	0.14	0.04	0.002	0.31	0.93	0.03	0.83	1.00
EJH/12/072A	Boundary	0.13	0.03	0.10	0.16	0.94	0.05	0.87	0.98
EJH/12/072A	Nepheline Syenite	0.13	0.02	0.10	0.22	0.98	0.003	0.97	0.99
EJH/12/072B	Phonolite	0.21	0.05	0.04	0.33	0.88	0.01	0.84	0.97
EJH/12/073	Micro-nephelinolite	0.15	0.02	0.03	0.20	0.92	0.01	0.84	0.97
EJH/12/073	Nepheline Syenite	0.12	0.04	0.003	0.26	0.95	0.01	0.90	0.98
EJH/12/074	Micro-nephelinolite	0.12	0.03	0.04	0.04	0.89	0.02	0.85	0.85
EJH/12/074	Nepheline Syenite	0.08	0.04	0.05	0.11	0.97	0.01	0.96	0.98
EJH/12/076	Phonolite	0.30	0.01	0.26	0.32	0.89	0.01	0.87	0.91
EJH/12/078	Micro-nephelinolite	0.17	0.07	0.07	0.44	0.93	0.01	0.90	0.90
EJH/12/078	Nepheline Syenite	0.12	0.03	0.06	0.24	0.96	0.02	0.91	1.00
EJH/12/091	Phonolite	0.31	0.07	0.15	0.71	0.87	0.01	0.80	0.91
EJH/12/092	Phonolite	0.26	0.08	0.12	0.35	0.83	0.03	0.80	0.88
Mean Compositions									
Phonolite		0.88	0.01	0.03	1.52	0.32	0.06	0.65	0.99
Micro-nephelinolite		0.90	0.01	0.002	0.44	0.17	0.02	0.67	1.00
Boundary		0.88	0.03	0.10	0.32	0.18	0.03	0.83	0.87
Nepheline Syenite		0.92	0.01	0.003	0.31	0.14	0.01	0.83	1.00

Table 8.6: Mean, Minimum and Maximum values for geochemical ratios measured in amphiboles from the phonolite, micro-nephelinolite and syenite samples. Precision (±) to 95% confidence.

An EPMA traverse was performed across a large amphibole crystal in nepheline syenite (EJH/12/073). The Ca/(Na+K) ratio ranges from 0.06 to 0.17 and the X_{Fe} ratio from 0.91 to 0.94, indicating no significant chemical evolutionary trends from core to margin (Fig. 8.18).

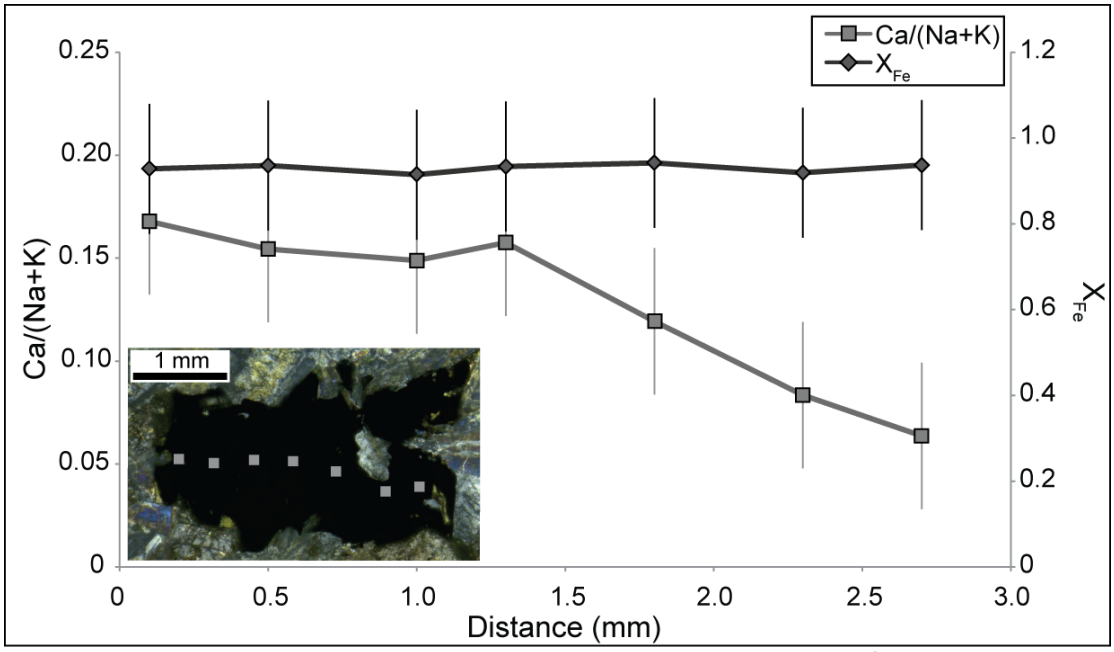

Figure 8.18: EPMA traverse across large amphibole crystal (inset) from sample EJH/12/073, measuring Ca/(Na+K) and X_{Fe} ratios. Note amphibole appears opaque in thick section.

8.7 Development of the Phonolite/Micro-nephelinolite Sequence.

The phonolite, micro-nephelinolite and nepheline syenite sequence has been described variously as: lujavrite that underlays the kakortokite (Ussing, 1912); a fine-grained unlayered kakortokite termed a 'hybrid' (Ferguson, 1970); and an unlayered kakortokite formed through slumping of unconsolidated kakortokite crystal mush (Bohse *et al.*, 1971). The latter hypothesis is the most commonly quoted, however the mineralogical, textural and chemical evidence presented above indicates inconsistencies between these rocks and kakortokite.

The sequence is distinct to the kakortokite; it crosscuts the layering (Figs. 8.1b and 8.19) and is texturally heterogeneous on a centimetre- to metre-scale, while the layered kakortokite is homogeneous over similar scales. Most noticeably the phonolite and micro-nephelinolite contain nepheline syenite veins (Fig. 8.3a) and pillows (Fig. 8.3b). The rock sequence contains fabrics, both at metre- and centimetre-scale, for example, the foliation fabric that passes from the micro-nephelinolite into the syenite (Fig. 8.3h). While these features may have given rise to the hypothesis that the sequence was generated through slumping, formation of these textural features through magmatic flow is equally plausible.

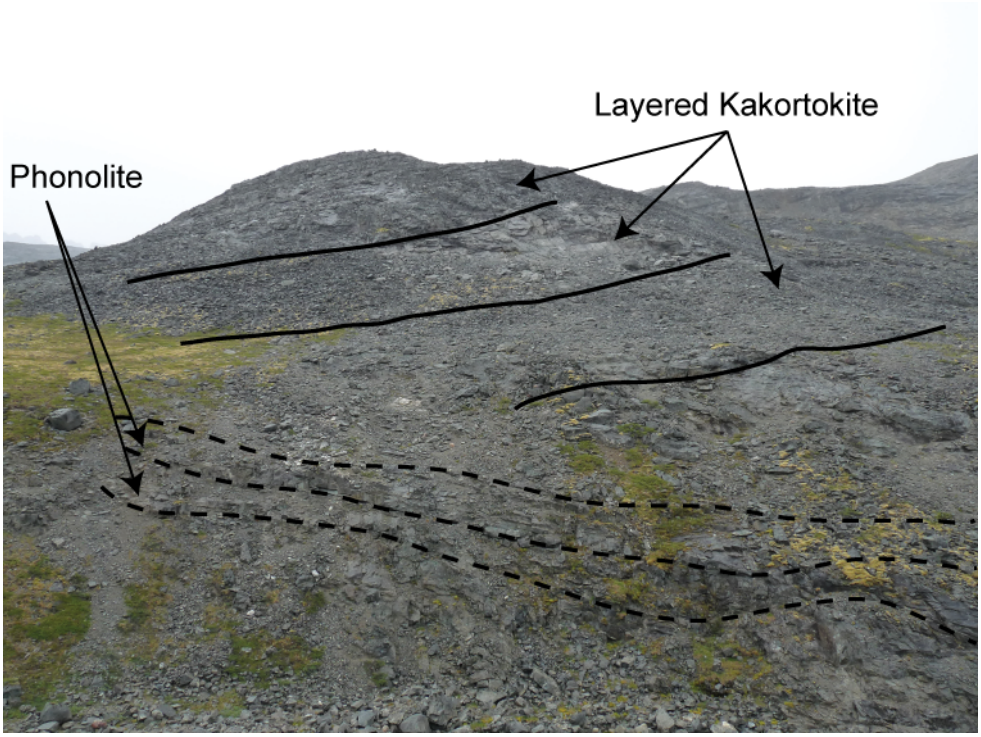

Figure 8.19: phonolite cross-cuts the layered kakortokite in Lakseelv valley, view to South, arrowed on Fig. 8.1a as outcropping at approximately Unit -4.

The mineralogy of the phonolite and micro-nephelinolite differs from layered kakortokite and lujavrite as the phonolite and micro-nephelinolite are typically eudialyte-poor and contain aenigmatite and augite. This highlights a difference

between these rocks and the layered kakortokite as aenigmatite is less abundant in the kakortokite; augite, which occurs as large euhedral crystals, is not present in kakortokite.

CSD analysis was performed on all three rock types, phonolite, micro-nephelinolite and nepheline syenite, to investigate the processes of nucleation and growth during the formation of each and to compare them to black, red and white kakortokite samples (Unit 0 marker horizon). The crystal sizes in the phonolite and micro-nephelinolite are dissimilar to the layered kakortokite; the crystal sizes are much smaller (Fig. 8.9) and in the case of alkali feldspar there is a greater proportion of the finest crystals. Slope profiles for alkali feldspar and arfvedsonite display kinks (Fig. 8.9 b&d) indicating mixed crystal populations. This is inferred to derive from interaction and movement of crystals between rock types. The CSDs for the nepheline syenite compare well to the layered kakortokite (Fig. 8.9a,c,e), the range of crystal sizes is similar, although the syenite typically displays a greater number of the smallest crystal sizes compared to the layered kakortokite. Similar to the phonolite and micro-nephelinolite samples the CSDs for alkali feldspar and arfvedsonite are kinked (Fig. 8.9a,c). This again indicates mixing of crystal populations and likely interactions between the three rock types.

The CSDs for eudialyte in nepheline syenite are typically flatter than their equivalents from layered red kakortokite (Fig. 8.9e) and show a decreased number of the smallest crystals. This flattening of slope profiles is associated with post-nucleation textural coarsening, i.e. coalescence of crystals and the growth of large crystals at the expense of the smallest (Higgins, 2010, Marsh, 1998). The exceptionally large eudialyte crystals in nepheline syenite from sample EJH/12/073 suggest that some eudialyte crystals underwent extreme textural coarsening as they have much greater crystal sizes than those in the red kakortokite.

The differences between the CSD profiles for the phonolite and micro-nephelinolite and for the layered kakortokite indicate that the crystals were not sourced from remobilised kakortokite; instead they underwent a distinct crystallisation history. This is also indicated by the whole rock chemistry. The samples range from the phonolite samples, which have the lowest peralkalinity indices and are relatively enriched in TiO_2, to the micro-nephelinolite samples, which have higher peralkalinity indices, are peralkaline to agpaitic in composition, and are relatively less enriched in TiO_2. The micro-nephelinolite samples that texturally and mineralogically resemble black kakortokite have the highest peralkalinity and lowest TiO_2 contents. They also plot in a similar location to the layered kakortokite (Fig.

8.12). This reflects an evolutionary trend from the finest-grained phonolite to the medium/coarse-grained rocks that are kakortokitic in appearance and composition.

The compositions of the amphibole in phonolite to micro-nephelinolite to nepheline syenite also indicate an evolutionary trend. Individual samples display Ca/(Na+K) ratios that range from relatively primitive compositions in the phonolite, which increase through micro-nephelinolite and the boundary to nepheline syenite, and are greatest in amphiboles in the nepheline syenite (Fig. 8.17). This is consistent with mixing at the boundary between the micro-nephelinolite and syenite. The eudialyte in the syenite displays a range of compositions. The sample that resembles an arfvedsonite-rich black kakortokite (EJH/12/076) contains eudialyte that is typically in the range of black kakortokite compositions (Fig. 8.13). The eudialyte in the micro-nephelinolite is more primitive, falling between the ranges of black and red kakortokite. The nepheline syenite contains eudialyte in the range of red to white kakortokite (Fig. 8.13). The sample that resembles black kakortokite (EJH/12/076) is considered to be a remobilised lens of black kakortokite, based on its mineralogical and chemical similarities.

The phonolite samples have a very different chemical composition to the layered kakortokite. These chemistries show that the phonolite was not formed from kakortokite magma, rather it crystallised from a more primitive (i.e. less alkaline) and relatively Ti-rich magma. This could only have occurred through open-system magma chamber processes and the manner in which the sequence crosscuts the layering indicates an influx of replenishing magma, which cut through the unconsolidated layered kakortokite crystal mush (Fig. 8.20a). Intrusion of this primitive magma would lead to thermal, chemical and physical erosion of the crystal mush. Mixing of the intruding primitive magma with the kakortokite crystal mush (Fig. 8.20b-c) would form the range of compositions represented in the phonolite and micro-nephelinolite samples (Fig. 8.12).

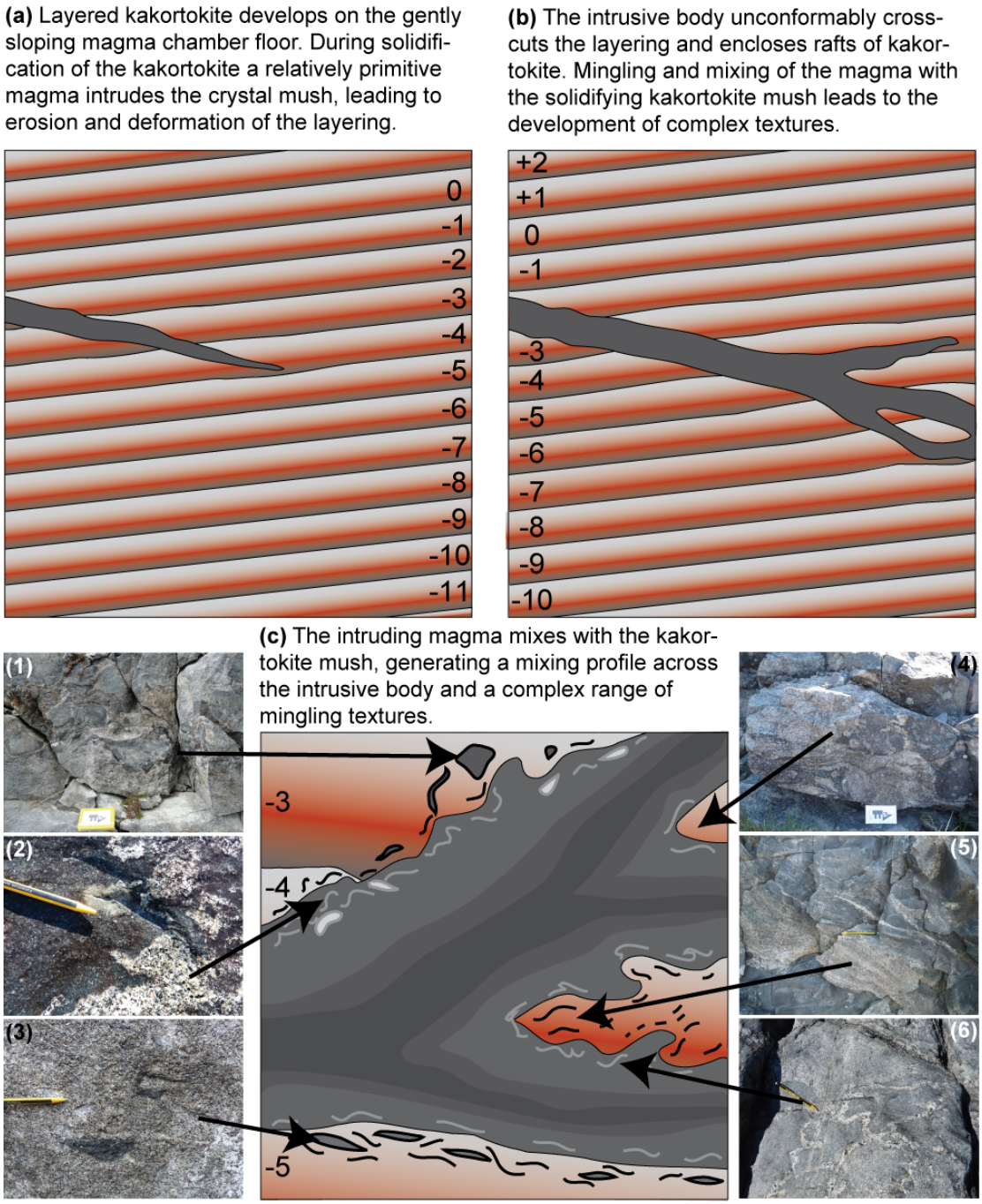

Figure 8.20: model of formation for the hybrid from initial development (a) to final complex range of mingling and mixing textures (c) (1) Blocks of phonolite with sharp margins in kakortokite. (2) Flames of nepheline syenite in micro-nephelinolite. (3) Sheared lenses of phonolite in kakortokite. (4) Sheared, anastomosing lenses of micro-nephelinolite in nepheline syenite. (5) Lenses of nepheline syenite in micro-nephelinolite. (6) Net veins of nepheline syenite in micro-nephelinolite.

The location of the feeder system through which the Ilímaussaq magma chamber was filled is unknown, as the base of the complex is not exposed (Larsen & Sørensen, 1987). However there are two fault systems that were active before the formation of the complex: the Tunulliarfik, which bisects the complex into north and south zones; and the Kangerluarsuk-Lakseelv, which divides the layered kakortokite

and the transitional layered kakortokite (Sørensen, 2006). While the Tunulliarfik fault is not suggested to have been active during the formation of the complex, the Kangerluarsuk-Lakseelv fault was (Sørensen, 2006). This seems to be the most likely emplacement path for the phonolite/micro-nephelinolite sequence due to the proximity of the rocks to the fault (Fig. 8.1a). Intrusion of magma along this fault would emplace the sequence at the stratigraphic level of Unit -2, where it then cut down through the crystal mush towards the southwest.

The intrusion of the primitive magma locally deformed the unconsolidated kakortokite crystal mush (Fig. 8.20c). The rafts of material at the upper portions of the phonolite (Fig. 8.1c,d), around the stratigraphic location of Unit -2, are explained in this model as intruding phonolite magma breaking off large fragments of layered kakortokite and including these either as competent rafts (Fig. 8.1c, sample EJH/12/076) or as deformed lenses of what would have been less competent kakortokite mush (Fig 8.20c-4, Fig 8.3e sample EJH/12/061) At the base of the intrusion magmatic flow developed sheared lenses of phonolite (Fig. 8.20c-3). These observations indicate emplacement of the rock sequence through processes of stoping and replacement of the kakortokite mush (cf. Paterson *et al.*, 2008).

The nepheline syenite is texturally and mineralogically similar to white kakortokite, and formation through remobilisation and potentially minor partial melting of the kakortokite mush during the intrusion of the phonolite/micro-nephelinolite is credible. It is represented in outcrop by the complex pods and pillows, which have crenulated margins (Fig 8.20c-2&5). Minor partial melting of the unconsolidated kakortokite mush would have allowed for the development of the complex network of veins of nepheline syenite through the sequence (Fig 8.20c-6). This is reflective of processes of mingling between the intruding primitive magma and the kakortokite crystal mush (cf. Vernon *et al.*, 1988).

The CSD data support this model as the plots for the phonolite and micro-nephelinolite samples indicate very different nucleation and growth histories compared to both the nepheline syenite and the layered kakortokite. The finer grain sizes indicate faster crystallisation in comparison to kakortokite and this would be associated with chilling of the primitive magma during the intrusion into the crystal mush. The kinked plots reflect mixing of crystal populations and this is associated with the incorporation of crystals from the kakortokite crystal mush into the infiltrating melt during partial melting and mingling. The nepheline syenite CSD plots are very similar to layered kakortokite, which reflects formation from remobilised, unconsolidated layered kakortokite. The increased number of the finest-grained crystals is associated with where the model indicates partial melting of the crystal

mush took place. The growth of the eudialyte megacrysts in some samples (e.g. EJH/12/073) can be explained through extreme textural coarsening of crystals inherited from kakortokite. Megacrysts can form in areas of enhanced melt flow through the crystal mush (Higgins, 2002) and partial melting associated with intrusion of the phonolite magma could have provided the conditions for enhanced crystal growth through textural coarsening.

8.8 Conclusions

Relatively little attention has been paid to the sequences of phonolite, micro-nephelinolite and nepheline syenite within the layered kakortokite, but they undoubtedly provide insights into magma chamber processes occurring at the time of kakortokite formation. This detailed petrographic, textural and chemical study of the unit is inconsistent with slumping of the unconsolidated kakortokite crystal mush, as the most commonly quoted model for their formation hypothesises (Bohse *et al.*, 1971). Instead a model is proposed whereby the unit is the result of open-system magma chamber behaviour. Where an influx of a relatively primitive and Ti-rich melt was forcefully emplaced within the unconsolidated kakortokite crystal mush and the associated chilling effect developed the much finer-grain size of the phonolite and micro-nephelinolite. The intrusion of the unit into the kakortokite mush resulted in mixing and the development of a compositional range from rocks that are alkaline to peralkaline and agpaitic. Magmatic flow led to the development of the textures previously interpreted as slumping, while mingling formed textures inconsistent with slumping, such as the complex net veining. Thus the terminology of Ferguson (1970) is supported, referring to the phonolite as a ‘hybrid’ , as the unit represents a relatively primitive magma that mixed and mingled with the unconsolidated kakortokite mush. It can further be inferred that the Ilímaussaq magma chamber acted as an open system during the formation of this unit. It must represent replenishment by a magma that was more primitive than the kakortokite, indicating an active feeder system below the Ilímaussaq magma chamber whilst the layered series was developing.

8.9 References

Bailey, J. C., Gwozdz, R., Rose-Hansen, J. & Sørensen, H. (2001). Geochemical overview of the Ilímaussaq alkaline complex, South Greenland. *Geology of Greenland Survey Bulletin* **190**, 35-53.

Bohse, H., Brooks, C. K. & Kunzendorf, H. (1971). Field observations on the kakortokites of the Ilimaussaq intrusion, South Greenland, including mapping and analyses by portable X-ray fluorescence equipment for zirconium and niobium. *Rapport Grønlands Geologiske Undersølgelse* **38**, 43 pp.

Di Carlo, I., Rotolo, S. G., Scaillet, B., Vincenzo, B. & Pichavant, M. (2010). Phase Equilibrium Constraints on Pre-eruptive Conditions of Recent Felsic Explosive Volcanism at Pantelleria Island, Italy. *Journal of Petrology* **51**, 2245-2276.

Ferguson, J. (1970). The significance of the kakortokite in the evolution of the Ilímaussaq intrusion, South Greenland. *Meddelelser om Grønland* **190**, 1-193.

Higgins, M. D. (2002). A crystal size-distribution study of the Kiglapait layered mafic intrusion, Labrador, Canada: evidence for textural coarsening. *Contributions to Mineralogy and Petrology* **144**, 314-330.

Higgins, M. D. (2010). Textural coarsening in igneous rocks. *International Geology Review* **1**, 1-23.

Krumrei, T. V., Pernicka, E., Kaliwoda, M. & Markl, G. (2007). Volatiles in a peralkaline system: Abiogenic hydrocarbons and F-Cl-Br systematics in the naujaite of the Ilímaussaq intrusion, South Greenland. *Lithos* **95**, 298-314.

Larsen, L. M. & Sørensen, H. (1987). The Ilímaussaq intrusion - progressive crystallisation and formation of layering in an agpaitic magma. *Geological Society London, Special Publications* **30**, 473-488.

Larsen, L. M. & Steenfelt, A. (1974). Alkali loss and retention in an iron-rich peralkaline phonolite dyke from the Gardar province, south Greenland. *Lithos* **7**, 81-90.

Le Maitre, R. W. (ed.) (2002). *Igneous Rocks A Classification and Glossary of Terms*. Cambridge: Cambridge University Press

Marks, M., Halama, R., Wenzel, T. & Markl, G. (2004). Trace element variations in clinopyroxene and amphibole from alkaline to peralkaline syenites and granites: implications for mineral-melt trace-element partitioning. *Chemical Geology* **211**, 185-215.

Marsh, B. D. (1998). On the interpretation of crystal size distributions in magmatic systems. *Journal of Petrology* **39**, 553-599.

Paterson, S. R., Pignotta, G. S., Farris, D., Memeti, V., Miller, R. B., Vernon, R. H. & Žák, J. (2008). Is stoping a volumetrically significant pluton emplacement process?: Discussion. *GSA Bulletin* **120**, 1075-1079.

Pfaff, K., Krumrei, T., Marks, M. A. W., Wenzel, T., Rudolf, T. & Markl, G. (2008). Chemical and physical evolution of the 'lowered layered sequence' from the nepheline syenitic Ilímaussaq intrusion, South Greenland: Implications for the origin of magmatic layering in peralkaline felsic liquids. *Lithos* **106**, 280-296.

Sørensen, H. (2006). The Ilímaussaq Alkaline Complex, South Greenland - an overview of 200 yeards of research and an outlook. *Meddeleser om Grønland* **342**, 1-70.

Ussing, N. V. (1912). Geology of the country around Julianehaab, Greenland. *Medeleser om Grønland* **38**, 1-426.

Vernon, R. H., Etheridge, M. A. & Wall, V. J. (1988). Shape and microstructure of microgranitoid enclaves: Indicators of magma mingling and flow. *Lithos* **22**, 1-11.

Chapter 9

Magma Chamber Dynamics During the Formation of the Layered Kakortokite

9.1 Introduction

The layered kakortokite series is one of the world's most spectacular occurrences of macrorhythmic layering and yet this type is one of the most poorly understood (Irvine, 1987). The layering is remarkably homogeneous, individual units can be traced across outcrop and through drill core (Fig. 9.1, Appendix B). Lateral consistencies in texture and composition indicate the layering must have developed through large-scale processes that operated across a quiescent magma chamber. Variations to the typical unit structure and the presence of rock sequences that crosscut the layered kakortokite (Fig. 9.1) reflect the complexity of processes operating during the development of the series. This chapter brings together observations and interpretations into a model of the magma chamber dynamics operating during the development of the layered series. Although parts of the model remain speculative, it is suggested that the ideas generated could drive further work on the complex and provide insights into the development of layering in other peralkaline complexes.

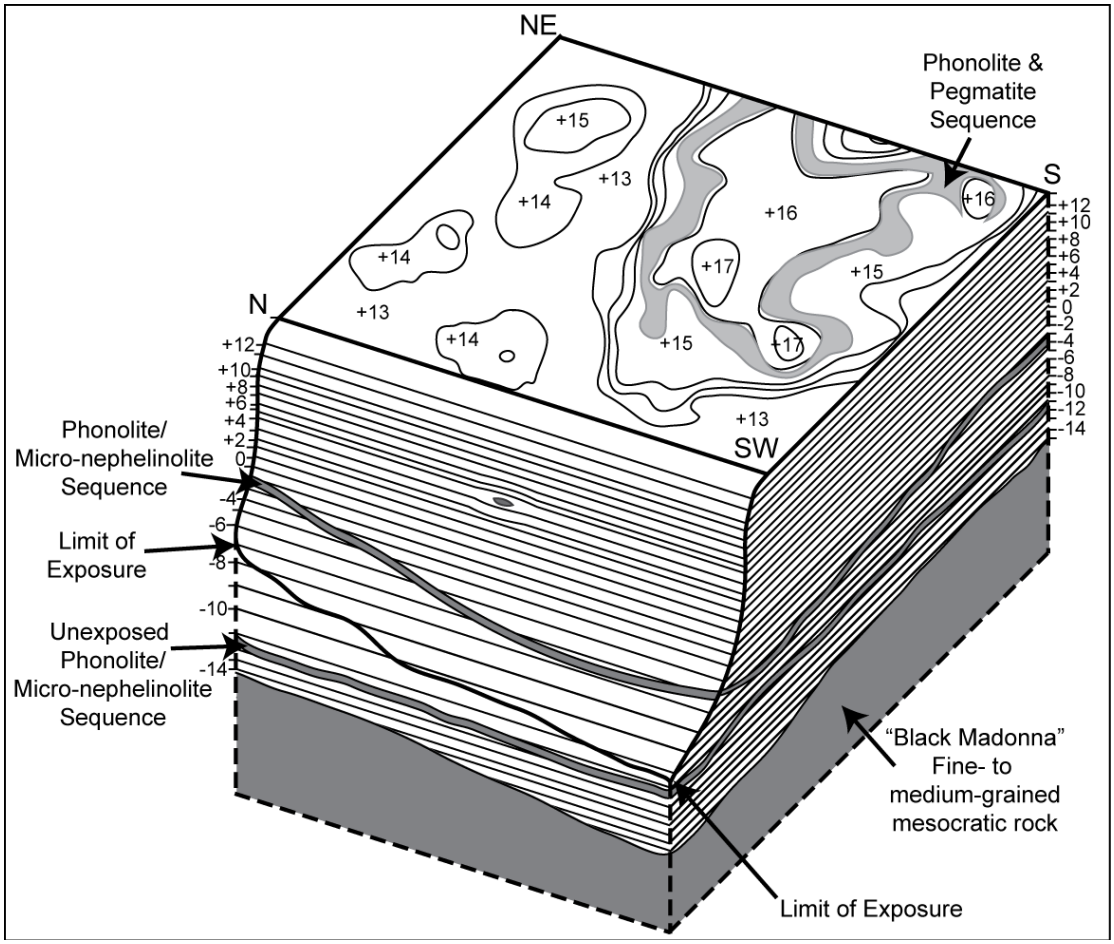

Figure 9.1: Schematic 3D model of layered kakortokite through Kringlerne cliff section and plateau. Thick solid lines indicate exposed rocks and dashed lines unexposed rocks recognised from drill cores.

9.2 Ilímaussaq Magma Chamber Dynamics

Layering is commonly cited to have developed through eutectic crystallisation of all phases (Larsen & Sørensen, 1987) followed by density sorting during gravitational settling (Ferguson, 1964, Larsen & Sørensen, 1987, Sørensen, 1969). This hypothesis is not however universally accepted at Ilímaussaq. Other workers have inferred that the depth of the magma through which the crystals settled was not great enough, at least during the development of the upper units, to separate the mineral phases according to density (Pfaff *et al.*, 2008). The textural analysis does not discount gravitational settling, however the data indicate that the majority of each unit formed through processes of *in situ* crystallisation. Further evidence for this is derived from the presence of the 'Wa' layers, principally composed of low-density alkali feldspar and nepheline beneath red layers principally composed of denser eudialyte, these are unlikely to have developed through gravitational settling.

The development of the tripartite layering is proposed to be controlled through the effects of an oscillating volatile pressure on the nucleation of each mineral phase, e.g Ussing (1912), Ferguson (1970), Sørensen & Larsen (1987). A similar process to the one proposed to have developed the layering in the Klokken Complex, S. Greenland (Parsons, 1986). The chemical discontinuities observed between units (Chapters 6.5 & 7.5) and the compositional variations through the phonolite/micro-nephelinolite sequence (Chapter 8) provide evidence for injections of magmas of varying compositions into the chamber. Therefore I further propose that the Ilímaussaq chamber operated as an open-system during the formation of the layered kakortokite and unit development was initiated by replenishment events.

The initial quiescent magma chamber conditions allow the injected melt to pool at the base of the magma chamber as a layer between the crystal mush and the overlying resident magma (Fig. 9.2a). This bottom layer initially acts as an isolated system and the inferred volatile-rich composition acts to supress nucleation of all phases, resulting in supersaturation of all mineral components. As the bottom magma starts to cool and equilibrate with the resident magma, the first phase that can nucleate is arfvedsonite, as this can nucleate at higher volatile pressures than any of the other phases (Sørensen, 1969). This nucleates *in situ* at the crystal mush – magma interface (Fig. 9.2b), with potential nucleation sites being controlled by epitaxy onto the crystal faces of the underlying layer.

Injection of magma with relatively pronounced compositional and/or thermal differences onto a semi-rigid crystal mush will develop the knife-sharp unit boundaries, such as the one associated with Units -1/0 (Chapter 6.2). This is due to

the combined processes of thermal and/or chemical erosion with *in situ* nucleation at the crystal mush – magma interface (Fig. 9.2a). Less pronounced compositional/thermal differences between the injected magma and the crystal mush and/or a less solidified crystal mush will develop less distinct unit boundaries, e.g. Units -11/-10 and -10/-9 (Chapter 7.2), due to greater mixing between the injected magma and the crystal mush.

Crystallisation of the black kakortokite resulted in a reduction of the F content of the bottom magma, due to uptake in arfvedsonite. Upwards loss of volatile elements (Larsen & Sørensen, 1987) to the coevally forming roof rocks (sodalite-rich naujaite) along concentration gradients developed in the quiescent magma chamber would also contribute, although in a lesser manner, to a reduction in the volatile pressure of the bottom magma layer. This progressive decrease in volatile pressure allows for the crystallisation of eudialyte, which is supersaturated in the melt. Combining this with desaturation in arfvedsonite results in the gradational boundary between the black and red kakortokite. It is inferred that this decrease in volatile pressure reduces the inhibition on growth of eudialyte and hence the red kakortokite layer develops (Fig. 9.2c). Where well developed, e.g. Unit 0, this layer is principally composed of eudialyte, however when poorly developed, e.g. Unit -9, eudialyte (25%) comprises a similar portion of the rock to alkali feldspar (30%) and nepheline (20%), thus in some cases, the volatile pressure must decrease sufficiently to allow for nucleation of all three minerals simultaneously.

Where a subordinate white kakortokite (‘Wa’), has developed between the black and red kakortokite, e.g. Unit -10, the ‘Wa’ rocks contain sodalite (10-30%). Up to now, the model has not included phases other than arfvedsonite, eudialyte, alkali feldspar and nepheline. However crystallisation of sodalite would substantially influence the Cl content of the magma, which is essential for the crystallisation of eudialyte. If Cl contents fall, then it is credible that eudialyte crystallisation becomes unfavourable, forming the subordinate white kakortokite.

During crystallisation of the red kakortokite the volatile pressure continues to decrease due to uptake of Cl, in eudialyte, combined with relatively minor processes of upwards loss of volatiles and equilibration of the bottom magma layer with the resident magma. This decrease in volatile pressure allows for nucleation of alkali feldspar and nepheline, which combined with desaturation of eudialyte in the melt, develops the white kakortokite above a gradational boundary (Fig. 9.2d).

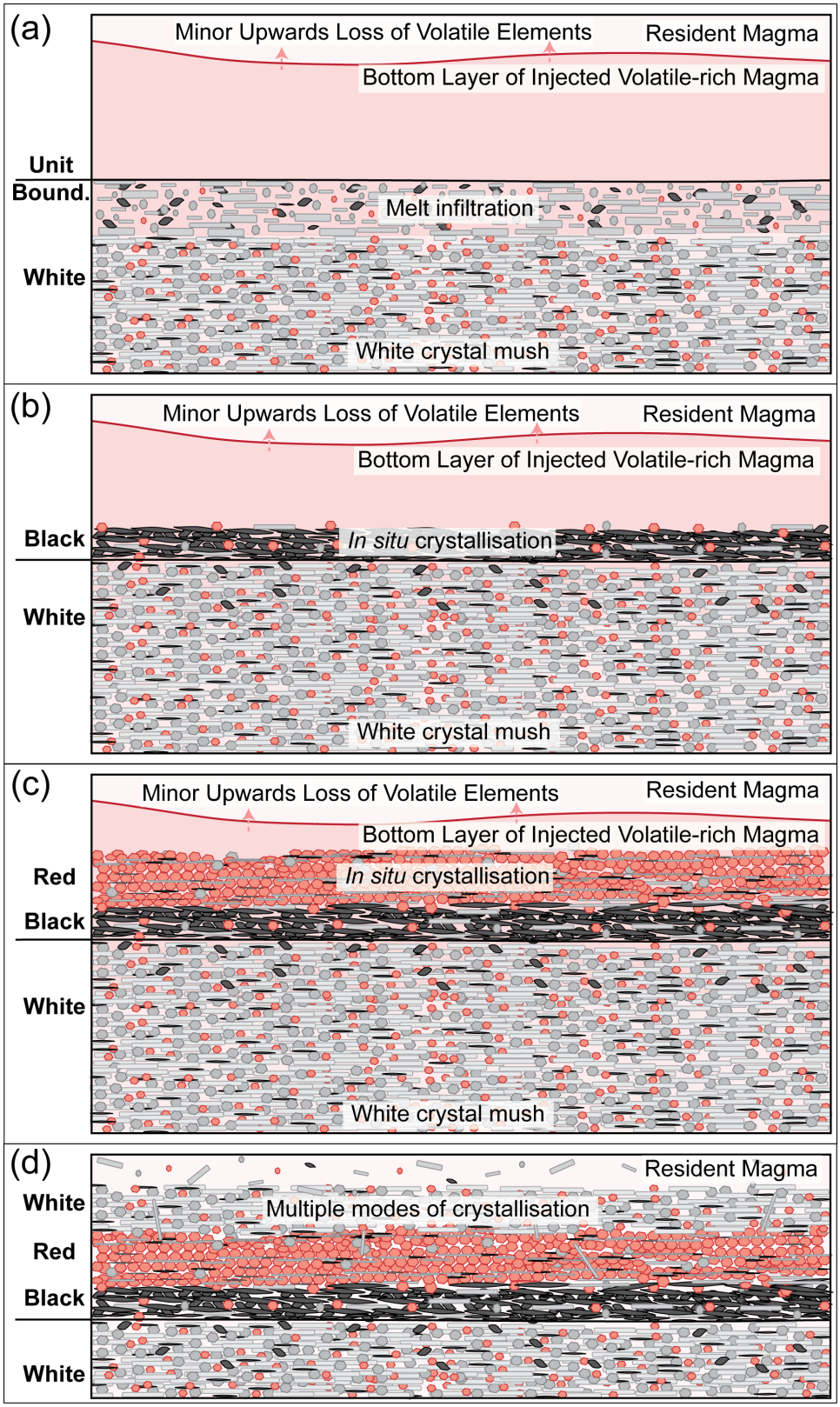

Figure 9.2: (a) Injection of a volatile-rich magma at the floor of a quiescent magma chamber results in thermal and/or chemical erosion during downwards infiltration of the melt into the crystal mush. (b) High volatile pressure in bottom layer of magma which inhibits nucleation of all phases except arfvedsonite. (c) Decreasing volatile pressure allows for crystallisation of eudialyte. (d) Equilibration of the bottom magma layer with the resident magma reduces volatile pressure enough for development of the white kakortokite.

9.3 Insights into the Ilímaussaq Plumbing System

I infer that the layering of the kakortokite was controlled by injections of volatile-rich magmas and their resultant effects on volatile pressure. Each unit potentially formed from a single event, the simplest explanation for which is periodic movement of magma into the chamber. The data do not indicate magmatic evolution upwards through the analysed kakortokite, as the eudialyte-group minerals in the black kakortokite (the most primitive rocks in each unit) have the greatest and most primitive $Fe_{(TOT)}$/Mn ratios in Unit 0 (mean = 12.10±0.23) while those in Units -10 (10.58±1.63), -9 (10.56±0.36) and -8 (10.69±0.54) are more evolved. Therefore the injected magmas were not sourced from a single fractionating and evolving sub-chamber. Instead it is proposed that they reflect a complex plumbing system that allowed upwards movements of magmas of differing compositions. This is highlighted by the phonolite and micro-nephelinolite sequences that occur in the lower layered kakortokite (below Unit 0, Fig. 9.1), as these reflect injection of magmas of sub-alkaline compositions into the Ilímaussaq chamber. Thus the source of the magmas must have been heterogeneous and pulses of magmas of differing composition must have occurred (Fig. 9.3). The presence of antecrysts in the black kakortokite is indicative of some crystals being sourced from a sub-chamber, however the relative scarcity of these crystals indicates that the injected magmas were predominantly aphanitic.

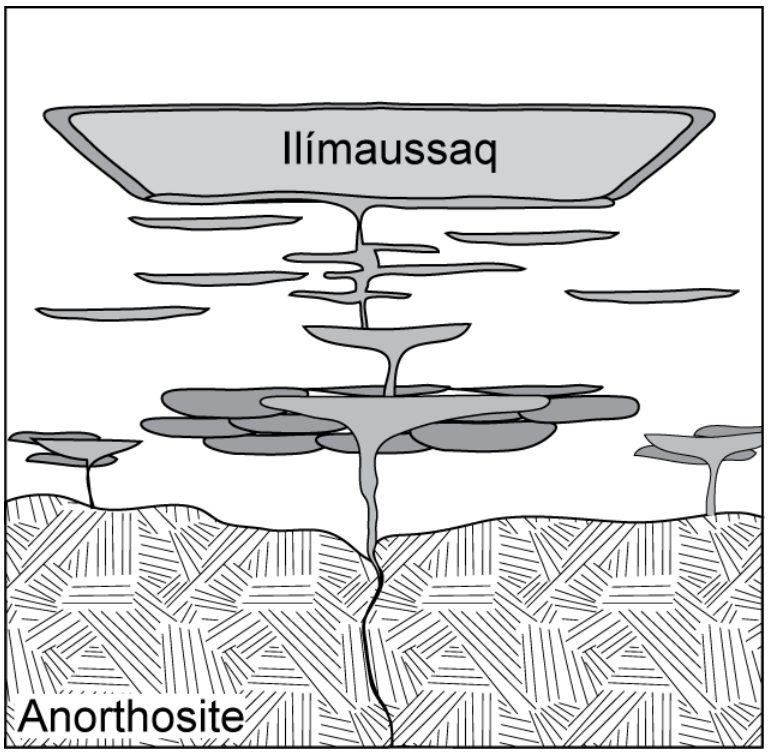

Figure 9.3: Speculative representation of crustal section beneath the Ilímaussaq magma highlighting the heterogeneous nature of the plumbing system.

Several authors have attempted to address the accommodation of the parental melt as Larsen & Sørensen (1987) inferred that the Ilímaussaq Complex magmas developed from fractionation of an alkali basalt parental magma. If the Ilímaussaq magmas formed during conventional fractionation, this would require 98% crystallisation of the parental magma (Larsen & Sørensen, 1987). However, if the magma body separated as it fractionated with the lighter, more evolved melts rising (Larsen & Sørensen, 1987), then the parent magma may not have had to crystallise to such a large extent before the highly evolved, peralkaline melts developed. There is evidence for separation of fractionating melts through the numerous anorthosite xenoliths found throughout the Gardar Province (Bridgwater, 1976, Bridgwater & Harry, 1968, Patchett *et al.*, 1976). Crystallisation of anorthosite underneath the Gardar Province at mid-depths in the crust (Fig. 9.3, Bridgwater, 1976) would accommodate the crystallising parental melt and allow for development of the peralkaline melts through fractionation and separation.

9.4 Future Work and Applications

This thesis focuses on interpreting peralkaline magma chamber dynamics through an analysis of the layered kakortokite of the Ilímaussaq Complex. The present study initially focused on the marker horizon, as this is the best-developed unit and provides a good insight into the processes that developed the igneous layering. The analysis was extended to the lowest exposed units (-11 to -8) as these are suggested to have coevally formed with naujaite at the roof and thus allows for a broader view of magma chamber processes. The ordered nucleation model developed in this thesis applies to both the marker horizon and the lowest exposed units. Future work on the development of the layered series should be extended to the upper units (above Unit 0) and transitionally layered kakortokite to determine if the magma chamber continued to operate as an open-system during the development of the top of the layered series.

The proposed open-system behaviour during the formation of the kakortokite should also be visible in the coevally formed roof rocks. It is recommended that a similar combined textural and mineral chemical analysis is performed on the naujaite, to investigate the effects of replenishment events and an oscillating volatile pressure on the development of these rocks. It is speculated that magmas with extremely rich volatile element contents would have a relatively low density and thus rise to the roof after injection, rather than sinking to the floor, potentially controlling the development of the weakly layered naujaite.

The Ilímaussaq Complex was chosen for the present study as it is one of the best-exposed and preserved layered peralkaline complexes and therefore allows the best chance for the interpretation of primary igneous processes. Peralkaline complexes are currently receiving attention from academia and industry as the extreme composition of the rocks allows them to host potentially economically viable deposits of elements that are scarce worldwide. The Ilímaussaq Complex itself is currently being explored for rare earth elements, zirconium, niobium and tantalum in the south by TANBREEZ Mining Greenland A/S and in the north for rare earth elements, uranium and zinc by Greenland Minerals and Energy Ltd. The model developed in the present study could be key to understanding the generation of the resources, as the repeated replenishment events during the development of the complex could have been essential in concentrating the extremely rich resources it hosts. The observations derived from the kakortokite are also useful for informing studies of some of the less well exposed and/or preserved peralkaline complexes. The poorly exposed and extensively altered Nechalacho Layered Alkaline Suite (N.W.T. Canada), which is currently being explored for rare earth elements, zirconium, niobium and tantalum by Avalon Rare Metals Inc. is a possible example. The resources are hosted by layered alkaline cumulates; however all primary eudialyte is decomposed (e.g. Chapter 6.6) and is identified from relict outlines (Sheard *et al.*, 2012). The CSD analysis pioneered in this thesis would allow for analysis of these relict eudialyte crystals and could assist in the interpretation of primary igneous processes, thus providing a vital insight into magma chamber dynamics during the development of the layered suite.

9.5 Summary

This thesis presents the results of a combined petrographic, quantitative textural (CSD) and mineral chemical analysis of the layered kakortokite of the Ilímaussaq Complex, S. Greenland. The data indicate that the magma chamber was operating as an open system during at least the formation of the lower layered kakortokite (Unit 0 and below) and repeated injections of volatile-rich magmas were key to generating the macrorhythmic layering. Complex feedback mechanisms and an oscillating volatile pressure are proposed to have controlled the order of nucleation. The occurrence of multiple replenishment events and the disruptions to the layered series by relatively primitive sequences of phonolite and micro-nephelinolite highlight the complexity and heterogeneity of the plumbing system beneath the Ilímaussaq magma chamber. The results of this study highlight the need to understand the complex magmatic processes that contributed to the development

of layered peralkaline rocks from complexes with good exposure and preservation, before interpreting relict igneous layering in more highly altered peralkaline complexes.

9.6 References

Bridgwater, D. (1976). Feldspathic inclusions in the Gardar igenous rocks of South Greenland and their relvance to the formation of major anorthosites in the Canadian Shield. *Canadian Journal of Earth Sciences* **4**, 995-1014.

Bridgwater, D. & Harry, W. T. (1968). Anorthosite Xenoliths and Plagioclase Megacrysts in Precambrian Intrusions of South Greenland. *Meddelelser om Grønland* **185**, 1-243.

Ferguson, J. (1964). Geology of the Ilímaussaq alkaline intrusion, South Greenland. Part I. Description of map and structure. *Meddelelser om Grønland* **172**, 1-81.

Ferguson, J. (1970). The significance of the kakortokite in the evolution of the Ilímaussaq intrusion, South Greenland. *Meddelelser om Grønland* **190**, 1-193.

Irvine, T. N. (1987). Processes involved in the formation and development of layered igneous rocks. In: Parsons, I. (ed.) *Origins of Igneous Layering*. Dordrecht: D. Reidel Publishing, 649-656.

Larsen, L. M. & Sørensen, H. (1987). The Ilímaussaq intrusion - progressive crystallisation and formation of layering in an agpaitic magma. *Geological Society London, Special Publications* **30**, 473-488.

Parsons, I. (ed.) (1986). *Origins of Igneous Layering*. Dordrecht: D. Riedel Publishing Company

Patchett, P. J., Hutchinson, J., Blaxland, A. B. & Upton, B. G. J. (1976). Origin of anorthosites, gabbros and potassic ultramafic rocks from the Gardar Province, South Greenland: Sr isotopic ratio studies. *Bulletin of the Geological Society of Denmark* **25**, 79-84.

Pfaff, K., Krumrei, T., Marks, M. A. W., Wenzel, T., Rudolf, T. & Markl, G. (2008). Chemical and physical evolution of the 'lowered layered sequence' from the nepheline syenitic Ilímaussaq intrusion, South Greenland: Implications for the origin of magmatic layering in peralkaline felsic liquids. *Lithos* **106**, 280-296.

Sheard, E. R., Williams-Jones, A. E., Heiligmann, M., Pederson, C. & Trueman, D. L. (2012). Controls on the Concentration of Zirconium, Niobium, and the Rare Earth Elements in the Thor Lake Rare Metal Deposit, Northwest Territories, Canada. *Economic Geology* **107**, 81-104.

Sørensen, H. (1969). Rythmic igneous layering in peralkaline intrusions: An essay review on Ilímaussaq (Greenland) and Lovozero (Kola, USSR). *Lithos* **2**, 261-283.

Sørensen, H. & Larsen, L. M. (1987). Layering in the Ilimaussaq alkaline intrusion, South Greenland. In: Parsons, I. (ed.) *Origins of Igneous Layering*. Dordrecht: D. Reidel Publishing, 1-28.

Ussing, N. V. (1912). Geology of the country around Julianehaab, Greenland. *Medeleser om Grønland* **38**, 1-426.

Appendix A
Sample List

Samples from Outcrop

Sample	Description	Location	Location Description	Latitude	Longitude
EJH/12/ 001	Unit -2, intraunit banding.	L002	Outcrop at base of hill above Lakse Elv	60.88080293	-45.82624108
EJH/12/ 002	Unit +14, foliated red kakortokite	L004	Top of hill above Lakse Elv	60.88145874	-45.82399833
EJH/12/ 003	Unit +13, fresh red kakortokite	L005	Top of hill above Lakse Elv	60.88146217	-45.82513601
EJH/12/ 004	Unit +11	L006	Outcrop on hillside above Lakse Elv	60.88175361	-45.82538369
EJH/12/ 005	Unit 0, laminated red kakortokite	L007	Outcrop on hillside above Laske Elv	60.88156912	-45.82889688
EJH/12/ 006A	Hybrid, medium grey	L008	In stream bed Lakse-tvær Elv	60.88158958	-45.82989927
EJH/12/ 006B	Hybrid, medium grey with veins	L008	In stream bed Lakse-tvær Elv	60.88158958	-45.82989927
EJH/12/ 007	Unit -1/0 Boundary	L009	In stream bed Lakse-tvær Elv	60.88119823	-45.82901414
EJH/12/ 008	Unit 0 black kakortokite	L009	In stream bed Lakse-tvær Elv	60.88119823	-45.82901414
EJH/12/ 009	Unit 0 red kakortokite	L009	In stream bed Lakse-tvær Elv	60.88119823	-45.82901414
EJH/12/ 010	Unit 0 white kakortokite	L009	In stream bed Lakse-tvær Elv	60.88119823	-45.82901414
EJH/12/ 011	Unit -3/-2 Boundary (friable)	L010	Outcrop at base of hill above Lakse Elv	60.88164322	-45.82928848
EJH/12/ 012	Unit 4 black kakortokite	L011	Outcrop on hillside above Lakse Elv	60.88157658	-45.82638156
EJH/12/ 013	Unit 3 white kakortokite	L011	Outcrop on hillside above Lakse Elv	60.88157658	-45.82638156
EJH/12/ 014	Unit 3/4 Boundary	L011	Outcrop on hillside above Lakse Elv	60.88157658	-45.82638156
EJH/12/ 014x	Unit 8 black kakortokite	L012	Outcrop on hillside above Lakse Elv	60.88151598	-45.8259773
EJH/12/ 015	Unit 7 white kakortokite	L012	Outcrop on hillside above Lakse Elv	60.88151598	-45.8259773
EJH/12/ 016	Unit 8 weathered black kakortokite	L012	Outcrop on hillside above Lakse Elv	60.88151598	-45.8259773
EJH/12/ 017	Unit 7(?) albite vein with eudialyte-rich pocket	L013	Outcrop on hillside above Lakse Elv	60.88146787	-45.82653738
EJH/12/ 018	Hybrid, dark grey	L014	In stream bed Lakse-tvær Elv	60.88161942	-45.83018543
EJH/12/ 019A	Hybrid, mid grey	L014	In stream bed Lakse-tvær Elv	60.88161942	-45.83018543
EJH/12/ 019B	Hybrid, mid grey	L014	In stream bed Lakse-tvær Elv	60.88161942	-45.83018543
EJH/12/ 020	Hybrid, fresh orange eudialyte	L015	In stream bed Lakse-tvær Elv	60.88232232	-45.83137776
EJH/12/ 021A	Hybrid, fissile & eudialyte-rich	L015	In stream bed Lakse-tvær Elv	60.88232232	-45.83137776
EJH/12/ 021B	Hybrid, fissile & eudialyte-rich	L015	In stream bed Lakse-tvær Elv	60.88232232	-45.83137776
EJH/12/ 022A	Hybrid, dark grey with white vein	L016	In stream bed Lakse-tvær Elv	60.88237136	-45.83191043

Sample	Description	Location	Location Description	Latitude	Longitude
EJH/12/ 022B	Hybrid, dark grey with white vein	L016	In stream bed Lakse-tvær Elv	60.88237136	-45.83191043
EJH/12/ 023	Unit -11/-10 Boundary	L018	S-side of Kangerluarsuk, Kringlerne	60.86913415	-45.86755137
EJH/12/ 024	Unit -10 Black, 90 cm above boundary	L018	S-side of Kangerluarsuk, Kringlerne	60.86913415	-45.86755137
EJH/12/ 025	Unit -11 White, 2m below -11/-10 boundary	L018	S-side of Kangerluarsuk, Kringlerne	60.86913415	-45.86755137
EJH/12/ 026A	Vug of analcime, fsp & arvf in -10B	L018	S-side of Kangerluarsuk, Kringlerne	60.86913415	-45.86755137
EJH/12/ 026B	Vug of analcime, fsp & arvf in -10B	L018	S-side of Kangerluarsuk, Kringlerne	60.86913415	-45.86755137
EJH/12/ 026C	Vug of analcime, fsp & arvf in -10B	L018	S-side of Kangerluarsuk, Kringlerne	60.86913415	-45.86755137
EJH/12/ 026D	Vug of analcime, fsp & arvf in -10B	L018	S-side of Kangerluarsuk, Kringlerne	60.86913415	-45.86755137
EJH/12/ 026E	Vug of analcime, fsp & arvf in -10B	L018	S-side of Kangerluarsuk, Kringlerne	60.86913415	-45.86755137
EJH/12/ 027	Unit -10 Red kakortokite	L019	S-side of Kangerluarsuk, Kringlerne	60.8694561	-45.86568497
EJH/12/ 028	Unit -10 White kakortokite	L020	S-side of Kangerluarsuk, Kringlerne	60.86944914	-45.86524844
EJH/12/ 029	Unit -9 Black kakortokite	L021	S-side of Kangerluarsuk, Kringlerne	60.86966196	-45.86525749
EJH/12/ 030	Unit -10/-9 Boundary	L021	S-side of Kangerluarsuk, Kringlerne	60.86966196	-45.86525749
EJH/12/ 031	Unit -9 Red kakortokite, poor red	L021	S-side of Kangerluarsuk, Kringlerne	60.86966196	-45.86525749
EJH/12/ 032	Unit -8 Black kakortokite	L022	S-side of Kangerluarsuk, Kringlerne	60.86965576	-45.86492934
EJH/12/ 033	Unit -9 White kakortokite	L022	S-side of Kangerluarsuk, Kringlerne	60.86965576	-45.86492934
EJH/12/ 034	Decimetre-scale layering at contact to marginal pegmatite	L024	S-side of Kangerluarsuk, Contact to marginal pegmatite	60.86782222	-45.8715741
EJH/12/ 035	Aegirine from fault cutting marginal kakortokite	L025	S-side of Kangerluarsuk, Contact to marginal pegmatite	60.86745509	-45.87204491
EJH/12/ 036	Kakortokite & pegmatite, layering aligned with pegmatite	L028	S-side of Kangerluarsuk, Contact to marginal pegmatite	60.86739524	-45.87252712
EJH/12/ 037	Pegmatite, marginal pegmatite	L028	S-side of Kangerluarsuk, Contact to marginal pegmatite	60.86739524	-45.87252712
EJH/12/ 038	Laminated black kakortokite from margin	L029	S-side of Kangerluarsuk, Contact to marginal pegmatite	60.86738845	-45.87239703
EJH/12/ 039	Black to white lamination at margin	L029	S-side of Kangerluarsuk, Contact to marginal pegmatite	60.86738845	-45.87239703

Sample	Description	Location	Location Description	Latitude	Longitude
EJH/12/ 040	White vein in red kakortokite at margin	L030	S-side of Kangerluarsuk, Contact to marginal pegmatite	60.86737655	-45.87205572
EJH/12/ 041	White kakortokite & pegmatite at margin	L030	S-side of Kangerluarsuk, Contact to marginal pegmatite	60.86737655	-45.87205572
EJH/12/ 042	Poikillitc naujaite	L031	Behind Henning's Hut	60.88240044	-45.8428722
EJH/12/ 043	Fresh naujaite	L032	Shoreline of Kangerluarsuk behind Henning Bohse's Hut	60.8835014	-45.84351936
EJH/12/ 044	Foliated green aegirine lujavrite	L033	Hill behind Henning Bohse's Hut	60.8831906	-45.8385753
EJH/12/ 045	Aegirine lujavrite with oikocrystic arfv	L033	Hill behind Henning Bohse's Hut	60.8831906	-45.8385753
EJH/12/ 046	Foliated green aegirine lujavrite	L034	Hill behind Henning Bohse's Hut	60.88365521	-45.83705993
EJH/12/ 047	Aegirine lujavrite, fsp carries foliation	L035	Hill behind Henning Bohse's Hut	60.88334961	-45.83685676
EJH/12/ 048	Aegirine lujavrite, fsp carries foliation, cut by fsp vein	L035	Hill behind Henning Bohse's Hut	60.88334961	-45.83685676
EJH/12/ 049	Nepheline-rich leucocratic vein through aegirine lujavrite	L036	Hill behind Henning Bohse's Hut	60.88320603	-45.83715809
EJH/12/ 050	Darker aegirine lujavrite, towards transitional kakortokite	L036	Hill behind Henning Bohse's Hut	60.88320603	-45.83715809
EJH/12/ 051	Transitional kakortokite (A?)	L037	Hill behind Henning Bohse's Hut	60.88309354	-45.83711534
EJH/12/ 052	Unit C trans kakortokite White	L038	Hill behind Henning Bohse's Hut	60.88265534	-45.83744324
EJH/12/ 053	Unit B trans kakortokite Black	L038	Hill behind Henning Bohse's Hut	60.88265534	-45.83744324
EJH/12/ 054	Unit B trans kakortokite Grey/White	L038	Hill behind Henning Bohse's Hut	60.88265534	-45.83744324
EJH/12/ 055	Unit B trans kakortokite Red	L038	Hill behind Henning Bohse's Hut	60.88265534	-45.83744324
EJH/12/ 056	Unit A trans kakortokite Red	L039	Hill behind Henning Bohse's Hut	60.88262332	-45.83822728
EJH/12/ 057	Ilvaite	L040	N-side of Kangerluarsuk, augite syenite	60.87468985	-45.8831195
EJH/12/ 058	Ilvaite or sulphides?	L041	N-side of Kangerluarsuk, augite syenite	60.87468985	-45.8831195
EJH/12/ 059	Ilvaite or sulphides?	L042	N-side of Kangerluarsuk, augite syenite	60.87468985	-45.8831195
EJH/12/ 060	Tugtupite in albite with polylithionite. Photo reactive	L032	Scree above shoreline of Kangerluarsuk behind Henning Bohse's Hut	60.8835014	-45.84351936

Sample	Description	Location	Location Description	Latitude	Longitude
EJH/12/ 061	Hybrid, very fissile similar to lujavrite	L041	S-side of Lakse Elv Valley	60.87932931	-45.84399906
EJH/12/ 062	White kakortokite, Unit -2?	L042	S-side of Lakse Elv Valley	60.88001755	-45.84242159
EJH/12/ 063	Red kakortokite, Unit -2?	L043	S-side of Lakse Elv Valley	60.88022534	-45.84195245
EJH/12/ 064	Foliated kakortokite, arfv carrying foliation	L044	S-side of Lakse Elv Valley	60.8804809	-45.84094578
EJH/12/ 065	Astrophyllite from pegmatite vein	L045	S-side of Lakse Elv Valley	60.8809777	-45.83685013
EJH/12/ 066A	Hybrid with xenocrysts of aegirine in disequilibrium	L045	S-side of Lakse Elv Valley	60.8809777	-45.83685013
EJH/12/ 066B	Hybrid with xenocrysts of aegirine in disequilibrium	L045	S-side of Lakse Elv Valley	60.8809777	-45.83685013
EJH/12/ 067	Hybrid and white kakortokite type rocks	L046	S-side of Lakse Elv Valley	60.88109798	-45.83632442
EJH/12/ 068	Hybrid, mixed	L046	S-side of Lakse Elv Valley	60.88109798	-45.83632442
EJH/12/ 069A	Potential rinkite sample	L048	Hill behind Henning Bohse's Hut	60.8902853	-45.82883427
EJH/12/ 069B	Potential rinkite, single crystal	L048	Hill behind Henning Bohse's Hut	60.8902853	-45.82883427
EJH/12/ 069C	Potential rinkite, single crystal	L048	Hill behind Henning Bohse's Hut	60.8902853	-45.82883427
EJH/12/ 070	Rinkite	L048	Hill behind Henning Bohse's Hut	60.8902853	-45.82883427
EJH/12/ 071	Kakortokite with rusty eudialyte	L048	Hill behind Henning Bohse's Hut	60.8902853	-45.82883427
EJH/12/ 072	Hybrid, ball from load structure	L049	S-side of Kangerluarsuk, Kringlerne	60.86969549	-45.86419559
EJH/12/ 073	Hybrid with eudialyte-rich veins, eud upto 1 cm	L049	S-side of Kangerluarsuk, Kringlerne	60.86969549	-45.86419559
EJH/12/ 074	Hybrid, load structure or vein with aligned fsp	L049	S-side of Kangerluarsuk, Kringlerne	60.86969549	-45.86419559
EJH/12/ 075	Hybrid mafic enclave from kakortokite	L049	S-side of Kangerluarsuk, Kringlerne	60.86969549	-45.86419559
EJH/12/ 076	Hybrid, arfv rich top	L050	S-side of Kangerluarsuk, Kringlerne	60.86987184	-45.86362554
EJH/12/ 077	Hybrid, fsp rich base	L050	S-side of Kangerluarsuk, Kringlerne	60.86987184	-45.86362554
EJH/12/ 078	Hybrid, white veins with arfv reaction rim at contact to hybrid	L053	S-side of Kangerluarsuk, Kringlerne	60.86970999	-45.86300695
EJH/12/ 079	Units -1/0 Boundary and black kakortokite	L054	Western Kringlerne Cliff	60.86570989	-45.86138279

Sample	Description	Location	Location Description	Latitude	Longitude
EJH/12/ 080	Unit 0 red kakortokite	L054	Western Kringlerne Cliff	60.86570989	-45.86138279
EJH/12/ 081	Unit -1 white kakortokite	L054	Western Kringlerne Cliff	60.86570989	-45.86138279
EJH/12/ 082	Unit 0 white kakortokite	L054	Western Kringlerne Cliff	60.86570989	-45.86138279
EJH/12/ 083	Unit 3? Intralayer lamination (not in situ)	L055	Western Kringlerne Cliff	60.86547051	-45.86206474
EJH/12/ 084	Neptunite	L056	Lilleelv Valley	60.89300229	-45.84461991
EJH/12/ 085A	Tugtupite, photo reactive	L056	Lilleelv Valley	60.89300229	-45.84461991
EJH/12/ 085B	Bag of tugtupite pieces	L056	Lilleelv Valley	60.89300229	-45.84461991
EJH/12/ 086	Black arfvedsonite lujavrite, similar features to hybrid	L057	Lilleelv Valley, first waterfall	60.89543363	-45.84089792
EJH/12/ 087	Black arfvedsonite lujavrite, fissile & foliated	L057	Lilleelv Valley, first waterfall	60.89543363	-45.84089792
EJH/12/ 088	Polylithionite plates	L058	Sørensen's Island	60.881015	-45.86440665
EJH/12/ 089	Aenigmatite, single crystal	L058	Sørensen's Island	60.881015	-45.86440665
EJH/12/ 090	Hybrid, nepheline in disequilibrium	L059	S-side Kangerluarsuk, Shoreline	60.87754112	-45.84730337
EJH/12/ 091	Hybrid, layered & coarse-grained	L059	S-side Kangerluarsuk, Shoreline	60.87754112	-45.84730337
EJH/12/ 092	Hybrid, with very fresh eudialyte	L061	S-side Kangerluarsuk, Shoreline	60.87632566	-45.84935199
EJH/12/ 093	Hybrid, arfvedsonite vein	L061	S-side Kangerluarsuk, Shoreline	60.87632566	-45.84935199
EJH/12/ 094	Units -1/0 Boundary	L063	Eastern Kringlerne Cliff	60.87424921	-45.84738024
EJH/12/ 095	Unit 0 red kakortokite	L063	Eastern Kringlerne Cliff	60.87424921	-45.84738024
EJH/12/ 096	Unit 0 white kakortokite	L063	Eastern Kringlerne Cliff	60.87424921	-45.84738024
EJH/12/ 097	Unit 0 white kakortokite (from scree slope)	L064	Eastern Kringlerne scree slope	60.87470627	-45.84954226
EJH/12/ 098	Lujavrite dyke with devitrification textures? and foyaite margin	L066	S. Ilímaussaq roof zone	60.90734046	-45.84956213
EJH/12/ 099	Lujavrite dyke with devitrification textures?	L066	S. Ilímaussaq roof zone	60.90734046	-45.84956213
EJH/12/ 100	Lujavrite dyke with devitrification textures? More homogenous	L067	S. Ilímaussaq roof zone	60.9067497	-45.8524559

Sample	Description	Location	Location Description	Latitude	Longitude
EJH/12/ 101	Natrolite? Replacement of arfvedsonite	L068	S Ilímaussaq roof zone	60.90471667	-45.85162047
EJH/12/ 102	Unit +16 Red kakortokite	L071	Kringlerne Plateau	60.86763337	-45.84460977
EJH/12/ 103	Unit +16 White kakortokite	L072	Kringlerne Plateau	60.86759666	-45.844909
EJH/12/ 104	Unit +16 Pegmatite	L073	Kringlerne Plateau	60.86777486	-45.84441992
EJH/12/ 105	Unit +13? Black kakortokite	L074	Kringlerne Plateau	60.86919308	-45.84650349
EJH/12/ 106	Unit +16 Black kakortokite	L075	Kringlerne Plateau Margin	60.87351604	-45.81033625
EJH/12/ 107	Unit +16 Red kakortokite	L075	Kringlerne Plateau Margin	60.87351604	-45.81033625
EJH/12/ 108	Unit +16 White kakortokite	L075	Kringlerne Plateau Margin	60.87351604	-45.81033625
EJH/12/ 109	Lujavrite dyke with devitrification textures? Similar to spherulites	L076	N Ilímaussaq, Taseq?	60.94644212	-45.92151322
EJH/12/ 110A	Lujavrite dyke with devitrification textures? And cross-cutting bands	L076	N Ilímaussaq, Taseq?	60.94644212	-45.92151322
EJH/12/ 110B	Lujavrite dyke with devitrification textures? And cross-cutting bands	L076	N Ilímaussaq, Taseq?	60.94644212	-45.92151322
EJH/12/ 111	Lujavrite dyke with devitrification textures? Elongated segregates light & dark bands	L076	N Ilímaussaq, Taseq?	60.94644212	-45.92151322
EJH/12/ 112	Lujavrite dyke with devitrification textures? Nucleation onto naujaite?	L076	N Ilímaussaq, Taseq?	60.94644212	-45.92151322
EJH/12/ 113	Eudialyte single crystal from hybrid	L077	S-side of Kangerluarsuk, Kringlerne	60.87004476	-45.86197388
EJH/12/ 114	Hybrid arfvedsonite veins through white kakortokitic	L078	S-side of Kangerluarsuk, Kringlerne	60.86939357	-45.86447245
EJH/12/ 115	Unit +10 'sewer' black kakortokite	L079	Kringlerne Plateau	60.87186498	-45.82266829
EJH/12/ 116	Unit +10 'sewer' red kakortokite	L079	Kringlerne Plateau	60.87186498	-45.82266829
EJH/12/ 117	Unit +10 'sewer' white kakortokite	L079	Kringlerne Plateau	60.87186498	-45.82266829
EJH/12/ 118	Unit +10 'sewer' boundary with oikocrystic arfv	L079	Kringlerne Plateau	60.87186498	-45.82266829
EJH/12/ 119	Unit +10 'sewer' alteration with rinkite	L079	Kringlerne Plateau	60.87186498	-45.82266829
EJH/12/ 120	Unit +10 'sewer' pegmatite with aegirine & rinkite	L079	Kringlerne Plateau	60.87186498	-45.82266829
EJH/12/ 121	Unit +10 'sewer' single crystal of unknown (rinkite?)	L079	Kringlerne Plateau	60.87186498	-45.82266829

Sample	Description	Location	Location Description	Latitude	Longitude
EJH/12/ 122	Unit +10 'sewer' alteration with oikocrystic arfvedsonite	L080	Kringlerne Plateau	60.87185986	-45.82265647
EJH/12/ 123	Unit +10 'sewer' alteration 70% eudialyte	L080	Kringlerne Plateau	60.87185986	-45.82265647
EJH/12/ 124	Unit +10 'sewer' phonolite within boundary pegmatite	L081	Kringlerne Plateau	60.87211283	-45.82235623

Samples collected during fieldwork by A. Finch in 1999

Sample	Description	Location	Location Description	Latitude	Longitude
AF/99/ 191	Unit 0 white kakortokite		NE of Lakse-tvær Elv	60.88124	-45.83117
AF/99/ 192	Unit 0 black kakortokite		NE of Lakse-tvær Elv	60.88124	-45.83117
AF/99/ 193	Unit 0 red kakortokite		NE of Lakse-tvær Elv	60.88124	-45.83117
AF/99/ 195	Unit -1/0 boundary		NE of Lakse-tvær Elv	60.88124	-45.83117

Samples from Drill Core (Owned by TANBREEZ Mining Greenland A/S)

Sample	Unit	Core	Top Depth (m)	Base Depth (m)
EJH/12/ 125	16 R	DX-01	6.95	6.99
EJH/12/ 126	16 B	DX-01	9.59	9.63
EJH/12/ 127	15 R	DX-01	31.40	31.46
EJH/12/ 128	15 B	DX-01	32.52	32.57
EJH/12/ 129	14 W	DX-01	34.10	34.15
EJH/12/ 130	14 R	DX-01	35.49	35.54
EJH/12/ 131	14 B	DX-01	38.76	38.80
EJH/12/ 132	13 W	DX-01	40.12	40.22
EJH/12/ 133	13 R	DX-01	42.09	42.15
EJH/12/ 134	13 B	DX-01	42.85	42.90
EJH/12/ 135	12 W	DX-01	44.00	44.05
EJH/12/ 136	12 R	DX-01	46.94	47.00
EJH/12/ 137	12 B	DX-01	52.39	52.43
EJH/12/ 138	11 W	DX-01	55.23	55.28
EJH/12/ 139	11 R	DX-01	57.39	57.45
EJH/12/ 140	11 B	DX-01	58.48	58.54
EJH/12/ 141	11 B / 10 W	DX-01	59.09	59.14
EJH/12/ 142	10 W	DX-01	59.72	59.87
EJH/12/ 143	10 R	DX-01	60.89	60.93
EJH/12/ 144	10 Wa	DX-01	65.51	65.56
EJH/12/ 145	10 B	DX-01	67.45	67.50
EJH/12/ 146	10 B / 9 W	DX-01	67.80	67.86
EJH/12/ 147	9 W	DX-01	70.39	70.45
EJH/12/ 148	9 R	DX-01	73.20	73.25
EJH/12/ 149	9 B	DX-01	76.80	76.85
EJH/12/ 150	9 B / 8 W	DX-01	77.55	77.61
EJH/12/ 151	8 W	DX-01	78.84	78.89
EJH/12/ 152	8 R	DX-01	81.24	81.28
EJH/12/ 153	8 B	DX-01	83.61	83.66
EJH/12/ 154	8 B / 7 W	DX-01	84.94	85.01
EJH/12/ 155	7 W	DX-01	89.78	89.83
EJH/12/ 156	7 R	DX-01	91.76	91.81
EJH/12/ 157	7 B	DX-01	92.42	92.46
EJH/12/ 158	7 B / 6 W	DX-01	92.70	92.76
EJH/12/ 159	6 W	DX-01	93.10	93.15
EJH/12/ 160	6 R	DX-01	95.45	95.50
EJH/12/ 161	6 B	DX-01	96.45	96.50
EJH/12/ 162	5 W	DX-01	98.23	98.27
EJH/12/ 163	5 R	DX-01	99.01	99.07
EJH/12/ 164	5 Wa	DX-01	101.05	101.11
EJH/12/ 165	5 B	DX-01	101.99	102.04
EJH/12/ 166	5 B / 4 W	DX-01	102.51	102.58
EJH/12/ 167	4 W	DX-01	104.68	104.73
EJH/12/ 168	4 R	DX-01	106.88	106.93
EJH/12/ 169	4 B	DX-01	109.21	109.26
EJH/12/ 170	3 W	DX-01	110.16	110.21

Appendix 1 – Sample List

Sample	Unit	Core	Top Depth (m)	Base Depth (m)
EJH/12/ 171	3 R	DX-01	112.13	112.19
EJH/12/ 172	3 B	DX-01	112.29	112.35
EJH/12/ 173	2 W	DX-01	115.23	115.30
EJH/12/ 174	2 R	DX-01	124.46	124.51
EJH/12/ 175	2 B	DX-01	128.33	128.39
EJH/12/ 176	1 W	DX-01	132.04	132.09
EJH/12/ 177	1 R	DX-01	133.44	133.49
EJH/12/ 178	1 B	DX-01	134.44	134.48
EJH/12/ 179	1 B / 0 W	DX-01	134.82	134.90
EJH/12/ 180	0 W	DX-01	139.19	139.23
EJH/12/ 181	0 R	DX-01	141.67	141.71
EJH/12/ 182	0 B	DX-01	142.30	142.35
EJH/12/ 183	0 B / -1 W	DX-01	142.68	142.75
EJH/12/ 184	-1 W	DX-01	144.43	143.49
EJH/12/ 185	-1 R	DX-01	146.56	146.60
EJH/12/ 186	-1 B	DX-01	147.32	147.37
EJH/12/ 187	-1 B / -2 W	DX-01	147.69	147.76
EJH/12/ 188	-2 W	DX-01	148.13	148.18
EJH/12/ 189	-2 R	DX-01	150.28	150.33
EJH/12/ 190	-2 B	DX-01	151.20	151.25
EJH/12/ 191	-3 W	DX-01	153.42	153.47
EJH/12/ 192	-3 R	DX-01	160.32	160.38
EJH/12/ 193	-3 B	DX-01	161.65	161.69
EJH/12/ 194	-4 W	DX-01	164.02	164.07
EJH/12/ 195	-4 R	DX-01	167.71	167.76
EJH/12/ 196	-4 Wa	DX-01	175.15	171.20
EJH/12/ 197	-4 B	DX-01	174.68	174.73
EJH/12/ 198	-4 B / -5 W	DX-01	176.51	176.53
EJH/12/ 199	-5 W	DX-01	180.21	180.26
EJH/12/ 200	-5 R	DX-01	181.80	181.86
EJH/12/ 201	Hybrid	DX-01	198.78	198.82
EJH/12/ 202	-6 W	DX-01	205.00	205.05
EJH/12/ 203	-6 R	DX-01	206.57	206.61
EJH/12/ 204	-6 B	DX-01	207.95	208.00
EJH/12/ 205	-6 B / -7 W	DX-01	208.02	208.10
EJH/12/ 206	-7 W	DX-01	212.25	212.31
EJH/12/ 207	-7 R	DX-01	214.07	214.11
EJH/12/ 208	-7 B	DX-01	214.82	214.85
EJH/12/ 209	-7 B / -8 W	DX-01	215.37	215.42
EJH/12/ 210	-8 W	DX-01	225.41	225.21
EJH/12/ 211	-8 R	DX-01	228.60	228.65
EJH/12/ 212	-8 B	DX-01	231.70	231.76
EJH/12/ 213	-8 B / -9 W	DX-01	232.79	232.83
EJH/12/ 214	-9 W	DX-01	235.30	235.35
EJH/12/ 215	-9 R	DX-01	237.92	237.97
EJH/12/ 216	-9 B	DX-01	239.36	239.41
EJH/12/ 217	-10 W	DX-01	242.00	242.08
EJH/12/ 218	-10 R	DX-01	246.83	246.87
EJH/12/ 219	-10 Wa	DX-01	250.23	250.30

Sample	Unit	Core	Top Depth (m)	Base Depth (m)
EJH/12/ 220	-10 B	DX-01	251.60	251.66
EJH/12/ 221	-10 B / -11 W	DX-01	252.11	252.18
EJH/12/ 222	-11 W	DX-01	258.36	258.41
EJH/12/ 223	-11 R	DX-01	259.95	259.99
EJH/12/ 224	-11 B	DX-01	261.35	261.38
EJH/12/ 225	-11 B / -12 W	DX-01	261.56	261.61
EJH/12/ 226	-12 W	DX-01	264.56	264.60
EJH/12/ 227	-12 R	DX-01	265.58	265.63
EJH/12/ 228	-12 B	DX-01	266.08	266.15
EJH/12/ 229	-12 B / -13 W	DX-01	266.45	266.54
EJH/12/ 230	-13 W	DX-01	266.62	266.67
EJH/12/ 231	Leucocratic Lense	DX-01	268.41	268.50
EJH/12/ 232	-13 R	DX-01	270.78	270.81
EJH/12/ 233	-13 B	DX-01	273.31	272.37
EJH/12/ 234	-14 W	DX-01	275.02	275.09
EJH/12/ 235	-14 R	DX-01	275.83	275.89
EJH/12/ 236	-14 B	DX-01	278.04	278.09
EJH/12/ 237	-14 B / -15 W	DX-01	278.51	278.57
EJH/12/ 238	-15 W	DX-01	279.44	279.49
EJH/12/ 239	-15 R	DX-01	280.56	280.61
EJH/12/ 240	-15 B	DX-01	282.24	282.29
EJH/12/ 241	-15 B /-16 W	DX-01	282.70	282.77
EJH/12/ 242	-16 W	DX-01	283.76	283.80

Appendix B
Drill Core Logs

Drill Core Key

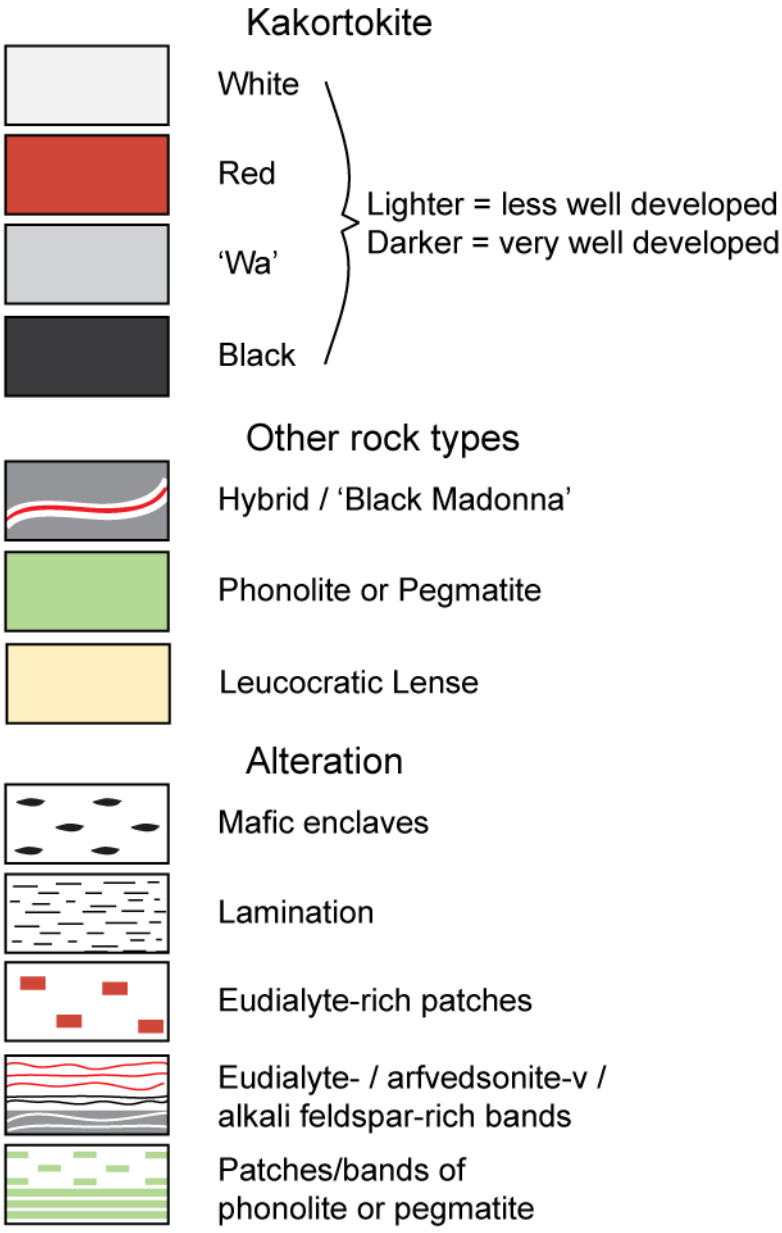

Drill Core: DX-01 - Sheet 1 of 6		Elevation (top):	General Comments
Date Logged: 11th-15th August 2012	Geologist: E. J. Hunt	Elevation (base):	Recovery >95% Core depth = 338m
Units: metres		Locality:	

Depth	Unit	Lithology	Texture	Unit Thickness	Sample No.	Photo No.	Description and Interpretation
6							
8	16 R				EJH/12/125 6.95-6.99 m		Strong red, saccharoidal, patchy alteration. No foliation 30-40% eud, 20% sod, 5% arfv, 5% aeg, 20% fsp & neph Gradational boundary to black.
10	16 B			1.98 m	EJH/12/126 9.59-9.63 m		Poor foliation, aligned fsp lathes. 55% arfv, 30% sod, 5% fsp, 5% eud, 5% neph Sharp contact to pegmatite.
12				19.5 m			Pegmatite and phonolite. Sharp contact between pegmatite and overlying U+16B. Dipping contact between phonolite and underlying U+15W
14							
16							
18							
20							
22							
24							
26							
28							
30	15 W			0.06 m			15 W: Not foliated. 35% fsp, 20% neph, 20% eud, 15% aeg, 10% arfv. 2 sodalite xtls within 6 cm of core. Relatively sharp boundary to 15 R.
32	15 R			1.59 m	EJH/12/127 31.40-31.46 m		Dark red unit, poor foliation - fsp & arfv. Eudialyte altered in patches. 30% eud, 20% aeg, 15% sod, 15% arfv, 15% fsp, 5% neph.
	15 B			1.32 m	EJH/12/128 32.52-32.57 m		Moderate foliation - fsp & arfv. 25% aeg, 20% arfv, 20% fsp, 10% sod, 10% eud, 10% neph. Sharp contact to 14 W.
34	14 W			1.31 m	EJH/12/129 34.10-34.15 m		Spotty texture - aeg, poor foliation - fsp. Sod increases upwards to 15 B. 30% fsp, 20% aeg, 20% neph, 15% eud, 5% arfv, 5% sod.
36	14 R			2.77 m	EJH/12/130 35.49-35.54 m		Spotty texture - aeg, no sod. 30% fsp, 25% eud, 20% aeg, 15% arfv, 5% neph.
38	14 B			1.82 m	EJH/12/131 38.76-38.80 m		Sod appears, moderate foliation - fsp & arfv. 25% arfv, 20% aeg, 20% fsp, 15% eud, 15% neph, 5% sod.
40	13 W			2.61 m	EJH/12/132 40.12-40.22 m		Sharp boundary to 15 B. Sod generally <5%, v. poor foliation. 30% fsp, 20% neph, 20% aeg, 15% arfv, 10% eud, 5% sod.
42	13 R			0.53 m	EJH/12/133 42.09-42.15 m		Thin red, patchy alteration, eud decreases upwards. 50% eud, 25% arfv, 10% aeg, 10% fsp, 5% sod.
	13 B			0.91 m	EJH/12/134 42.85-42.90 m		Good black, sod appears 10 cm above 12/13 boundary. 60% arfv, 15% sod, 10% eud, 10% fsp, 5% aeg.
44	12 W			3.19 m	EJH/12/135 44.00-44.05 m		Sharp 12/13 boundary. Good white, v. leucocratic, sod increases upwards to 13B (0-10%-20%). 40% fsp, 15% sod, 15% aeg, 10% eud, 10% arfv, 5% neph.
46							
48	12 R			3.83 m	EJH/12/136 46.94-47.00 m		Eud greatest in centre of unit. Occasional sod. 35% eud, 30% fsp, 20% aeg, 10% arfv, 5% neph.
50							
52	12 B			2.71 m	EJH/12/137 52.39-52.43 m		Sod is patch 0-8%, good black. 30% arfv, 25% aeg, 20% fsp, 10% eud, 10% neph, 5% sod. Presumed sharp 11/12 boundary, core broken.
54	11 W			4.15 m	EJH/12/138 55.23-55.28 m		Dark white - aeg-rich, patchy sod 0-5%. 35% fsp, 30% aeg, 20% neph, 10% eud, 3% arfv, 2% sod.
56							

Drill Core: DX-01 - Sheet 2 of 6		Elevation (top):	General Comments
Date Logged: 11th-15th August 2012	Geologist: E. J. Hunt	Elevation (base):	Recovery >95% Core depth = 338m
Units: metres		Locality:	

Depth	Unit	Lithology	Texture	Unit Thickness	Sample No.	Photo No.	Description and Interpretation
54	11 W			4.15 m	EJH/12/138 55.23-55.28 m		Dark white - aeg-rich, patchy sod 0-5%. 35% fsp, 30% aeg, 20% neph, 10% eud, 3% arfv, 2% sod.
56					EJH/12/139 57.39-57.45 m		Eud decreases upwards, saccharoidal at base to foliated (fsp). Patchy alteration, 40% eud, 30% fsp, 20% aeg, 10% arfv, 8% neph, 2% sod.
	11 R			0.45 m			
58	11 B			1.52 m	EJH/12/140 58.48-58.54 m		Strong black, sod increases upwards to 11R up to 5%. 70% arfv, 20% fsp, 5% eud, 5% aeg.
	10 W			1.18 m	EJH/12/142 59.72-59.87 m		Patchy aeg, sod decreases upwards to 11B (35-5%). 40% fsp, 20% aeg, 15% eud, 10% sod, 5% arfv.
60	10 R			1.16 m	EJH/12/143 60.89-60.93 m		Patchy alteration, sod-rich. 40% eud, 35% sod, 20% aeg, 5% fsp.
62							
64	10Wa			4.79 m	EJH/12/144 65.51-65.56 m		Dark white & sod-rich. 30% fsp, 30% sod, 15% arfv, 15% aeg, 10% eud.
66							
	10 B			1.59 m	EJH/12/145 67.45-67.50 m		Good black, foliated-fsp, sod decreases upwards to 0%. 40% arfv, 30% fsp, 15% aeg, 10% eud, 5% sod.
68					EJH/12/146 67.80-67.86 m		
70	9 W			3.32 m	EJH/12/147 70.39-70.45 m		Good white, patchy sod (0-10%). 50% fsp, 15% neph, 15% arfv, 10% eud, 5% sod, 5% aeg.
72							
74	9 R			4.65 m	EJH/12/148 73.20-73.25 m		Patchy alteration to pink eud, sod decreased in altered patches. Good red & saccharoidal. 40% eud, 20% sod, 20% aeg, 20% fsp.
76	9 B			1.76 m	EJH/12/149 76.80-76.85 m		Poor foliation - fsp, small sod xtls (~1 mm), patchy eud alteration. 40% arfv, 20% aeg, 15% sod, 15% fsp, 10% eud.
					EJH/12/150 77.55-77.61 m		
78	8 W			3.36 m	EJH/12/151 78.84-78.89 m		Sharp boundary from 9B, marked by fsp band. Well developed white, less sod than 8R. 50% fsp, 15% sod, 10% eud, 10% neph, 10% arfv, 5% aeg.
80							
82	8 R			2.17 m	EJH/12/152 81.24-81.28 m		Patchy alteration with 1 syenite band. 40% eud, 20% sod, 15% fsp, 15% aeg, 10% arfv.
84	8 B			1.88 m	EJH/12/153 83.61-83.66 m		Strong black, patches of sod throughout, no foliation. 40% arfv, 20% aeg, 20% fsp, 10% neph, 5% eud, 5% sod.
					EJH/12/154 84.94-85.01 m		
86							Sharp & distinct 7/8 boundary.
88	7 W			5.75 m	EJH/12/155 89.78-89.83 m		Aegirine decreases upwards. 30% fsp, 20% aeg, 15% sod, 10% eud, 5% arfv.
90							
	7 R			1.43 m	EJH/12/156 91.76-91.81 m		Good red, sharp boundary to 7B below. 50% eud, 20% aeg, 20% fsp, 10% neph.
92	7 B			0.58 m	EJH/12/157 92.42-92.46 m		Aeg-rich black. 40% aeg, 30% arfv, 20% fsp, 10% eud.
94	6 W			2.36 m	EJH/12/159 93.10-93.15 m		Moderate foliation - fsp. 60% fsp, 20% aeg, 10% sod, 5% eud, 5% neph.
96	6 R			1.24 m	EJH/12/160 95.45-95.50 m		Altered & aeg-rich. No foliation. 40% eud, 30% aeg, 20% fsp, 10% neph.
	6 B			1.66 m	EJH/12/161 96.45-96.50 m		Some pegmatite alteration in centre of unit over 30 cm (aeg & fsp). 60% aeg, 15% fsp, 10% eud, 5% sod.
98	5 W			0.93 m	EJH/12/162 98.23-98.27 m		Core missing at 5/6 boundary, presumed sharp contact. Aeg-rich, no foliation. 50% fsp, 30% aeg, 10% eud, 5% arfv, 5% sod.
	5 R			0.99 m	EJH/12/163 99.01-99.07 m		Saccharoidal, pink eud. 30% eud, 30% aeg, 25% fsp, 5% sod, 5% arfv.
100	5 Wa			1.52 m	EJH/12/164 101.05-101.11 m		Aeg-rich. 40% aeg, 20% eud, 20% fsp, 10% sod, 10% neph.
102	5 B			1.05 m	EJH/12/165 101.99-102.04 m		Strong black. 70% arfv, 15% eud, 10% fsp, 5% sod.

Drill Core: DX-01 - Sheet 3 of 6		Elevation (top):	General Comments
Date Logged: 11th-15th August 2012	Geologist: E. J. Hunt	Elevation (base):	Recovery >95% Core depth = 338m
Units: metres		Locality:	

Depth	Unit	Lithology	Texture	Unit Thickness	Sample No.	Photo No.	Description and Interpretation
104	4 W			3.17 m	EJH/12/167 104.68-104.73 m		Sharp 4/5 boundary. Fsp randomly orientated, up to 40% sod. 50% fsp, 20% aeg, 10% sod, 10% neph, 10% eud.
106	4 R			1.62 m	EJH/12/168 106.88-106.93 m		Patchy aeg, no foliation. 30% aeg, 30% eud, 30% fsp, 15% sod, 5% arfv.
108	4 B			2.61 m	EJH/12/169 109.21-109.26 m		Aeg-rich black, 40% aeg, 20% arfv, 20% fsp, 10% eud, 5% neph, 5% sod. 3/4 boundary cut by syenite.
110	3 W			0.89 m	EJH/12/170 110.16-110.21 m	P1030650 P1030651	Phonolitic alteration, leached bands of fsp & eud. 40% aeg, 30% fsp, 15% sod, 10% aeg, 5% arfv.
112	3 R			1.21 m	EJH/12/171 112.13-112.19 m		Saccharoidal, some phonolitic alteration. 40% eud, 30% fsp, 15% sod, 10% aeg, 5% arfv.
	3 B			0.52 m	EJH/12/172 112.29-112.35 m		Poor black with phonolitic patches. 20% arfv, 20% aeg, 20% fsp, 20% eud, 15% sod, 5% neph.
114	2 W			10.63 m	EJH/12/173 115.23-115.30 m	P1030649	2/3 boundary: indistinct with phonolite patches. Altered with phonolite patches, eud-rich. 30% fsp, 30% eud, 15% aeg, 15% sod.
116							
118							
120							
122							
124	2 R			4.26 m	EJH/12/174 124.46-124.51 m		Not foliated. 30% eud, 30% sod, 25% aeg, 10% fsp, 5% arfv.
126							
128	2 B			1.41 m	EJH/12/175 128.33-128.39 m		Poor foliation - fsp, dark black. 50% arfv, 30% sod, 15% fsp, 5% eud.
				0.28 m			Aegirine-rich phonolite.
130	1 W			4.12 m	EJH/12/176 124.46-124.51 m		Dark white, spotted aeg & arfv. 40% fsp, 20% aeg, 15% arfv, 10% neph, 10% sod, 5% eud.
132							
	1 R			0.68 m	EJH/12/177 133.44-133.49 m		Patchy alteration. 40% eud, 30% fsp, 20% mafic, 10% sod.
134	1 B			1.20 m	EJH/12/178 134.44-134.48 m		Occasional sod xtls, poor foliation-fsp. 50% arfv, 25% neph, 20% fsp, 5% eud.
136	0 W			5.14 m	EJH/12/179 134.82-134.90 m EJH/12/180 139.19-139.23 m		Sharp 0/1 boundary. Sod increases up from 0R to max 30% then decreases to 1B boundary. 40% fsp, 20% neph, 15% sod, 10% arfv, 10% aeg, 5% eud.
138							
140							
	0 R			1.91 m	EJH/12/181 141.67-141.71 m		Strong red, saccharoidal, up to 5% sod, localised patchy alteration. 40% eud, 20% fsp, 20% neph, 10% arfv, 10% aeg.
142	0 B			0.71 m	EJH/12/182 142.30-142.35 m		Strong black, no foliation, <1% sod. 60% arfv, 15% fsp, 10% eud, 5% neph.
144	-1 W			3.31 m	EJH/12/184 144.43-144.49 m		Sharp -1/0 boundary. Dark white, poor foliation - fsp, Sod decreases upwards (20-0%). 40% fsp, 30% neph, 20% aeg, 15% arfv, 10% eud, 5% sod.
146	-1 R			0.80 m	EJH/12/185 146.56-146.60 m		Poor red, patchy alteration. 30% eud, 155 fsp, 20% arfv, 30% sod, 5% aeg.
	-1 B			0.87 m	EJH/12/186 147.32-147.37 m		V poor black. 30% aeg, 30% arfv, 25% fsp, 10% sod, 10% eud, 5% neph.
148	-2 W			2.44 m	EJH/12/188 148.13-148.18 m		Indistinct boundary (-2/-1). Rel dark white, large aeg phenocrysts (~1 cm), sod 0-5%. 40% fsp, 20% aeg, 20% neph, 10% arfv, 5% eud, 5% sod.
150	-2 R			0.56 m	EJH/12/189 150.28-150.33 m		Strong red, patchy alteration. 40% eud, 25% sod, 20% arfv, 10% fsp, 5% neph.
	-2 B			1.30 m	EJH/12/190 151.20-151.25 m		Strong black, poor foliation - fsp. 50% arfv, 30% sod, 15% fsp, 5% eud.
152							

Drill Core: DX-01 - Sheet 4 of 6		Elevation (top):	General Comments
Date Logged: 11th-15th August 2012	Geologist: E. J. Hunt	Elevation (base):	Recovery >95% Core depth = 338m
Units: metres		Locality:	

Depth	Unit	Lithology	Texture	Unit Thickness	Sample No.	Photo No.	Description and Interpretation
152							
	-3 W			7.11 m	EJH/12/191 153.42-153.47 m		Sharp -3/-2 boundary. Sod increases upwards (0-20%), poor foliation - fsp. 40% fsp, 15% sod, 15% neph, 15% arfv, 10% aeg, 5% eud.
154							
156							
158							
160	-3 R			2.26 m	EJH/12/192 160.32-160.38 m		Patchy alteration above contact to -3B, least alteration in centre, contact to -3W develops spotted arfv oikocrysts. Potentially 3 phases of eud: red, pink & altered yellow. Centre: 50% eud, 30% arfv, 15% fsp, 10% neph, 5% sod.
	-3 B			0.48 m	EJH/12/193 161.65-161.69 m		Strong black, no foliation. 50% arfv, 20% neph, 15% sod, 10% fsp, 5% eud.
162				0.19 m			Phonolite: aegirine-rich with fsp veins.
164	-4 W			4.77 m	EJH/12/194 164.02-164.07 m		Good foliation - fsp. Sodalite xtls variable (secondary?) from <1 mm to >1 cm. 40% fsp, 35% aeg, 10% eud, 10% arfv, 5% sod.
166							
168	-4 R			2.86 m	EJH/12/195 167.71-167.76 m		Moderate foliation - fsp. Patchy alteration. 30% eud, 30% fsp, 20% aeg, 10% neph, 5% sod, 5% arfv.
170				0.10 m			Phonolite: aegirine, nepheline & eudialyte.
172	-4 Wa			4.31 m	EJH/12/196 175.15-171.20 m		Sod varies from 0-10%, some eud-rich bands. Avg: 40% fsp, 20% aeg, 20% neph, 10% sod, 5% arfv, 5% eud.
174							
	-4 B			1.32 m	EJH/12/197 175.68-175.73 m		Foliated - fsp. 30% arfv, 30% aeg, 20% fsp, 10% neph, 10%, eud.
176					EJH/12/198 176.51-176.53 m		Sharp -5/-4 boundary (sample taken just above boundary).
178	-5 W			6.33 m	EJH/12/199 180.21-180.26 m		Strong fsp - no preferred orientation. 50% fsp, 15% aeg, 15% sod, 10% neph, 10% eud.
180							
182	-5 R			1.89 m	EJH/12/200 181.80-181.86 m		Altered at contact to hybrid with large aeg (up to 3 cm). Strong red with oikocrystic arfv. 30% eud, 20% arfv, 20% fsp, 2-% sod, 10% aeg.
184							
186							
188							
190	Hybrid			14.62 m		P1030610 P1030611	Complex textures, light & dark banding. Eud-rich and arfv-rich bands.
192							
194							
196							
198							
	Arfv Hybrid			0.74 m	EJH/12/201 198.78-198.82 m		Very arfv-rich band, laminated with fsp.
200							
202	Hybrid						

Drill Core: DX-01 - Sheet 5 of 6		Elevation (top):	General Comments
Date Logged: 11th-15th August 2012	Geologist: E. J. Hunt	Elevation (base):	Recovery >95% Core depth = 338m
Units: metres		Locality:	

Depth	Unit	Lithology	Texture	Unit Thickness	Sample No.	Photo No.	Description and Interpretation
200							
202	Hybrid			5.90 m		P1030609 P1030612	Medium grey, signs of flow banding. Resorption of white at base. Reaction eud present in veins at top.
204							
	-6 W			1.89 m	EJH/12/202 205.00-205.05 m		Good foliation- fsp. Mostly missing due to hybrid. Less sod than -6R (<5%). 40% fsp, 30% aeg, 10% eud, 10% neph, 5% arfv, 5% sod.
206	-6 R			2.54 m	EJH/12/203 206.57-206.61 m		V strong & thick red, patchy alteration. Aeg coarsens upwards at contact to -6W. 50% eud, 25% aeg, 10% fsp, 10% sod, 5% neph. Potentially recrystallised.
208	-6 B			0.41 m	EJH/12/204 207.95-208.00 m		Aeg-rich black, 30% aeg, 25% arfv, 25% sod, 15% fsp, 5% eud.
	-7 W			0.30 m			Foliated - fsp. 40% fsp, 10% sod.
210				4.14 m			Sharp inclined boundaries to -7W above & below. Phonolite composed of fsp & aeg.
212					EJH/12/206 212.25-212.31 m		Rel dark white, aeg-rich, prob altered due to pegmatite. 25% fsp, 20% neph, 15% sod, 5% eud, 35% aeg.
	-7 W			0.22 m			
214	-7 R			2.10 m	EJH/12/207 214.07-214.11 m		Good red, saccharoidal, patchy alteration. 40% eud, 25% fsp, 20% aeg, 10% arfv, 5% neph. Patches of sodalite.
	-7 B			0.88 m	EJH/12/208 214.82-214.85 m		Strong black, no foliation, no sod. 70% arfv, 15% fsp, 10% neph, 5% eud.
216					EJH/12/209 215.37-215.42 m		Sharp -8/-7 boundary.
218							
220							
	-8 W			12.58 m	EJH/12/210 225.41-225.21 m		Poor foliation, eud very altered. 60% fsp, 15% sod, 15% eud, 15% neph, 5% aeg, 5% arfv. Sod decreases upwards to <5%.
222							
224							
226							
228							
230	-8 R			3.54 m	EJH/12/211 228.60-228.65 m		Saccharoidal, patchy alteration. 40% eud, 20% sod, 20% fsp, 10% arfv, 10% neph.
	-8 B			0.83 m	EJH/12/212 231.70-231.76 m		Foliated - fsp & arfv. <5% sod. 30% arfv, 30% fsp, 15% aeg, 15% eud, 10% neph.
234	-9 W			4.27 m	EJH/12/213 232.79-232.83 m EJH/12/214 235.30-235.35 m		Sharp -9/-8 boundary Sod reappears from boundary to pegmatite. No foliation, 35% fsp, 20% neph, 15% sod, 15% aeg, 10% eud, 5% arfv.
236							
				0.52 m			Pegmatite. Sharp boundaries to -9W each side. Aeg & fsp, no sod.
	-9 W			0.13 m			Fsp-rich, rel sharp boundary from -9R. 10% sod.
238	-9 R			1.43 m	EJH/12/215 237.92-237.97 m		Localised sod (0-5%), foliated - fsp. 40% fsp, 30% eud, 20% aeg, 7% neph, 3% arfv.
	-9 B			1.07 m	EJH/12/216 239.36-239.41 m		Dark black, <1% sod, poor foliation. 50% fsp, 25% neph, 15% eud, 5% aeg, 5% arfv.
240							Sharp -10/-9 boundary
242	-10 W			6.63 m	EJH/12/217 242.00-242.08 m		Dark white, <1% sod, poor foliation. 50% fsp, 25% neph, 15% eud, 5% aeg, 5% arfv.
244							
246							
	-10 R			1.34 m	EJH/12/218 246.83-246.87 m		Poor foliation - arfv. Patchy alteration. 40% eud, 30% fsp, 15% aeg, 10% neph, 5% aeg. <1% sod.
248							
	-10 Wa						

Drill Core: DX-01 - Sheet 6 of 6		Elevation (top):	General Comments
Date Logged: 11th-15th August 2012	Geologist: E. J. Hunt	Elevation (base):	Recovery >95% Core depth = 338m
Units: metres		Locality:	

Depth	Unit	Lithology	Texture	Unit Thickness	Sample No.	Photo No.	Description and Interpretation
248							
	-10 Wa			3.51 m	EJH/12/219 250.23-250.30 m		Intermediate white unit, transition over 5 cm. 30% fsp, 20% sod, 20% aeg, 15% eud, 15% arfv.
250							
	-10 B			0.95 m	EJH/12/220 251.60-251.66 m		Well developed, well foliated - fsp. 45% arfv, 25% fsp, 20% sod, 5% neph, 5% eud.
252	-11 W			0.18 m			Mingling contact with hybrid, 20% sod.
	Hybrid			2.00 m	Top Eud Bottom	P1030608 P1030607 P1030606	Sharp contacts, partially melted -11 W. Xenocrystic, reaction eud bands.
254							
256							
	-11 W			5.28 m	EJH/12/222 258.36-258.41 m		More foliated upwards, <5% sod. 50% fsp, 20% neph, 10% aeg, 10% eud, 5% sod, 5% aeg.
258							
260	-11 R			1.55 m	EJH/12/223 259.95-259.99 m		Gradual increase in eud from -11 B. No sod, eud in bands not evenly distributed. 15-40% eud.
	-11 B			0.45 m	EJH/12/224 261.35-261.38 m		Well developed, v dark, no sod. 70% arfv, 15% neph, 13% fsp, 2% eud.
262							Sharp -12/-11 boundary, but very melanocratic white.
	-12 W			3.49 m	EJH/12/226 264.56-264.60 m		Foliation increases to -11 B, no sod. 60% fsp, 20% aeg, 10% neph, 8% arfv, 2% eud.
264							
	-12 R			0.64 m	EJH/12/227 265.58-265.63 m		Poor red, foliated fsp & arfv, no sod. 40% fsp, 20% neph, 15% eud, 15% arfv, 10% aeg.
266	-12 B			0.74 m	EJH/12/228 266.08-266.15 m		Well foliated - fsp & arfv, no sod. 40% arfv, 35% fsp, 10% neph, 10% aeg, 5% eud. Sharp -13/-12 boundary, steeply dipping.
	-13 W			0.38 m	EJH/12/230 266.62-266.67 m		No sod, moderate lamination - fsp. 60% fsp, 20% neph, 10% arfv, 8% aeg, 2% eud.
	-13 R			0.49 m			
268				0.22 m			Phonolite composed of aeg & fsp. Banded with fsp-rich laminations.
							Same as below, highly altered, ~40% eud plus aeg & fsp.
				1.32 m	EJH/12/231 268.41-268.50 m		Leucratic lense. Coarse grained >3 mm, resembles altered naujaite from Core 89-36. 40% fsp, 30% neph, 25% aeg, 5% altered eud.
270				1.97 m			Pegmatite: aeg, fsp & purple fluorite?
	-13 R			0.43 m	EJH/12/232 270.78-270.81 m		V altered in middle of pegmatite. No sod, ~40% altered eud.
				0.86 m			Pegmatite band.
272	-13 B			0.25 m	EJH/12/233 273.31-273.37 m		Dark black, no sod. 60% arfv, 10% fsp, 10% eud, 10% neph.
	-14 W			3.18 m	EJH/12/234 275.02-275.09 m		Poor foliation - fsp & arfv. No sod. 35% fsp, 25% neph, 20% aeg, 15% arfv, 5% eud.
274							
276	-14 R			1.83 m	EJH/12/235 275.83-275.89 m		Poor red, no sod, no foliation. 30% aeg, 20% fsp, 20% eud, 20% neph, 10% arfv.
278	-14 B			1.22 m	EJH/12/236 278.04-278.09 m		Good lamination - arfv & fsp, <1% sod. 40% arfv, 30% fsp, 10% aeg, 10% eud, 10% neph.
	-15 W			1.49 m	EJH/12/238 279.44-279.49 m		Sharp -15/-14 boundary. Rel eud-rich, oikocrystic arfv, laminated - fsp. 30% fsp, 20% neph, 15% sod, 15% eud, 10% arfv, 10 % aeg.
280	-15 R			1.35 m	EJH/12/239 280.56-280.61 m		No foliation, 35% eud, 20% fsp, 15% sod, 15% neph, 15% mafics.
282	-15 B			1.19 m	EJH/12/240 282.24-282.29 m		Moderate foliation - fsp & arfv, sod decreases upwards. 40% arfv, 20% aeg, 20% fsp, 10% eud, 7% neph, 2% sod.
	-16 W			1.20 m	EJH/12/242 283.76-283.80 m		Sharp -16/-15 boundary, poor foliation. 40% fsp, 20% sod, 20% neph, 10% arfv, 5% aeg, 5% eud.
284							
286	Transition			7.31 m			Transitional sequence from layered kakortokites to black madonna. Thinner banding, no distinguishable layers.
288							
290							
292							
294	Black Madonna						Black madonna.
296							
298							

Drill Core: DDH-01 - Sheet 1 of 1		Elevation (top):	General Comments
Date Logged: 11th-15th August 2012	Geologist: E. J. Hunt	Elevation (base):	Recovery >95% Core depth = 338m
Units: metres		Locality:	

Depth	Unit	Lithology	Texture	Unit Thickness	Sample No.	Photo No.	Description and Interpretation
6							-11 W: Eudialyte-rich, patchy sod (secondary?), 40% fsp, 10% sod, 20% eud, 20% aeg, 10% arfv. -11 R: Coarse-grained eud up to 3 mm, recrystallised?. 35% eud, 30% sod, 15% fsp, 15% arfv, 5% aeg.
8	-11 B						-11 B: Strong black, 40% aeg, 20% arfv, 15% fsp, 15% eud, 10% sod.
10	-12 W			4.81 m		P1030613	Strong white, moderate foliation - fsp. 40% fsp, 30% sod, 15% eud, 10% arfv, 5% aeg.
12							
14	-12 R			0.76 m		P1030613	Dark red, eud xtls <1 mm to 2 mm. 40% eud, 30% fsp, 15% aeg, 10% sod, 5% aeg.
	-12 B			0.74 m		P1030614	Finer grained than other units, laminated - fsp. 40% arfv, 20 % aeg, 20% fsp, 10% sod, 10% eud.
	Hybrid			0.77 m		P1030614	Melanocratic bands & reaction eud. Occurs at -13/-12 boundary.
16	-13 W			3.14 m		P1030614	Recrystallised at ~18 m - eud-rich up to 40%, may be assoc with hybrid below. Alteration over 1 m then white again. 40% fsp, 25% sod, 20% aeg, 15% eud.
18							
	Hybrid			0.77 m		P1030614	Looks like partial melting of -13W & recrystallisation. Then typical hybrid banding & eud reaction bands
20	-13 R			1.48 m		P1030614	Strong, saccharoidal red kakortokite.
	-13 B			0.21 m		P1030615	Altered? Bands of fsp 5 mm thick. Poor foliation - fsp. 50% arfv, 30% eud, 10% sod, 10% fsp.
22	-14 W			3.78 m		P1030615	Foliated - fsp, relatively dark white. 40% fsp, 30% sod, 15% aeg, 10% eud, 5% arfv.
24							
				0.86 m		P1030615	Leucocratic with large arfv (7 mm, 10%), eud (6 mm, 5%), sod (6 mm, 10%), fsp (3 mm, 10%). Siliceous matrix?
26	-14 R			0.59 m		P1030615	Relatively unaltered, foliated - fsp. 30% eud, 30% fsp, 20% aeg, 10% sod, 10% arfv.
	-14 B			1.24 m		P1030615	Poor lamination - fsp & arfv. 25% arfv, 25% aeg, 20% sod, 20% fsp, 10% eud.
28	-15 W			2.49 m		P1030616	Not very distinct -15/-14 boundary but sharp. Sod-rich white & leucocratic. 40% fsp, 30% sod, 15% aeg, 10% eud, 5% arfv.
30							
32	-15 R			2.45 m		P1030616	Saccharoidal, some fsp lathes aligned. Some eud xtls altered at margins. 40% eud, 20% fsp, 20% aeg, 10% eud, 5% arfv.
	-15 B			0.74 m		P1030616	Strong black, moderate foliation - fsp. 40% arfv, 20% aeg, 15% eud, 15% sod, 10% fsp.
34	-16 W			2.93 m		P1030617	Melanocratic white, arfv-rich. 30% fsp, 30% sod, 15% eud, 15% aeg, 10% arfv.
36						P1030617	Saccharoidal, patchy alteration. 40% eud, 20% fsp, 20% sod, 10% aeg, 10% arfv.
	-16 R			0.45 m			
38	-16 B			1.71 m		P1030617	Leucocratic black, patches of eud. 30% arfv, 20% sod, 20% aeg, 20% fsp, 10% eud.
40	-17 W			2.47 m		P1030617	Sharp & distinct -17/-16 boundary. Arfv-rich band in centre of unit. Foliated - fsp. 50% fsp, 15% aeg, 15% eud, 10% sod, 10% arfv.
	-17 R			0.62 m		P1030618	Patchy, saccharoidal, fsp lamination. 40% eud, 30% fsp, 15% sod, 10% aeg.
42				0.96 m		P1030618	Pegmatite composed of sodalite, fsp, aeg, arfv & eud. Must replace -17 B.
44	-18 W			2.14 m		P1030618	Foliated - fsp & arfv. 40% fsp, 20% sod, 15% arfv, 10% aeg, 10% neph, 5% eud.
46	-18 R			2.91 m		P1030618	Strong red, patchy alteration. 60% eud, 20% sod, 15% arfv, 10% aeg, 10% neph, 5% eud.
	-18 B			0.25 m		P1030618	Strong black, laminated - fsp lathes. 50% arfv, 30% fsp, 10% sod, 10% eud.
48	-19 W			2.91 m		P1030619	Sharp & distinct -19/-18 boundary. Melanocratic white. 40% fsp, 20% arfv, 15% sod, 10% neph, 10% eud, 5% aeg.
50							
	-19 R			0.49 m		P1030619	Thin red, foliated - fsp lathes. Minor alteration, esp at rims of eud xtls. 40% eud, 30% fsp, 20% arfv, 5% sod, 5% aeg.
	-19 B			0.17 m		P1030620	Small unit before alteration above B.M. Strong black, no foliation. 60% arfv, 20% eud, 15% fsp, 5% sod.
52							
54				3.68 m		P1030620	Eudialyte-rich material, 40% fsp, 20% eud, 20% arfv, 10% sod, 10% aeg. With enclaves of f-grained mafic material. Eud rich layer: 50% eud with patchy alteration & 10% sod. Darkens to laminated (fsp) black, 60% arfv, 5% sod.
56						P1030620 - P1030644	Sharp contact to Black Madonna